Universidade do Minho
Escola de Engenharia

Óscar José Maciel Barros

Tailored recovery of rare earth elements from fluorescent lamps industry leachates towards new catalytic applications

October 2023

Tailored recovery of rare earth elements from fluorescent lamps industry leachates towards new catalytic applications

Óscar José Maciel Barros

UMinho | 2023

Universidade do Minho
Escola de Engenharia

Óscar José Maciel Barros

Tailored recovery of rare earth elements from fluorescent lamps industry leachates towards new catalytic applications

Dissertation for PhD degree in
Chemical and Biological Engineering

Work carried out under the supervision of:
Maria Teresa de Jesus Simões Campos Tavares, PhD
Maria Isabel Pontes Correia Neves, PhD

October 2023

Acknowledgements

Developing this thesis would not be possible without the support of several people, for which I am and will be deeply thankful. Each one contributed to my growth not only at a personal level but also as a scientist through the share of knowledge and advice.

I would start by expressing my gratitude to my supervisor, Professor Teresa Tavares, for allowing me to join her research group as a researcher and later as a PhD student. Also, I want to thank her for the support these last 4 years regarding my work and progress, but primarily for believing in my work and my capacity to overcome all the difficulties during this journey. To my co-supervisor, Professor Isabel Neves, for all the support, help and confidence boost given me during this journey, especially when my confidence levels were low. To Professor Pier Parpot, for all the availability to help me and teaching regarding the Machine Learning algorithms. To the Centre of Biological Engineering (CEB) and to all its technical staff for the excellent support. To all the people from the LEQ lab at CEB for all the help given, healthy discussions and friendship created.

I also want to thank my friends who accompanied me from the start of this new adventure that we called university. I want to thank my friends from LTEB lab at CEB for all the support, conversations, help and friendship created. To a new friend I made during the last months of this adventure, I want to thank you for your patience and comprehension during this short time we have known each other.

My truly and deeply felt thanks to my parents, who gave unconditional love, education, support, and the hours they listened to me. Thank you for all of these and for making me the person I am today. To my brothers, for all the love and understanding and for being at my side, always making me push forward and never give up.

All of them were essential to me during this time. Adding to them, I also want to thank myself for fighting, working, believing, dreaming and realizing what I aimed to do.

Finally, I would like to thank the Portuguese Foundation for Science and Technology (FCT) for my PhD grant (SFRH/BD/140362/2018) and all the funding entities that supported the work.

FCT under the scope of the strategic funding of UID/BIO/04469/2020 and UID/QUI/0686/2020 units and BioTecNorte operation (NORTE-01-0145-FEDER-000004) funded by the European Regional Development Fund under the scope of Norte2020—Programa Operacional Regional do Norte, Portugal.

STATEMENT OF INTEGRITY

I hereby declare having conducted this academic work with integrity. I confirm that I have not used plagiarism or any form of undue use of information or falsification of results along the process leading to its elaboration. I further declare that I have fully acknowledged the Code of Ethical Conduct of the University of Minho.

Resumo

Recuperação de terras raras de lixiviados de lâmpadas fluorescentes para aplicações catalíticas

As terras raras são elementos químicos conhecidos como REE (do inglês, Rare Earth Elements), essenciais em diversas aplicações tecnológicas que fazem parte do quotidiano. A procura destes elementos químicos tem vindo a aumentar devido ao seu grande consumo e aplicações. Os zeólitos são aluminossilicatos sólidos porosos, bastante utilizados na recuperação de metais de águas contaminadas, podendo ainda ser aplicados como catalisadores heterogéneos em reações de interesse industrial. Esta tese tem como objetivos o desenvolvimento de um sistema de recuperação de terras raras de águas contaminadas em múltiplos ciclos de adsorção e dessorção e a validação da utilização das terras raras suportadas em zeólitos em reações catalíticas. A modificação química da superfície de diferentes zeólitos foi efetuada com vista à otimização da recuperação de terras raras de águas contaminadas. Verificou-se que o melhor zeólito modificado consegue remover mais de 80 % de todos as terras raras presentes na solução de ensaio e obtiveram-se recuperações acima de 90 % por posterior lixiviação dos sorventes. A estes resultados foram aplicadas, com sucesso, técnicas de *machine learning (ML)*, nomeadamente *supervised e unsurpervised learning*. Em regime de *supervised learning* foram aplicados algoritmos de classificação aos dados experimentais e a possibilidade de regressão. Em *unsupervised learning*, foram aplicados algoritmos para redução da dimensionalidade dos dados utilizados na elaboração dos *clusters*. A segunda parte é a continuação natural da anterior, em que o melhor zeólito passa de testes *batch* para ensaios em coluna, nos quais se atingiu mais de 70 % de remoção e uma recuperação, após a otimização, acima de 80 % para todas as REE testadas. As mesmas análises de *ML* foram aplicadas com sucesso aos resultados obtidos neste sistema aberto. A capacidade catalítica das REE suportadas nos zeólitos foi testada em reações tipo Fenton para a degradação de dois corantes, a tartrazina e o índigo de carmim, após a adição de ferro aos referidos zeólitos com REE. A degradação obtida para a tartrazina foi superior a 80 %, enquanto para o índigo de carmim foi superior a 95 %. Algoritmos de *ML* foram aplicados eficazmente na análise dos resultados obtidos de degradação.

Palavras-chave: Terras Raras; Adsorção; Dessorção; Machine learning; Catálise

Abstract

Tailored recovery of rare earth elements from fluorescent lamps industry leachates towards new catalytic applications

Rare earth elements, known as REE, are essential chemical elements with diverse technological applications that are part of everyday life. The demand for these elements has increased due to their high consumption and applications. Zeolites are porous solid aluminosilicates, widely used to recover metals from contaminated water and can also be applied as supports for heterogeneous catalysis. This thesis aims to develop a system for recovering REE in multiple adsorption and desorption cycles and to verify the possible use of REE supported on zeolites in catalytical reactions. Finally, machine learning (ML) algorithms were tested to select and to predict the behavior of REE and zeolite systems. Chemical surface modifications of different zeolites were carried out to optimize the recovery REE from contaminated water. The best modified zeolites can remove more than 80 % of all tested REE present in the test solution and recover above 90 % have been obtained by leaching the sorbents. ML techniques were successfully applied to these results namely unsupervised and supervised learning. Within the supervised learning, classification algorithms were applied to the collected data to select the best modified zeolites and to test the possibility of regression, validating the predictive ability of these algorithms on the removal of REE from wastewater. Within the unsupervised learning, algorithms were applied to reduce the dimensionality of the data used to create the clusters. The second part is the natural follow up of the previous work, where the best zeolites were used in continuous flow assays. A total REE removal above 70 % was obtained and a total REE recovery above 80 % for all REE tested after optimization. The same ML analyses were successfully applied. The catalytical capacity of the REE/zeolite was tested in Fenton-type reactions for the degradation of two dyes, tartrazine and indigo carmine, after the addition of iron to the REE/zeolite. The degradation for tartrazine was above 80%, while for indigo carmine, it was higher than 95 %. As previously described, ML algorithms were successfully applied to analyze the obtained results.

Keywords: Rare Earths Elements; Adsorption; Desorption; Machine learning; Catalysis

List of Contents

List of Figures

Chapter 1

Chapter 2

Chapter 3

Chapter 4

Chapter 5

List of Tables

Chapter 3

Chapter 4

Chapter 5

List of Abbreviations and Acronyms

A

A3 – catalyst $La_{10}Fe_{10}NaX$, FAU (NaX in powder) with the metals added via impregnation method

A7 – catalyst $La_{10}Fe_{10}NaX$, FAU (NaX in pellet) with the metals added via impregnation method

AOP – Advanced Oxidation Processes

ATR-FTIR Attenuated Total Reflectance Fourier Transform Infrared spectroscopy

B

BET – Brunauer-Emmett-Teller

C

$C/C_{0\,out}$ – C/C_0 concentration of REE that leave the continuous flow assays

C_o – initial concentration (mg/L) of the REE

Conc. – concentration

CT – Catalytic Tests

C_t – concentration (mg/L) of REE at a time (t)

D

dH_2O – distilled water (dH_2O)

DVD – Digital Versatile Disc

E

E_a – activation energy

EU – European Union (EU)

F

FAU – *Faujasite* structure

FCC – Fluid Cracking Catalysis

FTIR – Fourier-transform infrared spectroscopy

H

HDD – hard disk drives

HREE – heavy REE

I

ICP-AES – Inductively Coupled Plasma Atomic Emission Spectroscopy

ICP-OES – Inductively Coupled Plasma – Optical Emission Spectrometry

IS – Initial Screening

IUPAC – International Union of Pure and Applied Chemistry

K

k_1 – rate constant (min^{-1}) for PFO

k_2 – parameter related to the initial concentration of solute (g/(mg × min))

k_a – rate constants of adsorption

k_d – rate constants of desorption

KNN – K-nearest neighbors Classifier

L

L.E.D. – light-emitting diodes

LREE – light REE

LTA – Linde Type A structure

M

m – the mass (g) of the adsorbent used.

MAE – Mean absolute error

MFI – Mobil-type five structure

ML – Machine learning

MSE – Mean squared error

N

NW – without washing with NaOH 0.01 M – between the desorption and adsorption cycles

P

PCA – Principal Component Analysis

PFO – Pseudo-first order

pH_assay – pH value of the adsorption solution

pH_treatment – pH value of the treatment solution

pH_{final} – final pH

$pH_{initial}$ – initial pH

pH_{PZC} – pH of zero point charge

ppm – parts per million

PSO – Pseudo-second order

Q

q – uptake, mass of adsorbate per unit mass of adsorbent (mg/g)

q_e – mass of adsorbate per unit mass of adsorbent at equilibrium (mg/g)

q_t – mass of solute retained per mass of solid at time (t)

R

R_c – recovery percentage during the continuous flow assays

REE – Rare Earth Elements

REE_2O_3 or REEO- rare earth oxides

R_m – removal percentage during the continuous flow assays

RMSE – Root mean squared error

S

SEM-EDS – Scanning Electron Microscopy/Energy Dispersive X-Ray spectroscopy

SSR – Sum of Squares due to Regression

Sy.x – Standard Deviation of the Residuals

V

V_0 – the initial volume (L) of the REE solution

V_t – volume (L) of the solution at a given time (t)

W

WW – with washing with NaOH 0.01 M between the desorption and adsorption cycles

X

XPS – X-ray Photoelectron Spectroscopy

XRD – X-ray diffraction

Z

Z1 – catalyst $La_{10}Fe_{10}$ZSM5, MFI (ZSM5 in powder) with the metals added via impregnation method

Z10 – catalyst $Pr_{10}Fe_{10}$NaY, FAU (NaY in powder) with the metals added via ion exchange method

Z11 – catalyst $Pr_{25}Fe_{10}$ZSM5, MFI (ZSM5 in powder) with the metals added via ion exchange method

Z12 – catalyst $Pr_{25}Fe_{10}$NaY, FAU (NaY in powder) with the metals added via ion exchange method

Z13X – zeolite 13X without modification (control for FAU 13X)

Z13X_NW – zeolite 13X with no chemical modification and without washing with NaOH 0.01 M between the desorption and adsorption cycles

Z13X_WW – zeolite 13X with no chemical modification and with washing with NaOH 0.01 M between the desorption and adsorption cycles

Z15 – catalyst $La_{10}Fe_{10}$ZSM5, MFI (ZSM5 in powder) with the metals added via ion exchange method

Z16 – catalyst $La_{25}Fe_{10}$ZSM5, MFI (ZSM5 in powder) with the metals added via ion exchange method

Z17 – catalyst $La_{25}Fe_{10}$NaY, FAU (NaY in powder) with the metals added via ion exchange method

Z2 – catalyst $La_{10}Fe_{10}$NaY, FAU (NaY in powder) with the metals added via impregnation method

Z3 – catalyst $La_{25}Fe_{10}$ZSM5, MFI (ZSM5 in powder) with the metals added via impregnation method

Z4 – catalyst $La_{25}Fe_{10}$NaY, FAU (NaY in powder) with the metals added via impregnation method

Z4A – zeolite 4A without modification (control for LTA 4A)

Z5 – catalyst $Ce_{10}Fe_{10}$ZSM5, MFI (ZSM5 in powder) with the metals added via ion exchange method

Z6 – catalyst $Ce_{10}Fe_{10}$NaY, FAU (NaY in powder) with the metals added via ion exchange method

Z7 – catalyst $Ce_{25}Fe_{10}$ZSM5, MFI (ZSM5 in powder) with the metals added via ion exchange method

Z8 – catalyst $Ce_{25}Fe_{10}$NaY, FAU (NaY in powder) with the metals added via ion exchange method

Z9 – catalyst $Pr_{10}Fe_{10}$ZSM5, MFI (ZSM5 in powder) with the metals added via ion exchange method

ZA _H_2O – zeolite 4A only washed with H_2O (control for LTA 4A)

ZA_KOH 0.10 M – zeolite 4A modified with KOH solution at 0.10 M

ZA_KOH 0.25 M – zeolite 4A modified with KOH solution at 0.25 M

ZA_KOH 0.50 M – zeolite 4A modified with KOH solution at 0.50 M

ZA_NaOH 0.10 M – zeolite 4A modified with NaOH solution at 0.10 M

ZA_NaOH 0.25 M – zeolite 4A modified with NaOH solution at 0.25 M

ZA_NaOH 0.50 M – zeolite 4A modified with NaOH solution at 0.50 M

ZNaOH_NW – zeolite 13X with chemical modification with NaOH 0.1 M and without washing with NaOH 0.01 M between the desorption and adsorption cycles

ZNaOH_WW – zeolite 13X with chemical modification with NaOH 0.1 M and with

washing with NaOH 0.01 M between the desorption and adsorption cycles

ZSM5 – Zeolite Socony Mobil-type 5

ZX_H_2O – zeolite 13X only washed with H_2O (control for FAU 13X)

ZX_H2SO4 0.25 M – zeolite 13X modified with H2SO4 solution at 0.25 M

ZX_HCl 0.25 M – zeolite 13X modified with HCl solution at 0.25 M

ZX_HNO3 0.25 M – zeolite 13X modified with HNO3 solution at 0.25 M

ZX_KOH 0.10 M – zeolite 13X modified with KOH solution at 0.10 M

ZX_KOH 0.25 M – zeolite 13X modified with KOH solution at 0.25 M

ZX_KOH 0.50 M – zeolite 13X modified with KOH solution at 0.50 M

ZX_NaOH – zeolite 13X modified with NaOH solution at 0.10 M for the continuous flow assays

ZX_NaOH 0.10 M – zeolite 13X modified with NaOH solution at 0.10 M

ZX_NaOH 0.25 M – zeolite 13X modified with NaOH solution at 0.25 M

ZX_NaOH 0.50 M – zeolite 13X modified with NaOH solution at 0.50 M

"Be true to yourself. Make each day a masterpiece. Help others. Drink deeply from good books. Make friendship a fine art. Build a shelter against a rainy day."

John Wooden

Chapter 1 – Motivation and Outline

This chapter presents an overview of the work developed in this thesis. The motivation and outline of the research work and the main scientific outputs are also described.

1.1. Context and Motivation

In modern days, we are surrounded by technology like phones, computers, wind turbines, electric cars, photovoltaic panels and many others. In this technological world, our constant requirement for new devices and energy associated with the growth of the population is leading to an increase in the need for diversified chemicals to manufacture these products.

There are 118 chemical elements that make up everything that surrounds us and 44 of those will face supply limitations in the coming years [1]. Some of the critical elements include precious metals as gold (Au), silver (Ag), Rare Earth Elements (REE), phosphorus (P), lithium (Li), copper (Cu), aluminum (Al) and many others [1,2]. These elements may suffer from market pressure due to the high demand for diverse applications as the production of low-carbon energy technologies intensifies [2]. For example, the production of electric cars has been growing by over 50 % yearly for a decade and might reach an international value of 100 million of electric cars by 2023 [3,4]. The Li production would need to double in the next decade to achieve such goal [5]. Another example is the higher amounts of metal to produce the same power as their fossil fuels counterparts by low-carbon energies [6]. For example, photovoltaic power requires up to 40 times more Cu than fossil fuel combustion and wind power up to 14 times more Fe [6].

Metals are one of the most crucial resources in the world, with 2.8 billion tons mined, with some diversified applications, as shown in **Figure 1.1**.

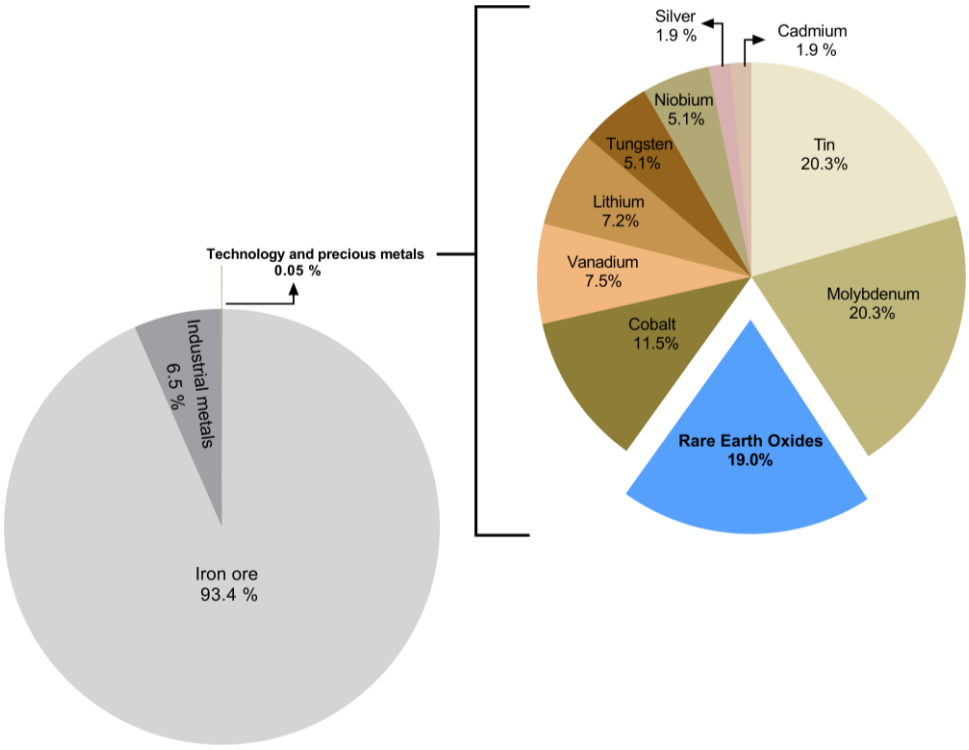

Figure 1.1: World metal production in 2021 [7].

In the technology and precious metals sector, which accounts for 0.05% of the world metal production, rare earth oxides represent 19% of metals used and the trend is upwards. REE have played a crucial role in the materials industry across various domains such as phosphors, magnets, metallurgy, catalysts and glass since the 1950s. They are frequently employed as additives or dopants in materials. What makes REE particularly valuable is their ability to induce significant changes in material properties, even when used in small quantities. Consequently, they have earned the reputation of being the "vitamins" of modern industry, and the creation of materials doped with rare earths has emerged as a relevant technological advancement [6,8].

This work will focus on the recovery of REE from industry leachates by porous materials, so that they may be used in new catalytic applications. The REE are more abundant than Au or Pb [9] but their extraction is quite challenging, not always justifiable. Therefore, recycling becomes a new possible source of REE but their recovery is still in the first steps, and a good system that allows their recovery and tackles the accumulation of contaminating waste is required.

The increased resource requirement leads to a growth in mining exploration and it is important to remember that mineral extraction contributes to diverse problems such as environment degradation, population displacement and other adverse impacts [10]. Moreover, not all the various final mining products are recycled, which can lead to water contamination from these chemicals.

To increase the REE life cycle, zeolites were used to retain REE and the resultant systems, REE supported on zeolites were evaluated as catalysts in oxidation reactions. Zeolites, which are aluminosilicate minerals, are extensively utilized as catalysts, adsorbents and ion exchangers due to their crystalline microporous nature. Some zeolites are naturally found in nature and are excellent supports for REE [11]. As a result of this research project, we can address the following issues:

- **Can REE be removed by zeolites from wastewater and recovered in multiple adsorption and desorption cycles?**
- **Can REE-zeolite serve as a heterogeneous catalyst for environmental purposes?**
- **Can Machine Learning (ML) algorithms aid in selecting and predicting outcomes for the REE/zeolite systems?**

For that, a zeolite-based removal system was developed to extract REE from wastewater and it was associated with a recovery step to allow the cyclic use of the system. To enhance the natural metal removal capacity of zeolites, chemical treatments were employed to modify their surfaces. These chemically modified zeolites were utilized for REE adsorption and subsequent desorption tests to recover both the REE and the zeolite, which may be utilized for further REE removal purposes. In addition to the

desorption tests, the zeolite loaded with REE was evaluated for its effectiveness in degrading various food dyes through heterogeneous catalysis in a Fenton-type reaction. The successful implementation of ML algorithms in this study allowed selecting the best REE/ zeolite systems.

This thesis was carried out mainly at the Centre of Biological Engineering (CEB) and Centre of Chemistry of the University of Minho (Braga, Portugal).

1.2. Thesis outline

The thesis is divided in 6 chapters. Chapters 1, 2 and 6 correspond to the introduction, state-of-the-art, the main conclusions and the suggestions for future work, respectively. The main core of the thesis is constituted by chapters 3, 4 and 5, which are based on scientific papers under submission for publication.

Chapter 1, the current chapter, describes the context, motivation, research plan and the thesis outline.

Chapter 2 introduces a general background and a review of the state of the art required for the understanding of the work presented in four subchapters: I) Rare Earths Elements, REE; II) Zeolites, III) Sorption processes and IV) catalysis.

Chapter 3 describes the methodologies used for the different pre-treatments of the zeolites. Subsequently, these zeolites were characterized and tested for their REE adsorption capacity in batch trials to select the best options. The selection process used a machine learning approach, ML, classification and regression algorithms to choose the most promising adsorbents for REE. Desorption and kinetics assessment was carried out with the most promising zeolites and from these data the most adequate was selected.

Chapter 4 explores the experimental data from column assays to evaluate the possibility of a scale-up assay with the zeolite selected from the previous chapter. The column assays were carried out with 4 cycles of adsorption, desorption and wash and the results were analyzed using the classification of ML algorithms.

Chapter 5 addresses the production of different REE/Fe-zeolite catalysts resulting from the combination of REE, iron (Fe) and zeolites. These catalysts were tested on the degradation of two food dyes through a Fenton-like reaction. Based on these results, the most promising catalysts for dye degradation was selected using the classification from ML algorithms. The kinetics assessment allowed an even narrower selection of the most suitable catalyst.

Finally, the breakthroughs of this thesis are briefly discussed in **Chapter 6** and suggestions for future work in this field are given.

1.3. Scientific outputs

The development of the experimental work during this Ph.D. thesis originated the following publications in international scientific journals and the participation in several scientific meetings by oral and poster communications.

Publications in peer-reviewed journals:

- **Barros, O.**; Parpot, P.; Neves, I. C.; Tavares, T.; *Chemical modification of zeolites for the recovery of Rare Earth Elements using Machine Learning algorithms* – under revision.
- **Barros, O.**; Parpot, P.; Neves, I. C.; Tavares, T.; *Exploring optimization of zeolites as adsorbents for Rare Earth Elements using Machine Learning techniques in continuous flow assays* – under revision.
- **Barros, O.**; Parpot, P.; Rombi, E.; Tavares, T.; Neves, I. C; *Machine learning approach for classification of REE/Fe-zeolite catalysts for Fenton-like reaction* – under revision.
- Lago, A., Rocha, V., **Barros, O.,** Silva, B., Tavares, T., *Bacterial biofilm attachment to sustainable carriers as a clean-up strategy for wastewater treatment: a review* – under revision.
- Rocha, V., Lago, A., **Barros, O,** Silva, B., Tavares, T., *Immobilization of biogenic metal nanoparticles on sustainable materials - green approach applied to wastewater treatment: a systematic review* – under revision.
- Assila, O.; **Barros, O.**; Fonseca, A. M. F.; Parpot, P.; Soares, O. S. G. P.; Pereira, M. F. R.; Zerrouq, F.; Kherbeche, A.; Rombi, E.; Tavares, T.; Neves, I. C.; *Degradation of pollutants in water by Fenton-like oxidation over LaFe-catalysts: Optimization by experimental design*; Microporous and Mesoporous Materials, 2023, 349, 112422, https://doi.org/10.1016/j.micromeso.2022.112422

Book Chapter:

- Costa, F.; Lago, A.; **Barros, O.**; Rocha, V.; Vipotnik, Z.; Silva, B.; Tavares, T.; *Chapter 14 - Retention of organic micro-pollutants by sorption processes*; Current Developments in Biotechnology and Bioengineering, Emerging Organic Micro-pollutants; 2020; 331-362, https://doi.org/10.1016/B978-0-12-819594-9.00014-0

Oral communication in scientific meetings

- **Barros, O.**; Neves, I. C.; Tavares, T.; *Recovery of rare earth elements by zeolite materials*, XVth International Symposium on Environment, Catalysis and Process Engineering, 23 to 25 November 2021, Morocco;

- Assila, O.; **Barros, O.**; Zerrouq, F.; Kherbeche, A.; Fonseca, A. M. F.; Parpot, P.; Tavares, T.; Neves, I. C.; *Optimization of Fenton-type reaction for water treatment using bimetallic catalysts based in porous materials by Box-Behnken Design*, at XVth International Symposium on Environment, Catalysis and Process Engineering, 23 to 25 November 2021, Morocco;
- Assila, O.; **Barros, O.**; Zerrouq, F.; Kherbeche, A.; Fonseca, A. M. F.; Parpot, P.; Tavares, T.; Neves, I. C.; *Box-Behnken Desing for optimization of Fenton-type reaction for water treatment using heterogeneous catalysts*, XXVII Encontro Nacional da Sociedade Portuguesa de Química, 14 to 16 July 2021, Braga, Portugal.

Poster communications in scientific meetings

- **Barros, O.**; Assila, O.; Neves, I. C.; Tavares, T.; *Comparison of the catalytic behaviour of rare earth elements loaded in zeolites as heterogeneous catalysts,* XI National Meeting on Catalysis and Porous Materials (XI ENCMP) and the II Meeting of the Carbon Group (II RGC), 9 and 10 December 2021, Aveiro, Portugal.

1.4. References

1. American Chemical Society The Periodic Table of Endangered Elements - American Chemical Society Available online: https://www.acs.org/greenchemistry/research-innovation/endangered-elements.html (accessed on Jul 1, 2023).
2. Church, C.; Crawford, A. *Green Conflict Minerals: The fuels of conflict in the transition to a low-carbon economy. IISD Report*; 2018;
3. IEA *Global EV Outlook 2019 - Análise - IEA*; 2019;
4. United Nations Climate Change Conference Paris Declaration on Electro-Mobility and Climate Change & Call to Action Available online: https://unfccc.int/news/the-paris-declaration-on-electro-mobility-and-climate-change-and-call-to-action (accessed on Jul 1, 2023).
5. Ballinger, B.; Stringer, M.; Schmeda-Lopez, D.R.; Kefford, B.; Parkinson, B.; Greig, C.; Smart, S. The vulnerability of electric vehicle deployment to critical mineral supply. *Appl. Energy* **2019**, *255*, 113844.
6. Lèbre, É.; Stringer, M.; Svobodova, K.; Owen, J.R.; Kemp, D.; Côte, C.; Arratia-Solar, A.; Valenta, R.K. The social and environmental complexities of extracting energy transition metals. *Nat. Commun.* **2020**, *11*, 4823.
7. Visual Capitalist All the Metals We Mined in 2021: Visualized - Visual Capitalist Available online: https://www.mining.com/web/all-the-metals-we-mined-in-2021-visualized/ (accessed on Jul 1, 2023).
8. Zheng, B.; Fan, J.; Chen, B.; Qin, X.; Wang, J.; Wang, F.; Deng, R.; Liu, X. Rare-Earth Doping in Nanostructured Inorganic Materials. *Chem. Rev.* **2022**, *122*, 5519–5603.
9. Barrett, S.D.; Dhesi, S.S. *The Structure of Rare-Earth Metal Surfaces*; PUBLISHED BY IMPERIAL COLLEGE PRESS AND DISTRIBUTED BY WORLD SCIENTIFIC PUBLISHING CO., 2001; ISBN 978-1-86094-165-8.
10. UN Sustainable Development Solutions Network (UNSDSN) *Mapping Mining to the Sustainable Development Goals: An Atlas*; 2016;
11. Pérez-Botella, E.; Valencia, S.; Rey, F. Zeolites in Adsorption Processes: State of the Art and Future Prospects. *Chem. Rev.* **2022**, *122*, 17647–17695.

Chapter 2 – Literature Review

This chapter presents an overview of the Rare Earth Elements, especially in what concerns their characteristics, processing, applications and the importance of recovering and recycling these elements. The definition, characteristics, importance and applications of zeolites will be discussed. The concepts and importance underlining adsorption processes will be explained. An overview on heterogeneous catalysis and on Fenton-type reactions will be forwarded. Finally, the application of machine learning techniques to adsorption and to catalysis will be reviewed to understand how these algorithms can benefit for the selection of the best outcomes.

2.1. Rare Earth Elements

The rare earth group includes seventeen elements (lanthanide group of the periodic table with scandium (Sc) and yttrium (Y)) as defined by the International Union of Pure and Applied Chemistry (IUPAC). The fifteen lanthanides are the elements with the atomic numbers from 57 to 71, being listed as: lanthanum (La), cerium (Ce), praseodymium (Pr), neodymium (Nd), promethium (Pm), samarium (Sm), europium (Eu), gadolinium (Gd), terbium (Tb), dysprosium (Dy), holmium (Ho), erbium (Er), thulium (Tm), ytterbium (Yb) and lutetium (Lu).

These elements are divided into light REE (LREE) and heavy REE (HREE), with Z of the LREE ranging from 57 to 64,while the atomic number of the HREE goes from 65 to 71, including Y [1,2]. The main difference between the HREE and the LREE is related to the paired electrons (both clockwise and counter-clockwise spinning electrons) present in the HREE [3]. Yttrium is included in the HREE since this element presents some similarities, both in ionic radius and chemical properties with that group. Sometimes the REE are divided into three categories: (i) light REE - La, Ce, Pr, and Nd; (ii) medium REE – Sm, Eu, and Gd and (iii) heavy REE - Tb, Dy, Ho, Er, Tm, Yb, Y and Lu [4–6]. This work will consider the REE division into light and heavy.

Sc is considered an REE as it was discovered simultaneously with other REE and its characteristics resemble more the ones of Y rather than those of Al or Ti [6]. However, this element is not considered a LREE or a HREE [3,7]. Pm is considered a REE as it is the last element of the lanthanide group to assume double c-axis hcp (*dhcp*) structure at ambient conditions [8]. This element is the only one that does not occur in nature due to its radioactivity instability [9,10].

Understanding the REE and their various applications, which will be summarized in section **2.1.1 REE applications**, will be more straightforward when the characteristics of these elements are known. Diverse studies and reviews have been published to explain the versatility of REE [3,7,11].

The REE possess different oxidation states, although the most common oxidation is 3^+, as it is more stable, and due to that, most of the REE are represented as REE_2O_3 [3,12].

A critical characteristic of all metals is their precipitation pH, mainly for purification purposes, and the REE are no exception. It is essential to understand that the REE precipitation may occur at different pH, depending on the anion present in the solution and its concentration. The work of Han [13] shows that it is possible to induce REE precipitation even at low pH values by using different precipitants. Some examples of REE precipitation described in the literature use carbonate [14,15], fluoride [16,17], phosphate [18,19], sulfate [20–24] and oxalate [7,25–28].

The REE are elements that do not exist as individual native metals such as gold (Au), copper (Cu) or silver (Ag), due to their reactivity. Instead, they occur together in diverse minerals as minor or major constituents [29]. REE are found in a great variety of minerals, over 250 minerals [30], although the primary sources of REE of economic interest are bastnaesite, monazite, loparite and the lateritic ion-adsorption clays [29]. The bastnaesite ore is found in China and the United States and constitutes the most significant percentage of the world's REE source. In contrast, the monazite ore is found in countries such as Australia, Brazil, China, India, Malaysia, South Africa, Sri Lanka, Thailand and the United States. It constitutes the second largest deposit of REE [31,32]. Although with minor impact , other sources of REE are apatite, cheralite, eudialyte, loparite, phosphorites, rare-earth-bearing (ion adsorption) clays, secondary monazite, spent uranium solutions and xenotime [33]. Apatite ore does not present a high concentration, varying from 0.1 % to 1 %, of rare earth oxides (REE_2O_3 or designed as REEO) [34–36]. However, this ore is abundant and is found worldwide, making it an essential source of REE [37,38]. The work by Liu *et al.* [39] summaries the updated state regarding the different REE deposits, active mines and 146 projects at an advanced stage, shown in **Figure 2.1**.

Figure 2.1: Current global distribution of REE projects, including active mines and advanced projects. The REE deposit types are represented by various colors accordingly. Active mines (☆) and advanced projects (○) are also marked. Adapted from Liu et al. [39].

Over the most recent years, the REE production suffered enormous growth, from 1.814 kilotonnes (kt) before 1960 to 112.491 kt in 2010, with an average growth rate of around 10 % per year [40,41]. The global production of rare earth oxide (REO) was 263.054 kt in 2021 and 272.155 kt in 2022

[42]. The global REE market reached 9.5 billion US $ in 2022 [43], with a global consumption of REE oxides around 164 kt [44].

China is the major REE producer, followed by the United States, Australia and Burma, as the percentage of the total production from 2022 [42] reveals in **Figure 2.2**.

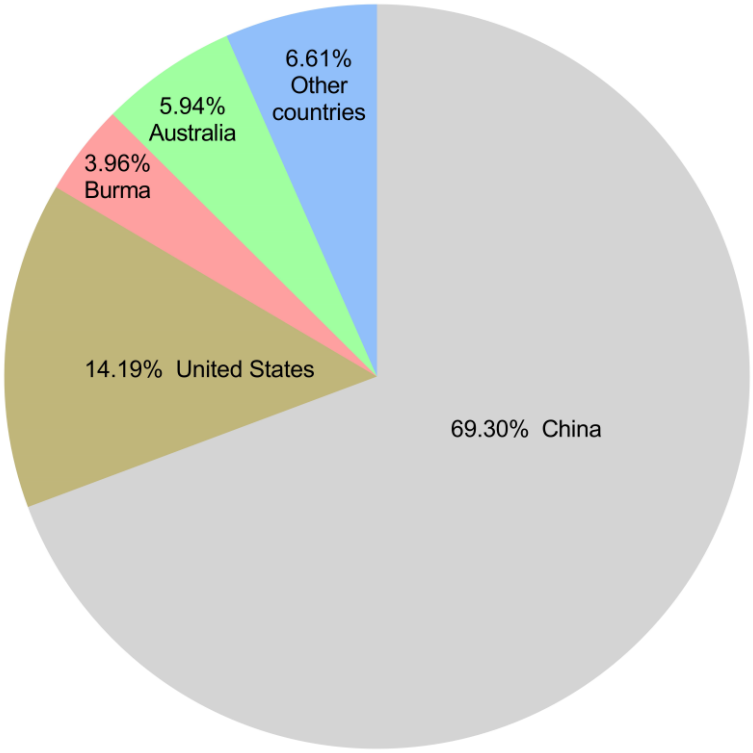

Figure 2.2: World production of REE in 2022. Adapted from the U.S. Geological Survey 2023 [42].

The REE purification from ores involves significant energy and resource consumption, high pollution levels and relevant environmental impacts. The REE processing is much more complex than the production of other metals [45,46], due to their similar reactivity. Adding to that, REE production is associated with radioactive pollution and toxicity due to the presence of radioactive elements in the REE deposits like uranium (U) or thorium (Th) [47]. For these reasons, REE production is attracting more attention globally [48,49]. For the extraction of 0.907 t of REE in Bayan Obo in Mongolia, it is required 4.001 t of sulfuric acid (H_2SO_4), 11.177 t of sodium chloride (NaCl), 1.488 t of sodium hydroxide (NaOH), 1.061 t of hydrochloric acid (HCl), 1.724 t of water and the grinding of almost 45.359 t of mineral ore [50,51]. Additionally, the energy required to obtain 1 ton of an individual REE varies from 38 to 48 GJ, except for Sc and Y, which requires 148 or 75 GJ per ton, respectively [50].

In 2011, REE were sold at record high prices, which had driven some countries to re-open mines, as the Mountain Pass mine in California re-opened in 2012 [52]. Some countries like Japan and most of

the European Union (EU) do not have any REE deposits, so they have to invest in developing alternative sources of REE [52].

Kato and co-workers reported a rich REE mud around Minamitorishima Island in 2011 [53] and further studies verified that the referred mud had almost 8000 ppm of total REE , corresponding to more than 14.515 million tonnes (Mt) of REEO in the studied area [54]. In 2021, Ohta *et al.* [55] reported a rich REE mud with contents between 2000 and 4500 ppm in the Central Pacific Basin. Although the mud presents high concentrations of REE, it will be a challenge to isolate them. The challenge begins with collecting, concentrating and transporting the mud from the seabed by the lowest cost possible. New technologies are required as well as the adaptation of other ones to process this deep mud and to recover the valuable REE.

Another possible source of REE is coal, mainly coal ash or coal-based materials [56–58]. Coal ash is reported to eventually release toxic elements, such as As, Se, Cr and Cd by naturally leaching from the ash deposit sites, which is harmful to the environment and to human health [59]. Some critical metals can also be found in coal like Ge, Ga, Nb, Zr, V, Re, Au and base metals such as Al [59–61]. Luttrel *et al.* [62] reported that more than 80 % of REE associated with the run-of-mine coals are refused streams after coal preparation. Therefore, the coal refuse or even the coal ash could be a more suitable REE source as higher concentrations of REE mean a more cost-effective and efficient recovery. However, it is essential to note that the feasibility of using such a source depends on various factors, such as the actual concentration of REE in the refuse, the efficiency of extraction methods, environmental considerations and economic viability. Some developments have been reported such as the methods used by Wang *et al.* [59] to recover REE from coal ash. While for coal refuse, physical and hydrometallurgical approaches usually provide low recoveries [57], a previous calcination step before the acid leaching has encouraging results [63,64].

2.1.1.REE applications

REE are a group of chemical elements with a huge application potential and this is related to their diversified properties of interest, which vary from chemical, optical, electrical, metallurgical and catalytical to magnetic [42,65–67]. The diverse electronic, manufacturing, and technological applications of the properties of the REE show that these elements are present in a significant part of the products that surround us in our daily lives. Due to their importance in diverse areas, several international institutions and governments coded REE as critical materials [1,29,68,69].

REE do have diverse applications such as in metal alloys, lasers, lighter flints, batteries, fluorescent materials (lamps), information storage (Digital Versatile Discs or computer memories),

catalysts, magnets and super magnets, glass additives, military technologies, transport of energy, phosphors, mobile phones, medical applications (nanomedicine, imaging), light-emitting diodes (L.E.D.), light bulbs, high-temperature superconductors, renewable energy sources (solar panels, wind turbines), polishing compounds, military and aerospace systems [29,42,70–72]. The primary applications of these elements in 2021 are shown in **Figure 2.3**.

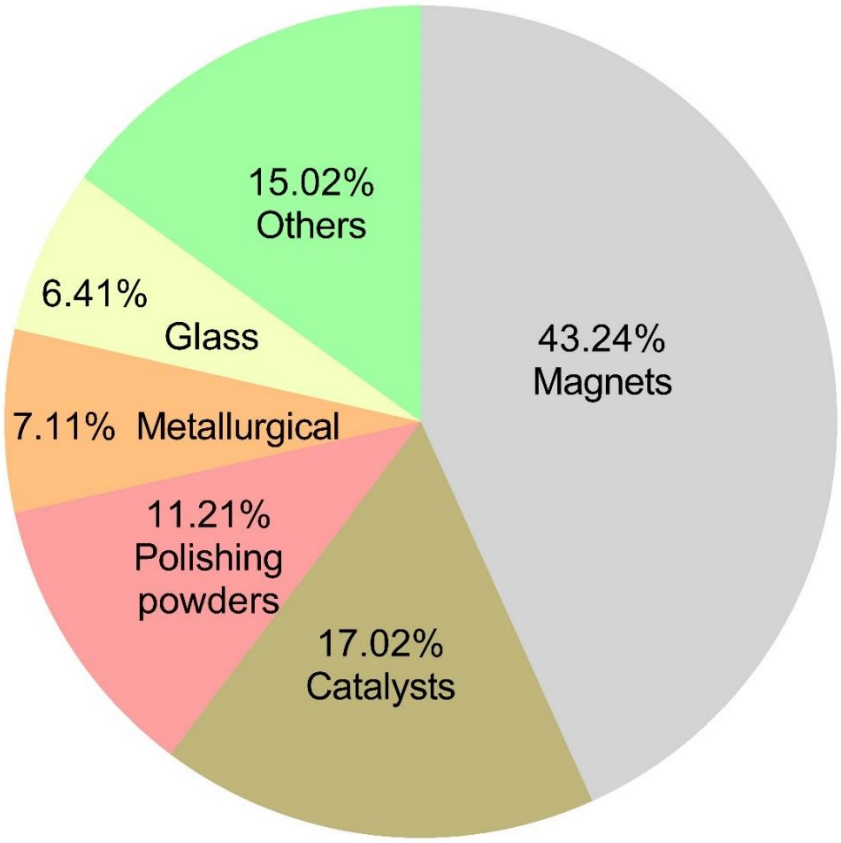

Figure 2.3: Distribution of rare earth element consumption in 2021 (adapted from Statista [73]).

2.1.2.Recovery and recycling importance of REE

REE are relevant for different applications and are nonrenewable strategic resources [74]. The undirected development in recent years has caused a severe depletion of REE and irreversible damage to such resources since the supply of these elements is widening year by year [75]. Therefore, recycling the REE from urban or industrial waste is critical to moving from a linear economy to a circular economy [72]. However, the recycling of REE is quite complex due to the number of such elements and the quantities of those elements (that range from mg to several kgs) present in the end-products [72]. Combining the varying amounts with the complexity of their uses, the inherent difficulty of separating individual REE, the possible extended life usage of specific applications, it is justifiable that less than 1 % of the REE used today is recycled [72,76]. Some relevant efforts have been made to develop new REE recycling methods [77–79]. Over the last years, extensive efforts have been made regarding the recycling

of fluorescent lamps [77,80], of NdFeB magnets from hard disk drives (HDD) [24,81], from wind turbines [82,83] or from magnets production waste [84].

One of the most important secondary sources is electronic waste, e-waste [85]. This waste consists of electric and electronic devices (equipment that required electricity to work) which were discarded at the end of their economic life span when no longer used by consumers [86,87]. Those devices include computers, audio-visual and communication equipment [88,89]. In 2016, each inhabitant produced, on average, 6.1 kg of this waste, a total of 44.7 Mt worldwide and it was estimated to reach 52.2 Mt in 2021 [90]. In 2016, it was estimated that this waste was worth around 55 billion euros [91] and the European market for REE recycling could be worth 1 billion euros [92].

Some factors play a crucial role in the growth of this waste such as the decreasing economic lifespan of electronic devices [93], lack of international consensus on e-waste management [94] and inadequate use awareness [87]. One big challenge for its disposal is its quantification since there is no appropriate waste tracking systems. As an alternative to disposal, e-waste could be redirected for material recycling and reprocessing [95], resulting in new raw materials able to substitute primary materials, more commonly designed as virgin materials obtained from ores. This idea may help to construct a new economy based on circular zero-waste [96].

One important concept is the technosphere, a material stockpile established by human activities and technological processes where different metals and alloys can be found [97]. These metal deposits changed the mining perspective since some metals can be recycled from previous applications and used in new ones [97]. This idea will help to supply the markets with the needed metals, as technosphere mining is a secondary source of many metals, promoting a circular economy and reducing the amount of end-of-life products in e-waste. Jowitt *et al.* [98] state that the recycling of REE could be divided into different types, namely direct recycling of manufacturing scrap or residues, recycling of solid and liquid industrial wastes and urban mining or technosphere mining of end-of-life products also in accordance to the work of Li *et al.* [99].

Technosphere mining can be applied for recycling REE from end-of-life products such as permanent magnets, lamp phosphors from fluorescent lamps, batteries, urban solid waste, stocks of landfilled industrial processes residues such as mine tailing bauxite residue, REE catalysts used within the chemical industry and some others [52,98,100–104]. One big obstacle to recycling REE from end-of-life products is the vestigial elemental amounts present in most of them. On the other hand, significant amounts of those products could raise the total quantity of REE potentially recovered. Other problems

have held back the recycling of REE up to date such as the difficulty of collecting, extracting and recovering [98].

With correct e-waste management, as summarized in **Figure 2.4**, it could be possible to perform a technosphere mining of REE, in other words, the REE recycling. On the other hand, tracking the amounts of e-waste produced and recycled could enhance that recycling as it is. However, new recycling methods with good recovery yields even starting from low concentrations, high selectivity, economic, non-toxic and not harmful to human health and to the environment are needed. Diverse processes have been studied and used. However, some of them require chemicals to allow a high recovery capacity, which will lead to a growth of waste while the idea is to reduce it as much as possible. The different sorption processes may be a possible solution for this problem. The focus of this thesis is the recovery of the soluble REE using adsorption techniques, being some of the main reasons for the possible use of this technique with lower concentration of the pollutant and other characteristics that will be explored in 2.3 Sorption Processes.

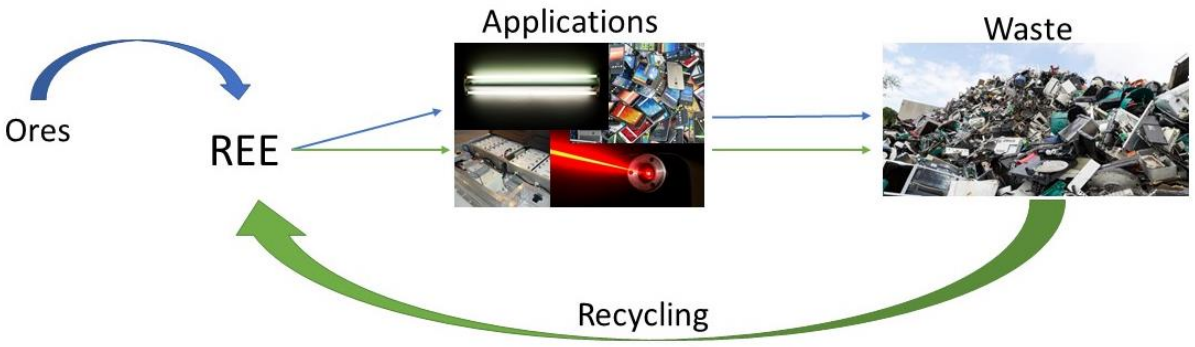

Figure 2.4: REE life cycle: REE are obtained from ores and transformed into different applications (blue), resulting in waste. In green, it is possible to get REE through recycling the e-waste by technosphere mining and re-use those elements into new applications.

One main problem after the solubilization of the REE will be their separation from the solution, overcame by precipitation with specific anions. However, as explained in the section 2.1 Rare Earth Elements, precipitation depends on several factors to be successful and economically viable.

2.2. Zeolites

Zeolites are crystalline microporous aluminosilicates solids [105], which can be used for incorporating within their structure different cations from a solution by ion exchange reaction. Zeolites which belong to the tectosilicate-type minerals and some of them occur naturally, present a high specific surface area, and are used as catalysts, adsorbents, ion-exchangers, and other aplications [105–107].

The variation of the synthesis conditions, use of more reactive silica sources and more alkaline media led to the obtention of zeolites A and X and 14 new zeolite materials. In this work, it was used MFI, Mobil-type five (Zeolite Socony Mobil-type 5, ZSM5), faujasite, FAU (Y and X) and Linde Type A, LTA (4A) structures. Therefore, these zeolite structures will be the focus and the respective structures are shown in **Figure 2.5**.

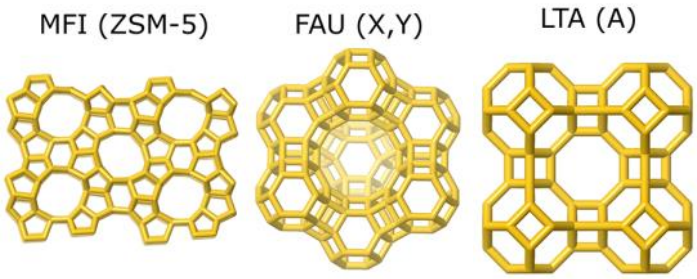

Figure 2.5: Front view of the structure of the selected zeolites for this work. Each zeolite has the official name given to each structure by the International Zeolite Association, while their common name is shown in parentheses, adapted from [105].

Zeolites have a three-dimensional structure of SiO_4 and AlO_4 tetrahedras, in which replacing the Si^{4+} with Al^{3+} give the zeolite a negative charge [108]. This negative charge justifies the strong affinity for cations, such as transition metals, and a little affinity for anions and non-polar organic molecules [108,109].

The zeolites can be classified according to their Si/Al ratio as low-silica (Si/Al ratios below 2, highly polar), medium-silica zeolites (Si/Al ratio between 2 and 5, intermediate polarity) and high-silica zeolites (Si/Al ratios above 5) [110]. Also, by the size of the pore diameters [110–112]:

- Small pores: between 3 and 4 Å, corresponding to 8 or 9 oxygen rings.
- Medium pore: between 5 and 6 Å, corresponding to 10 oxygen rings.
- Large pore: between 6 and 7.5 Å, corresponding to 12 oxygen rings.
- Extra-large: above 7.5 Å, corresponding to more than 12 oxygen rings.

2.2.1.Applications

Zeolites present high thermal and moderate to high chemical stabilities [113,114], which allow them to be used in diverse applications. This section will further explore the main uses of each selected zeolite structure. The FAU and LTA are frequently addressed in all applications, due to their physicochemical properties.

The usage as ion exchangers of the zeolites depend on the relative sizes between the cations (with possible inclusion of their hydration shell) and the pores [105]. This size exclusion associated with the different stereo-affinities of ions when using zeolites as exchangers allows ion separation and, more specifically, ion sieving [115,116]. Diverse studies have been published using natural and synthetic zeolites, including FAU, LTA and MFI, in terms of the ion-exchange isotherms and selectivity. These data were reviewed by Dyer in 2007 [116] and the main conclusions [105] are:

- Zeolites with higher Si/Al ratios (as MFI) work better with cations with low charge density (large and monovalent), while zeolites with lower Si/Al ratios (as FAU or LTA) are more adequate for cations with high charge density (small and multivalent).
- Cations with high level of hydration (as lithium, Li^{+}, or magnesium, Mg^{2+}) tend to have slow exchange kinetics.
- Other cations are usually preferred over transition metal cations depending on the exchanger material.

Some zeolite structures, including FAU and LTA, have been used to mitigate the effects of nuclear accidents and the presence of radioactive waste, more specifically, to remove radioactive cesium [105,116]. The usage of zeolites for water treatment may include processes other than ion exchange, such as filtration, surface precipitation or adsorption [117].

The industrial application of zeolites in catalysis was first envisioned by the Union Carbide zeolite research group in the 1950s [105]. The studies of Milton and Breck using a partially H^{+}-exchanged X zeolite for the cracking of hydrocarbons defined a much more active catalyst than the ones being used till then [118]. In the same year, they began developing new catalysts with metal dispersion on A, X and Y zeolites, resulting in some relevant patents [119,120]. These findings led to other studies conducted by other companies using zeolites for their potential use as catalysts. In 1959, Union Carbide commercialized the zeolite Y as an acid catalyst for isomerization and cracking processes [121,122]. These innovations led to the preferential usage of zeolite cracking catalysts instead of the old amorphous silica-alumina catalyst in every refinery [105]. Other applications were found for catalysts based on zeolites with MFI and FAU structures, such as:

- MFI: oil refining and petrochemistry interface (fluid catalytic cracking (FCC), dewaxing of lubricants, catalytic reforming of naphtha, catalytic cracking for propene production, aromatization of light paraffin and olefins); petrochemistry (xylene isomerization, toluene disproportionation-transalkylation, alkylation of toluene with methanol) [105].
- FAU: oil refining (FCC with FAU Y type catalysts with REE) [105].

The usage of zeolites as adsorbents comes from their microporosity and regular pore size [105]. Zeolites 3A, 4A, 5A from LTA structure and 13X from FAU are the ones with more adsorption evaluations and the ones mostly used in industrial separations, due to their physicochemical properties and relatively low production cost [105].

2.3. Sorption Processes

As previously seen, solutions for recycling the REE from e-waste or other solid sources are under study. However, what to do when leaching from an e-waste deposit contaminates water reservoirs? For this, the sorption process can be employed.

Sorption is defined by the physical-chemical processes through which one substance, called sorbate, is retained at the surface of another substance, called sorbent. Depending on the depth of the sorbate transference into the sorbent, sorption can be divided into adsorption (first atomic/molecular layers) and absorption (deeper in the surface layer). The term sorption is only used when there is indeterminacy in the specific process but acts as a global definition [123]. With the use of sorbents of biological origin, the term biosorption is also included in the sorption class.

Adsorption processes happen when there is a physical-chemical adherence or bonding of the sorbate, which can be ions or molecules, onto the sorbent surface [1,68,123,124]. This process has numerous vantages such as environment friendliness, wide-range availability of sorbents and competitive economics [1,68,123–125]. Specific parameters must be considered for the adsorption process when selecting the most suitable adsorbent [126]. The ideal adsorbent should be:

- Selective towards one or more components of the mixture to be treated.
- Present a large adsorption capacity.
- Easily regenerable.
- Durable and stable under relevant conditions.
- Shaped to achieve optimal mechanical and dynamical properties.
- Sustainable and competitive.

Unfortunately, finding an adsorbent that fulfills all the above characteristics for a given separation is quite challenging. Many separation processes require compromises to achieve the best overall performance.

Many conventional adsorbents such as activated carbon, make the adsorption process less competitive for extensive use in water treatment [127]. Using non-convention low-cost sorbents like agriculture wastes, makes this process more appealing as it becomes more competitive while reducing solid wastes [124]. Alongside activated carbon, zeolites are another class of adsorbents widely used in diverse applications, as described in section **2.2 Zeolites**.

Due to its versatility, adsorption is widely used in water treatment (removal of diverse pollutants as heavy metals [128–130] or micro-pollutants [131–133]), drying, hydrogen purification, air separation or hydrocarbon separation [134].

The desorption process is used when it is intended to reuse the sorbent for new cycles of sorption or to reuse it in new applications [124]. It is required to use eluents that remove the sorbate from the sorbent and this treatment may change the sorbate sorption capacity. The eluents used in desorption processes should be non-toxic, cause no damage to the sorbent, allow the sorbent reuse and enable a maximum sorbate recovery at the lowest possible eluent concentration and contact time [135–137].

The sequential association of the adsorption and the desorption processes will remove an element/ compound from wastewater and will allow its eventual reuse into a new application, reducing the ore mining and all associated problems and promoting the valorization of wastes within a circular economy perspective.

2.4. Catalysis

Catalysts are used in chemical reactions in order to accelerate those processes or to reduce their reaction temperatures. They do not appear in the stoichiometry equation of the reaction and they are not consumed by the reactional processes themselves. Catalysts interfere in reactions by reducing their activation energy (E_a) which is translated into a faster reaction. That change in the E_a increases the rates of both forward and reverse reactions likewise.

Catalytic reactions are intensively used in industrial processing. Most chemical processes (85 to 90 %) involve at least one catalytical step within food, health, fuels and energy processes [138]. Catalysis is divided into three major classes: heterogeneous, homogeneous and enzymatic catalysis. Heterogeneous catalysis is used in the production of fuels, of a variety of chemicals, in water treatment and mitigation of hazardous gaseous or liquid emissions into the environment [139–142]. This work will be focused on the design of catalysts prepared from REE supported on zeolites to be used in

heterogeneous processes as the catalysts are in solid state and the reactional environment will be in liquid phase.

With the growing concern about the environment and according to the green chemistry principles, the usage of catalysis is more and more justifiable, since it offers advantages such as higher reaction kinetics, higher selectivity and/or lower energy requirements [143–145]. These processes have improved efficiencies compared to homogeneous chemical processes, with reduced energy and material consumption and reduced environmental impact [146].

The heterogeneous catalysts have obtained increased attention from the chemical industry [147,148], mainly due to the high activity and selectivity resulting in more efficient processes from both economic and environmental points of view [149].

Environmental catalysis presents some specific aspects when compared to other catalytic processes [150]:

1. Developed technology able to operate efficiently at conditions defined by upstream units.
2. Different applications include refineries, chemical processes, treatment of emissions, and household or indoor applications.
3. Operation in smoother conditions than classical catalysts for chemical production, with efficient operation with various feeds and fast changes in feed composition.

2.4.1.Catalysts using zeolites and REE

Zeolites are another essential piece in the catalytic processes and have been mainly used in petroleum refining, in the case of FCC, in which significant improvements have been reached due to high activity for gasoline production, low coke and gas yields and good thermal and hydrothermal stabilities [151–153]. Zeolite Y which belongs to FAU is the active component for the cracking catalyst, which is modified to achieve higher stability and activity [151]. Usually, zeolite Y is submitted to an ion-exchange with rare earth salts followed by a calcination process, improving the stability of the zeolite and increasing the activity of the catalyst [151].

Many studies of zeolite Y containing REE were performed in recent years to assess the catalyst selectivity and stability, as Sousa-Aguiar et al. referred to in their review of the subject [151]. New applications were found for those catalysts such as converting hydrocarbon fractions of crude petroleum oils to more valuable products [154,155]. The presence of REE in the zeolite Y reduces the framework dealumination under hydrothermal conditions [152], which translates into increased activity and enhances the hydrogen transfer rate.

REE are used not only for FCC reactions but also in other industrial essential reactions such as hydrocarbon cracking, isomerization and alkylation [72,151,156].

The recovery of REE from wastewater using zeolite is possible, as supported by some literature [157]. After being recovered from wastewater, the REE supported on the zeolite may have two different fates. One is the leaching of the REE present inside the zeolite for further applications, which may define a secondary source of REE. Another fate is the application of these zeolites loaded with REE as heterogeneous catalyst in catalytical reactions. For the catalytical assessment of these zeolites loaded with REE, some reactions are considered valuable test reactions such as the transalkylation of ethylbenzene [156]. Dye degradation may also be used as reaction models, as they are easily evaluated as reported in literature [158].

The idea of removing metal from wastewater followed by a catalyst definition is already described in the literature [159,160]. One example is the work of Figueiredo *et al.* [159], who used chromium adsorbed on zeolite to catalyze oxidation reactions in mild conditions [161,162].

2.5. Machine Learning

Machine learning (ML) tools are an evolving branch of computational algorithms whose development led to statistical models that can make predictions and decisions without being explicitly programmed [163–166]. ML can integrate multimodality multi-fidelity data to reveal correlations between different features [167].

The learning process is divided into two steps: training and testing. In the training part, samples from the dataset are taken as input in which learning algorithms learn features, the designer is the learner, and the model is built [168]. In this part, both features and characteristics of the data, designed as x, and the target labels, designed as Y, are used in this process. This happens so the model can learn that the characteristics of the data, the *x*, will originate a particular response, *y*. In the testing process, the model predicts the test data [168]. The resulting data is the output of the learning model, which gives the final prediction or classified data [169]. In other words, the *x* values of the dataset are given to the model so it can process and give a prediction to those characteristics. The predicted *y* value is usually compared to the real y value, and the model can be evaluated from there.

ML can be organized into the following categories accordingly to the nature of the learning signal or feedback available to a learning system used [168,169]. The most common categories are supervised learning, unsupervised learning and reinforcement learning.

Supervised learning uses labelled data and provides a dataset consisting of features or characteristics and labels [168]. The tasks used in this approach are divided into two categories,

classification and regression, as shown in **Figure 2.6**. Classification is used with discrete labels, when the y values have fixed categorical outcomes, presented by whole numbers designed as integers. Regression is used with continuous labels, when the *y* values have floating point values, such as temperature or prices. Some application examples are predictive analytics (such as house prices and stock exchange prices), text recognition, spam detection, customer sentiment analysis and object detection (such as face detection).

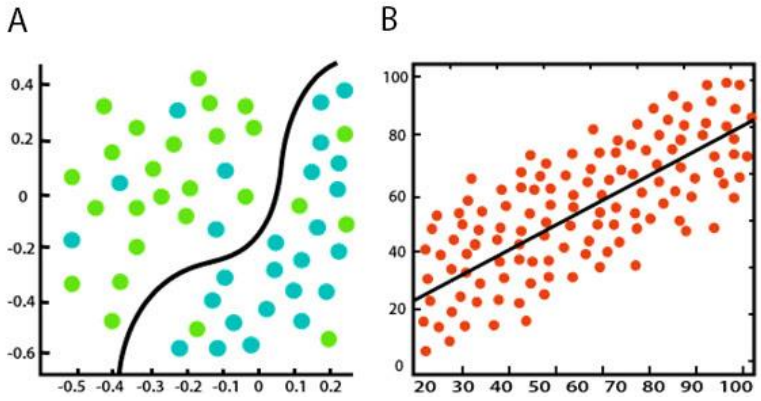

Figure 2.6: Representation of the main supervised ML techniques: **A)** Classification and **B)** Regression.

Unsupervised learning uses data with no labels and aims to explore the data and find similarities between them [168]. The idea is to make the model discover "hidden" labels within the data. Some application examples are anomaly detection, customer behavior prediction and recommendation engines.

The reinforcement learning technique interacts with a dynamic environment in which it must approach a certain goal without being explicitly told that it is close to its goal [168]. Here, the algorithm identifies which actions yield the most significant reward through trial and error. It is often used for robotics, gaming and navigation.

2.5.1.ML algorithms

An extensive set of ML algorithms are developed to build ML models and they can be classified based on the learning styles [168], as shown in **Figure 2.7**. The ones that will be used in this work are the following:

- Regression algorithms: related to modeling the relationships between variables that are continuous.
- Instance-based algorithms: based on a learning model, a decision problem with instances or examples of training data deemed essential or required by the model.
- Decision Tree algorithms: use a decision tree as a predictive model that maps observations about an item to conclude about its target value.

- Clustering algorithms: it is the classification method of objects into different groups.
- Dimensionality Reduction algorithms: aims to remove irrelevant and redundant data to reduce the computational cost and improve data quality for efficient data organization strategies.

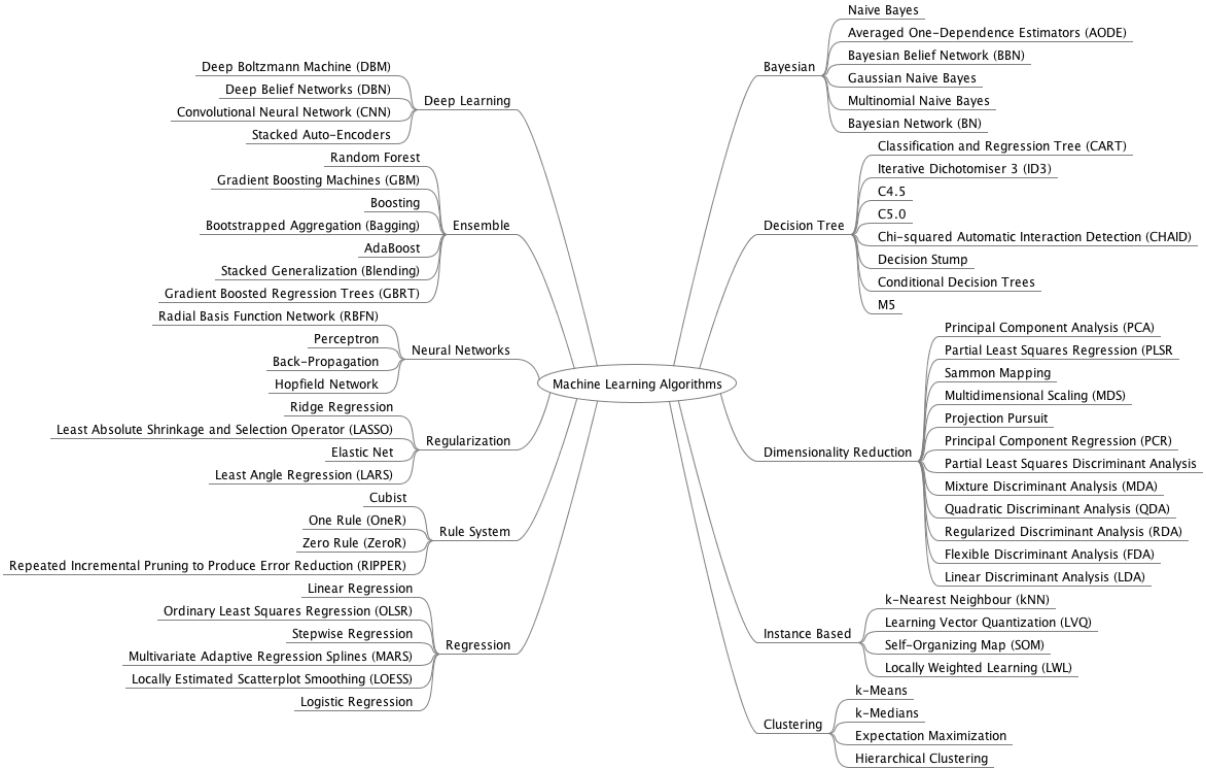

Figure 2.7: Representation of the classification of all ML algorithms (adapted from [170]).

2.5.2.ML applications

ML has been successfully applied in diverse fields such as pattern recognition, medicine, science, computer vision, spacecraft engineering, engineering, biomedicine, psychology, catalysis, neurobiology and many other disciplines [166,169,171]. This broad application allows a faster treatment of tremendous amounts of data since ML is able to analyze and correlate those data to achieve better interpretations and, therefore, to take better decisions.

ML models and their importance have been recognized and appreciated in wastewater treatment [172,173]. Some developments were achieved in ML algorithms or deep learning neural networks for the optimization of the adsorption of antibiotics [174,175], of organic compounds [176,177] and of metals [178–180].

The capacity of ML algorithms to evaluate large amounts of data from catalytic reactions and catalyst characterization can help to design the best catalyst for a given reaction [181,182]. Various homogeneous and heterogeneous catalytic applications have been using ML [183].

2.6. References

1. Anastopoulos, I.; Bhatnagar, A.; Lima, E.C. Adsorption of rare earth metals: A review of recent literature. *J. Mol. Liq.* **2016**, *221*, 954–962.
2. Moldoveanu, G.A.; Papangelakis, V.G. Recovery of rare earth elements adsorbed on clay minerals: I. Desorption mechanism. *Hydrometallurgy* **2012**, *117–118*, 71–78.
3. Voncken, J.H.L. Physical and Chemical Properties of the Rare Earths. In *The Rare Earth Elements - An Introduction*; Springer, Cham, 2016; pp. 53–72 ISBN 978-3-319-26809-5.
4. Xiao, Y.; Huang, L.; Long, Z.; Feng, Z.; Wang, L. Adsorption ability of rare earth elements on clay minerals and its practical performance. *J. Rare Earths* **2016**.
5. CHEN, Z. Global rare earth resources and scenarios of future rare earth industry. *J. Rare Earths* **2011**, *29*, 1–6.
6. Gupta, C.K.; Krishnamurthy, N. *Extractive Metallurgy of Rare Earths*; Taylor & Francis: Abingdon, UK, 2004; ISBN 978-0-203-68517-4.
7. Ganguli, R.; Cook, D.R. Rare earths: A review of the landscape. *MRS Energy Sustain.* **2018**, *5*, 6.
8. Samudrala, G.K.; Vohra, Y.K. Structural Properties of Lanthanides at Ultra High Pressure. In *Including Actinides*; Bünzli, J.-C.G., Pecharsky, V.K.B.T.-H. on the P. and C. of R.E., Eds.; Elsevier, 2013; Vol. 43, pp. 275–319 ISBN 0168-1273.
9. Lambert, C.E.; Ledrich, M.-L. Lanthanide Series of Metals. In *Encyclopedia of Toxicology*; Wexler, P.B.T.-E. of T. (Third E., Ed.; Elsevier: Oxford, 2014; pp. 43–47 ISBN 978-0-12-386455-0.
10. Zhang, J.; Liu, Q.; He, Q.; Nozaki, Y. Rare Earth Elements and Their Isotopes in the Ocean. In *Encyclopedia of Ocean Sciences*; Cochran, J.K., Bokuniewicz, H.J., Yager, P.L.B.T.-E. of O.S. (Third E., Eds.; Elsevier: Oxford, 2019; pp. 181–197 ISBN 978-0-12-813082-7.
11. Barrett, S.D.; Dhesi, S.S. *The Structure of Rare-Earth Metal Surfaces*; PUBLISHED BY IMPERIAL COLLEGE PRESS AND DISTRIBUTED BY WORLD SCIENTIFIC PUBLISHING CO., 2001; ISBN 978-1-86094-165-8.
12. Choppin, G.R.; Rizkalla, E.N. Chapter 128 Solution chemistry of actinides and lanthanides. In *Handbook on the Physics and Chemistry of Rare Earths*; 1994; pp. 559–590.
13. Han, K.N. Characteristics of Precipitation of Rare Earth Elements with Various Precipitants. *Minerals* **2020**, *10*, 178.
14. de Vasconcellos, M.E.; da Rocha, S.M.R.; Pedreira, W.R.; Queiroz, C.A. da S.; Abrão, A. Solubility behavior of rare earths with ammonium carbonate and ammonium carbonate plus ammonium hydroxide: Precipitation of their peroxicarbonates. *J. Alloys Compd.* **2008**, *451*, 426–428.
15. Kim, P.; Anderko, A.; Navrotsky, A.; Riman, R.E. Trends in Structure and Thermodynamic Properties of Normal Rare Earth Carbonates and Rare Earth Hydroxycarbonates. *Minerals* 2018, *8*.
16. Tokunaga, S.; Haron, M.J.; Wasay, S.A.; Wong, K.F.; Laosangthum, K.; Uchiumi, A. Removal of fluoride ions from aqueous solutions by multivalent metal compounds. *Int. J. Environ. Stud.* **1995**, *48*, 17–28.
17. Yan, C.; Jia, J.; Liao, C.; Wu, S.; Xu, G. Rare Earth Separation in China. *Tsinghua Sci. Technol.* **2006**, *11*, 241–247.
18. Wu, S.; Zhao, L.; Wang, L.; Huang, X.; Zhang, Y.; Feng, Z.; Cui, D. Simultaneous recovery of rare earth elements and phosphorus from phosphate rock by phosphoric acid leaching and selective precipitation: Towards green process. *J. Rare Earths* **2019**, *37*, 652–658.
19. Zakharova, B.; Komissarova, L.; Traskin, V.; Naumov, S.; Melnikov, P. Precipitation of Rare Earth Phosphates from H3PO4 Solutions. *Phosphorus. Sulfur. Silicon Relat. Elem.* **1996**, *111*, 2.
20. Moeller, T.; Kremers, H.E. Observations on Rare Earths Double Sodium Sulfate Precipitation for Separation of the Terbium and Yttrium Earths. *Ind. Eng. Chem. Anal. Ed.* **1945**, *17*, 44–45.

21. Vijayalakshmi, R.; Mishra, S.L.; Singh, H.; Gupta, C.K. Processing of xenotime concentrate by sulphuric acid digestion and selective thorium precipitation for separation of rare earths. *Hydrometallurgy* **2001**, *61*, 75–80.
22. Han, K.N. Effect of Anions on the Solubility of Rare Earth Element-Bearing Minerals in Acids. *Mining, Metall. Explor.* **2019**, *36*, 215–225.
23. Han, K.N. Effect of Metal Complexation on the Solubility of Rare Earth Compounds. In *Critical and Rare Earth Elements*; CRC Press, 2019; pp. 59–84 ISBN 9780429023545.
24. Ciro, E.; Alzate, A.; López, E.; Serna, C.; Gonzalez, O. Neodymium recovery from scrap magnet using ammonium persulfate. *Hydrometallurgy* **2019**, *186*, 226–234.
25. Gupta, C.K.; Krishnamurthy, N. Extractive metallurgy of rare earths. *Int. Mater. Rev.* **1992**, *37*, 197–248.
26. Chi, R.; Xu, Z. A solution chemistry approach to the study of rare earth element precipitation by oxalic acid. *Metall. Mater. Trans. B* **1999**, *30*, 189–195.
27. Khawassek, Y.M.; Eliwa, A.A.; Gawad, E.A.; Abdo, S.M. Recovery of rare earth elements from El-Sela effluent solutions. *J. Radiat. Res. Appl. Sci.* **2015**, *8*, 583–589.
28. He, L.; Xu, Q.; Li, W.; Dong, Q.; Sun, W. One-step separation and recovery of rare earth and iron from NdFeB slurry via phosphoric acid leaching. *J. Rare Earths* **2022**, *40*, 338–344.
29. Balaram, V. Rare earth elements: A review of applications, occurrence, exploration, analysis, recycling, and environmental impact. *Geosci. Front.* **2019**, *10*, 1285–1303.
30. Dostal, J. Rare Earth Element Deposits of Alkaline Igneous Rocks. *Resources* 2017, *6*.
31. King, H. REE - Rare Earth Elements - Metals, Minerals, Mining, Uses Available online: https://geology.com/articles/rare-earth-elements/ (accessed on Apr 27, 2020).
32. Gholz, E. Rare Earth Elements and National Security. *Energy Rep.* **2014**, 1–20.
33. King, H. *REE - Rare Earth Elements - Metals, Minerals, Mining, Uses*; 2016;
34. Habashi, F. The recovery of the lanthanides from phosphate rock. *J. Chem. Technol. Biotechnol. Chem. Technol.* **1985**, *35*, 5–14.
35. Preston, J.S.; Cole, P.M.; Craig, W.M.; Feather, A.M. The recovery of rare earth oxides from a phosphoric acid by-product. Part 1: Leaching of rare earth values and recovery of a mixed rare earth oxide by solvent extraction. *Hydrometallurgy* **1996**.
36. Ihlen, P.M.; Schiellerup, H.; Gautneb, H.; Skår, Ø. Characterization of apatite resources in Norway and their REE potential - A review. *Ore Geol. Rev.* 2014.
37. U.S. Geological Survey *Mineral Commodity Summaries*; 2019; Vol. 3;.
38. Emsbo, P.; McLaughlin, P.I.; Breit, G.N.; du Bray, E.A.; Koenig, A.E. Rare earth elements in sedimentary phosphate deposits: Solution to the global REE crisis? *Gondwana Res.* 2015.
39. Liu, S.-L.; Fan, H.-R.; Liu, X.; Meng, J.; Butcher, A.R.; Yann, L.; Yang, K.-F.; Li, X.-C. Global rare earth elements projects: New developments and supply chains. *Ore Geol. Rev.* **2023**, *157*, 105428.
40. Gschneidner Jr., K.A. *The rare earth crisis – the supply/demand situation for 2010-2015*; 2011; Vol. 6;.
41. Voncken, J.H.L. *The Rare Earth Elements*; SpringerBriefs in Earth Sciences; Springer International Publishing: Cham, 2016; Vol. 53; ISBN 978-3-319-26807-1.
42. U.S. Geological Survey *Mineral commodity summaries 2023*; 2023;
43. IMARC Group *Rare Earth Elements Market Share, Size & Forecast 2028* |;
44. Supply and Demand - Arafura Available online: https://www.arultd.com/products/supply-and-demand/ (accessed on Aug 8, 2023).
45. Khan, A.M.; Bakar, N.K.A.; Bakar, A.F.A.; Ashraf, M.A. Chemical speciation and bioavailability of rare earth elements (REEs) in the ecosystem: a review. *Environ. Sci. Pollut. Res.* **2017**, *24*, 22764–22789.

46. Yin, X.; Martineau, C.; Demers, I.; Basiliko, N.; Fenton, N.J. The potential environmental risks associated with the development of rare earth element production in Canada. *Environ. Rev.* **2021**, *29*, 354–377.
47. Cardoso, C.E.D.; Almeida, J.C.; Lopes, C.B.; Trindade, T.; Vale, C.; Pereira, E. Recovery of rare earth elements by carbon-based nanomaterials—a review. *Nanomaterials* 2019.
48. Gwenzi, W.; Mangori, L.; Danha, C.; Chaukura, N.; Dunjana, N.; Sanganyado, E. Sources, behaviour, and environmental and human health risks of high-technology rare earth elements as emerging contaminants. *Sci. Total Environ.* **2018**, *636*, 299–313.
49. Ma, L.; Dang, D.H.; Wang, W.; Evans, R.D.; Wang, W.-X. Rare earth elements in the Pearl River Delta of China: Potential impacts of the REE industry on water, suspended particles and oysters. *Environ. Pollut.* **2019**, *244*, 190–201.
50. Talens Peiró, L.; Villalba Méndez, G. Material and Energy Requirement for Rare Earth Production. *JOM* **2013**, *65*, 1327–1340.
51. Oladipo, H.J.; Tajudeen, Y.A.; Taiwo, E.O.; Muili, A.O.; Yusuf, R.O.; Jimoh, S.A.; Oladipo, M.K.; Oladunjoye, I.O.; Egbewande, O.M.; Sodiq, Y.I.; et al. Global Environmental Health Impacts of Rare Earth Metals: Insights for Research and Policy Making in Africa. *Challenges* **2023**, *14*, 20.
52. Binnemans, K.; Jones, P.T.; Blanpain, B.; Van Gerven, T.; Pontikes, Y. Towards zero-waste valorisation of rare-earth-containing industrial process residues: a critical review. *J. Clean. Prod.* **2015**, *99*, 17–38.
53. Kato, Y.; Fujinaga, K.; Nakamura, K.; Takaya, Y.; Kitamura, K.; Ohta, J.; Toda, R.; Nakashima, T.; Iwamori, H. Deep-sea mud in the Pacific Ocean as a potential resource for rare-earth elements. *Nat. Geosci.* **2011**, *4*, 535–539.
54. Takaya, Y.; Yasukawa, K.; Kawasaki, T.; Fujinaga, K.; Ohta, J.; Usui, Y.; Nakamura, K.; Kimura, J.-I.; Chang, Q.; Hamada, M.; et al. The tremendous potential of deep-sea mud as a source of rare-earth elements. *Sci. Rep.* **2018**, *8*, 5763.
55. Ohta, J.; Yasukawa, K.; Nakamura, K.; Fujinaga, K.; Iijima, K.; Kato, Y. Geological features and resource potential of deep-sea mud highly enriched in rare-earth elements in the Central Pacific Basin and the Penrhyn Basin. *Ore Geol. Rev.* **2021**, *139*, 104440.
56. Wang, Z.; Xu, G.; Lin, R.; Wang, H.; Ren, J. Energy performance contracting, risk factors, and policy implications: Identification and analysis of risks based on the best-worst network method. *Energy* **2019**, *170*, 1–13.
57. Zhang, W.; Noble, A.; Yang, X.; Honaker, R. A Comprehensive Review of Rare Earth Elements Recovery from Coal-Related Materials. *Minerals* **2020**, *10*, 451.
58. Huang, Z.; Fan, M.; Tian, H. Rare earth elements of fly ash from Wyoming's Powder River Basin coal. *J. Rare Earths* **2020**, *38*, 219–226.
59. Wang, Z.; Dai, S.; Zou, J.; French, D.; Graham, I.T. Rare earth elements and yttrium in coal ash from the Luzhou power plant in Sichuan, Southwest China: Concentration, characterization and optimized extraction. *Int. J. Coal Geol.* **2019**, *203*, 1–14.
60. Dai, S.; Finkelman, R.B. Coal as a promising source of critical elements: Progress and future prospects. *Int. J. Coal Geol.* **2018**, *186*, 155–164.
61. Dai, S.; Yan, X.; Ward, C.R.; Hower, J.C.; Zhao, L.; Wang, X.; Zhao, L.; Ren, D.; Finkelman, R.B. Valuable elements in Chinese coals: a review. *Int. Geol. Rev.* **2018**, *60*, 590–620.
62. Luttrell, G.H.; Kiser, M.J.; Yoon, R.-H.; Noble, A.; Rezaee, M.; Bhagavatula, A.; Honaker, R.Q. A Field Survey of Rare Earth Element Concentrations in Process Streams Produced by Coal Preparation Plants in the Eastern USA. *Mining, Metall. Explor.* **2019**, *36*, 889–902.
63. Zhang, W.; Honaker, R. Characterization and recovery of rare earth elements and other critical metals (Co, Cr, Li, Mn, Sr, and V) from the calcination products of a coal refuse sample. *Fuel* **2020**, *267*, 117236.

64. Zhang, W.; Honaker, R. Calcination pretreatment effects on acid leaching characteristics of rare earth elements from middlings and coarse refuse material associated with a bituminous coal source. *Fuel* **2019**, *249*, 130–145.
65. Ji, B.; Li, Q.; Zhang, W. Leaching recovery of rare earth elements from the calcination product of a coal coarse refuse using organic acids. *J. Rare Earths* **2022**, *40*, 318–327.
66. Commission, E.; Directorate-General for Internal Market Entrepreneurship and SMEs, I.; Grohol, M.; Veeh, C. *Study on the critical raw materials for the EU 2023 : final report*; Publications Office of the European Union, 2023;
67. Burton, J. U.S. Geological Survey Releases 2022 List of Critical Minerals Available online: https://www.usgs.gov/news/national-news-release/us-geological-survey-releases-2022-list-critical-minerals (accessed on Aug 4, 2023).
68. Zhao, F.; Repo, E.; Meng, Y.; Wang, X.; Yin, D.; Sillanpää, M. An EDTA-β-cyclodextrin material for the adsorption of rare earth elements and its application in preconcentration of rare earth elements in seawater. *J. Colloid Interface Sci.* **2016**, *465*, 215–224.
69. Rostami, I.; Rezvani, H.; Hu, Z.; Shahmoradian, S.H. Breakthroughs in medicine and bioimaging with up-conversion nanoparticles. *Int. J. Nanomedicine* **2019**, *14*, 7759–7780.
70. Evans, C.H. Medical Uses of the Rare Earths. In *Episodes from the History of the Rare Earth Elements*; Springer Netherlands: Dordrecht, 1996; pp. 205–228.
71. Giese, E. Rare Earth Elements: therapeutic and diagnostic applications in modern medicine. *Clin. Med. Reports* **2018**, *2*.
72. Binnemans, K.; Jones, P.T.; Blanpain, B.; Van Gerven, T.; Yang, Y.; Walton, A.; Buchert, M. Recycling of rare earths: a critical review. *J. Clean. Prod.* **2013**, *51*, 1–22.
73. Statista REE share of consumption worldwide by end use 2021 Available online: https://www.statista.com/statistics/604190/distribution-of-rare-earth-element-consumption-worldwide-by-end-use/ (accessed on Aug 9, 2023).
74. Bonfante, M.C.; Raspini, J.P.; Fernandes, I.B.; Fernandes, S.; Campos, L.M.S.; Alarcon, O.E. Achieving Sustainable Development Goals in rare earth magnets production: A review on state of the art and SWOT analysis. *Renew. Sustain. Energy Rev.* **2021**, *137*, 110616.
75. Yang, Y.; Walton, A.; Sheridan, R.; Güth, K.; Gauß, R.; Gutfleisch, O.; Buchert, M.; Steenari, B.-M.; Van Gerven, T.; Jones, P.T.; et al. REE Recovery from End-of-Life NdFeB Permanent Magnet Scrap: A Critical Review. *J. Sustain. Metall.* **2017**, *3*, 122–149.
76. Eggert, R.; Wadia, C.; Anderson, C.; Bauer, D.; Fields, F.; Meinert, L.; Taylor, P. Rare Earths: Market Disruption, Innovation, and Global Supply Chains. *Annu. Rev. Environ. Resour.* **2016**, *41*, 199–222.
77. Tan, Q.; Li, J.; Zeng, X. Rare Earth Elements Recovery from Waste Fluorescent Lamps: A Review. *Crit. Rev. Environ. Sci. Technol.* **2015**, *45*, 749–776.
78. Fujita, Y.; McCall, S.K.; Ginosar, D. Recycling rare earths: Perspectives and recent advances. *MRS Bull.* **2022**, *47*, 283–288.
79. El Ouardi, Y.; Virolainen, S.; Massima Mouele, E.S.; Laatikainen, M.; Repo, E.; Laatikainen, K. The recent progress of ion exchange for the separation of rare earths from secondary resources – A review. *Hydrometallurgy* **2023**, *218*, 106047.
80. Machacek, E.; Richter, J.L.; Habib, K.; Klossek, P. Recycling of rare earths from fluorescent lamps: Value analysis of closing-the-loop under demand and supply uncertainties. *Resour. Conserv. Recycl.* **2015**, *104*, 76–93.
81. Niskanen, J.; Lahtinen, M.; Perämäki, S. Acetic acid leaching of neodymium magnets and iron separation by simple oxidative precipitation. *Clean. Eng. Technol.* **2022**, *10*, 100544.
82. Pietrantonio, M.; Pucciarmati, S.; Sebastianelli, L.; Forte, F.; Fontana, D. Materials recovery from end-of-life wind turbine magnets. *Int. J. Environ. Sci. Technol.* **2022**, *19*, 8019–8026.

83. Kumari, A.; Sinha, M.K.; Pramanik, S.; Sahu, S.K. Recovery of rare earths from spent NdFeB magnets of wind turbine: Leaching and kinetic aspects. *Waste Manag.* **2018**, *75*, 486–498.
84. Kumar Parhi, P.; Kumari Misra, P.; Kumar Jyothi, R. Integrated hydrometallurgical investigation for extraction and recovery of neodymium (Nd) from waste permanent Nd-Fe-B magnet. *Inorg. Chem. Commun.* **2023**, *148*, 110251.
85. Gutiérrez-Gutiérrez, S.C.; Coulon, F.; Jiang, Y.; Wagland, S. Rare earth elements and critical metal content of extracted landfilled material and potential recovery opportunities. *Waste Manag.* **2015**, *42*, 128–136.
86. Royen, H.; Fortkamp, U. *Rare Earth Elements - Purification, Separation and Recycling*; 2016; ISBN 9789188319128.
87. Işıldar, A.; Rene, E.R.; van Hullebusch, E.D.; Lens, P.N.L. Electronic waste as a secondary source of critical metals: Management and recovery technologies. *Resour. Conserv. Recycl.* **2018**, *135*, 296–312.
88. Akcil, A.; Erust, C.; Gahan, C.S.; Ozgun, M.; Sahin, M.; Tuncuk, A. Precious metal recovery from waste printed circuit boards using cyanide and non-cyanide lixiviants – A review. *Waste Manag.* **2015**, *45*, 258–271.
89. Kaya, M. Recovery of metals and nonmetals from electronic waste by physical and chemical recycling processes. *Waste Manag.* **2016**, *57*, 64–90.
90. Baldé, C.P.; Forti, V.; Gray, V.; Kuehr, R.; Stegmann, P. *The Global E-waste Monitor 2017*; 2017; ISBN 9789280890532.
91. Tsamis, A.; Coyne, M. *Recovery of Rare Earths from Electronic wastes: An opportunity for High-Tech SMEs*; 2015;
92. European Commision *Report on Critical Raw Materials for the EU*; 2014;
93. Zhang, Y.; Liu, S.; Xie, H.; Zeng, X.; Li, J. Current Status on Leaching Precious Metals from Waste Printed Circuit Boards. *Procedia Environ. Sci.* **2012**, *16*, 560–568.
94. Friege, H. Review of material recovery from used electric and electronic equipment-alternative options for resource conservation. *Waste Manag. Res. J. a Sustain. Circ. Econ.* **2012**, *30*, 3–16.
95. Jones, P.T.; Geysen, D.; Tielemans, Y.; Van Passel, S.; Pontikes, Y.; Blanpain, B.; Quaghebeur, M.; Hoekstra, N. Enhanced Landfill Mining in view of multiple resource recovery: a critical review. *J. Clean. Prod.* **2013**, *55*, 45–55.
96. Ongondo, F.O.; Williams, I.D.; Whitlock, G. Distinct Urban Mines: Exploiting secondary resources in unique anthropogenic spaces. *Waste Manag.* **2015**, *45*, 4–9.
97. Johansson, N.; Krook, J.; Eklund, M.; Berglund, B. An integrated review of concepts and initiatives for mining the technosphere: towards a new taxonomy. *J. Clean. Prod.* **2013**, *55*, 35–44.
98. Jowitt, S.M.; Werner, T.T.; Weng, Z.; Mudd, G.M. Recycling of the rare earth elements. *Curr. Opin. Green Sustain. Chem.* **2018**, *13*, 1–7.
99. Li, J.; He, X.; Zeng, X. Designing and examining e-waste recycling process: methodology and case studies. *Environ. Technol.* **2017**, *38*, 652–660.
100. Tan, Q.; Deng, C.; Li, J. Innovative Application of Mechanical Activation for Rare Earth Elements Recovering: Process Optimization and Mechanism Exploration. *Sci. Rep.* **2016**, *6*, 19961.
101. Jones, P.T.; Van Gerven, T.; Van Acker, K.; Geysen, D.; Binnemans, K.; Fransaer, J.; Blanpain, B.; Mishra, B.; Apelian, D. CR3: Cornerstone to the sustainable inorganic materials management (SIM2) research program at K.U.Leuven. *JOM* **2011**, *63*, 14–15.
102. Reid, S.; Tam, J.; Yang, M.; Azimi, G. Technospheric Mining of Rare Earth Elements from Bauxite Residue (Red Mud): Process Optimization, Kinetic Investigation, and Microwave Pretreatment. *Sci. Rep.* **2017**, *7*, 15252.
103. Bian, Y.; Guo, S.; Jiang, L.; Liu, J.; Tang, K.; Ding, W. Recovery of Rare Earth Elements from NdFeB Magnet by VIM-HMS Method. *ACS Sustain. Chem. Eng.* **2016**, *4*, 810–818.

104. Rombach, E.; Friedrich, B. Chapter 10 - Recycling of Rare Metals. In *Handbook of Recycling*; Elsevier, 2014; pp. 125–150 ISBN 9780123964595.
105. Pérez-Botella, E.; Valencia, S.; Rey, F. Zeolites in Adsorption Processes: State of the Art and Future Prospects. *Chem. Rev.* **2022**, *122*, 17647–17695.
106. Laurino, C.; Palmieri, B. Zeolite: "the magic stone"; main nutritional, environmental, experimental and clinical fields of application. *Nutr. Hosp.* **2015**, *32*, 573–81.
107. Hammond, C.; Padovan, D.; Tarantino, G. Porous metallosilicates for heterogeneous, liquid-phase catalysis: perspectives and pertaining challenges. *R. Soc. Open Sci.* **2018**, *5*, 171315.
108. Silva, B.; Figueiredo, H.; Quintelas, C.; Neves, I.C.; Tavares, T. Zeolites as supports for the biorecovery of hexavalent and trivalent chromium. *Microporous Mesoporous Mater.* **2008**, *116*, 555–560.
109. Vaca Mier, M.; López Callejas, R.; Gehr, R.; Jiménez Cisneros, B.E.; Alvarez, P.J.J. Heavy metal removal with mexican clinoptilolite: multi-component ionic exchange. *Water Res.* **2001**, *35*, 373–378.
110. Kulprathipanja, S. *Zeolites in Industrial Separation and Catalysis*; Kulprathipanja, S., Ed.; Wiley, 2010; ISBN 9783527325054.
111. Breck DW *Zeolite molecular sieves, chemistry, and use,*; Wiley, 1974; ISBN 978-0-471-09985-7.
112. McCusker, L.B.; Liebau, F.; Engelhardt, G. Nomenclature of structural and compositional characteristics of ordered microporous and mesoporous materials with inorganic hosts(IUPAC Recommendations 2001). *Pure Appl. Chem.* **2001**, *73*, 381–394.
113. Flanigen, E.M. Molecular sieve zeolite technology - the first twenty-five years. *Pure Appl. Chem.* **1980**, *52*, 2191–2211.
114. Flanigen, E.M.; Broach, R.W.; Wilson, S.T. Chapter 1: Introduction. In *Zeolites in Industrial Separation and Catalysis*; Wiley-VCH Verlag GmbH & Co. KGaA: Weinheim, Germany, 2010; pp. 1–26 ISBN 9783527325054.
115. Townsend, R.P.; Coker, E.N. Chapter 11: Ion exchange in zeolites. In *Introduction to Zeolite Science and Practice*; van Bekkum, H., Flanigen, E.M., Jacobs, P.A., Jansen, J.C.B.T.-S. in S.S. and C., Eds.; Elsevier, 2001; Vol. 137, pp. 467–524 ISBN 0167-2991.
116. Dyer, A. Chapter 16: Ion-Exchange Properties of Zeolites and Related Materials. In *Introduction to Zeolite Science and Practice*; Čejka, J., van Bekkum, H., Corma, A., Schüth, F.B.T.-S. in S.S. and C., Eds.; Elsevier, 2007; Vol. 168, pp. 525–553 ISBN 0167-2991.
117. Inglezakis, V.J. The concept of "capacity" in zeolite ion-exchange systems. *J. Colloid Interface Sci.* **2005**, *281*, 68–79.
118. Milton, R.M. Chapter 1: Molecular Sieve Science and Technology. In *Zeolite Synthesis*; Occelli, M.L., Robson, H.E., Eds.; American Chemical Society (ACS), 1989; pp. 1–10.
119. Breck, D.W.; Milton, R.M. Cadmium-loaded molecular sieve 1961.
120. Breck, D.W.; Milton, R.. Metal Loading of Molecular Sieves 1961.
121. Rabo, J.A.; Pickert, P.E.; Boyle, J.E. Hydrocarbon Conversion Process with the Use of a Y Type Crystalline Zeolite 1966.
122. Rabo, J.A.; Pickert, P.E.; Boyle, J.E. Hydrocarbon Conversion Catalysts 1968.
123. Gadd, G.M. Biosorption: critical review of scientific rationale, environmental importance and significance for pollution treatment. *J. Chem. Technol. Biotechnol.* **2009**, *84*, 13–28.
124. Costa, F.; Lago, A.; Barros, Ó.; Rocha, V.; Vipotnik, Z.; Silva, B.; Tavares, T. Retention of organic micro-pollutants by sorption processes. In *Current Developments in Biotechnology and Bioengineering*; Elsevier, 2020; pp. 331–362.
125. Tareq, R.; Akter, N.; Azam, M.S. Biochars and Biochar Composites. In *Biochar from Biomass and Waste*; Elsevier, 2019; pp. 169–209.
126. Yang, R.T. *Adsorbents: Fundamentals and Applications*; Wiley, 2003; ISBN 9780471297413.

127. Ata, A.; Nalcaci, O.O.; Ovez, B. Macro algae Gracilaria verrucosa as a biosorbent: A study of sorption mechanisms. *Algal Res.* **2012**, *1*, 194–204.
128. Lee, S.-Y.; Choi, H.-J. Persimmon leaf bio-waste for adsorptive removal of heavy metals from aqueous solution. *J. Environ. Manage.* **2018**, *209*, 382–392.
129. Nguyen, T.C.; Loganathan, P.; Nguyen, T.V.; Kandasamy, J.; Naidu, R.; Vigneswaran, S. Adsorptive removal of five heavy metals from water using blast furnace slag and fly ash. *Environ. Sci. Pollut. Res.* **2018**, *25*, 20430–20438.
130. Burakov, A.E.; Galunin, E. V; Burakova, I. V; Kucherova, A.E.; Agarwal, S.; Tkachev, A.G.; Gupta, V.K. Adsorption of heavy metals on conventional and nanostructured materials for wastewater treatment purposes: A review. *Ecotoxicol. Environ. Saf.* **2018**, *148*, 702–712.
131. Djilani, C.; Zaghdoudi, R.; Modarressi, A.; Rogalski, M.; Djazi, F.; Lallam, A. Elimination of organic micropollutants by adsorption on activated carbon prepared from agricultural waste. *Chem. Eng. J.* **2012**, *189–190*, 203–212.
132. Mailler, R.; Gasperi, J.; Coquet, Y.; Derome, C.; Buleté, A.; Vulliet, E.; Bressy, A.; Varrault, G.; Chebbo, G.; Rocher, V. Removal of emerging micropollutants from wastewater by activated carbon adsorption: Experimental study of different activated carbons and factors influencing the adsorption of micropollutants in wastewater. *J. Environ. Chem. Eng.* **2016**, *4*, 1102–1109.
133. Kim, E.; Jung, C.; Han, J.; Her, N.; Min Park, C.; Son, A.; Yoon, Y. Adsorption of selected micropollutants on powdered activated carbon and biochar in the presence of kaolinite. *Desalin. Water Treat.* **2016**, *57*, 1–13.
134. Henley, E.J.; Seader, J.D.; Keith Roper, D. *Separation process principles, 3rd Edition*; 2011; ISBN 9780470646113.
135. Das, N. Recovery of precious metals through biosorption — A review. *Hydrometallurgy* **2010**, *103*, 180–189.
136. Akpomie, K.G.; Dawodu, F.A.; Adebowale, K.O. Mechanism on the sorption of heavy metals from binary-solution by a low cost montmorillonite and its desorption potential. *Alexandria Eng. J.* **2015**, *54*, 757–767.
137. Wilhelm, B.S.; Duncan, J.R. Reusability of immobilised Saccharomyces cerevisiae with successive copper adsorption-desorption cycles. *Biotechnol. Lett.* **1996**, *18*, 531–536.
138. Rodríguez-Padrón, D.; Puente-Santiago, A.R.; Balu, A.M.; Muñoz-Batista, M.J.; Luque, R. Environmental Catalysis: Present and Future. *ChemCatChem* **2019**, *11*, 18–38.
139. Melián-Cabrera, I. Catalytic Materials: Concepts to Understand the Pathway to Implementation. *Ind. Eng. Chem. Res.* **2021**, *60*, 18545–18559.
140. Bartholomew, C.H.; Farrauto, R.J. *Fundamentals of Industrial Catalytic Processes*; Wiley, 2005; ISBN 9780471457138.
141. Moulijin, J.A.; Makkee, M.; van Diepen, A.E. *Chemical process technology*; 2013; Vol. 51; ISBN 978-1-444-32025-1.
142. Hagen, J. *Industrial Catalysis*; Wiley, 2015; ISBN 9783527331659.
143. Polshettiwar, V.; Varma, R.S. Green chemistry by nano-catalysis. *Green Chem.* **2010**, *12*, 743.
144. Centi, G.; Perathoner, S. Catalysis and sustainable (green) chemistry. *Catal. Today* **2003**, *77*, 287–297.
145. Anastas, P.T.; Kirchhoff, M.M.; Williamson, T.C. Catalysis as a foundational pillar of green chemistry. *Appl. Catal. A Gen.* **2001**, *221*, 3–13.
146. Védrine, J.C. Chapter 9: Concluding remarks and challenges of heterogeneous catalysis on metal oxides. In *Metal Oxides in Heterogeneous Catalysis*; Elsevier, 2018; pp. 551–569 ISBN 9780128116319.
147. Kalz, K.F.; Kraehnert, R.; Dvoyashkin, M.; Dittmeyer, R.; Gläser, R.; Krewer, U.; Reuter, K.; Grunwaldt, J.-D. Future Challenges in Heterogeneous Catalysis: Understanding Catalysts under

Dynamic Reaction Conditions. *ChemCatChem* **2017**, *9*, 17–29.
148. Fechete, I.; Wang, Y.; Védrine, J.C. The past, present and future of heterogeneous catalysis. *Catal. Today* **2012**, *189*, 2–27.
149. Descorme, C.; Gallezot, P.; Geantet, C.; George, C. Heterogeneous Catalysis: A Key Tool toward Sustainability. *ChemCatChem* **2012**, *4*, 1897–1906.
150. Centi, G.; Ciambelli, P.; Perathoner, S.; Russo, P. Environmental catalysis: trends and outlook. *Catal. Today* **2002**, *75*, 3–15.
151. Sousa-Aguiar, E.F.; Trigueiro, F.E.; Zotin, F.M.Z. The role of rare earth elements in zeolites and cracking catalysts. *Catal. Today* **2013**, *218–219*, 115–122.
152. Woltermann, G.M.; Magee, J.S.; Griffith, S.D. Chapter 4: Commercial Preparation and Characterization of FCC Catalysts. In *Studies in Surface Science and Catalysis*; Elsevier, 1993; Vol. 76, pp. 105–144 ISBN 9780444890375.
153. Scherzer, J. Chapter 5: Correlation Between Catalyst Formulation and Catalytic Properties. In *Studies in Surface Science and Catalysis*; Elsevier, 1993; Vol. 76, pp. 145–182 ISBN 9780444890375.
154. Malleswara Rao, T.V.; Dupain, X.; Makkee, M. Fluid catalytic cracking: Processing opportunities for Fischer–Tropsch waxes and vegetable oils to produce transportation fuels and light olefins. *Microporous Mesoporous Mater.* **2012**, *164*, 148–163.
155. Mante, O.D.; Agblevor, F.A.; Oyama, S.T.; McClung, R. The effect of hydrothermal treatment of FCC catalysts and ZSM-5 additives in catalytic conversion of biomass. *Appl. Catal. A Gen.* **2012**, *445–446*, 312–320.
156. Thomas, B.; Sugunan, S. Effect of rare earth metal ions on the structural and textural properties of NaFAU-Y zeolite and vapour phase alkylation of benzene with 1-octene. *Indian J. Chem. Technol.* **2005**, *12*, 676–688.
157. Barros, Ó.; Costa, L.; Costa, F.; Lago, A.; Rocha, V.; Vipotnik, Z.; Silva, B.; Tavares, T. Recovery of Rare Earth Elements from Wastewater Towards a Circular Economy. *Molecules* **2019**, *24*, 1005.
158. Assila, O.; Barros, Ó.; Fonseca, A.M.F.; Parpot, P.; Soares, O.S.G.P.; Pereira, M.F.R.; Zerrouq, F.; Kherbeche, A.; Rombi, E.; Tavares, T.; et al. Degradation of pollutants in water by Fenton-like oxidation over LaFe-catalysts: Optimization by experimental design. *Microporous Mesoporous Mater.* **2023**, *349*, 112422.
159. Figueiredo, H.; Silva, B.; Kuźniarska-Biernacka, I.; Fonseca, A.M.; Medina, R.; Rasmussen, S.; Bañares, M.A.; Neves, I.C.; Tavares, T. Oxidation of cyclohexanol and cyclohexene with triazenido complexes of chromium immobilized in biosorption FAU supports. *Chem. Eng. J.* **2014**, *247*, 134–141.
160. Figueiredo, H.; Neves, I.C.; Quintelas, C.; Tavares, T.; Taralunga, M.; Mijoin, J.; Magnoux, P. Oxidation catalysts prepared from biosorbents supported on zeolites. *Appl. Catal. B Environ.* **2006**, *66*, 274–280.
161. Figueiredo, H.; Silva, B.; Quintelas, C.; Neves, I.C.; Tavares, T. Effect of the supporting zeolite structure on Cr biosorption: Performance of a single-step reactor and of a sequential batch reactor—A comparison study. *Chem. Eng. J.* **2010**, *163*, 22–27.
162. Figueiredo, H.; Silva, B.; Quintelas, C.; Pereira, M.F.R.; Neves, I.C.; Tavares, T. Biosorption of hexavalent chromium based on modified y zeolites obtained by alkali-treatment. *Environ. Eng. Manag. J.* **2010**, *9*, 305–311.
163. Jordan, M.I.; Mitchell, T.M. Machine learning: Trends, perspectives, and prospects. *Science (80-.).* **2015**, *349*, 255–260.
164. Bi, Q.; Goodman, K.E.; Kaminsky, J.; Lessler, J. What is Machine Learning? A Primer for the Epidemiologist. *Am. J. Epidemiol.* **2019**, *188*, 2222–2239.

165. Samuel, A.L. Some studies in machine learning using the game of checkers. *IBM J. Res. Dev.* **2000**, *44*, 206–226.
166. El Naqa, I.; Murphy, M.J. Chapter 1: What Is Machine Learning? In *Machine Learning in Radiation Oncology*; Springer International Publishing: Cham, 2015; pp. 3–11 ISBN 9781119815075.
167. Peng, G.C.Y.; Alber, M.; Buganza Tepole, A.; Cannon, W.R.; De, S.; Dura-Bernal, S.; Garikipati, K.; Karniadakis, G.; Lytton, W.W.; Perdikaris, P.; et al. Multiscale Modeling Meets Machine Learning: What Can We Learn? *Arch. Comput. Methods Eng.* **2021**, *28*, 1017–1037.
168. Dhage, S.N.; Raina, C.K. A review on Machine Learning Techniques. *Int. J. Recent Innov. Trends Comput. Commun.* **2016**, *4*, 395–399.
169. Qin, S.J.; Chiang, L.H. Advances and opportunities in machine learning for process data analytics. *Comput. Chem. Eng.* **2019**, *126*, 465–473.
170. Mithun Sridharan Machine Learning Algorithms Mindmap | Jixta Available online: https://www.kaggle.com/discussions/getting-started/83518 (accessed on Aug 12, 2023).
171. Nasteski, V. An overview of the supervised machine learning methods. *HORIZONS.B* **2017**, *4*, 51–62.
172. Torregrossa, D.; Leopold, U.; Hernández-Sancho, F.; Hansen, J. Machine learning for energy cost modelling in wastewater treatment plants. *J. Environ. Manage.* **2018**, *223*, 1061–1067.
173. Pang, J.-W.; Yang, S.-S.; He, L.; Chen, Y.-D.; Cao, G.-L.; Zhao, L.; Wang, X.-Y.; Ren, N.-Q. An influent responsive control strategy with machine learning: Q-learning based optimization method for a biological phosphorus removal system. *Chemosphere* **2019**, *234*, 893–901.
174. Foroughi, M.; Ahmadi Azqhandi, M.H.; Kakhki, S. Bio-inspired, high, and fast adsorption of tetracycline from aqueous media using Fe3O4-g-CN@PEI-β-CD nanocomposite: Modeling by response surface methodology (RSM), boosted regression tree (BRT), and general regression neural network (GRNN). *J. Hazard. Mater.* **2020**, *388*, 121769.
175. Al-Gheethi, A.A.; Mohd Salleh, M.S.; Noman, E.A.; Mohamed, R.M.S.R.; Crane, R.; Hamdan, R.; Naushad, M. Cephalexin Adsorption by Acidic Pretreated Jackfruit Adsorbent: A Deep Learning Prediction Model Study. *Water* **2022**, *14*, 2243.
176. Zhang, K.; Zhong, S.; Zhang, H. Predicting Aqueous Adsorption of Organic Compounds onto Biochars, Carbon Nanotubes, Granular Activated Carbons, and Resins with Machine Learning. *Environ. Sci. Technol.* **2020**, *54*, 7008–7018.
177. Sigmund, G.; Gharasoo, M.; Hüffer, T.; Hofmann, T. Deep Learning Neural Network Approach for Predicting the Sorption of Ionizable and Polar Organic Pollutants to a Wide Range of Carbonaceous Materials. *Environ. Sci. Technol.* **2020**, *54*, 4583–4591.
178. Sadek, A.H.; Fahmy, O.M.; Nasr, M.; Mostafa, M.K. Predicting Cu(II) Adsorption from Aqueous Solutions onto Nano Zero-Valent Aluminum (nZVAl) by Machine Learning and Artificial Intelligence Techniques. *Sustainability* **2023**, *15*, 2081.
179. Abdi, J.; Mazloom, G. Machine learning approaches for predicting arsenic adsorption from water using porous metal–organic frameworks. *Sci. Rep.* **2022**, *12*, 16458.
180. Ke, B.; Nguyen, H.; Bui, X.-N.; Bui, H.-B.; Choi, Y.; Zhou, J.; Moayedi, H.; Costache, R.; Nguyen-Trang, T. Predicting the sorption efficiency of heavy metal based on the biochar characteristics, metal sources, and environmental conditions using various novel hybrid machine learning models. *Chemosphere* **2021**, *276*, 130204.
181. Kitchin, J.R. Machine learning in catalysis. *Nat. Catal.* **2018**, *1*, 230–232.
182. Li, Z.; Wang, S.; Xin, H. Toward artificial intelligence in catalysis. *Nat. Catal.* **2018**, *1*, 641–642.
183. Yang, W.; Fidelis, T.T.; Sun, W.-H. Machine Learning in Catalysis, From Proposal to Practicing. *ACS Omega* **2020**, *5*, 83–88.

Chapter 3 – Chemical modification of zeolites for the recovery of Rare Earth Elements

Rare earth elements (REE) are a significant group of valuable elements used in diverse and relevant applications in our daily lives. The mining and processing of the original ores, as well as the final wastes disposal, produce wastewater with variable concentrations of REE to be recovered. Adsorption processes have been used for the retention of various molecules from wastewater using sorbent materials such as zeolites. Modified zeolites were obtained by acid and alkali treatments in order to increase their sorption capacity compared to the controls. Desorption assays were also performed to evaluate the REE leaching from the sorbent. An overall removal of 80% by adsorption and over 90% recovery by desorption was achieved. The machine learning algorithms helped to classify the adsorption results and allowed the selection of the most suitable modified zeolites, which correspond to ZX_NaOH 0.10 M, ZX_KOH 0.10 M and ZA_NaOH 0.50 M. It is concluded that alkali modification of the zeolites surfaces increases their natural adsorption capacity for REE recovering. Unsupervised machine learning algorithms can also be used for pattern recognition.

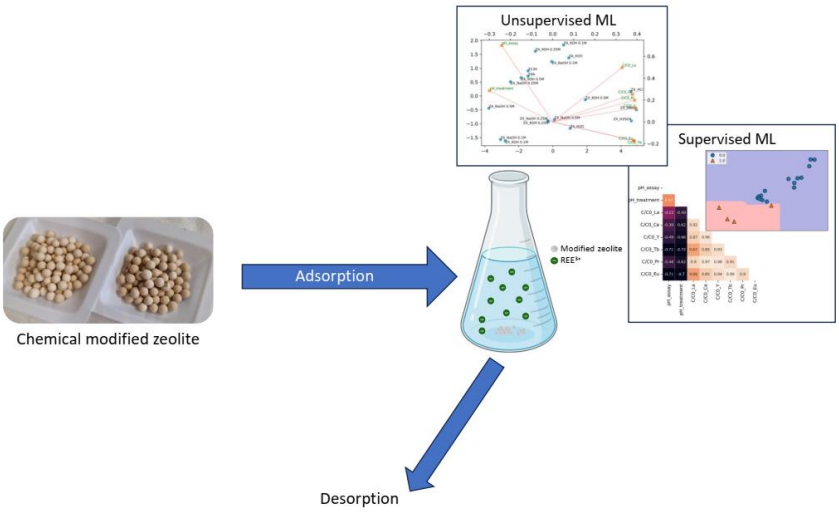

Adapted from: Barros, O.; Parpot, P.; Neves, I. C.; Tavares, T.; Chemical modification of zeolites for the recovery of Rare Earth Elements using Machine Learning algorithms – under revision.

3.1. Introduction

Rare earth elements (REE) are a group of seventeen elements, subdivided into light REE (La to Gd) or heavy REE (Tb to Lu, including Y) [1,2]. These elements are widely used in different applications (fluorescent lamps, batteries, lasers, information storage, conservation and transport of energy) due to their specific properties [1–3]. As they are becoming more and more essential, these elements are getting closer attention. There is almost no production of REE in European Union due to the complex exploitation of their deposits [4] and due to environmental impact [5] of REE extraction and refining [6]. For that reason, alternative methods for obtaining REE are quite attractive, such as REE-containing waste recycling [6]. Some efforts have been made in this context to implement the specific recycling of REE [7,8] and to achieve their recovery and possible reuse [9–11].

Adsorption processes have been extensively used to remove different pollutants from wastewater such as heavy metals [12,13], which led to their recognition as some of the most interesting separation processes. Adsorption is simple and competitive, with high recovery efficiency, with availability of a wide-range of sorbents, effective even with low concentrations of sorbate and environmentally sustainable [1,13–15], making it quite attractive for pollutant removal.

Different inorganic materials are used as sorbents like clays, carbon and zeolites [9,16,17]. Zeolites are crystalline microporous aluminosilicates that are used as catalysts, adsorbents and ion-exchangers [18]. Different surface treatments can be used to increase their applicability. The most common modifications of the zeolite structures are chemical [19–21] or hydrothermal [22,23] treatments that improve the access to the zeolite surface. Figueiredo *et al.* studied the modification of NaY zeolite by NaOH 2.0 M, with two different contact periods between the zeolite and the alkaline solution (1 h and 9 h), with the final purpose of removing hexavalent chromium from aqueous solutions. These newly modified zeolites preformed an efficient Cr removal [21]. Two different zeolites, FAU and ZSM5, was modified with $NaNO_3$ to obtain different acidity and sodium content for an improved removal of chromium [19].

This work aims to assess the effect of chemical treatments on different zeolite surfaces as FAU and LTA to improve their capacity for REE entrapment. Acid and alkali treatments with different concentrations were used to modify zeolites. The best chemical treatments were then selected in accordance to the results of REE adsorption-desorption and kinetics modeling assays. Furthermore, the adsorption results were analyzed by machine learning (ML) techniques to select the most suitable modified zeolite and predict the zeolite classification (as a good or bad adsorbents, accordantly to the

results and tested conditions) and residual concentration of pollutants. The supervised and unsupervised learning from ML will be used in this work. Supervised learning is related to classification (division of the different samples into good or bad, accordantly to the objective of the tests) and regression while unsupervised learning is related to clustering (group assembly accordantly to their affinity under the studied conditions) and dimension reduction (data compression to a smaller, different set of variables that can indicate the most important one of the original features) [24].

3.2. Materials and Methods

3.2.1.Materials

Stock solutions of each rare earth were prepared from the dissolution of the respective salt in distilled water (dH_2O) to obtain a solution with a concentration of 1000 mg/L and then used on the batch assays: europium ($EuCl_3.6H_2O$; 99.9 %) and cerium, ($Ce(NO_3)_3.6H_2O$; 99.5 %) were purchased from Acros Organics; lanthanum, ($La(NO_3)_3.6H_2O$; 99.9 %), praseodymium, ($PrCl_3.xH_2O$; 99.9 %), terbium, ($TbCl_3.6H_2O$; 99.9 %) and yttrium, ($YCl_3.xH_2O$; 99.9 %) were purchased from Alfa Aesar. The multi-element ICP quality control standard solution, with a concentration of each element of 200 mg/L, was purchased from CPAchem. Two zeolite structures were used, FAU (13X) and LTA (4A), typical adsorbents supplied by Acros Organics and Sigma-Aldrich, respectively. The particle size for 13X beads is 4 to 8 mesh with an average pore size of 7 Å, while 4A pellets have a diameter of 1.6 mm with an average pore size of 4 Å.

3.2.2.Zeolite modifications

The 13X and 4A zeolites modifications were carried out on flow columns using different basic and acid solutions. NaOH and KOH solutions at concentrations of 0.10, 0.25 and 0.50 M were used and HNO_3, HCl and H_2SO_4 solutions were tested at a concentration of 0.25 M. The procedure was divided into two steps. In the first step, 20 g of zeolite were washed with 500 mL dH_2O for 6 h with a flow rate of 23 mL/min. In the second step, 500 mL of the acid or of base solutions were used for 22 h with a flow rate of 3 mL/min. The resulting modified zeolites will be identified with the respective pre-treatment and concentration. Control of the pre-treatment process was also performed. The control zeolites were designated as ZX_H_2O or ZA_H_2O and were produced by performing the pre-treatment second step with dH_2O. After this procedure, the zeolites were dried at 60ºC for 48 h before characterization or adsorption-desorption assays. A list of the designation for each sample that will be tested and a description of the chemical modifications performed is shown in **Table 3.1**.

Table 3.1: Description of the modification of each tested zeolite with the respective name.

Designation	*Modification description*
Z13X	zeolite 13X (Z13X) - control
ZX_H_2O	ZX washed with H_2O - control
ZX_NaOH 0.10 M	ZX modified with NaOH 0.10 M
ZX_NaOH 0.25 M	ZX modified with NaOH 0.25 M
ZX_NaOH 0.50 M	ZX modified with NaOH 0.50 M
ZX_KOH 0.10 M	ZX modified with KOH 0.10 M
ZX_KOH 0.25 M	ZX modified with KOH 0.25 M
ZX_KOH 0.50 M	ZX modified with KOH 0.50 M
ZX_HCl 0.25 M	ZX modified with HCl 0.25 M
ZX_HNO_3 0.25 M	ZX modified with HNO_3 0.25 M
ZX_H_2SO_4 0.25 M	ZX modified with H_2SO_4 0.25 M
Z4A	zeolite 4A (Z4A) - control
ZA_H_2O	ZA washed with H_2O - control
ZA_NaOH 0.10 M	ZA modified with NaOH 0.10 M
ZA_NaOH 0.25 M	ZA modified with NaOH 0.25 M
ZA_NaOH 0.50 M	ZA modified with NaOH 0.50 M
ZA_KOH 0.10 M	ZA modified with KOH 0.10 M
ZA_KOH 0.25 M	ZA modified with KOH 0.25 M
ZA_KOH 0.50 M	ZA modified with KOH 0.50 M

3.2.3.Characterization

The modified zeolites were characterized by Scanning Electron Microscopy/Energy Dispersive X-Ray spectroscopy (SEM-EDS), Fourier-transform infrared spectroscopy (FTIR) and pH of zero point charge (pH_{PZC}).

The samples were characterized using a desktop scanning electron microscope (SEM) coupled with energy-dispersive X-ray spectroscopy (EDS) analysis (Phenom ProX with EDS Phenom-World BV, Netherlands). All data were acquired using the ProSuite software (Phenom-World BV, The Netherlands) integrated with Phenom Element Identification software (Phenom-World), used for the quantification of the concentration of the elements present in the samples, expressed in either weight or atomic concentration. The samples of zeolite were placed into aluminum pin stubs with electrically conductive carbon adhesive tape (PELCO Tabs, Manchester, NH, USA) and processed without coating. The

aluminum pin stub was then placed inside a Phenom Sample Holder (SR) and different points were analyzed for elemental composition. EDS analyses were conducted at 15 kV with intensity map.

The pHzpc values for zeolite were measured: a solution of 0.01 M NaCl was prepared, previously bubbled with nitrogen in order to stabilize the pH by preventing the dissolution of CO_2 and the pH was adjusted to different values (1 to 10) by adding diluted HCl or NaOH. For each pH value, 0.10 g of adsorbent was added to 25 mL of NaCl. All the flasks were sealed to avoid contact with air and left under moderate agitation (110 rpm) at 25 ◦C ± 1 ◦C, for 24 h. The samples were then filtered, using 0.2 μm nylon filters and the pH of the final filtrate was measured and plotted against the initial pH value. The pH at which the curve crosses the line of initial pH ($pH_{initial}$) equals to final pH (pH_{final}) is taken as pHzpc

FTIR spectroscopy measurements were performed on different samples using an attenuated total reflectance, ATR-FTIR, PerkinElmer Spectrum Two spectrometer equipped with an ATR accessory. A diamond prism was used as the waveguide. Firstly, the samples were reduced to powder and then all spectra were recorded with a resolution of 2 cm^{-1} in the wavelength region 4000-400 cm^{-1} by averaging 50 scans. The analyses were carried out at room temperature.

3.2.4.Analytical quantification of REE

All liquid samples were analyzed at the Inductively Coupled Plasma - Optical Emission Spectrometry, ICP-OES, (Optima 8000, PerkinElmer). The liquid sample was filtered through a pore size membrane of 0.22 μm and some drops of nitric acid, HNO_3 (Fisher, Loughborough, UK, 69%) were added to avoid the pKa value change. This analysis was performed under the following operating conditions: RF power at 1400 W, argon plasma flow at 12 L/min, auxiliary gas flow at 0.2 L/min and nebulizer gas flow at 0.70 L/min. The wavelengths (nm) used for each element were: La — 408.672, Ce — 413.764, Eu — 381.967, Y — 371.029, Tb — 350.917 and Pr—390.844, with an axial plasma view for La, Ce, Tb and Pr, while for Y and Eu, a radial view was used.

3.2.5.Selection of modified zeolite by adsorption assays

3.2.5.1. Adsorption assays

The adsorption assays were carried out using a concentration of 6 g/L of the modified zeolites with a mixed REE solution with a concentration of 10 mg/L of each REE tested. The uptake assays were carried out at room temperature in batch vessels placed in rotary shakers at 130 rpm for 24 h. The same procedure was used in kinetics assays that lasted 125 h. The pH was controlled and the desired values ranged between 3 and 4. When pH was higher than 4, a drop of a diluted solution of HCl would be added.

The uptake for each REE at a given time was calculated by equation 3.1:

$$q_t = \frac{(C_0 * V_0) - (C_t * V_t)}{m} \quad \text{(Eq .3.1)}$$

C_0 (mg/L) is the initial concentration of the REE present in solution, C_t (mg/L) is the concentration of REE at a time, t. V_0 (L) is the initial volume of the REE solution, while V_t is the volume of the solution at a given time, t, and m (g) is the weight of the adsorbent used.

3.2.5.2. Kinetics modeling

The kinetics modeling was performed using the non-linear forms of the Pseudo-first order (PFO), equation 3.2, and of the Pseudo-second order (PSO) models, equation 3.3. The use of non-linear equations aims to avoid some errors associated with the linearization of the models by changing the error structure or altering their distribution, possibly distorting the fitting as referenced in literature [25–30].

This fitting was performed using the non-linear equations of both models and the least-squares regression method, using Origin Pro 8.5 software. The equations used are the following:

$$q_t = q_e * (1 - e^{-k_1 * t}) \quad \text{(Eq. 3.2)}$$

$$q_t = \frac{k_2 * q^2 * e^t}{1 + k_2 * q_e * t} \quad \text{(Eq. 3.3)}$$

In these equations, q_t (mg/g) is the mass of solute retained per mass of solid at time, t; q_e (mg/g) is the mass of solute per unit mass of solid at equilibrium; k_1 is a rate constant (min^{-1}) and reflects a combination of the rate constants of adsorption k_a and desorption k_d; k_2 (g/(mg × min)) is a complex parameter related to the initial concentration of solute.

3.2.6.Desorption assays

Desorption assays were carried out using 3 different acid solutions: HNO_3, H_2SO_4 and HCl, at a concentration of 0.10 M each in distilled water. The zeolites loaded with REE produced previously were used in these tests. The assays were carried out at room temperature in rotary shakers at 120 rpm, for 5 h, using a volume of 0.1 L of leaching solution and 0.35 g of loaded zeolite. Samples of the solution were taken and then analyzed by ICP.

The recovery percentage (% recovery) was calculated using equation 3.4:

$$\%\, recovery = \frac{C_t * V_t}{m_{REE}} \quad \text{(Eq. 3.4)}$$

Where C_t is the concentration of one REE (mg/L) at a given time, V_t is the solution volume (L) of a given time, and m_{REE} is the total mass (g) of a given REE retained by the zeolite.

3.2.7.Machine learning

The ML analysis was performed using a table, named DataFrame, with labeled axes (rows and columns). The rows are related with the samples used, while the columns are the different elements that are being used to evaluate the different samples. The different features used were the C/C_0 results after 24h for each tested REE, the pH of the zeolite treatment and the pH of the adsorption solution after the 24 h time point.

The DataFrame was evaluated under unsupervised learner (Principal Component Analysis, K-Means Analysis) and supervised learner (classification and regression). The Principal Component Analysis, PCA, is a method for reducing the dimensionality of data, leading to an increased interpretation and minimizing information lost, while the K-Means divides the samples into groups or clusters that are more compatible with each other accordantly to the studied conditions.

K-nearest neighbors Classifier (KNN), Decision Tree Classifier and Random Forest Classifier were used to classify the samples. These classifiers are often used in binary classification, as explained in **Table 3.2**. The data was divided into two sets, a training set (70 % of the data), which contains a known output and where the model learns to generalize and then apply to other data and a test set (30 % of the data), where the model's prediction is tested. It also added a stratify option to the data division, allowing both test and train sets to have the same percentage of positive cases (in this case, a good adsorbent) as the complete set.

Table 3.2: The binary classification for the different REE. The C/C_0 values were given a classification accordantly. The mean value of these intervals was taken and given the respective binary classification.

C/C_0 intervals	*C/C_0 Classification*	*Binary Classification*
$0.8 < C/C_0 < 1.0$	1	
$0.6 < C/C_0 < 0.8$	2	> 4.0 is 1
$0.4 < C/C_0 < 0.6$	3	
$0.2 < C/C_0 < 0.4$	4	< 4.0 is 0
$0.0 < C/C_0 < 0.2$	5	

For the regression, the training test split was 70% for training and 30 % for testing. Different metrics were used to evaluate the regression prediction, which were the mean absolute error (MAE), the mean squared error (MSE), the root mean squared error (RMSE) and the R-Squared (R^2). These metrics

were used to evaluate the test data. MAE is calculated by the sum of the absolute differences between the real and predicted values of each tested observation and then divided by the number of observations. All tests were performed using Spyder (Python 3.9) and the respective needed modules as pandas, numpy, scikit-learn, matplotlib and seaborn.

3.2.8.Statistical analysis

The adsorption results were analyzed using the One-Way ANOVA, where the obtained values for each pre-treated zeolite and the respective controls were compared between each other. The Two-Way ANOVA was used for the statistical analysis of the desorption results. The Bonferroni's multiple comparison test was used for both data sets.

The ANOVA analyses were performed using the software Graph Pad Prism version 8.0.2 (Graph Pad Software, Inc, San Diego, CA, USA). The results were only considered significantly different when the probability (*p*-value) was lower than 0.05, assuming a 95 % confidence interval.

3.3. Results and Discussion

3.3.1.Modified zeolites characterization

Two different zeolite structures, FAU (13X) and LTA (4A), were subjected to chemical treatments with acid and basic solutions at room temperature. From the SEM observations it was concluded that the modifications had slight effects on the zeolite morphology, which were more noticeable at higher concentrations. These results do not give any specific information regarding the modifications and their eventual impact on the surface characteristics or on the zeolite behaviour.

The elementary quantification of the pristine zeolites and the modified ones were evaluated using EDS. The results for zeolite 13X and its modified forms are shown in **Table 3.3**.

These data prove that the different chemical treatments affect the surface of the zeolite. In the case of the acid treatments, the sodium present in the framework was entirely replaced by protons of the acid solutions and a dealumination was observed. An opposed effect was observed for the alkali treatments. A decrease in the Si/Al ratio was perceived in the same magnitude for both strong bases, NaOH and KOH, and its values ranged between 1.20 and 1.34, showing that both alkali solutions affect the zeolite structure in the same extension.

Table 3.3: EDS surface analysis of modified 13X zeolite and controls.

Chemical treatment		Element (wt %)					Si/Al
Samples	Conc. (M)	O	Si	Al	Na	K	
ZX_HCl	0.25	56.0 ± 1.0	27.3 ± 1.7	5.5 ± 0.0	0	-	4.8
ZX_HNO_3	0.25	57.0 ± 4.3	27.0 ± 2.4	5.9 ± 0.4	0	-	4.4
ZX_H_2SO_4	0.25	56.6 ± 6.1	27.0 ± 2.9	5.3 ± 0.4	0	-	4.9
ZX_NaOH	0.10	68.0 ± 0.4	15.2 ± 0.3	12.2 ± 0.2	3.6 ± 0.2	-	1.2
	0.25	57.6 ± 1.5	14.2 ± 1.0	10.2 ± 0.6	9.6 ± 0.7	-	1.3
	0.50	57.7 ± 1.0	16.8 ± 0.6	12.3 ± 0.2	10.8 ± 0.6	-	1.3
ZX_KOH	0.10	58.2 ± 1.0	16.9 ± 0.3	12.2 ± 0.3	7.5 ± 0.4	0	1.3
	0.25	58.0 ± 1.5	16.0 ± 0.7	12.1 ± 0.4	6.0 ± 0.2	6.2 ± 0.7	1.3
	0.5	56.5 ± 4.7	15.9 ± 1.3	11.5 ± 0.7	4.9 ± 0.9	8.6 ± 3.4	1.3
ZX_H_2O		57.3 ± 1.7	18.1 ± 1.3	10.6 ± 1.2	12.0 ± 1.0	-	1.6
Z13X		57.3 ± 1.7	18.1 ± 1.3	10.6 ± 1.2	12.0 ± 1.0	-	1.6

Considering that the acid treatment provokes more modifications to the zeolite framework in the case of Z13X, this treatment was not carried out on the LTA structure. The other reason is related with the poor adsorption capacity that the acid treatment had on the Z13X, as will be analyzed in the **3.3.2 Selection of the most suitable chemical treatment** section of this chapter. The EDS results for the zeolite 4A and the modified samples are shown in **Table 3.4**. In the case of LTA, the alkali treatments do not affect the Si/Al ratio since is similar between the samples and close to the values found for the controls.

Table 3.4: EDS analyses of the zeolite 4A, the alkali pre-treated samples and controls.

Chemical treatment		Element (wt %)					Si/Al
Samples	Conc. (M)	O	Si	Al	Na	K	
ZA_NaOH	0.10	56.6 ± 2.3	13.5 ± 2.5	12.5 ± 1.8	9.5 ± 1.7		1.0
	0.25	56.7 ± 1.6	16.71 ± 1.2	15.2± 0.7	11.4 ± 0.3		1.1
	0.50	60.5 ± 3.1	14.27 ± 1.6	13.33 ± 1.4	11.7 ± 0.1		1.0
ZA_KOH	0.10	57.2 ± 2.7	15.76 ± 0.7	14.1 ± 0.3	7.0 ± 1.0	5.6 ± 2.9	1.1
	0.25	55.9 ± 1.9	16.1 ± 0.7	14.5 ± 0.5	6.3 ± 0.5	7.0 ± 1.1	1.1
	0.50	56.2 ± 0.5	15.2 ± 0.3	14.2 ± 0.3	4.5 ± 0.1	9.4 ± 0.57	1.0
ZA_H_2O		58.1 ± 0.8	16.5 ± 1.2	14.9 ± 0.6	10.4 ± 1.0		1.1
Z4A		55.9 ± 1.2	17.2 ± 0.4	15.5 ± 0.4	11.2 ± 0.4		1.1

An increase of K^+, without the loss of Si or Al from the framework, was observed for the samples treated with KOH solutions with different concentrations. This effect was more pronounced on LTA structure than on FAU structure, where the presence of K^+ was detected at the higher concentrations of KOH (**Table 3.3**). As the washing step of the zeolites preparation may lead to the Na removal and, consequently to a negative charge of the solid surfaces, the presence of the K^+ may be related to the counterbalance of such charge.

The profiles of pH_{PZC} and the FTIR spectra for both zeolite structures, FAU and LTA, and respective modified samples are shown in **Figure 3.1** and **Figure 3.2**.

The alkali treated 13X and 4A zeolites have similar pH_{PZC} to the ones of the respective controls, closer to 10, **Figure 3.1**. Although there was no difference regarding the pH_{PZC} values between the modified and the control samples, the treated zeolites show a different behavior during the adsorption. It should be mentioned that higher pH_{PZC} values probably could lead to REE precipitation during the adsorption assays, which is not intended. All the acid treated 13X samples decreased their pH_{PZC} compared to the pristine zeolite, 9.6 [9]. The samples ZX_HNO_3 and ZX_H_2SO_4 had lower values, 5.6 and 4.4, respectively, but the effect was not so evident on the ZX_HCl, 8.4. The acid treatment with HNO_3 or H_2SO_4 greatly decreases the pH_{ZPC} values as expected as the H^+ from the chemical modification was incorporated into the zeolites to reduce their natural negative charge. The pH_{PZC} value for one of the controls, ZX_H_2O, is 7.5 while ZA_H_2O presents a pH_{PZC} value close to 7.0. As previously stated, the modification of these zeolites was performed using only dH_2O, with a pH value of 7.00. However, due the absorption of carbon dioxide from the atmosphere, the pH value will be slightly acidic with a value around 5.8. This acidification of the water used for the chemical modification of the controls can explain the difference of the pH_{PZC} value when compared to the zeolites without modification (Z13X and Z4A).

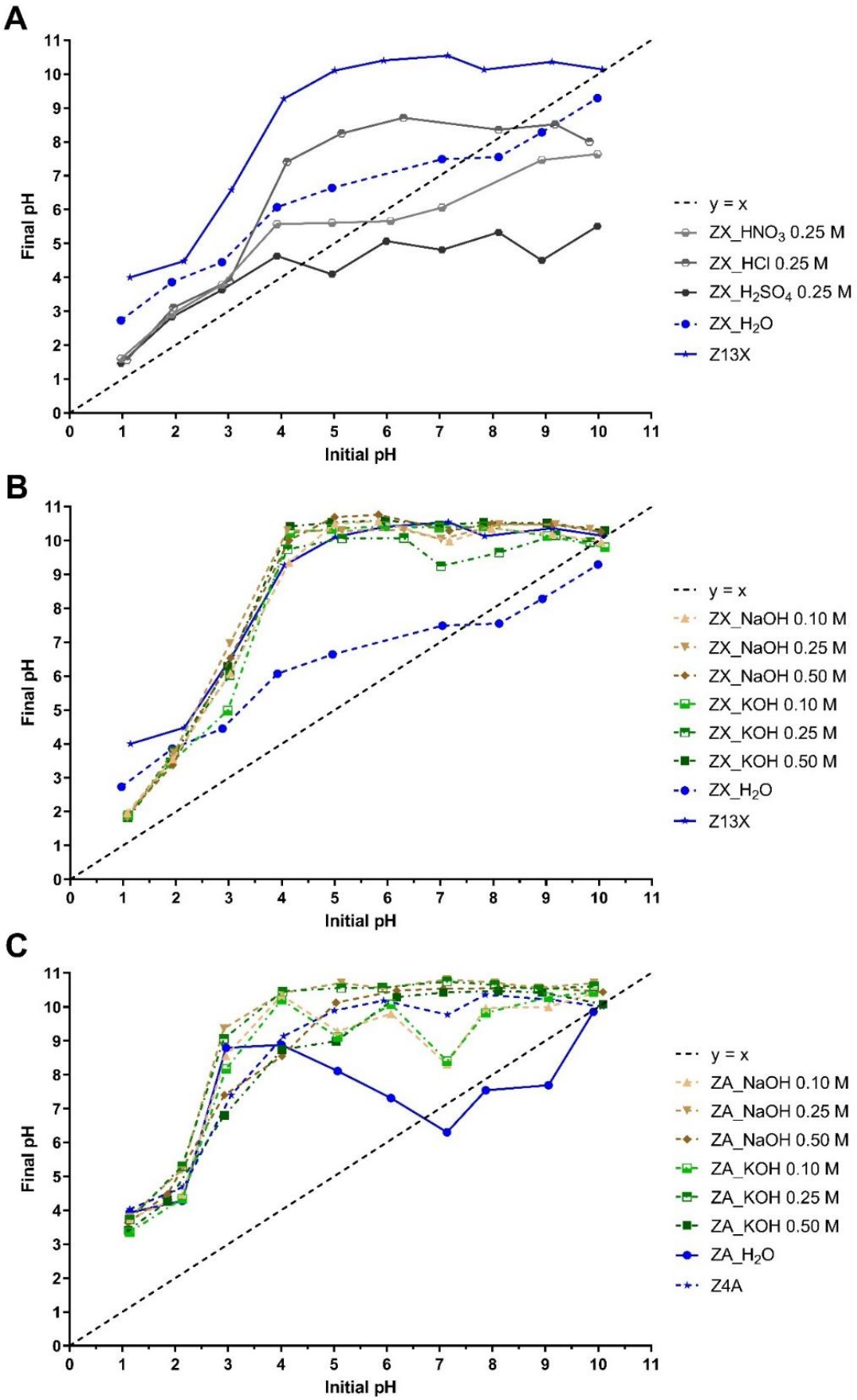

Figure 3.1: pH_{PZC} results: **A** - acid modified 13X, **B** - alkali modified 13X, and **C** – alkali modified 4A.

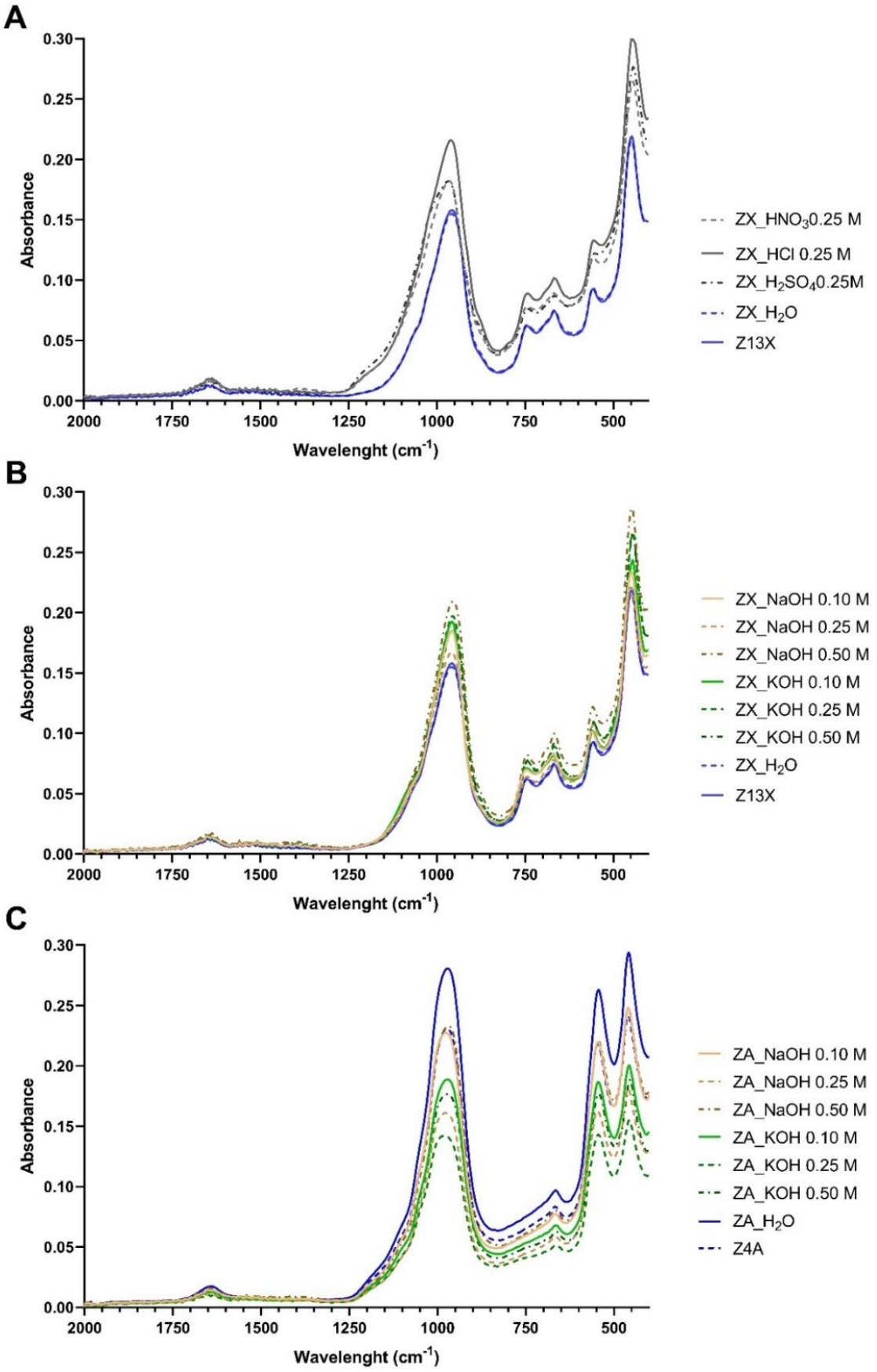

Figure 3.2: FTIR analyses: **A** - acid modified 13X, **B** - alkali modified 13X and **C** - alkali modified 4A.

FTIR spectra of zeolites 13X and 4A, **Figure 3.2**, are very similar to the ones of FAU zeolite structures. In **Figure 3.2** is possible to see a band at 1640 cm^{-1} characteristic of $\delta(H_2O)$ vibration of absorbed water on the zeolite. The characteristic bands of the lattice vibrations of the framework are evidenced in 1330 to 450 cm^{-1}. The band at 960 cm^{-1} is attributed to the asymmetric stretching of Si-O and Al-O belonging to the TO_4 tetrahedras (T = Si or Al) [31–33]. The bands at 670 cm^{-1} and near 750 cm^{-1} are related to the Si–O symmetric stretching and oscillations of aluminosilicate oxygen tetrahedral chains [32,33]. At the same time, the band near 550 cm^{-1} is attributed to the symmetric stretching vibrations of the bridge bonds Si-O-Si and to the bending vibrations of O-Si-O [34]. Comparing the modified samples to the respective controls, the same bands in the same positions are observed indicating that the pre-treatments had no effect on the pristine zeolites. In addition, Si/Al ratio of the FAU samples can be determined by FTIR analysis using the equation 5:

$$x = 3.857 - 0.00621W_{DR} \quad \text{(Eq. 5)}$$

In here x = $(1+Si/Al)^{-1}$ and W_{DR} is the wavenumber at 500-650 cm^{-1}, related to the vibrations of the FAU lattice [35]. The results are shown in **Table 3.5.**

Table 3.5: Si/Al ratios based on FTIR and EDS analyses.

Zeolite	*Conc. (M)*	*Si/Al from FTIR*	*Si/Al from EDS*
ZX_HCl	0.25	1.50	4.75
ZX_HNO_3	0.25	1.42	4.38
ZX_H_2SO_4	0.25	1.42	4.88
ZX_NaOH	0.10	1.58	1.20
	0.25	1.42	1.34
	0.50	1.58	1.31
ZX_KOH	0.10	1.50	1.33
	0.25	1.42	1.26
	0.50	1.50	1.33
ZX_H_2O		1.50	1.64
Z13X		1.50	1.64

From the results of **Table 3.5** show that the zeolites modification was mostly superficial, as supported by the Si/Al ratio values shown in **Table 3.3**. The Si/Al ratio given by FTIR gives an indication of the framework ratio. However, the difference between the EDS and the FTIR results supports that the modification affects the most external surface. Any modification of the zeolite structure would become

irrelevant to the adsorption as this is a surface phenomenon. For the same reason, it is expected that acid modified zeolites may act as poor adsorbents, as acids tend to reduce the available specific surface.

3.3.2.Selection of the most suitable chemical treatment

3.3.2.1. Selection based on adsorption results

The REE ionic radii are small enough, between 0.9 to 1.032 Å [36,37], so the zeolites Z13X and Z4A are expected to remove those ions from the liquid solution considering their average pore size, 7 Å and 4 Å, respectively. The adsorption data from the mixed REE solution with the pre-treated zeolites are presented in **Figure 3.3**.

Overall, independently of the REE, the alkali treated zeolites t showed higher adsorption performance than the acid treated ones. Statistical differences (**Table S-3.1**) were found between the pre-treated sorbents, especially the acid modified zeolites and ZX_KOH 0.50 M, and the controls, for the retention of some REE. As the acid treated 13X zeolite did not show any enhancement of its adsorption ability, in accordance to the data in **Table 3.5**, it was not considered in the forward experiments. The adsorption process occurs on the material surface and the acid modified zeolites may suffer a reduction of the microporosity and an increase of the mesoporosity, which leads to a reduced specific surface area and explains the poorer results. The C/C_0 results obtained after the alkali modification of surfaces are similar for both the zeolites treated with 0.25 M solutions and for ZX_NaOH 0.50 M, when compared to the controls. The ZX_KOH 0.50 M presented worse results, with two significant differences found for Tb and Eu when compared with Z13X (**Table S-3.1)**. The samples modified with 0.10 M of NaOH and KOH were the ones that reached the lowest C/C_0 in solution after 24 h, **Figure 3.3**. ZX_NaOH 0.10 M reached removals over 80 % for five REE, apart from Ce. The results are similar between the controls, Z13X and ZX_H_2O, except for Tb and Eu, for which Z13X presented lower C/C_0, suggesting that the pristine zeolite washing with distilled water does not improve or even worsened the adsorption capacity, as expected. The increased removal for the ZX_NaOH 0.1 M and ZX_KOH 0.1 M, when compared with the controls, could be related with the increase of the surface area of the zeolite resulting from the treatment. K^+ was detected in the EDX analysis (**Table 3.3**) after the treatment with KOH, which can reduce the negative charge of the zeolite and this explains the lower adsorption for the zeolites treated with 0.25 and 0.5 M. For the treatment with NaOH, there was no increase in the Na^+ in the EDX analysis (**Table 3.3**), probably due to a competition between the REE and the Na^+. More Na^+ was detected in the zeolite for the higher concentrations. The presence of high quantities of Na^+ shown in analysis could be related with a poor performance, as happened for the controls. Therefore, the higher concentrations in the NaOH treatment

may lead to a low REE removal from the solution, assuming that what happened to the controls could also happen for these samples.

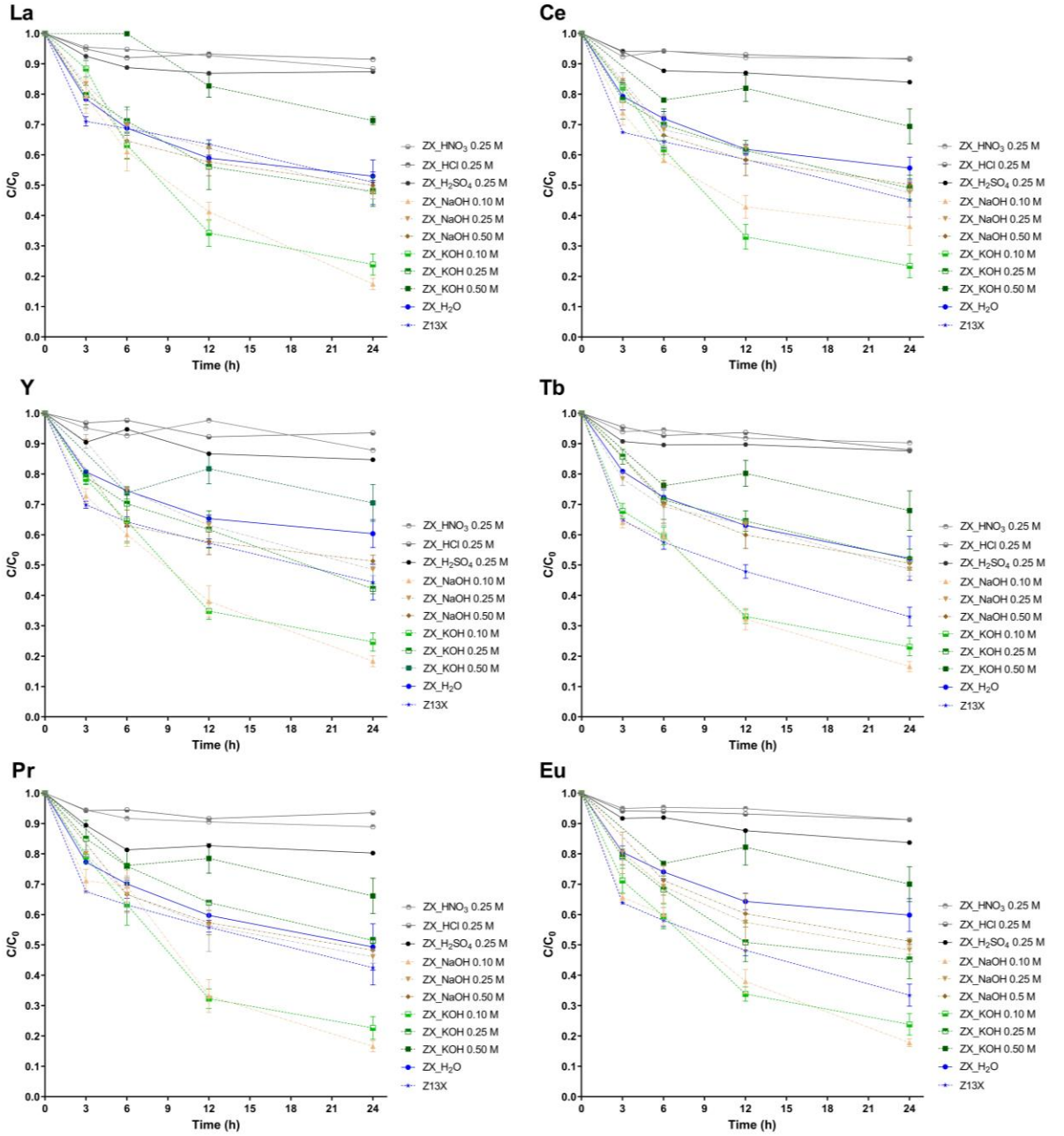

Figure 3.3: REE adsorption on Z13X and modified samples. The assays were carried out with a multi solution of REE previously described.

The pH solution was monitored during each of the assays with 13X zeolites, as presented in **Figure 3.4**, and for that, the precipitation of the REE can be discharged alkali treatment solutions with lower concentrations. However, some REE precipitation was observed 3 h after the beginning of the assay with zeolites treated with NaOH or with KOH, 0.50 M. For this reason, the concentration of 0.50 M for

both alkali treatment solutions are considered inadequate for the REE recovery. The Z13X zeolite presented a constant growth regarding the pH value that could be related with the presence of sodium in the zeolite, which tends to increase the pH value of water.

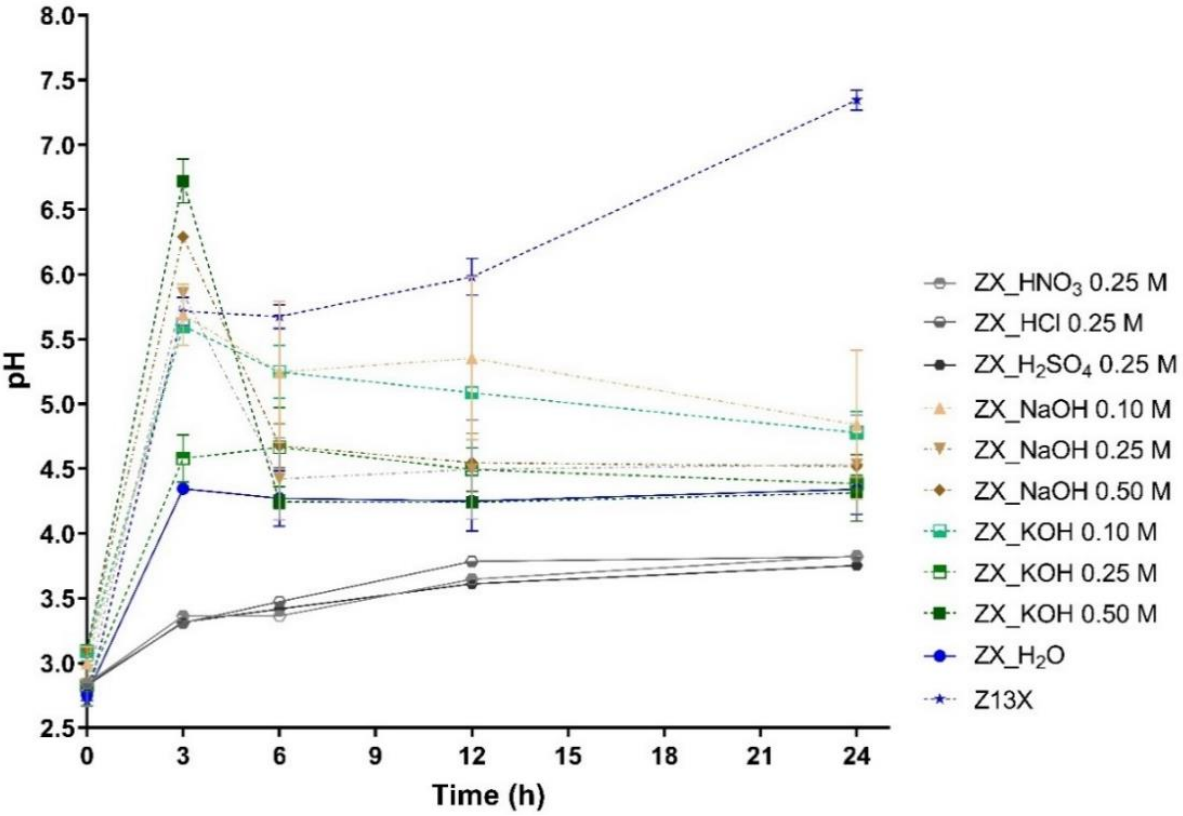

Figure 3.4: pH values during the adsorption assays for the basic and acid pretreatment to the Z13X.

The REE adsorption tests were also performed with the zeolite 4A and respective modified samples, **Figure 3.5**.

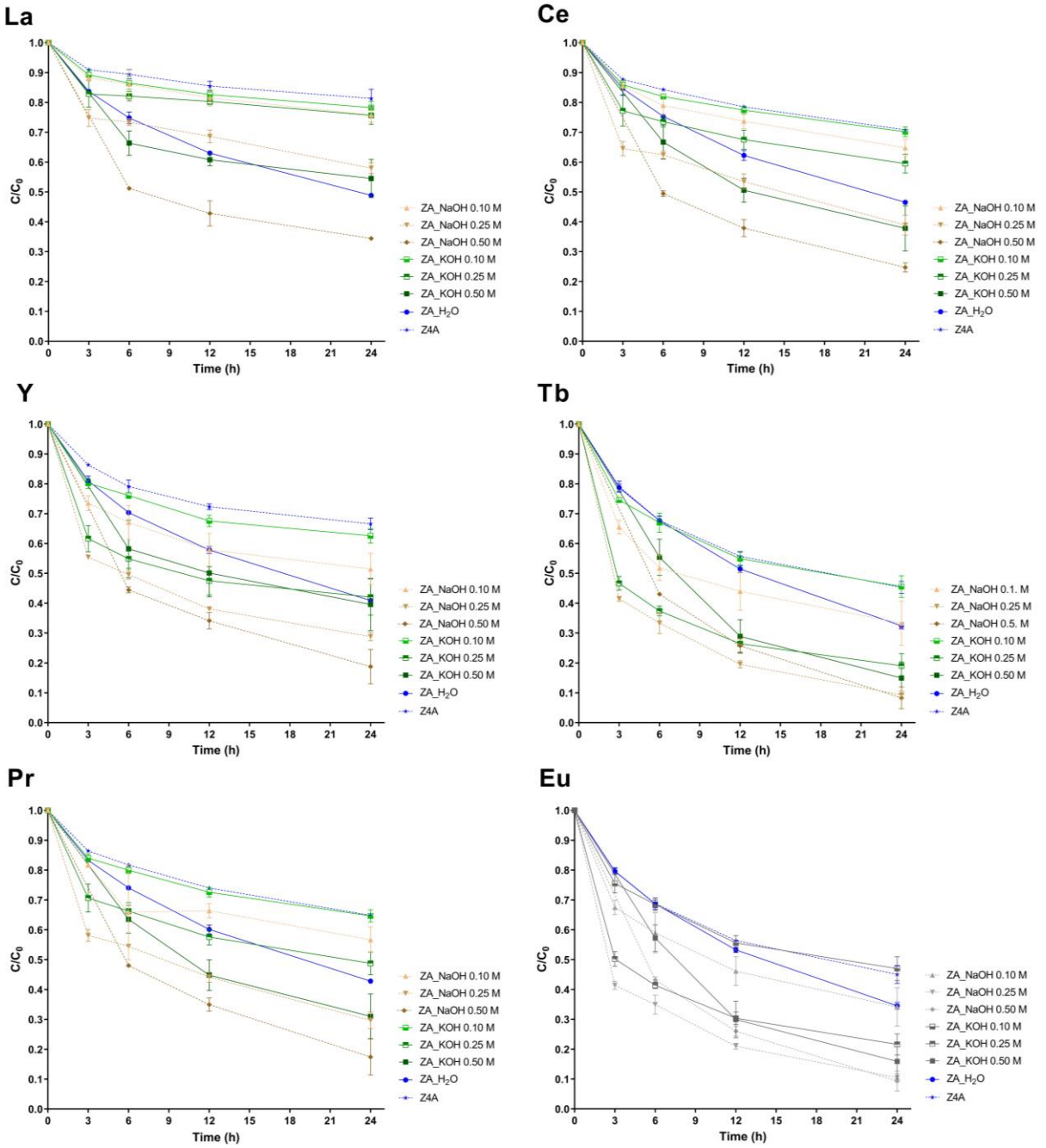

Figure 3.5: REE adsorption on zeolite 4A and modified zeolites, without pH adjustment. The assays were carried out with a multi solution of REE previously described.

It is also shown that one of the controls, Z4A, had the worst results in terms of the different REE adsorption, even with significant differences when compared to the modified zeolites (**Table S-3.2**). The overall adsorption capacity of the LTA structure increased with the alkali treatments and ZA_NaOH 0.50 M was the best sorbent with removals above 80 %, except for La and Ce. The pH monitoring along assays with 4A zeolite is presented in **Figure 3.6**. As with 13 X zeolite, ZA_NaOH 0.50 M and ZA_KOH 0.50 M used in adsorption tests presented some REE precipitation after 3 h of assay, the values greatly decrease

from 0 to 3 h, increasing till 6 h. This increase could be correlated with the addition of the diluted solution of HCl so the pH values ranged between 3.0 and 4.0.

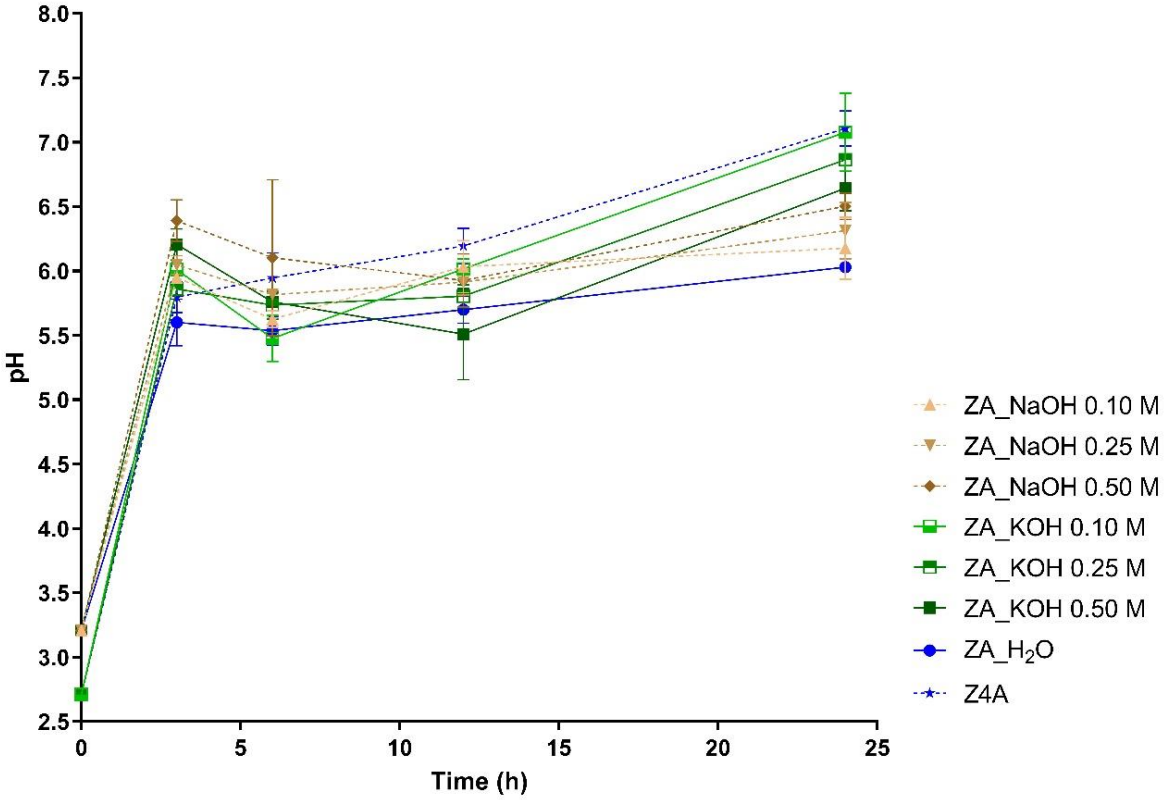

Figure 3.6: pH values during the adsorption assays for the basic pretreatment to the zeolite 4A.

From data of **Figure 3.3** and **Figure 3.5**, the uptake, *q*, was calculated after 24 h of assay. The uptake is defined by the mass of sorbate per mas of sorbent. Its values are presented in **Table 3.6** and **Table 3.7** for 13X and 4A zeolite samples, respectively.

As expected, the ZX_NaOH 0.10 M presented the highest uptake values for most of the REE, except for Y and Pr, suggesting a selective REE adsorption by the zeolite, **Table 3.6**. It is evidenced that the pristine zeolite has better uptake except for Y, when compared to ZX_H_2O, which suggests that the washing of the zeolite is not enough to improve its natural adsorption capacity. These uptake values are a good indicator that the alkali treatment with the lowest concentration solutions, improved the adsorption capacity of the zeolite surface.

Table 3.6: Uptake, q (mg/g), at 24 h sampling, for each REE tested by Z13X and by modified zeolites with alkali treatment.

Pre-treatment		REE					
Samples	Conc. (M)	La	Ce	Y	Tb	Pr	Eu
NaOH	0.10	1.40 ± 0.07	1.35 ± 0.07	0.95 ± 0.11	1.35 ± 0.08	1.19 ± 0.08	1.54 ± 0.10
	0.25	0.95 ± 0.02	0.97 ± 0.01	1.02 ± 0.14	0.87 ± 0.02	0.83 ± 0.03	0.88 ± 0.04
	0.50	0.89 ± 0.01	0.88 ± 0.01	0.48 ± 0.01	0.90 ± 0.02	0.85 ± 0.01	0.92 ± 0.01
KOH	0.10	1.28 ± 0.04	1.31 ± 0.04	1.04 ± 0.02	1.34 ± 0.03	1.21 ± 0.04	1.31 ± 0.04
	0.25	0.98 ± 0.07	1.00 ± 0.12	1.20 ± 0.39	0.85 ± 0.13	0.83 ± 0.15	0.93 ± 0.07
	0.50	0.61 ± 0.06	0.59 ± 0.07	0.32 ± 0.04	0.63 ± 0.08	0.60 ± 0.06	0.62 ± 0.07
ZX_H_2O		0.92 ± 0.06	0.96 ± 0.05	1.02 ± 0.20	0.86 ± 0.06	0.82 ± 0.06	0.81 ± 0.11
Z13X		0.93 ± 0.08	1.51 ± 0.10	0.83 ± 0.06	1.17 ± 0.03	1.07 ± 0.07	1.43 ± 0.05

Table 3.7: Uptake, q (mg/g), at 24h sampling, for each REE tested by 4A and modified zeolites with alkali treatment.

Pre-treatment		REE					
Sample	Conc. (M)	La	Ce	Y	Tb	Pr	Eu
NaOH	0.10	0.53 ± 0.04	1.07 ± 0.07	0.75 ± 0.06	1.17 ± 0.11	0.85 ± 0.06	1.42 ± 0.12
	0.25	0.82 ± 0.03	1.71 ± 0.07	1.04 ± 0.03	1.54 ± 0.04	1.30 ± 0.04	1.88 ± 0.04
	0.50	1.28 ± 0.11	2.15 ± 0.12	1.17 ± 0.05	1.55 ± 0.04	1.49 ± 0.07	1.90 ± 0.04
KOH	0.10	0.47 ± 0.03	0.88 ± 0.02	0.55 ± 0.02	0.96 ± 0.04	0.69 ± 0.02	1.15 ± 0.07
	0.25	0.51 ± 0.03	1.13 ± 0.06	0.80 ± 0.06	1.36 ± 0.05	0.94 ± 0.05	1.62 ± 0.04
	0.50	0.78 ± 0.15	1.51 ± 0.20	0.88 ± 0.04	1.42 ± 0.05	1.17 ± 0.12	1.71 ± 0.08
ZAH$_2$O		0.94 ± 0.02	1.45 ± 0.02	0.80 ± 0.01	1.15 ± 0.02	1.05 ± 0.01	1.39 ± 0.02
Z4A		0.44 ± 0.04	0.90 ± 0.05	0.52 ± 0.01	0.98 ± 0.02	0.71 ± 0.03	1.21 ± 0.03

The uptake values from **Table 3.7** showed that the 4A zeolite modified with NaOH 0.50 M reached the highest *q* values. ZA_H_2O presents higher *q* values when compared to Z4A, contrary to what happened with the zeolite 13X, suggesting that the water washing improved the adsorption capacities of the zeolite 4A. The alkali treatments with NaOH and KOH enhance, in general, better results compared to the ones obtained with the untreated zeolite. The best results were obtained with 0.50 M for both solutions, probably by an improvement in the microporosity of the structure, facilitating the incorporation of the REE into the zeolite matrix.

Comparing the *q* values of the best treated zeolites, ZA_NaOH 0.50 M and ZX_NaOH 0.10 M, (**Table 3.6** and **Table 3.7**)**,** it is noticeable that the LTA zeolite have the highest *q* of all tested REE, except for La. The main difference between the LTA and FAU is the connection of the β cages. For the LTA, the β cages are linked via oxygen bridges, which form an α cages [38] with small pores of approximately 4.1 Å [39], while for the FAU, the β cages are linked by double six-membered rings, forming "supercages" [38] with pores approximately of 7.4 Å [39]. The chemical treatment with the alkali solution may justify the alterations in the surface. However, for the ZA_NaOH 0.50 M, the solution pH remained between 5.5 and 6.5, a range in which the REE can precipitate, as mentioned before. Although this zeolite was the best performing LTA, the risk of a possible REE precipitation is high and therefore, it will not be considered in the following sections.

Overall and just based on the adsorption results, the best modified zeolites for the purpose are ZX_NaOH 0.10 M and ZX_KOH 0.10 M. These modified zeolites are the most promising ones to be used in continuous assays. However, it is required to assess their behaviour regarding desorption and the kinetics of both processes, adsorption and desorption.

3.3.2.2. Sorbents selection using ML algorithms

Some ML algorithms were used to select the most suitable modified zeolite to be used in continuous flow assays. Therefore, this analysis used data obtained for each modified zeolite, for the various REE and pH values after 24 h adsorption, as well as the pH_{PZC} values. The collected results are shown in **Figure 3.7**, which show a biplot where the bottom *x* and left *y* are used for the samples distribution, while the top *x* and right *y* are used for the distribution of the different features.

The process starts with a scaling or normalization of the data, that consists in the removal of the mean value and its division by the standard deviation, so the proper weight of the different features may be evaluated. Afterwards, a dimension reduction of the data and cluster samples was performed, accordantly to their similarity using a PCA. The selection of the correct number of features to use is required, so that the weight (variance) of each feature contributing to the PCA may be evaluated. The green circle in **Figure S-3.1A**, shows the selected values**.** The Knee Locator method was also used [40] to confirm the value of selected components. Accordantly to the graph and to the value given by the Knee locator, 2 principal components, PCA 1 and PCA 2, were selected as they explain over 92 % of the sample variation. The features distribution of the data are seen in **Figure 3.7A** that clarifies how they are related to each other, using the *cos* of the angle between the features analyzed and the resulting values (variables with a coefficient correlation close to 1 are directly proportional, while those close to –1 are inversely related). The coefficient correlation between the pH values of the assay (pH_assay) and those of the

treatment pH (pH_treatment) is close to 1. As expected, these values are positively correlated since a higher solution pH of the zeolite chemical treatment should provoke a higher pH during the adsorption assay. Overall, a positive correlation was detected between each REE C/C_0 ratios and the other REE C/C_0 ratios. Nevertheless, when the pH values are correlated with the C/C_0 of the different REE, values closer to −1 are obtained and this shows that as the pH increases, the C/C_0 in the solution decreases.

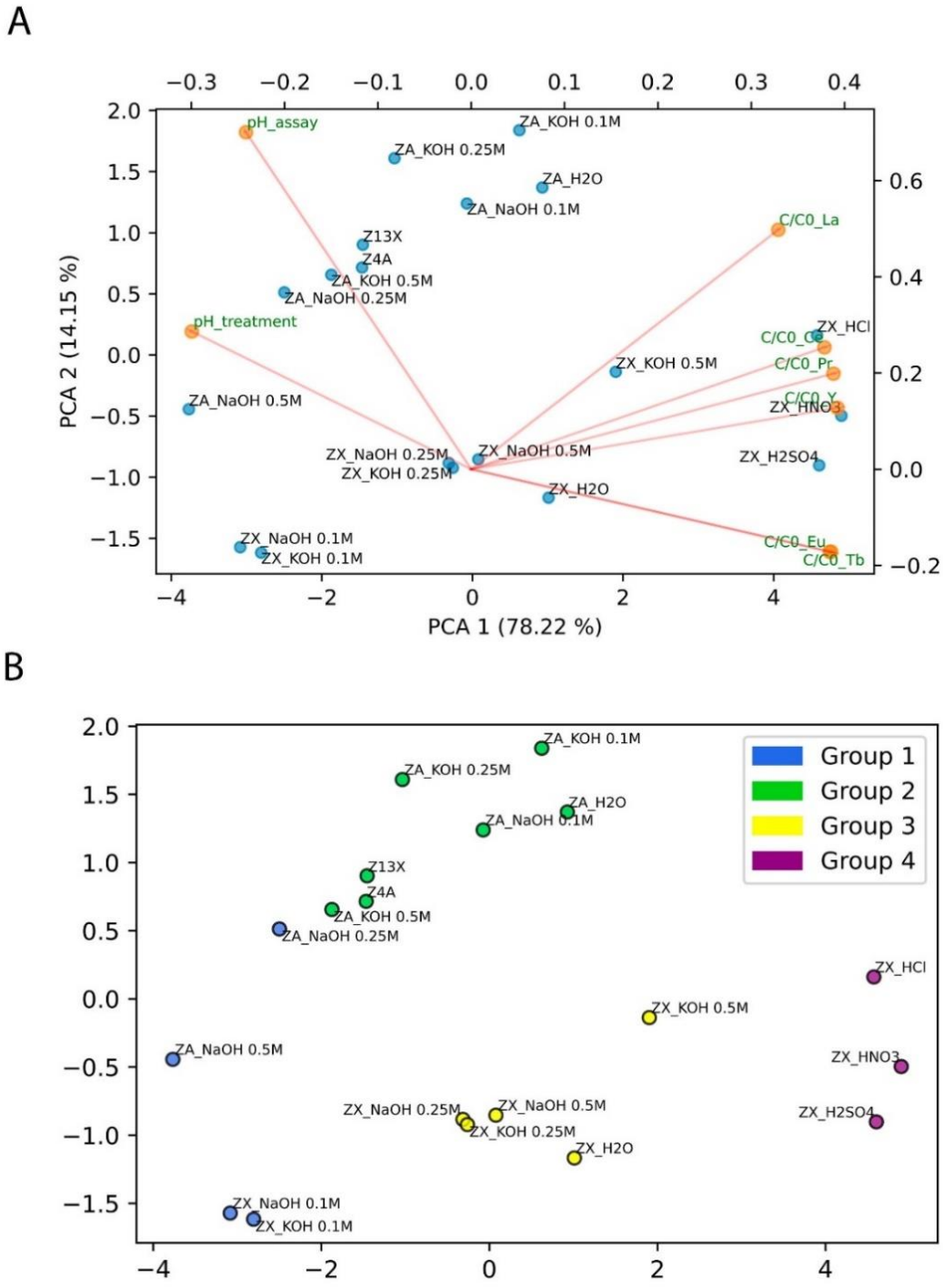

Figure 3.7: Graphical representation ML algorithms analysis of the data obtained at 24 h assay: **A)** PCA analysis and **B)** K-Means algorithm.

The weight of the different features on the behavior of the modified zeolites is described in **Figure 3.7A**. The values of the C/C_0 have high influence on the behavior of the acid treated 13X zeolite, since for these samples the C/C_0 was still high after 24h, meaning that there was little or no adsorption. The same happened with ZX_KOH 0.50 M. The zeolites modified with KOH 0.25 M, NaOH 0.50 M and the ZX_H_2O are closer to the center, showing that none of the features have a relevant influence on the results obtained with those sorbents. On the other hand, the variable pH of the assay has a stronger impact on the behavior of the different modified 4A zeolites and on the Z13X. For ZA_NaOH 0.50 M and ZA_NaOH 0.25 M, the influence of pH_treatment is notorious. The modified zeolites ZX_NaOH 0.1 M and ZX_KOH 0.10 M are in the opposite position of the C/C_0 values, which could be associated with the improved adsorption performance that these modified zeolites.

The data was then processed by the K-Means algorithm, presented in **Figure 3.7B**, to evaluate the number of groups that the zeolite samples can be divided into. The correct number of groups, which was 4, shown in **Figure S-3.1B,** was confirmed using the Knee Locator, as was done for the PCA. Group 4, in purple, shown in **Figure 3.7B**, contains the acid treated zeolites, indicating that these treatments are not the most suitable to improve the adsorption capacity of zeolites with a strong correlation with C/C_0 ratios, as previously suggested by the results shown in **Figure 3.3**. Group 1, highlighted in blue, includes the 13X modified zeolites with NaOH and KOH 0.10 M and the 4A modified with NaOH 0.25 M and 0.50 M. This group is situated in the opposite side of the C/C_0, which is translated into lower C/C_0. In consequence, the zeolites with the best adsorption performance, ZX_NaOH 0.10 M and ZX_KOH 0.10 M (**Figure 3.3**), and the ZA_NaOH 0.50M (**Figure 3.5**) are included in this group. The only unexpected presence in this group is the ZA_NaOH 0.25 M, since it was not included in the group of the best zeolites in the adsorption analysis. However, the ZA_NaOH 0.25 M was the second best zeolite in terms of q values (**Table 3.7**). Group 2, shown in green, includes the others Z4A modified zeolites and Z13X. Group 3, in yellow, has the remaining zeolites 13X. These groups include materials with middle-term adsorption performance, especially zeolites 13X, between a bad performance corresponding to group 4 and a good performance belonging to group 1. The presence of the Z13X in the group dominated by the zeolite 4A indicates that, for these features, the Z13X is more similar to the zeolite 4A than initially thought.

After an assessment of the experimental data using the PCA and K-Means algorithms, the possibility of the modified zeolites classification was verified. Therefore, it was attributed to each sample a binary classification, where 0 is considered bad (the zeolite had low adsorption) and 1 is considered a good performance (the zeolite had a high adsorption), which was made in agreement with **Table 3.2**. The results of this classification are shown in **Figure 3.8**.

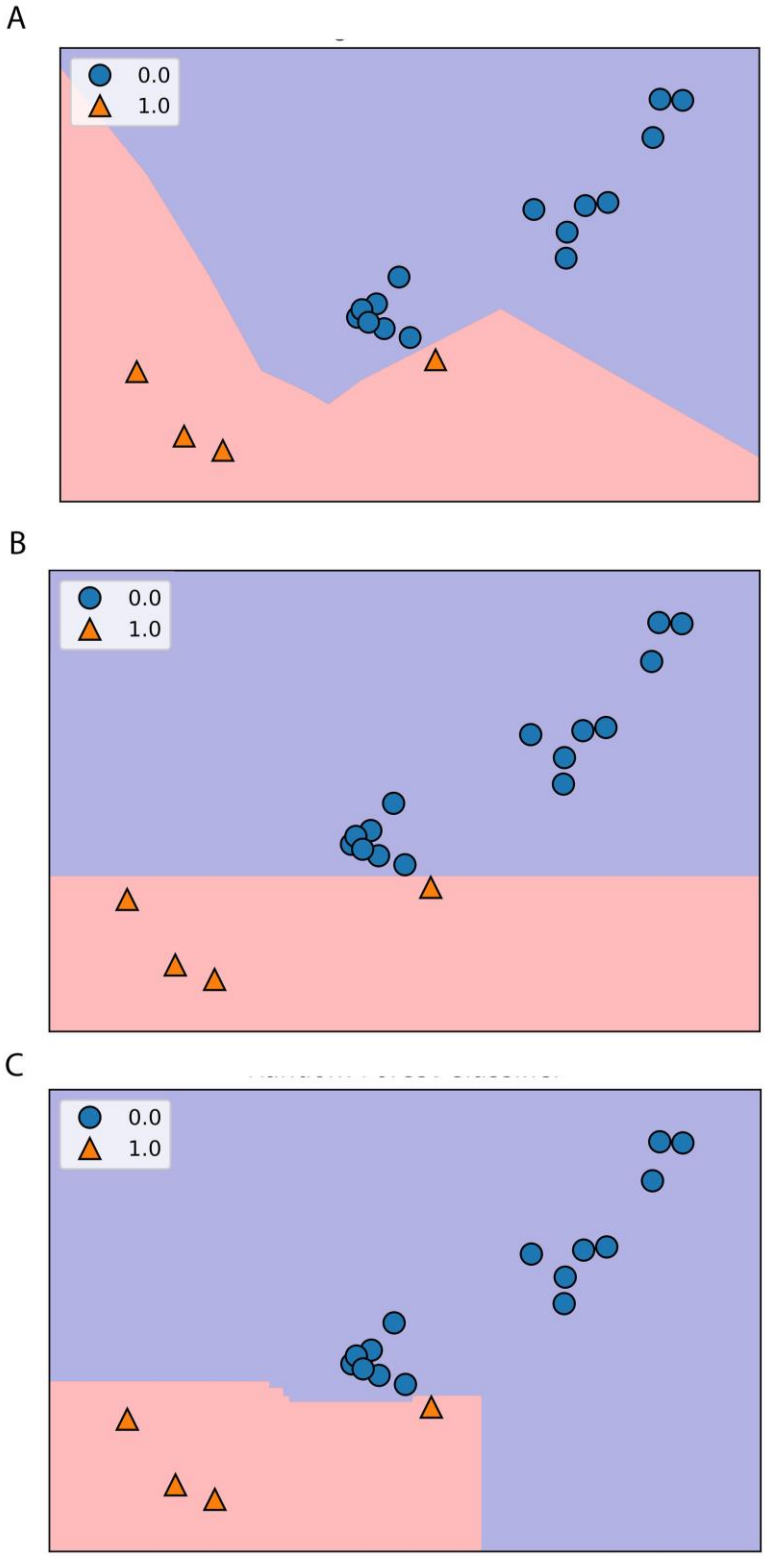

Figure 3.8: Representative display of the classification of the different modified zeolites based on the experimental data obtained after 24 h of assay using ML algorithms. The classification algorithms used were KNN classifier (**A**), Decision Tree classifier (**B**) and Random Forest classifier (**C**). The 1 represents a good adsorbent, while the 0 is a bad adsorbent accordantly to the evaluation performed. The different colors, violet and orange, represent the zone of a good or bad sorbent, respectively.

The classification was performed using 3 different classifiers: KNN, Decision Tree and Random Forest to evaluate its sustainability by using ML. The classification will help to select suitable new materials for REE removal from wastewater using zeolites as adsorbents and may be implemented for other pollutants removal to determine the best approach. The zeolites that had a good classification (binary classification of 1) were ZX_KOH 0.1 M, ZX_NaOH 0.1 M and ZA_NaOH, 0.25 and 0.5 M.

The selection of the best suitable number of neighbors (n_neighbors) by the KNN Classifier, is shown in **Figure S-3.1C**, from which 1 neighbor is selected depending on the accuracy values for both training and test sets. The accuracy for the precision, recall and f1-score for each classifier used and for both test and training sets is determined. The precision of each classifier is related to the probability of making good predictions, which was 100 % for every classifier, as happens for the recall (value of the correctly identified positive predictions) and for f1-score (harmonic mean of the precision and the recall).

In these approaches, it should be noticed that having 100 % accuracy on the training sets with a relatively low value for the test set means that overfitting occurs for the training set, which is not the best-case scenario. The idea of the training set is to get a good generalization of the results and then the model is used for unseen data, a test set, which serves to evaluate the capacity of the model to classify new data. All classifiers presented a 100 % score for the training set. The same value was reached forthe test sets, in terms of precision, recall and f1-scores of the prediction done by the model, considering the actual classification.

These results were validated by the confusion matrix, **Figure 3.9**, that confirms that there were only true positives (the model predicted good adsorption results and the results were actually good, that is the model predicted it was true and it was actually true) and true negatives (the model predicted poor adsorption results and the results were actually poor, that is the model predicted it was false and it was actual false).

Overall, this study shows that it is possible to use ML algorithms to support the selection of the best suitable zeolite for the removal of REE as the models used were able to select the best adsorbents within the starting list with very good metric results.

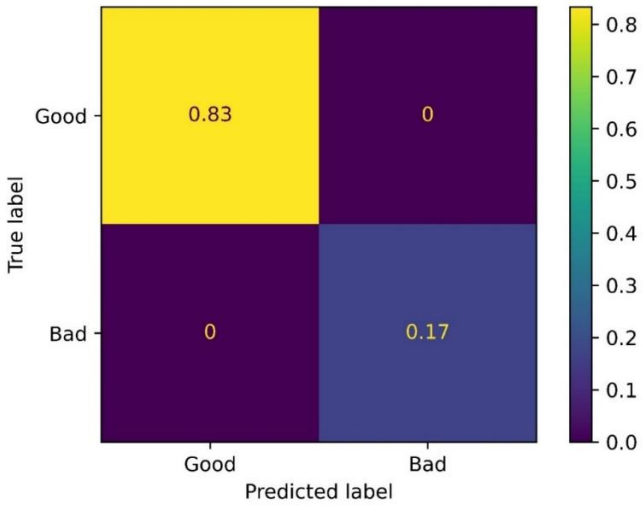

Figure 3.9: Confusion matrix for the test data for the different classifiers. The values shown refer to the fraction of the true correct predictions (when the model got it right) and false incorrect predictions (when the model got it wrong).

3.3.2.3. Predicting unseen data using ML algorithms

The Pearson correlation was calculated from the DataFrame used in the previous analysis and the results are displayed in a heatmap, **Figure 3.10**.

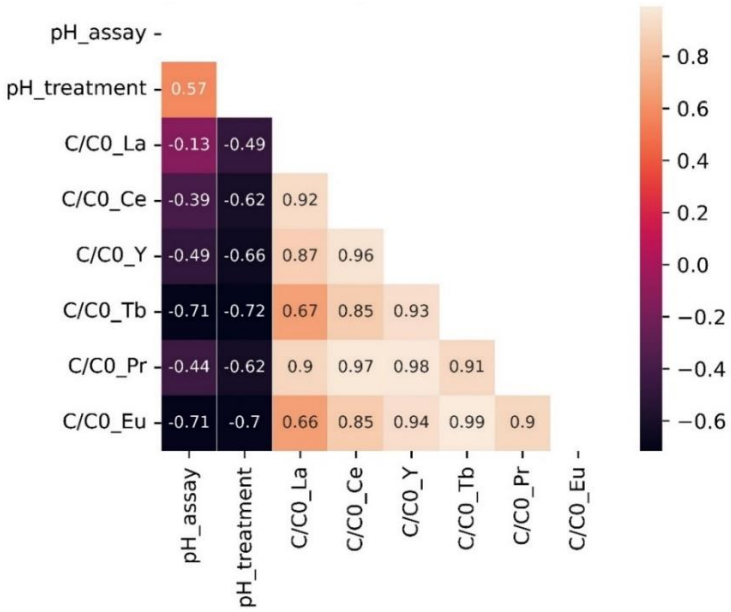

Figure 3.10: Heatmap representing the Pearson correlation between the different features considered in adsorption assays. The left scale represents the different correlation values and the respective colors.

It may be seen that the different pH values (pH_assay and pH_treatment) have a moderate positive correlation (between 0.50 and 0.70) [41]. The pH_assay has a negligible correlation (between

0.00 and - 0.30) [41] with the C/C_0 for La, a low negative correlation (between - 0.30 and - 0.5) [41] with the results for Ce, Y and Pr and a high negative correlation (between -070 and -0.90) [41] with the adsorption of Tb and Eu. It would be expected that C/C_0 would be lower as the pH increases till a certain degree (pH values that do not lead to REE precipitation) and this was verified during the adsorption assays. The pH_treatment had moderate negative correlation (between - 0.50 and - 0.70) with the adsorption of Ce, Y and Pr, a high negative correlation (between -0.70 and -0.90) [41] with Tb and Eu and a low negative correlation (between - 0.30 and - 0.5) with La, following the same explanation as before. The C/C_0 correlation between the REE is high (between 0.70 and 0.90) or very high positive (between 0.70 to 0.90) [41], with 2 exceptions: between La and Tb, 0.67, and between La and Eu, 0.66, which are moderate positive correlations. These results suggest that the entrapment values of the REE have a direct correlation with each other, meaning that for the samples used in this study it could be possible to predict the final C/C_0 of one REE using the known values of another REE. It is essential to mention that the correlation is stronger for REE of the same group, light REE – from La to Gd or heavy REE – from Tb to Lu, including Y [1,2]. Pr presented the best correlation with the other tested REE, with values over 0.9, as shown in **Figure 3.10**. This leads to the possibility of only using Pr to estimate the adsorption values of other REE present in the solution, considering all zeolites tested during 24h assays. The results for the tested linear regressions are shown in **Table 3.8**.

Table 3.8: Regression parameters for the C/C_0 values prediction using Pr (as x) and the other REE (as y).

Metrics and scoring	*Pr vs. La*	*Pr vs. Ce*	*Pr vs. Y*	*Pr vs. Tb*	*Pr vs. Eu*
Mean absolute error (MAE)	0.058	0.018	0.024	0.088	0.089
Mean squared error (MSE)	0.005	0.000	0.001	0.010	0.011
Root mean squared error (RMSE)	0.069	0.021	0.027	0.101	0.104
R^2 for the model explaining test data	0.772	0.984	0.977	0.795	0.801
R^2 for the model explaining training data	0.787	0.931	0.956	0.819	0.804

Table 3.8 displayed different metrics used to evaluate the scoring of the estimation of the C/C_0 of the other REE, once the Pr values are known. MAE is related to the difference between the prediction and the real value of one observation, while the MSE metric is used to measure the quality of the model and RMSE helps to understand the performance of the model. The lower the values for these metrics, the closer are predicted values to the real ones, indicating that the model predictions are good. The R^2 value is also essential, as it validates a good fitting to the data. As shown, the values are higher than 0.77

for both test and training sets, which is good since it reveals a strong correlation. It may be concluded from the overall evaluated metrics that it is possible to determine the residual REE concentrations in solution, just knowing one of them. However, a larger dataset with more samples would allow a better training for the model and would mprove prediction capacity of the model.

Nevertheless, the REE concentrations prediction was tested for a time period using the data obtained with a single zeolite. Two different adsorption periods were considered, 24 h and 125 h , for the ZX_NaOH 0.10 M, which was the best zeolite. As before, a Pearson correlation was made for the different results of the REE C/C_0, as shown in **Figure 3.11**.

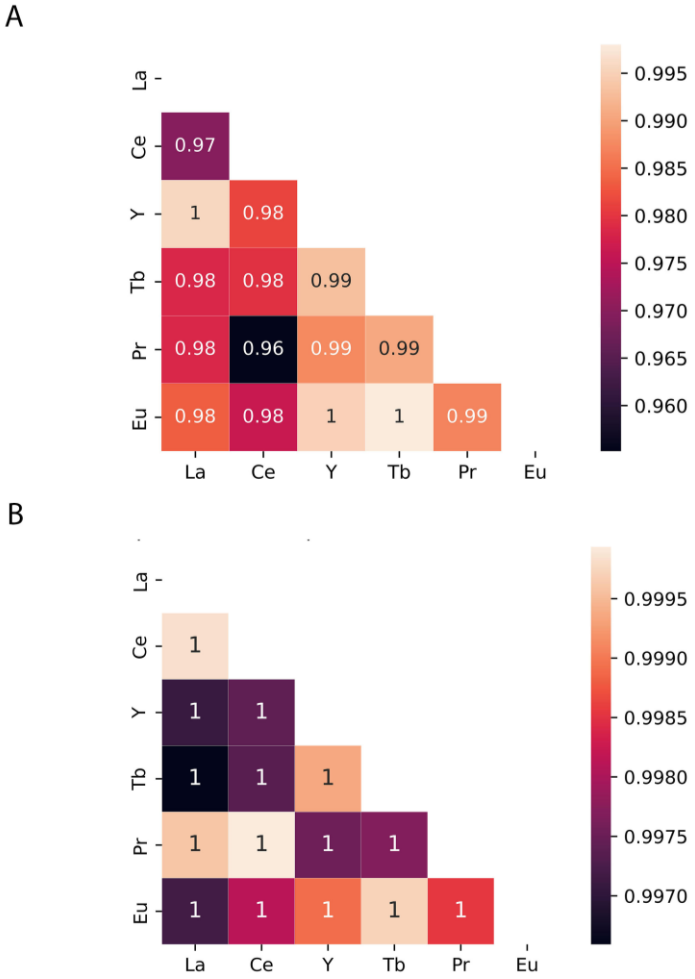

Figure 3.11: Heatmap representation of the Pearson correlations for the different REE after 24 h of contact with the sorbent(**A**) and after 125 h (**B**). The left scale represents the different correlation values and the respective colors.

Figure 3.11A shows the correlations of the C/C_0 of the different REE for the 24 h adsorption period. The correlation values are very high for every REE, including the correlation values obtained with Y, with values above 0.98. In this test, the Y will be used as the x value since this REE presented the

highest correlations with the other REE, with the results shown in **Table 3.9**. Every combination was tested during 125 h assays and the correlation values are shown in **Figure 3.11B**. Pr was used as the *x* value and the results are shown in **Table 3.10.** Comparing the Pearson Correlation values between the 2 assays, the longer tests present a better correlation between the tested REE. That is translated into better metrics and scorings for the models. The methodology was the same as the one performed for the estimation of the C/C_0 values of the zeolite. The data were divided into training and test sets and the metrics were evaluated to assess the model behavior.

Table 3.9: Scoring results for the 24 h adsorption assay regression between the different REE (as y) with Y (as x).

Metrics and scoring	Y vs. La	Y vs. Ce	Y vs. Pr	Y vs. Tb	Y vs. Eu
Mean absolute error (MAE)	0.072	0.081	0.072	0.072	0.072
Mean squared error (MSE)	0.005	0.008	0.005	0.005	0.005
Root mean squared error (RMSE)	0.071	0.089	0.071	0.071	0.071
R^2 for the model explaining test data	0.943	0.762	0.943	0.943	0.943
R^2 for the model explaining training data	0.946	0.907	0.946	0.946	0.946

Table 3.10: Scoring results for the 125 h adsorption assay regression between the different REE (as y) with Pr (as x).

Metrics and scoring	Pr vs. La	Pr vs. Ce	Pr vs. Y	Pr vs. Tb	Pr vs. Eu
Mean absolute error (MAE)	0.011	0.004	0.011	0.011	0.011
Mean squared error (MSE)	0.000	0.000	0.000	0.000	0.000
Root mean squared error (RMSE)	0.000	0.000	0.000	0.000	0.000
R^2 for the model explaining test data	1.000	1.000	1.000	1.000	1.000
R^2 for the model explaining training data	0.998	1.000	0.998	0.998	0.998

The results are much better for the model that used the 125 h adsorption data. That is related to the minor errors and the higher R^2 values for the training and test sets that indicate that the predicted values are closer to the actual values, showing that increasing the measurements number is essential to construct a good model. For the sake of robustness validation, it was decided to use the model obtained from the 125 h assays to predict the C/C_0 values of the REE in the 24 h assay. The C/C_0 values of Pr were used as x, while the rest of the C/C_0 values for the other REE were predicted from the previously

mentioned model. The metrics and respective scorings between the predicted and actual values are shown in **Table 3.11**.

The metrics values in **Table 3.11** are low, showing that the predicted results are very similar to those obtained experimentally. Comparing these metrics to the ones presented in **Table 3.9** it may be concluded that the prediction capacity of the model improved on the base of the 125 h assay.

Table 3.11: Scoring results for estimating the C/C_0 values for the 24 h assay, using the model trained with the 125 h adsorption assay for the different REE (as y) based on Pr (as x).

Metrics and scoring	*Pr vs La*	*Pr vs Ce*	*Pr vs Y*	*Pr vs Tb*	*Pr vs Eu*
Mean absolute error (MAE)	0.054	0.091	0.038	0.043	0.048
Mean squared error (MSE)	0.004	0.013	0.003	0.004	0.003
Root mean squared error (RMSE)	0.063	0.114	0.055	0.063	0.055

It is demonstrated that it is possible to predict the final C/C_0 in solution for any REE, based on the values for one of the sorbates, as well as to predict the C/C_0 values for each REE along time, based on the measurements at one time point. It is demonstrated that it is possible to train and test a model with a robust prediction capacity and reduced associated errors. These models can be further improved and tested to ensure the best possible prediction. In the future, these models could be an excellent help for faster quantification of metal pollutants, REE or heavy metals, eventually some other pollutants in water streams. This could make the quantification of various contaminants in water resources more effortless and faster, leading to quicker treatment.

For the following tests, the selected modified zeolites are ZX_NaOH 0.10 M and ZX_KOH 0.10 M. The other zeolites, namely ZA_NaOH 0.25 and 0.50 M, although with a good potential for the REE removal from wastewater by the classification algorithm, they will not be considered for future assays due to the possible REE precipitation with ZA_NaOH 0.50 M, as previously explained, while ZA_NaOH 0.25 M did not really reach outstanding results during the adsorption. Therefore, only the selected modified zeolites will be used, as well as the controls, on the leaching assays and on the adsorption kinetics determination.

3.3.3.Leaching of REE

The selected modified zeolites prepared by alkali treatments were used for the evaluation of leaching processes. HCl, H_2SO_4 and HNO_3 solutions, 0.10 M, were used as eluents. The loaded zeolites

were subjected to leaching for 0.5h and circa 80 to 90% of the entrapped REE were recovered by the eluent. This period of contact is the one needed to achieve relevant recovery rates of the tested REE while avoiding any damage to the adsorbent. The recovery results after 0.5 h leaching are shown in **Figure 3.12** for the 13X zeolite.

Water leaching REE recovery (data not shown) from both zeolite structures was less than 5 %. This suggests that the presence of H^+ in the solution is required to enhance the removal of the REE from the zeolite eventually by a cationic exchange with the REE^{2+}.

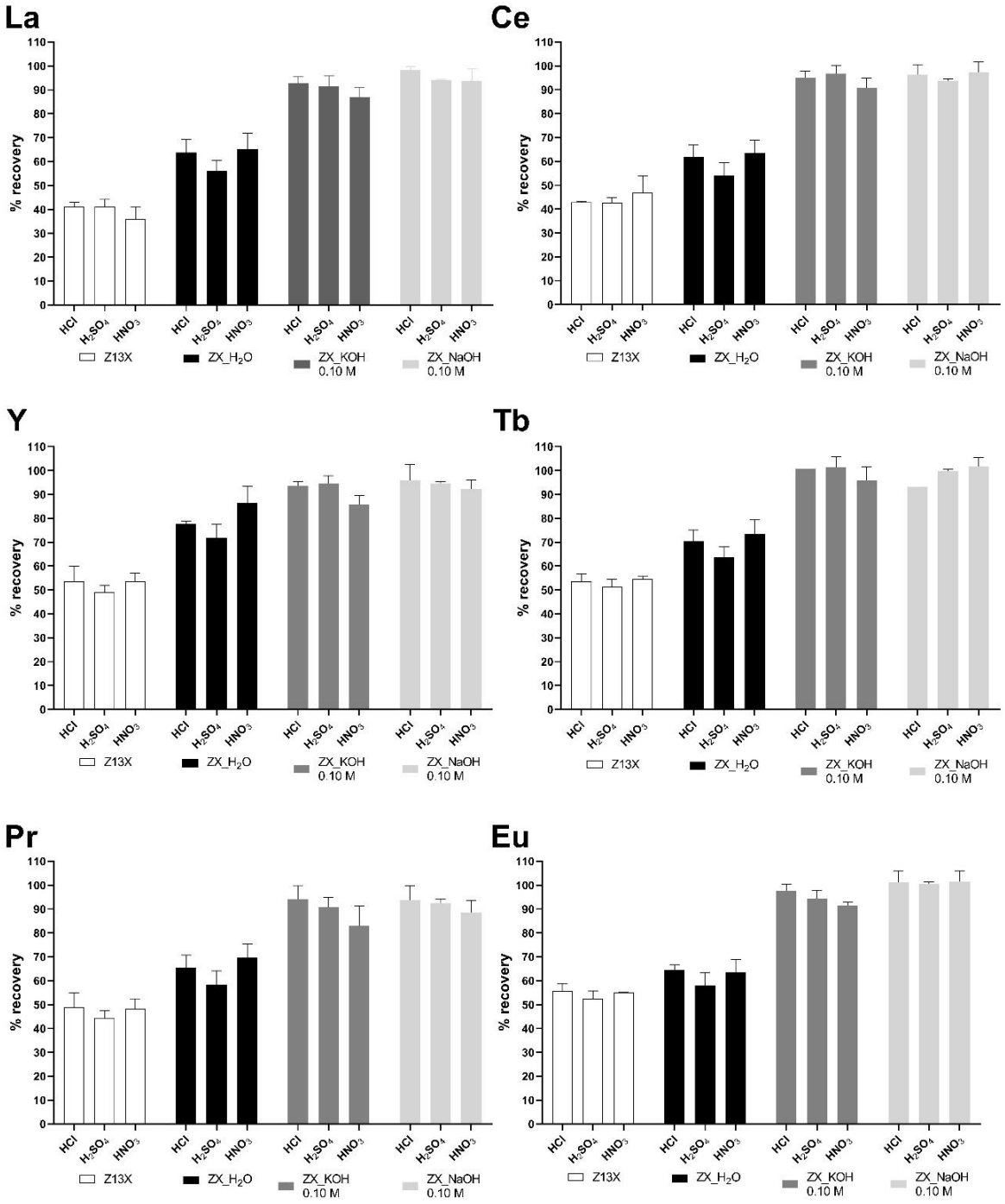

Figure 3.12: Recovery results for Z13X and respective controls, with HCl, H_2SO_4 and HNO_3 aqueous solutions.

Figure 3.12 shows that the zeolites modified with NaOH and KOH 0.10 M had the best recovery, with values near the 100 % for all the tested REE. They differ 40 to 45% from the Z13X and 20 to 35 % from the ZX_H_2O. A statistical analysis of the recovery values was performed and the results are shown in **Table S-3.3**. A significant difference for every REE and eluent was observed when comparing with the control Z13X and with the modified zeolites (NaOH or KOH 0.10 M). In addition, a significant difference was also found for most of the REE and eluents tested when comparing the referred recoveries with the ones obtained with the ZX_H_2O control. As expected, comparing the recovery results obtained with the zeolites treated with NaOH or KOH 0.10 M, no significant difference was observed, **Figure 3.12,** but some differences are seen between the controls ZXH_2O with Z13X. In general, it may be concluded that the initial alkali treatments applied to the zeolites improve their capacity to remove REE from wastewater as well as to recover the sorbates by acid leaching.

The tested eluents led to similar recoveries and present no significant difference between them. Therefore, for future assays, the selected eluent will be a solution of HNO_3 since this acid is weaker than the others and does not represent an environmental threat as the other ones.

A concentration step is the expected step to be performed after the desorption of the REE from the zeolite. Its complexity will depend on its final objective, on the presence of other metals and on the precipitant used. The purification of the individual REE requires a different approach than the recovery of a REE mixture. At the same time, the foreseen application of each element has also to be considered, depending on the anions used for the purpose. Some examples described in the literature include the precipitation with carbonate [42,43], fluoride [44,45], phosphate [46,47], sulfate [48–52] and oxalate [53–57].

3.3.4.Adsorption kinetics

The selected modified zeolites and the respective controls were used in kinetics evaluations to understand the mechanism of the whole process and its dependence on pre-treatments. Two fitting models were tested: the pseudo first-order, PFO, and the pseudo second-order, PSO. The parameters for both models is presented in **Table S-3.4** with the respective confidence intervals in **Table S-3.5** and the graphical representation in **Figure S-3.2**. The best fitting model was selected considering the correlation value, R^2, and the similarity of the q_e values from the model and the ones obtained experimentally. PFO fitted the experimental data better than PSO and assumes that a change of the solute uptake along time is directly proportional to the difference between sorbent saturation and the uptake along time [58]. The fitting parameters are shown in **Table 3.12**.

The q_e is the theoretical capacity of the zeolite to retain REE at equilibrium, the highest one being obtained with ZX_NaOH 0.10 M. This corroborates that for this zeolite, the alkali treatment increased the REE retention as demonstrated before. The k_1 is the affinity constant for the interaction between the REE and the zeolite.

Table 3.12: Fitting parameters for PFO for the modified 13 X zeolites and respective controls.

		ZX_KOH 0.1 M	ZX_NaOH 0.1 M	ZX_H_2O	Z13X
La	DF	22	22	37	21
	k_1	0.043	0.044	0.062	0.046
	q_e	3.346	3.380	3.245	3.364
	R^2	0.975	0.969	0.962	0.984
Ce	DF	21	26	26	21
	k_1	0.063	0.033	0.099	0.059
	q_e	2.813	4.442	3.220	3.747
	R^2	0.951	0.986	0.925	0.983
Y	DF	22	22	37	32
	k_1	0.051	0.045	0.059	0.045
	q_e	2.971	2.934	2.809	2.681
	R^2	0.964	0.974	0.958	0.970
Tb	DF	26	19	29	23
	k_1	0.046	0.048	0.052	0.032
	q_e	3.231	3.063	3.391	3.211
	R^2	0.962	0.967	0.970	0.945
Pr	DF	17	26	30	23
	k_1	0.056	0.040	0.075	0.042
	q_e	2.822	3.094	2.753	2.823
	R^2	0.982	0.985	0.977	0.962
Eu	DF	19	20	30	20
	k_1	0.056	0.044	0.055	0.029
	q_e	3.011	3.824	3.773	3.939
	R^2	0.969	0.980	0.962	0.949

DF – degrees of freedom; q_e – adsorption capacity at equilibrium calculated from the fitting (mg/g); k_1 – affinity constant of the pseudo-first order model (min^{-1}); R^2 – coefficient correlation.

The kinetic parameters for REE adsorption by ZX_NaOH 0.10 M were compared with the ones obtained with other inorganic materials and the results are shown in **Table 3.13**. ZX_NaOH 0.10 M has one of the highest q_e values among the considered sorbents and the kinetic parameters indicate a faster interaction of that modified zeolite with the REE in solution. The ratio between the different REE concentrations and the adsorbent concentration certainly also determine the differences noticed.

Table 3.13: The best kinetic model parameters for different inorganic adsorbents for the same REE.

Material	[REE] (mg/L)	[Adsorbent] (g/L)	Conditions	La	Ce	Y	Tb	Pr	Eu	Ref
Z13X ZX_NaOH 0.10 M	10	3	Non linear modulation; REE in water solution; zeolite pre-treated with NaOH 0.10 M	PFO: k_1 = 0.043; q_e = 3.346; R^2 = 0.975	PFO: k_1 = 0.063; q_e = 2.813; R^2 = 0.951	PFO: k_1 = 0.051; q_e = 2.971; R^2 = 0.964	PFO: k_1 = 0.046; q_e = 3.231; R^2 = 0.962	PFO: k_1 = 0.056; q_e = 2.822; R^2 = 0.982	PFO: k_1 = 0.056; q_e= 3.011; R^2 = 0.969	this work
FAU (13X) Zeolite 13X	20	5	Non linear modulation; REE in acetate buffer of 0.1 M solution; no pretreatment	PSO: k_2= 0.05; q_e = 4.35; R^2 = 0.997	PSO: k_2 = 0.039; q_e = 4.1; R^2 = 0.995	PSO: k_2 = 0.026; q_e = 3.64; R^2 = 0.954	PSO: k_2 = 0.033; q_e = 2.5; R^2 = 0.963	PSO: k_2 = 0.023; q_e = 5.13; R^2 = 0.993	PSO: k_2= 0.041; q_e = 2.74; R^2 = 0.955	[9]
Activated carbon AC0; ACK1; ACK3	0.1	0.25	Linear modulation; REE in water solution; without pretreatment (ACK0) and with KMnO4 at 0.01 (ACK1) and 0.03 mol/L (ACK3)	PSO: k_2= 0.129; q_e= 0.084; R^2 = 0.995		PSO: k_2 = 0.079; q_e = 0.094; R^2 = 0.993			PSO: k_2 = 0.063; q_e = 0.079; R^2 = 0.994	[16]
				PSO: k_2 = 0.232; q_e = 0.093; R^2 = 0.999		PSO: k_2 = 0.235; q_e = 0.098; R^2 = 1			PSO: k_2 = 0.203; q_e = 0.101; R^2 = 0.998	
				PSO: k_2 = 0.26; q_e = 0.1; R^2 = 0.999		PSO: k_2 = 0.272; q_e = 0.103; R^2 = 0.999			PSO: k_2= 0.402; q_e = 0.104; R^2 = 1	
Natural zeolite	2	10	Linear modulation; REE in water solution; no pretreatment	PSO: k_2 = 1.84; q_e = 0.47; R^2 = 0.99	PSO: k_2 = 1.78; q_e = 0.43; R^2 = 0.99	PSO: k_2 = 1.56; q_e = 0.46; R^2 = 0.99		PSO: k_2 = 3.54; q_e= 0.44; R^2 = 0.99	PSO: k_2 = 2.77; q_e= 0.45; R^2 = 0.99	[17]
Bentonite		5		PSO: k_2 = 98.4; q_e= 0.5; R^2 = 0.99	PSO: k_2 = 23.9; q_e= 0.45; R2 = 0.99	PSO: k_2 = 162; q_e = 0.49; R^2 = 0.99		PSO: k_2 = 36; q_e = 0.45; R^2 = 0.99	PSO: k_2 = 3126; q_e = 0.47; R^2 = 0.99	

[REE] — REE concentration; [Adsorbent] — adsorbent concentration; PFO – Pseud- First Order model; PSO – Pseudo-Second Order model; q_e — adsorption uptake at equilibrium calculated from the fitting (mg/g); k_1— affinity constant of the pseudo-first order model (min^{-1}); k_2 — affinity constant of the pseudo-second order model ($g \cdot mg^{-1} \cdot min^{-1}$); R^2 — correlation coefficient

3.4. Conclusions

The REE adsorption capacities of the FAU (13X) and the LTA (4A) zeolites were assessed after surface chemical treatments by acid and base solutions and the alkali treatment enhanced the REE recovery from aqueous solutions. The best results were obtained with alkali treatment for both zeolites, with 0.10 M NaOH for zeolite 13X and 0.50 M NaOH or KOH for zeolite 4A.

ML algorithms help to select the best modified zeolite for REE recovery. It was shown that even with a low number of features (19), it is possible to develop a model for classification and regression, successfully predicting the unseen data. These models can be further developed with more critical features, with more data and even with different algorithm parameters, promoting a better understanding of the process and, therefore, an improved model.

The best recoveries were obtained after 0.5 h desorption with diluted acids but there was almost no leaching of REE when the eluent was water. A significant improvement in the recoveries was detected when comparing the pre-treated zeolite with the controls. HNO_3 eluent at 0.10 M was selected for further assays because it presents good recoveries and is a weaker acid when compared to the others tested.

ZX_NaOH 0.10 M presented the best parameters in terms of the tested kinetic models, showing an overall improvement in both capacity and rate compared to the untreated zeolites. Therefore, this designed sorbent can be used in continuous flow assays to test its capacity for adsorption and desorption for REE recovery from wastewater.

3.5. References

1. Anastopoulos, I.; Bhatnagar, A.; Lima, E.C. Adsorption of rare earth metals: A review of recent literature. *J. Mol. Liq.* **2016**, *221*, 954–962.
2. Moldoveanu, G.A.; Papangelakis, V.G. Recovery of rare earth elements adsorbed on clay minerals: I. Desorption mechanism. *Hydrometallurgy* **2012**, *117–118*, 71–78.
3. Zhao, F.; Repo, E.; Meng, Y.; Wang, X.; Yin, D.; Sillanpää, M. An EDTA-β-cyclodextrin material for the adsorption of rare earth elements and its application in preconcentration of rare earth elements in seawater. *J. Colloid Interface Sci.* **2016**, *465*, 215–224.
4. Goodenough, K.M.; Schilling, J.; Jonsson, E.; Kalvig, P.; Charles, N.; Tuduri, J.; Deady, E.A.; Sadeghi, M.; Schiellerup, H.; Müller, A.; et al. Europe's rare earth element resource potential: An overview of REE metallogenetic provinces and their geodynamic setting. *Ore Geol. Rev.* **2016**, *72*, 838–856.
5. EPA Rare Earth Elements : A Review of Production , Processing , Recycling, and Associated Environmental Issues. *United States Environ. Prot. Agency* **2012**.
6. Peelman, S.; Kooijman, D.; Sietsma, J.; Yang, Y. Hydrometallurgical Recovery of Rare Earth Elements from Mine Tailings and WEEE. *J. Sustain. Metall.* **2018**, *4*, 367–377.
7. Otto, R.; Wojtalewicz-Kasprzak, A. Patent. Method for Recovery of Rare Earths from Fluorescent Lamps 2014, 1–11.

8. Lyman, J.W.; Palmer, G.R. Recycling of Rare Earths and Iron from NdFeB Magnet Scrap. *High Temp. Mater. Process.* **1993**, *11*, 175–188.
9. Barros, Ó.; Costa, L.; Costa, F.; Lago, A.; Rocha, V.; Vipotnik, Z.; Silva, B.; Tavares, T. Recovery of Rare Earth Elements from Wastewater Towards a Circular Economy. *Molecules* **2019**, *24*, 1005.
10. Yang, F.; Kubota, F.; Baba, Y.; Kamiya, N.; Goto, M. Selective extraction and recovery of rare earth metals from phosphor powders in waste fluorescent lamps using an ionic liquid system. *J. Hazard. Mater.* **2013**, *254–255*, 79–88.
11. Gutiérrez-Gutiérrez, S.C.; Coulon, F.; Jiang, Y.; Wagland, S. Rare earth elements and critical metal content of extracted landfilled material and potential recovery opportunities. *Waste Manag.* **2015**, *42*, 128–136.
12. Lee, S.-Y.; Choi, H.-J. Persimmon leaf bio-waste for adsorptive removal of heavy metals from aqueous solution. *J. Environ. Manage.* **2018**, *209*, 382–392.
13. Nguyen, T.C.; Loganathan, P.; Nguyen, T.V.; Kandasamy, J.; Naidu, R.; Vigneswaran, S. Adsorptive removal of five heavy metals from water using blast furnace slag and fly ash. *Environ. Sci. Pollut. Res.* **2018**, *25*, 20430–20438.
14. Xi, Z.; Chen, B. Removal of polycyclic aromatic hydrocarbons from aqueous solution by raw and modified plant residue materials as biosorbents. *J. Environ. Sci.* **2014**, *26*, 737–748.
15. Yakout, S.M.; Daifullah, A.A.M. Removal of selected polycyclic aromatic hydrocarbons from aqueous solution onto various adsorbent materials. *Desalin. Water Treat.* **2013**, *51*, 6711–6718.
16. Kano, N.; Pang, M.; Deng, Y.; Imaizumi, H. Adsorption of Rare Earth Elements (REEs) onto Activated Carbon Modified with Potassium Permanganate (KMnO4). *J. Appl. Solut. Chem. Model.* **2017**, *6*, 51–61.
17. Mosai, A.K.; Chimuka, L.; Cukrowska, E.M.; Kotzé, I.A.; Tutu, H. The Recovery of Rare Earth Elements (REEs) from Aqueous Solutions Using Natural Zeolite and Bentonite. *Water, Air, Soil Pollut.* **2019**, *230*, 188.
18. Silva, B.; Figueiredo, H.; Quintelas, C.; Neves, I.C.; Tavares, T. Zeolites as supports for the biorecovery of hexavalent and trivalent chromium. *Microporous Mesoporous Mater.* **2008**, *116*, 555–560.
19. Silva, B.; Figueiredo, H.; Soares, O.S.G.P.; Pereira, M.F.R.; Figueiredo, J.L.; Lewandowska, A.E.; Bañares, M.A.; Neves, I.C.; Tavares, T. Evaluation of ion exchange-modified Y and ZSM5 zeolites in Cr(VI) biosorption and catalytic oxidation of ethyl acetate. *Appl. Catal. B Environ.* **2012**, *117–118*, 406–413.
20. Martins, A.; Neves, V.; Moutinho, J.; Nunes, N.; Carvalho, A.P. Friedel-Crafts acylation reaction over hierarchical Y zeolite modified through surfactant mediated technology. *Microporous Mesoporous Mater.* **2021**, *323*, 111167.
21. Figueiredo, H.; Silva, B.; Quintelas, C.; Pereira, M.F.R.; Neves, I.C.; Tavares, T. Biosorption of hexavalent chromium based on modified y zeolites obtained by alkali-treatment. *Environ. Eng. Manag. J.* **2010**, *9*, 305–311.
22. Zou, C.; Sha, G.; Gu, H.; Huang, Y.; Niu, G. Facile solvothermal post-treatment to improve hydrothermal stability of mesoporous SBA-15 zeolite. *Chinese J. Catal.* **2015**, *36*, 1350–1357.
23. Qiu, Q.; Jiang, X.; Lv, G.; Chen, Z.; Lu, S.; Ni, M.; Yan, J.; Deng, X. Adsorption of heavy metal ions using zeolite materials of municipal solid waste incineration fly ash modified by microwave-assisted hydrothermal treatment. *Powder Technol.* **2018**, *335*, 156–163.
24. Müller, A.C.; Guido, S. *Introduction to Machine Learning with Python and Scikit-Learn*; 2015; ISBN 9781449369415.
25. Lin, J.; Wang, L. Comparison between linear and non-linear forms of pseudo-first-order and pseudo-second-order adsorption kinetic models for the removal of methylene blue by activated

carbon. *Front. Environ. Sci. Eng. China* **2009**, *3*, 320–324.
26. Chowdhury, S.; Saha, P. Pseudo-Second-Order Kinetic Model for Biosorption of Methylene Blue onto Tamarind Fruit Shell: Comparison of Linear and Nonlinear Methods. *Bioremediat. J.* **2010**, *14*, 196–207.
27. Chowdhury, S.; Das Saha, P. Comparative Analysis of Linear and Nonlinear Methods of Estimating the Pseudo-Second-Order Kinetic Parameters for Sorption of Malachite Green onto Pretreated Rice Husk. *Bioremediat. J.* **2011**, *15*, 181–188.
28. Ayawei, N.; Ebelegi, A.N.; Wankasi, D. Modelling and Interpretation of Adsorption Isotherms. *J. Chem.* **2017**, *2017*, 1–11.
29. Lataye, D.H.; Mishra, I.M.; Mall, I.D. Adsorption of 2-picoline onto bagasse fly ash from aqueous solution. *Chem. Eng. J.* **2008**, *138*, 35–46.
30. Kumar, K.V.; Porkodi, K.; Rocha, F. Isotherms and thermodynamics by linear and non-linear regression analysis for the sorption of methylene blue onto activated carbon: Comparison of various error functions. *J. Hazard. Mater.* **2008**, *151*, 794–804.
31. Boroglu, M.S.; Gurkaynak, M.A. Fabrication and characterization of silica modified polyimide–zeolite mixed matrix membranes for gas separation properties. *Polym. Bull.* **2011**, *66*, 463–478.
32. Wang, W.; Zhang, W.; Chen, H.; Zhang, S.; Li, J. Synergistic effect of synthetic zeolites on flame-retardant wood-flour/polypropylene composites. *Constr. Build. Mater.* **2015**, *79*, 337–344.
33. Aronne, A.; Esposito, S.; Ferone, C.; Pansini, M.; Pernice, P. FTIR study of the thermal transformation of barium-exchanged zeolite A to celsian. *J. Mater. Chem.* **2002**, *12*, 3039–3045.
34. Mozgawa, W.; Król, M.; Barczyk, K. FT-IR studies of zeolites from different structural groups. *Chemik* **2011**, *65*.
35. Kuźniarska-Biernacka, I.; Biernacki, K.; Magalhães, A.L.; Fonseca, A.M.; Neves, I.C. Catalytic behavior of 1-(2-pyridylazo)-2-naphthol transition metal complexes encapsulated in Y zeolite. *J. Catal.* **2011**, *278*, 102–110.
36. Voncken, J.H.L. Physical and Chemical Properties of the Rare Earths. In *The Rare Earth Elements - An Introduction*; Springer, Cham, 2016; pp. 53–72 ISBN 978-3-319-26809-5.
37. Shannon, R.D. Revised effective ionic radii and systematic studies of interatomic distances in halides and chalcogenides. *Acta Crystallogr. Sect. A* **1976**, *32*, 751–767.
38. McCusker, L.B.; Baerlocher, C. Chapter 3: Zeolite structures. In *Studies in Surface Science and Catalysis*; Elsevier, 2001; Vol. 137, pp. 37–67.
39. Luna, F.J. Modificação de zeólitas para uso em catálise. *Divulg. Quim. Nov.* **2001**, *24*, 885–892.
40. Satopaa, V.; Albrecht, J.; Irwin, D.; Raghavan, B. Finding a "Kneedle" in a Haystack: Detecting Knee Points in System Behavior. In Proceedings of the 2011 31st International Conference on Distributed Computing Systems Workshops; IEEE, 2011; pp. 166–171.
41. Mukaka, M.M. Statistics corner: A guide to appropriate use of correlation coefficient in medical research. *Malawi Med. J.* **2012**, *24*, 69–71.
42. de Vasconcellos, M.E.; da Rocha, S.M.R.; Pedreira, W.R.; Queiroz, C.A. da S.; Abrão, A. Solubility behavior of rare earths with ammonium carbonate and ammonium carbonate plus ammonium hydroxide: Precipitation of their peroxicarbonates. *J. Alloys Compd.* **2008**, *451*, 426–428.
43. Kim, P.; Anderko, A.; Navrotsky, A.; Riman, R.E. Trends in Structure and Thermodynamic Properties of Normal Rare Earth Carbonates and Rare Earth Hydroxycarbonates. *Minerals* 2018, *8*.
44. Tokunaga, S.; Haron, M.J.; Wasay, S.A.; Wong, K.F.; Laosangthum, K.; Uchiumi, A. Removal of fluoride ions from aqueous solutions by multivalent metal compounds. *Int. J. Environ. Stud.* **1995**, *48*, 17–28.
45. Yan, C.; Jia, J.; Liao, C.; Wu, S.; Xu, G. Rare Earth Separation in China. *Tsinghua Sci. Technol.* **2006**, *11*, 241–247.

46. Wu, S.; Zhao, L.; Wang, L.; Huang, X.; Zhang, Y.; Feng, Z.; Cui, D. Simultaneous recovery of rare earth elements and phosphorus from phosphate rock by phosphoric acid leaching and selective precipitation: Towards green process. *J. Rare Earths* **2019**, *37*, 652–658.
47. Zakharova, B.; Komissarova, L.; Traskin, V.; Naumov, S.; Melnikov, P. Precipitation of Rare Earth Phosphates from H3PO4 Solutions. *Phosphorus. Sulfur. Silicon Relat. Elem.* **1996**, *111*, 2.
48. Moeller, T.; Kremers, H.E. Observations on Rare Earths Double Sodium Sulfate Precipitation for Separation of the Terbium and Yttrium Earths. *Ind. Eng. Chem. Anal. Ed.* **1945**, *17*, 44–45.
49. Vijayalakshmi, R.; Mishra, S.L.; Singh, H.; Gupta, C.K. Processing of xenotime concentrate by sulphuric acid digestion and selective thorium precipitation for separation of rare earths. *Hydrometallurgy* **2001**, *61*, 75–80.
50. Han, K.N. Effect of Anions on the Solubility of Rare Earth Element-Bearing Minerals in Acids. *Mining, Metall. Explor.* **2019**, *36*, 215–225.
51. Han, K.N. Effect of Metal Complexation on the Solubility of Rare Earth Compounds. In *Critical and Rare Earth Elements*; CRC Press, 2019; pp. 59–84 ISBN 9780429023545.
52. Ciro, E.; Alzate, A.; López, E.; Serna, C.; Gonzalez, O. Neodymium recovery from scrap magnet using ammonium persulfate. *Hydrometallurgy* **2019**, *186*, 226–234.
53. Ganguli, R.; Cook, D.R. Rare earths: A review of the landscape. *MRS Energy Sustain.* **2018**, *5*, 6.
54. Gupta, C.K.; Krishnamurthy, N. Extractive metallurgy of rare earths. *Int. Mater. Rev.* **1992**, *37*, 197–248.
55. Chi, R.; Xu, Z. A solution chemistry approach to the study of rare earth element precipitation by oxalic acid. *Metall. Mater. Trans. B* **1999**, *30*, 189–195.
56. Khawassek, Y.M.; Eliwa, A.A.; Gawad, E.A.; Abdo, S.M. Recovery of rare earth elements from El-Sela effluent solutions. *J. Radiat. Res. Appl. Sci.* **2015**, *8*, 583–589.
57. He, L.; Xu, Q.; Li, W.; Dong, Q.; Sun, W. One-step separation and recovery of rare earth and iron from NdFeB slurry via phosphoric acid leaching. *J. Rare Earths* **2022**, *40*, 338–344.
58. Sahoo, T.R.; Prelot, B. Adsorption processes for the removal of contaminants from wastewater. In *Nanomaterials for the Detection and Removal of Wastewater Pollutants*; Elsevier, 2020; pp. 161–222 ISBN 9780128184899.

3.6. Supplementary material

Table S-3.1 Statistical differences using the Bonferroni's multiple comparisons test between the modified zeolite and the controls (Z13X and ZX_H_2O).

REE	Modified zeolite	Significantly different from	
		ZX_H_2O	Z13X
La	ZX_KOH 0.10 M	No (ns)	No (ns)
	ZX_KOH 0.25 M	No (ns)	No (ns)
	ZX_KOH 0.50 M	No (ns)	No (ns)
	ZX_NaOH 0.10 M	No (ns)	No (ns)
	ZX_NaOH 0.25 M	No (ns)	No (ns)
	ZX_NaOH 0.50 M	No (ns)	No (ns)
	ZX_H_2SO_4 0.25 M	No (ns)	No (ns)
	ZX_HCl 0.25 M	Yes (*)	Yes (*)
	ZX_HNO_3 0.25 M	Yes (*)	Yes (*)
Ce	ZX_KOH 0.10 M	No (ns)	No (ns)
	ZX_KOH 0.25 M	No (ns)	No (ns)
	ZX_KOH 0.50 M	No (ns)	No (ns)
	ZX_NaOH 0.10 M	No (ns)	No (ns)
	ZX_NaOH 0.25 M	No (ns)	No (ns)
	ZX_NaOH 0.50 M	No (ns)	No (ns)
	ZX_H_2SO_4 0.25 M	No (ns)	Yes (**)
	ZX_HCl 0.25 M	Yes (*)	Yes (***)
	ZX_HNO_3 0.25 M	Yes (*)	Yes (**)
Y	ZX_KOH 0.10 M	No (ns)	No (ns)
	ZX_KOH 0.25 M	No (ns)	No (ns)
	ZX_KOH 0.50 M	No (ns)	No (ns)
	ZX_NaOH 0.10 M	No (ns)	No (ns)
	ZX_NaOH 0.25 M	No (ns)	No (ns)
	ZX_NaOH 0.50 M	No (ns)	No (ns)
	ZX_H_2SO_4 0.25 M	No (ns)	Yes (*)
	ZX_HCl 0.25 M	No (ns)	Yes (**)
	ZX_HNO_3 0.25 M	No (ns)	Yes (**)
Tb	ZX_KOH 0.10 M	No (ns)	No (ns)
	ZX_KOH 0.25 M	No (ns)	No (ns)
	ZX_KOH 0.50 M	No (ns)	Yes (*)
	ZX_NaOH 0.10 M	No (ns)	No (ns)
	ZX_NaOH 0.25 M	No (ns)	No (ns)
	ZX_NaOH 0.50 M	No (ns)	No (ns)
	ZX_H_2SO_4 0.25 M	No (ns)	Yes (***)
	ZX_HCl 0.25 M	Yes (*)	Yes (***)
	ZX_HNO_3 0.25 M	Yes (*)	Yes (***)

Pr	ZX_KOH 0.10 M	No (ns)	No (ns)
	ZX_KOH 0.25 M	No (ns)	No (ns)
	ZX_KOH 0.50 M	No (ns)	No (ns)
	ZX_NaOH 0.10 M	No (ns)	No (ns)
	ZX_NaOH 0.25 M	No (ns)	No (ns)
	ZX_NaOH 0.50 M	No (ns)	No (ns)
	ZX_H_2SO_4 0.25 M	No (ns)	Yes (*)
	ZX_HCl 0.25 M	Yes (*)	Yes (**)
	ZX_HNO_3 0.25 M	Yes (*)	Yes (**)
Eu	ZX_KOH 0.10 M	No (ns)	No (ns)
	ZX_KOH 0.25 M	No (ns)	No (ns)
	ZX_KOH 0.50 M	No (ns)	Yes (*)
	ZX_NaOH 0.10 M	No (ns)	No (ns)
	ZX_NaOH 0.25 M	No (ns)	No (ns)
	ZX_NaOH 0.50 M	No (ns)	No (ns)
	ZX_H_2SO_4 0.25 M	No (ns)	Yes (***)
	ZX_HCl 0.25 M	No (ns)	Yes (***)
	ZX_HNO_3 0.25 M	No (ns)	Yes (****)

Table S-3.2: Statistical differences using the Bonferroni's multiple comparisons test between the modified zeolite and the controls (Z4A and ZA_H_2O).

REE	Modified zeolite	Significantly different from	
		ZX_H_2O	Z13X
La	ZA_KOH 0.10 M	No (ns)	No (ns)
	ZA_KOH 0.25 M	No (ns)	No (ns)
	ZA_KOH 0.50 M	No (ns)	Yes (**)
	ZA_NaOH 0.10 M	No (ns)	No (ns)
	ZA_NaOH 0.25 M	No (ns)	Yes (*)
	ZA_NaOH 0.50 M	Yes (*)	Yes (****)
Ce	ZA_KOH 0.10 M	No (ns)	No (ns)
	ZA_KOH 0.25 M	No (ns)	No (ns)
	ZA_KOH 0.50 M	No (ns)	Yes (**)
	ZA_NaOH 0.10 M	No (ns)	No (ns)
	ZA_NaOH 0.25 M	No (ns)	Yes (***)
	ZA_NaOH 0.50 M	Yes (**)	Yes (****)
Y	ZA_KOH 0.10 M	No (ns)	No (ns)
	ZA_KOH 0.25 M	No (ns)	Yes (***)
	ZA_KOH 0.50 M	No (ns)	Yes (**)
	ZA_NaOH 0.10 M	No (ns)	No (ns)
	ZA_NaOH 0.25 M	Yes (*)	Yes (****)
	ZA_NaOH 0.50 M	Yes (**)	Yes (****)
Tb	ZA_KOH 0.10 M	No (ns)	No (ns)
	ZA_KOH 0.25 M	Yes (**)	Yes (***)
	ZA_KOH 0.50 M	No (ns)	Yes (**)
	ZA_NaOH 0.10 M	No (ns)	No (ns)
	ZA_NaOH 0.25 M	Yes (***)	Yes (****)
	ZA_NaOH 0.50 M	Yes (**)	Yes (***)
Pr	ZA_KOH 0.10 M	No (ns)	No (ns)
	ZA_KOH 0.25 M	No (ns)	No (ns)
	ZA_KOH 0.50 M	No (ns)	Yes (**)
	ZA_NaOH 0.10 M	No (ns)	No (ns)
	ZA_NaOH 0.25 M	Yes (*)	Yes (***)
	ZA_NaOH 0.50 M	Yes (**)	Yes (****)
Eu	ZA_KOH 0.10 M	No (ns)	No (ns)
	ZA_KOH 0.25 M	Yes (**)	Yes (***)
	ZA_KOH 0.50 M	Yes (*)	Yes (**)
	ZA_NaOH 0.10 M	No (ns)	No (ns)
	ZA_NaOH 0.25 M	Yes (****)	Yes (****)
	ZA_NaOH 0.50 M	Yes (**)	Yes (***)

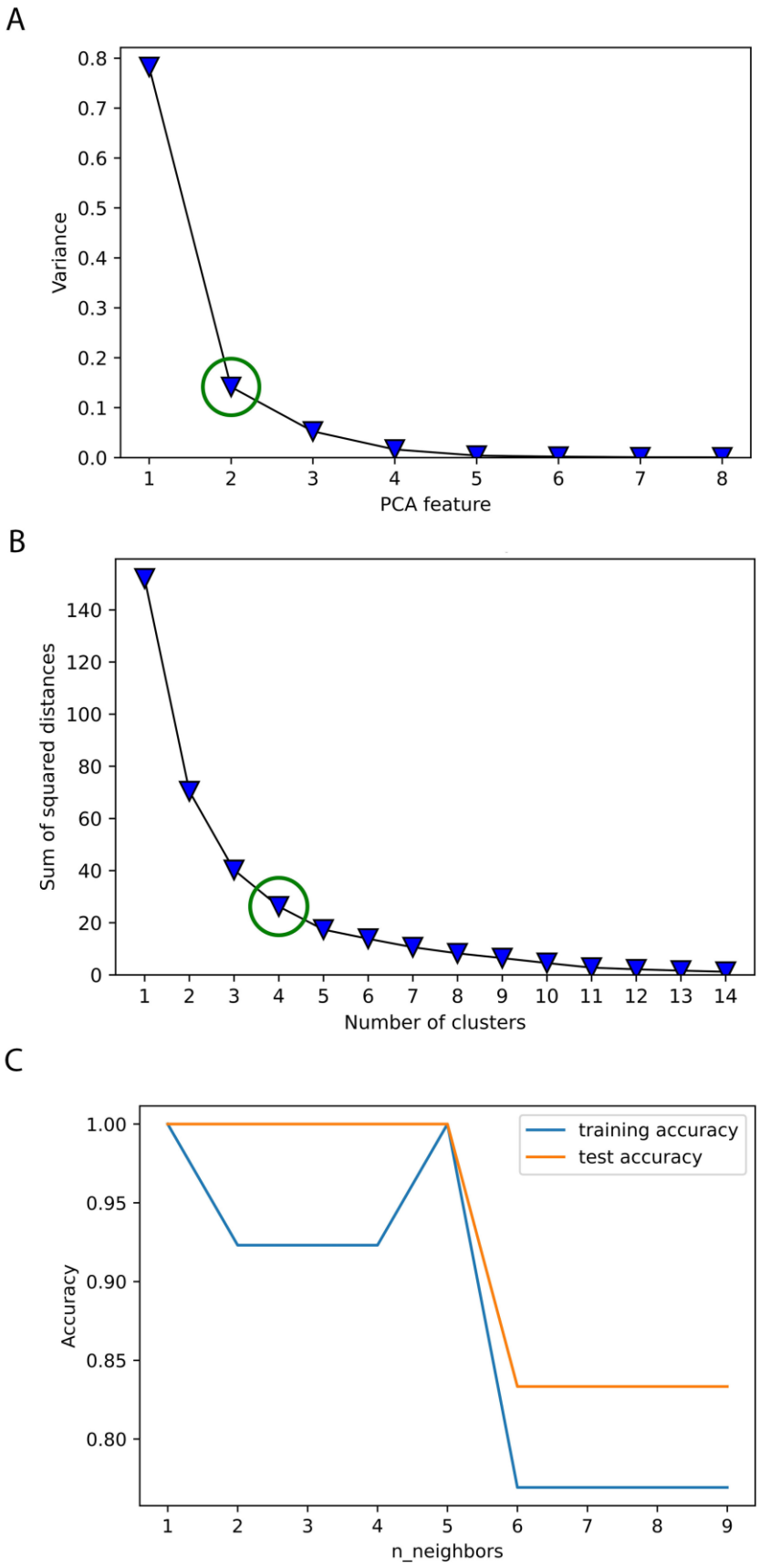

Figure S-3.1: Graphical representation of the elbow method to select the best option: **A)** PCA, **B)** K-Means and **C)** KNN Classifier accuracy for the training and test sets.

Table S-3.3: Statistical resume for the desorption from Z13X. A multi-comparison test of the results was performed where Y, yes, is used when there is a statistical difference between the conditions tested. N, no, means that there is no statistical difference. This test was performed for the different REE. The order of the results is: La, Ce, Y, Tb, Pr and Eu.

ZX_H_2O	HCl											
	H_2SO_4	N; N; N; N; N; N										
	HNO_3	N; N; N; N; N; N	N; N; N; N; N; N									
ZX_KOH 0.1 M	HCl	Y; Y; Y; Y; Y; Y	Y; N; Y; Y; Y; Y	Y; Y; N; Y; Y; Y								
	H_2SO_4	Y; Y; Y; Y; Y; Y	Y; Y; Y; Y; Y; Y	N; Y; N; Y; Y; Y	N; N; N; N; N; N							
	HNO_3	Y; Y; N; Y; N; Y	Y; Y; N; Y; Y; Y	Y; Y; N; Y; N; Y	N; N; N; N; N; N	N; N; N; N; N; N						
Z13X	HCl	Y; Y; Y; Y; N; N	N; N; Y; N; N; N	Y; Y; Y; Y; Y; N	Y; Y; Y; Y; Y; Y	Y; Y; Y; Y; Y; Y	Y; Y; Y; Y; Y; Y					
	H_2SO_4	Y; Y; Y; Y; Y; Y	Y; N; Y; N; N; N	Y; Y; Y; Y; Y; Y	Y; Y; Y; Y; Y; Y	Y; Y; Y; Y; Y; Y	Y; Y; Y; Y; Y; Y	N; N; N; N; N; N				
	HNO_3	Y; N; Y; Y; N; N	Y; N; Y; N; N; N	Y; Y; Y; Y; Y; N	Y; Y; Y; Y; Y; Y	Y; Y; Y; Y; Y; Y	Y; Y; Y; Y; Y; Y	N; N; N; N; N; N	N; N; N; N; N; N			
ZX_NaOH 0.1 M	HCl	Y; Y; Y; Y; Y; Y	Y; Y; Y; Y; Y; Y	Y; Y; N; Y; Y; Y	N; N; N; N; N; N	N; N; N; N; N; N	N; N; N; N; N; N	Y; Y; Y; Y; Y; Y	Y; Y; Y; Y; Y; Y	Y; Y; Y; Y; Y; Y		
	H_2SO_4	Y; Y; Y; Y; Y; Y	Y; Y; Y; Y; Y; Y	Y; Y; N; Y; Y; Y	N; N; N; N; N; N	N; N; N; N; N; N	N; N; N; N; N; N	Y; Y; Y; Y; Y; Y	Y; Y; Y; Y; Y; Y	Y; Y; Y; Y; Y; Y	N; N; N; N; N; N	
	HNO_3	Y; Y; N; Y; Y; Y	Y; Y; Y; Y; Y; Y	Y; Y; N; Y; Y; Y	N; N; N; N; N; N	N; N; N; N; N; N	N; N; N; N; N; N	Y; Y; Y; Y; Y; Y	Y; Y; Y; Y; Y; Y	Y; Y; Y; Y; Y; Y	N; N; N; N; N; N	N; N; N; N; N; N
		HCl	H_2SO_4	HNO_3	HCl	H_2SO_4	HNO_3	HCl	H_2SO_4	HNO_3	HCl	H_2SO_4	HNO_3
		ZX_H_2O			ZX_KOH 0.1 M			Z13X			ZX_NaOH 0.1 M		

Table S-3.4: Fitting parameters and square errors for Pseudo-First Order, PFO, and Pseudo-Second Order, PSO, models for the selected modified zeolite 13 X and respective controls.

REE	Zeolite designation	DF	PFO			PSO		
			k_1	q_e	R^2	k_2	q_e	R^2
La	ZX_KOH 0.1 M	22	0.043	3.346	0.975	0.010	4.132	0.963
	ZX_NaOH 0.1 M	22	0.044	3.380	0.969	0.009	4.325	0.951
	ZXH_2O	37	0.062	3.245	0.962	0.022	3.714	0.963
	Z13X	21	0.046	3.364	0.984	0.011	4.093	0.979
Ce	ZX_KOH 0.1 M	21	0.063	2.813	0.951	0.021	3.274	0.922
	ZX_NaOH 0.1 M	26	0.033	4.442	0.986	0.005	5.880	0.983
	ZXH_2O	26	0.099	3.220	0.925	0.036	3.571	0.923
	Z13X	21	0.059	3.747	0.983	0.015	4.436	0.972
Y	ZX_KOH 0.1 M	22	0.051	2.971	0.964	0.015	3.581	0.945
	ZX_NaOH 0.1 M	22	0.045	2.934	0.974	0.011	3.694	0.955
	ZXH_2O	37	0.059	2.809	0.958	0.023	3.235	0.955
	Z13X	32	0.045	2.681	0.970	0.015	3.224	0.963
Tb	ZX_KOH 0.1 M	26	0.046	3.231	0.962	0.011	3.998	0.944
	ZX_NaOH 0.1 M	19	0.048	3.063	0.967	0.013	3.727	0.949
	ZXH_2O	29	0.052	3.391	0.970	0.016	3.973	0.977
	Z13X	23	0.032	3.211	0.945	0.009	3.980	0.963
Pr	ZX_KOH 0.1 M	17	0.056	2.822	0.982	0.017	3.395	0.960
	ZX_NaOH 0.1 M	26	0.040	3.094	0.985	0.010	3.822	0.972
	ZXH_2O	30	0.075	2.753	0.977	0.031	3.116	0.976
	Z13X	23	0.042	2.823	0.962	0.006	4.365	0.970
Eu	ZX_KOH 0.1 M	19	0.056	3.011	0.969	0.016	3.621	0.947
	ZX_NaOH 0.1 M	20	0.044	3.824	0.980	0.009	4.781	0.962
	ZXH_2O	30	0.055	3.773	0.962	0.015	4.418	0.968
	Z13X	20	0.086	2.369	0.950	0.039	2.692	0.949

DF — degrees of freedom; q_e — adsorption uptake at equilibrium calculated from the fitting (mg/g); k_1 — affinity constant of the pseudo first-order model (min^{-1}); k_2 — affinity constant of the pseudo second-order model ($g \cdot mg^{-1} \cdot min^{-1}$); R^2 — coefficient correlation.

Table S-3.5: Confidence intervals for the parameters of Pseudo-First Order, PFO, and Pseudo-Second Order, PSO, kinetic models for every zeolite and REE tested.

REE	Designation		ZX_KOH 0.1 M	ZX_NaOH 0.1 M	ZXH_2O	Z13X
La	DF		22	22	37	21
	PFO	k_1	0.035 to 0.053	0.034 to 0.055	0.053 to 0.073	0.039 to 0.053
		q_e	3.187 to 3.523	3.169 to 3.622	3.139 to 3.356	3.233 to 3.500
	PSO	k_2	0.006 to 0.016	0.005 to 0.015	0.017 to 0.028	0.008 to 0.015
		q_e	3.766 to 4.606	3.834 to 4.993	3.545 to 3.900	3.822 to 4.414
Ce	DF		21	26	26	21
	PFO	k_1	0.049 to 0.080	0.028 to 0.038	0.075 to 0.131	0.051 to 0.069
		q_e	2.640 to 2.993	4.230 to 4.684	3.041 to 3.402	3.596 to 3.906
	PSO	k_2	0.012 to 0.035	0.004 to 0.006	0.02314 to 0.05449	0.011 to 0.021
		q_e	2.939 to 3.675	5.436 to 6.409	3.318 to 3.853	4.122 to 4.797
Y	DF		22	22	37	32
	PFO	k_1	0.041 to 0.064	0.037 to 0.054	0.050 to 0.070	0.038 to 0.052
		q_e	2.815 to 3.136	2.775 to 3.110	2.709 to 2.913	2.578 to 2.790
	PSO	k_2	0.009 to 0.023	0.007 to 0.018	0.017 to 0.031	0.011 to 0.020
		q_e	3.246 to 4.001	3.311 to 4.192	3.067 to 3.424	3.019 to 3.463
Tb	DF		26	19	29	23
	PFO	k_1	0.037 to 0.056	0.039 to 0.059	0.044 to 0.061	0.023 to 0.044
		q_e	3.056 to 3.419	2.873 to 3.266	3.253 to 3.537	2.880 to 3.650
	PSO	k_2	0.006969 to 0.01681	0.007903 to 0.02036	0.01229 to 0.02007	0.005 to 0.014
		q_e	3.618 to 4.471	3.330 to 4.211	3.774 to 4.194	3.529 to 4.579
Pr	DF		17	26	30	23
	PFO	k_1	0.047 to 0.066	0.034 to 0.045	0.066 to 0.086	0.033 to 0.053
		q_e	2.684 to 2.968	2.962 to 3.240	2.671 to 2.837	2.626 to 3.051
	PSO	k_2	0.011 to 0.027	0.007 to 0.012	0.025 to 0.039	0.009 to 0.019
		q_e	3.064 to 3.792	3.676 to 4.347	2.991 to 3.250	3.150 to 3.840
Eu	DF		19	20	30	20
	PFO	k_1	0.045 to 0.068	0.037 to 0.051	0.046 to 0.067	0.021 to 0.040
		q_e	2.827 to 3.207	3.629 to 4.032	3.607 to 3.950	3.505 to 4.530
	PSO	k_2	0.010 to 0.025	0.0057 to 0.013	0.011 to 0.020	0.003 to 0.010
		q_e	3.237 to 4.082	4.313 to 5.348	4.168 to 4.701	4.283 to 5.868

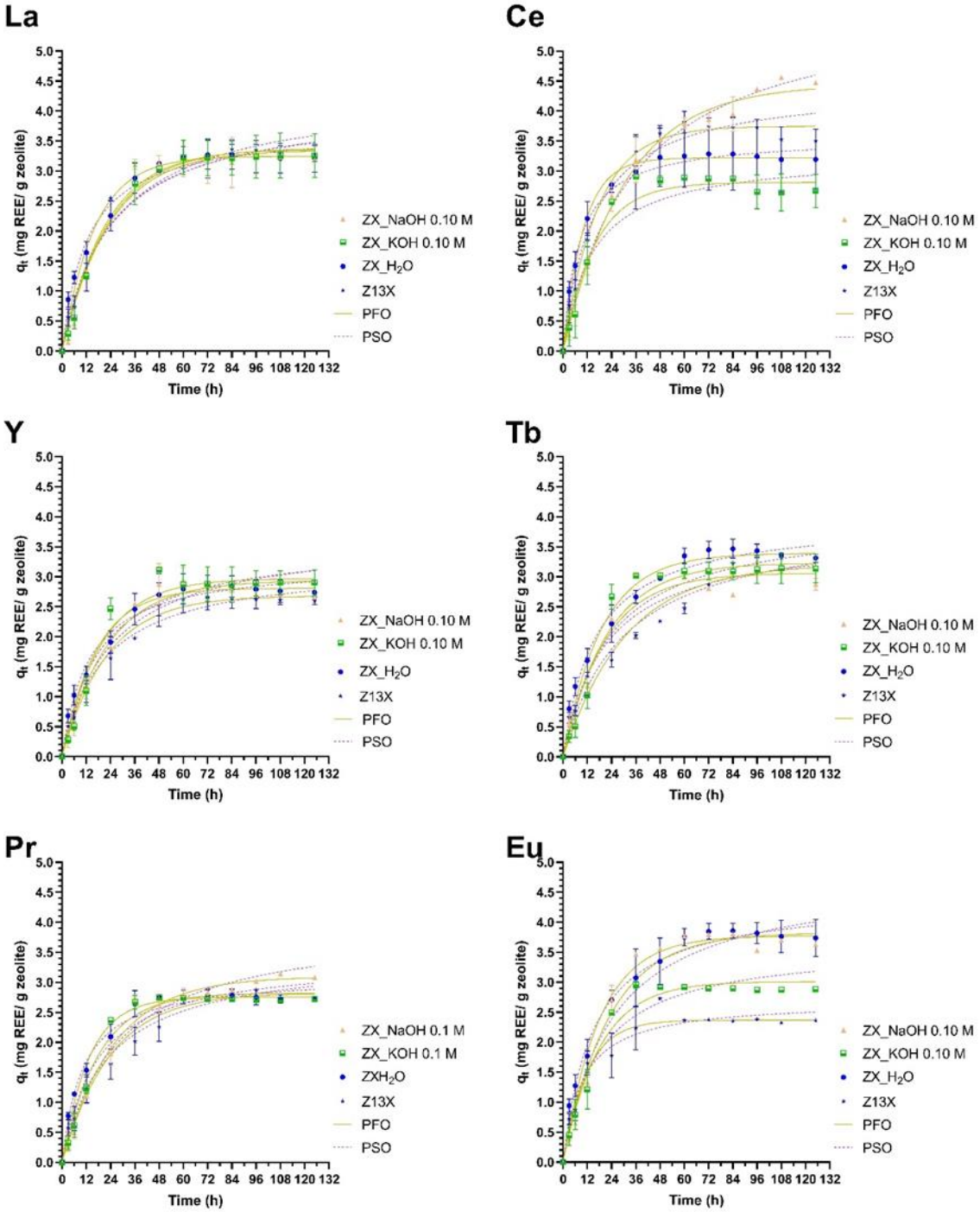

Figure S-3.2: Two kinetic models fitting to the different REE for the 13X zeolite.

Chapter 4 – Exploring optimization of zeolites as adsorbents for Rare Earth Elements in continuous flow assays

Unsupervised machine learning (ML) technique is applied to the characterization of the adsorption of Rare Earth Elements (REE) by zeolites in continuous flow. The successful application of PCA and K-means algorithms from ML allowed a wide range assessment of the adsorption results. This global approach permits the evaluation of the different stages of the sorption cycles and the development of possible optimizations and improvements. The results from ML are also used for the definition of a regression model to estimate other REE recoveries based on the known values of the tested REE. Overall, it was possible to remove more than 70% of all REE from aqueous solutions during the adsorption assays and to recover over 80% for the REE entrapped on the zeolite, using the optimized desorption cycle.

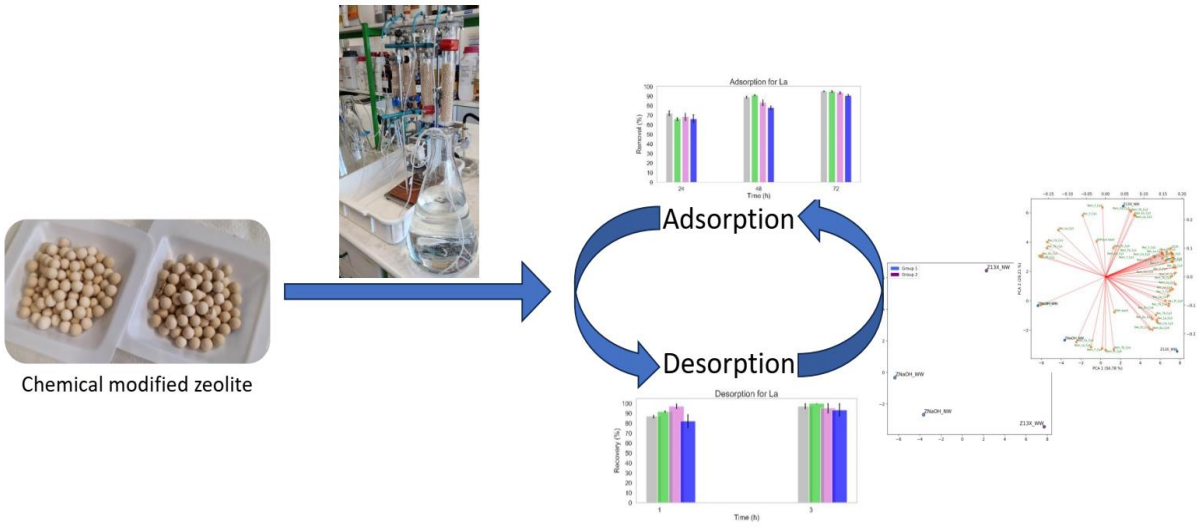

Adapted from: Barros, O.; Parpot, P.; Neves, I. C.; Tavares, T.; Exploring optimization of zeolites as adsorbents for Rare Earth Elements using Supervised Machine Learning techniques – under revision.

4.1. Introduction

The continuous research and progress have resulted in a significant surge of available data, motivating some sectors of our society to reposition themselves and harness the disruptive potential of data analytics and machine learning [1]. Machine learning (ML) is an evolving branch of computational algorithms, whose development led to statistical models that can make predictions and support decisions without being explicitly programmed [2–5]. ML can integrate multimodality multi-fidelity data to reveal correlations between different features [6]. It has been applied successfully in diverse fields such as pattern recognition, medicine, science, computer vision, spacecraft engineering, engineering, biomedicine, psychology, catalysis, neurobiology and many other disciplines [1,5,7]. This wide application allows a faster treatment of great amounts of data and therefore ML can be used to analyze and correlate those data to achieve better interpretations and, therefore, to make better decisions.

ML models and their importance have been recognized and appreciated in wastewater treatment [8–10]. Some developments have been made to use ML algorithms or deep learning neural networks for the optimization of the adsorption of antibiotics [11,12], organic compounds [13,14] and metals [15–17].

The advantages of the ML techniques applied to the recovery of Rare Earth Elements (REE) from aqueous solutions using zeolites as adsorbents are described. REE represents 19% of the metals used in the technology and in the precious metals sectors, which accounts for 0.05% of world metal production and the trend is upwards [18,19]. REE plays a crucial role in the materials industry across various domains such as phosphors, magnets, metallurgy, catalysts and glass since the 1950s. They are frequently employed as additives or dopants in materials formulations. REE are particularly valuable due to their ability to induce significant changes in material properties, even when used in small quantities. Consequently, they have earned the reputation of being the "vitamins" of modern industry and the design of materials doped with rare earths has emerged as indispensable for technological advances [19].

Zeolites are porous aluminosilicate materials known for their highly structured crystalline network composed of alumina and silica tetrahedra (TO_4). The presence of alumina induces a negative charge on the structure that is compensated by cations. Within the zeolitic structures available in the commercial market, zeolites of the LTA type and FAU type (faujasite, including zeolites X and Y) are commonly applied in various fields [20].The FAU structure exhibits a low Si/Al ratio, which results in a high cation exchange capacity mainly for cations with high charge density [20], such as rare earth elements (REE ions). So, this structure present goods properties for adsorption of these metals.

The application of ML algorithms has been applied to REE separation techniques [21] and to adsorption [22]. Therefore, the objective of this study is to optimize the removal of REE (La, Eu, Pr, Ce, Tb and Y) by adsorption on FAU structures in continuous flow assays, employing ML techniques for evaluation and system development.

4.2. Material and Methos

4.2.1.Materials

The materials used in this chapter (REE, zeolite FAU – 13X) are the same as the ones described in **Chapter 3**, **3.2.1 Materials.**

4.2.2.Analytical quantification of REE

The analytical quantification of the REE was performed as explained in the **Chapter 3**, **3.2.4 Analytical quantification of REE**.

4.2.3.Continuous flow assays

The continuous flow assays were carried out using 150 g of zeolite with and without modifications as the bed of column (height of 30 cm and diameter of 4.2 cm) set-ups with up-flow feeding, as represented in **Figure 4.1**.

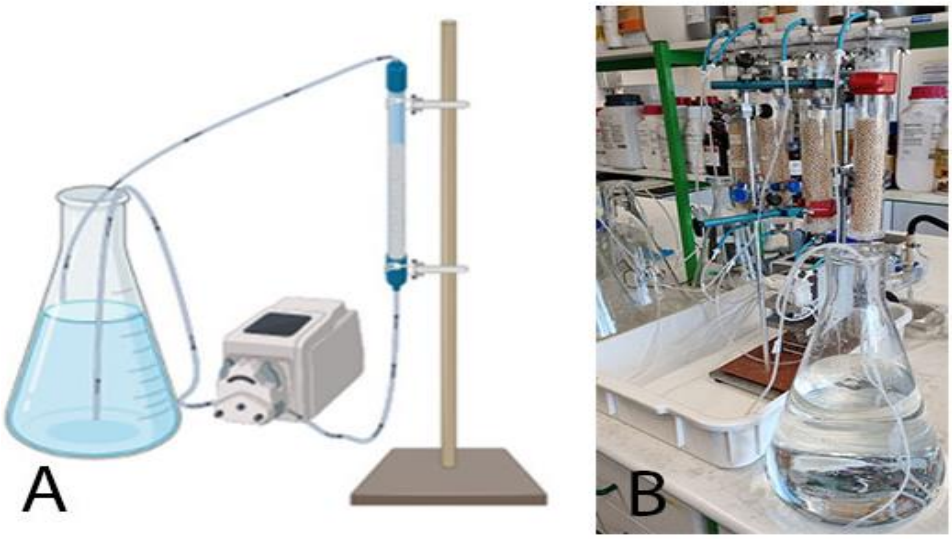

Figure 4.1: Schematic representation of the columns set-up (**A**) and the real system (**B**).

The zeolite modification was the same as the one selected as the most suitable one in the **Chapter 3**. The modified zeolite will be designed as ZX_NaOH, while the zeolite without modification will be designed as Z13X. The column designations are shown in **Table 4.1**.

Table 4.1: Column designations for the continuous flow assays

Column designation	Zeolite used	Modification	Washing between sorption assays
Z13X_NW	Z13X	No chemical modification	Without washing
Z13X_WW			With washing
ZNaOH_NW		Modified with NaOH 0.1 M	Without washing
ZNaOH_WW			With washing

Each column was tested in 4 cycles, which consisted in an adsorption step and a desorption one. Two of the four columns (ZX_WW and ZNaOH_WW, **Table 4.1**) had a washing step between the desorption and adsorption, which was only performed 3 times. The cycle description with concentrations, pump rate and duration are described in **Table 4.2**.

Table 4.2: Operational parameters of the assays. Each column had 4 adsorption and desorption cycles, only two of them had a washing step between the desorption and adsorption.

Step	*Cycle*	*Solution*	*Pump rate (mL/min)*	*Duration (h)*
Adsorption	1	C_i = 60 mg/L for each REE; V_i = 5 L	4	72
	2	C_i = 10 mg/L for each REE; $V_i \approx$ 5 L		
	3	C_i = 60 mg/L for each REE; V_i = 5 L		
	4	C_i = 25 mg/L for each REE; $V_i \approx$ 5 L		
Desorption	1	1 L of HNO_3 0.1 M for each desorption step	8	6
	2			
	3			
	4			
Wash	1	1 L of NaOH 0.01 M for each washing step	15	2
	2			
	3			

The adsorption assays were carried out using a prepared solution with the six different REE: La, Eu, Pr, Ce, Y and Tb, in a closed loop. Cycles 1 and 3 were run with a 60 mg/L solution of each of REE, while for cycles 2 and 4, the initial concentration of each REE was 10 and 25 mg/L, respectively. Samples were taken at 3, 6, 12, 24, 36, 48, 60 and 72 h from the outflow and the measured concentrations were used to build the C/C_0 versus time graph. Samples from the feeding solution in the retention Erlenmeyer were also taken at 0, 24, 48 and 72 h, and the measured concentrations were used to describe the

function of the removal (%) versus time. At the end of the adsorption, the REE solution was removed from the columns and afterwards the desorption solution, HNO_3 at 0.10 M, was pumped in. Samples were taken from the solution in the retention Erlenmeyer at 0, 1, 2, 4 and 6 h. Finally, in the last phase, NaOH 0.01 M was used for pH equilibration and washing. This step was performed for one column of each zeolite, namely Z13X_WW and ZNaOH_WW, with samples taken at 0 and after 2 h from the solution in the retention Erlenmeyer.

4.2.4.Machine Learning

The ML algorithms were supported by the DataFrame, a table where the rows list the samples used, while the columns are the different parameters used to evaluate the samples.

The first ML evaluation objective is the selection of the most suitable tested condition (considering the zeolite and the washing option). For that, the 4 different conditions tested, **Table 4.1**, are listed as rows, with 50 characteristics (24 adsorption and 24 desorption results – considering 4 different samples and 6 REE, plus the zeolite used and the eventual washing between adsorption and desorption), which are mainly the results of the adsorption (removal) and of the desorption (recovery) for each REE tested in each cycle.

The second ML evaluation was meant to validate any good cycle regarding the removal and recovery of the different REE. For that, 16 samples were used (the previous four samples were divided accordingly to the four cycles of adsorption and desorption for each REE) and 15 columns with the respective results (6 removals and 6 recoveries for each REE, the cycle number, the zeolite used and the eventual washing between adsorption and desorption) were used to assist in the selection of the best cycles.

The DataFrame was processed under unsupervised learner (Principal Component Analysis, K-Means analysis) and supervised learner (classification). Briefly, the Principal Component Analysis, PCA, is used to reduce the dimensions of a DataFrame without losing information and maximizing the interpretation, while the K-Means makes data clusters accordingly to the considered conditions.

The algorithms used for the classification were K-nearest neighbors Classifier (KNN), Decision Tree Classifier, Random Forest and Logistic Regressor Classifier. The classification algorithm is normally applied in a binary system and so it was used for each result of the adsorption (removal) and of the desorption (recovery) steps. The classification for the removal was done accordantly to the remaining REE present in solution (the lower remaining percentage, the higher the removal). For the recovery, it was the opposite (the higher percentage of REE in solution, the higher the recovery). The classification for removal and for recovery was established for every REE, and then the mean value was calculated. Next, the binary

classification was assigned depending on the mean value relatively to the chosen cut-off value. The process is summarized in **Table 4.3**.

The data used for the classification was divided into two sets, training set (70 % of the data), which contains the known output of the assays and will be used to train the model. The other set is the test set (30%), which is used to test the model prediction capacity. The stratify option was also used, so both training and test sets have the same percentage of positive cases, which for this analysis would represent high removals and recoveries.

Table 4.3: Binary classification used for each sample evaluated regarding the data from the adsorption (removal) and the desorption (recovery) assays.

Removal (R_m), %		Recovery (R_c), %		Classification Means	Binary Classification
Interval	Classification	Interval	Classification		
$80 < R_m < 100$	1	$80 < R_c < 100$	5	≥ 3.5	1
$60 < R_m < 80$	2	$60 < R_c < 80$	4		
$40 < R_m < 60$	3	$40 < R_c < 60$	3		
$20 < R_m < 40$	4	$20 < R_c < 40$	2	< 3.5	0
$00 < R_m < 20$	5	$00 < R_c < 20$	1		

4.2.5.Statistical analysis

Two-Way ANOVA was performed on the removal percentages of the adsorption assays, in which the conditions were compared between each other for the same time points. The desorption results were analyzed using a Two-Way ANOVA similarly to the removal percentage analysis.

All these analyses were conducted using the software Graph Pad Prism version 8.0.2 (Graph Pad Software, Inc, San Diego, CA, USA). A significant difference was only considered when the probability (*p*-value) was lower than 0.05, assuming a 95 % confidence interval.

4.3. Results and Discussion

The overall analysis of the results for the adsorption and desorption cycles simultaneously (**Figure S-4.1**) revealed the complexity of observing data without noticeable differences. The solution pH (data not shown) was monitored and when required, some drops of HCl were added to avoid the eventual REE precipitation. The same happens for the desorption assays as for the adsorption ones (**Figure S-4.2**).

The sorbent washing with NaOH 0.01 M was performed after cycles 1, 2 and 3 and no washing was performed after the last cycle. No REE leaching was detected during this procedure. During the analysis, removal will refer to the adsorption results, while the recovery will refer to the desorption ones.

4.3.1.Machine Learning analysis

4.3.1.1. Selection of the best sample in the continuous flow assays

The ML analysis of the continuous flow assays was used to evaluate and to select the best conditions among the tested ones, as previously described. Before applying the unsupervised ML algorithms, it is required to perform a data scaler, which consists in a data normalization.

The significance of each principal component weight in PCA was assessed (**Figure S-4.3A**) and two features were selected to build the PCA as they justified 85.99 % of the variance. The two features selection was not confirmed by the Knee Locator method [23]. The resulting PCA representation is shown in **Figure 4.2A**. The PCA is too crowded with features for the evaluation and it is hard to read the influence of each one on the tested conditions. Nevertheless, the majority of the features seem to have a high impact on the pristine Z13X C1 and C2 (without and with a NaOH 0.01 M washing after the desorption). The PCA analyses, **Figure 4.2A**, are represented in a biplot where the bottom *x* and left *y* are references for the samples distribution, while the top *x* and right *y* are for the features distribution.

The division using the K-Means algorithm created two different groups, shown in **Figure S-4.3B**. Similar to the PCA, the Knee Locator method did not identify any value for the best number of clusters. In **Figure 4.2B,** the four zeolite samples were divided into two groups, one for the pristine zeolite (Z13X_NW and Z13X_WW) and the other for the modified Z13X with NaOH 0.1 M (ZNaOH_NW and ZNaOH_WW), without any other division regarding the washing.

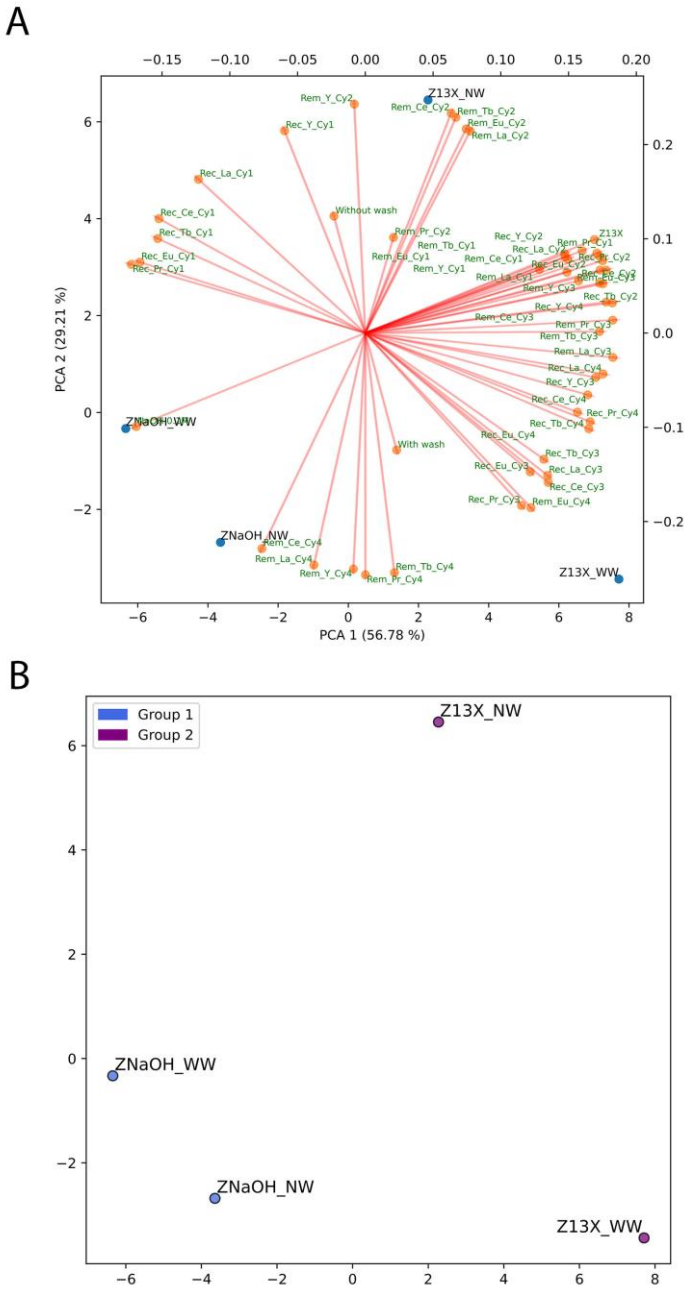

Figure 4.2: ML analysis of the four conditions used: **A**) PCA analysis; **B**) K-Means algorithm. The Rem refers to each REE removal (adsorption), Rec refers to each tested REE recovery (desorption) and the Cy regards each cycle.

The ML classification algorithms were used to assess one of the four tested samples (**Table 4.1**). Each sample must be classified using a binary system, where a value of 0 indicates poor performance, whereas a value of 1 is indicative of good performance. The binary classification was performed accordantly to **Table 4.3:** Binary classification used for each sample evaluated regarding the data from the adsorption (removal) and the desorption (recovery) assays.**Table 4.3**. The cut-off for satisfactory results is a classification mean equal to or above 3.5 and none of the 4 tested conditions was classified as 1. The classification means were calculated following **Table 4.3** and the results for the four conditions

ranged between 2.00 and 2.50, and since each part (adsorption or desorption) has a possible total weight of 2.5 out of 5.0, it is very likely that one of them underperformed. From overall results of the adsorption (**Figure S-4.1**) and desorption (**Figure S-4.2**), it is concluded that the desorption underperformed with recoveries below 25 %. Somehow this was unexpected as the zeolite with the NaOH 0.1 M treatment was reported in the previous work as performing much better REE removal and recovery than the Z13X itself. An incomplete recovery may negatively affect subsequent adsorption due to previous occupation of the different adsorption sites of the zeolite by the REE retained during the first adsorption steps.

4.3.1.2. Selection of the best cycle in the continuous flow assays

The inability of the approach to select the best condition for the continuous removal of REE from the solution was disappointing. Therefore, a test was performed to identify a cycle in which a good adsorption and desorption of the REE occurred. For that, the results of the four cycles (adsorption and desorption) performed in 4 columns defined 16 samples and the same ML analysis was performed.

From **Figure S-4.4A**, three features were selected to build the PCA, confirmed by the Knee Locator method [23]. A 3D graphic is shown in **Figure S-4.5** that confirms that the first two components explain 69.64 % of the variance of the samples. The 2D graphical representation is also shown in **Figure 4.3A.**

The group division using the K-Means algorithms created 4 different groups (**Figure S-4.4B)** and the same value was obtained with the Knee Locator method. In **Figure 4.3B,** the 4 zeolite samples were divided into 4 groups, with one of each condition tested, with one exception. That division could be majority related to the different cycles. Group 1 (blue) is the results for the first cycle; Group 2 (green) is the second cycle and group 3 (yellow) is the fourth cycle and one element from the third cycle. Finally, group 4 (purple) is the rest of the third cycle. The feature related to each cycle has more influence on the respective group, as previously described. The REE recoveries have a more substantial influence on group 1, while the REE removals have a similar impact on groups 1 and 2, as shown in **Figure 4.3A**. This stronger influence or affinity related to the recovery might suggest that the other 3 cycles do not have similar results to the ones obtained in the first cycle of the column assays. The same interpretation could be forwarded regarding the similar affinity of the removals for the first and second cycles of the assay. The other 2 features, namely the washing between sorption assays (with or without) and zeolite type (Z13X or ZX_NaOH), were more centered and did not have a relevant influence on any of the groups.

The ML classification algorithms were used to divide the samples into different groups, one of those groups will possibly include the cycles with the best performance, using the same strategy as before with the same classification mean for the cut-off. Again, no condition with a good classification was

obtained and from these results, it can be concluded that no condition achieved optimal removal and recovery in the same cycle.

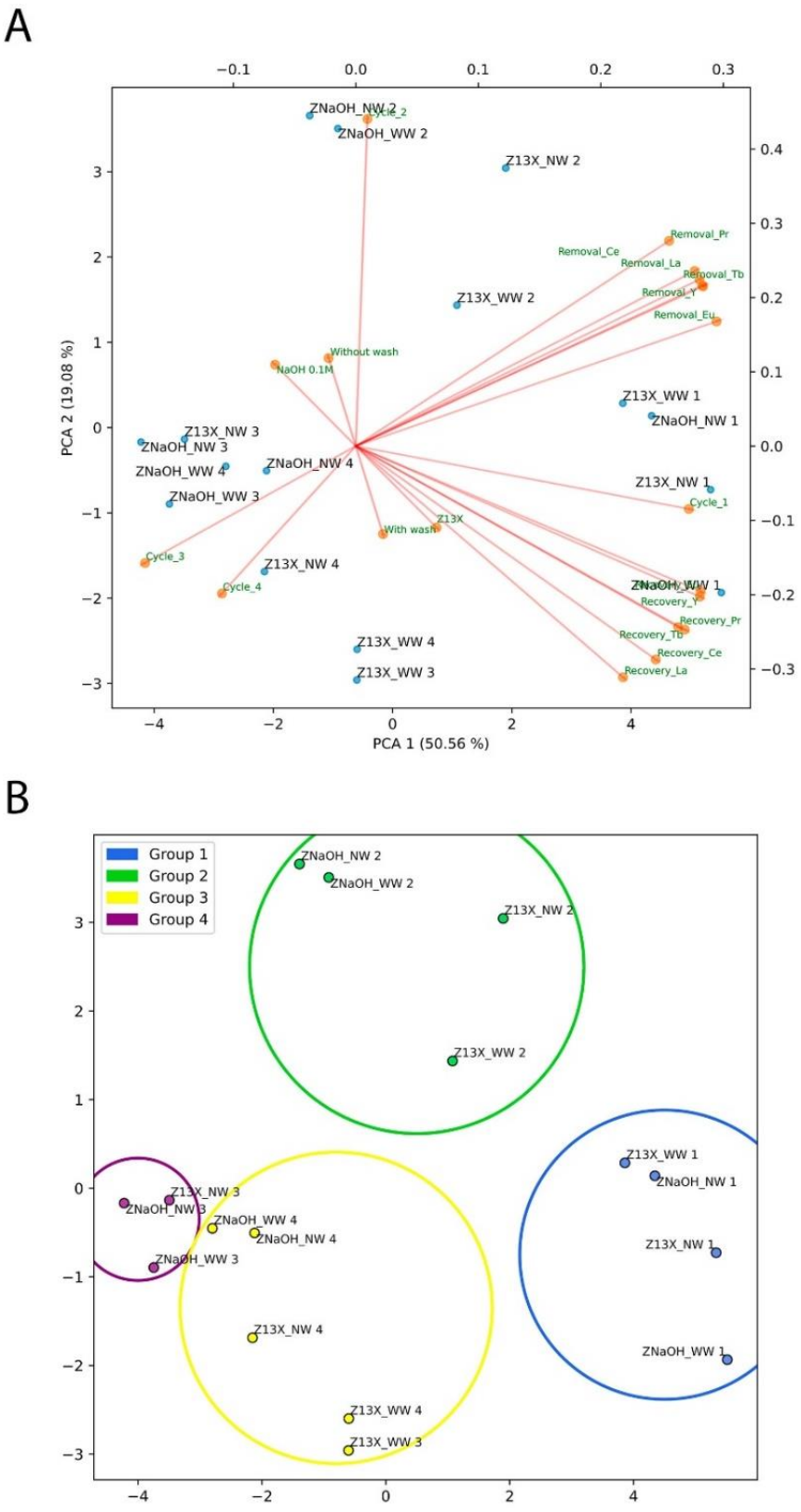

Figure 4.3: ML analysis for the second analysis to select the best condition cycle: **A)** PCA analysis; **B)** K-Means algorithm. The numbers after the designations are referencing to their respective cycles.

A heatmap showing the Pearson correlations of the tested features is presented in **Figure 4.4**.

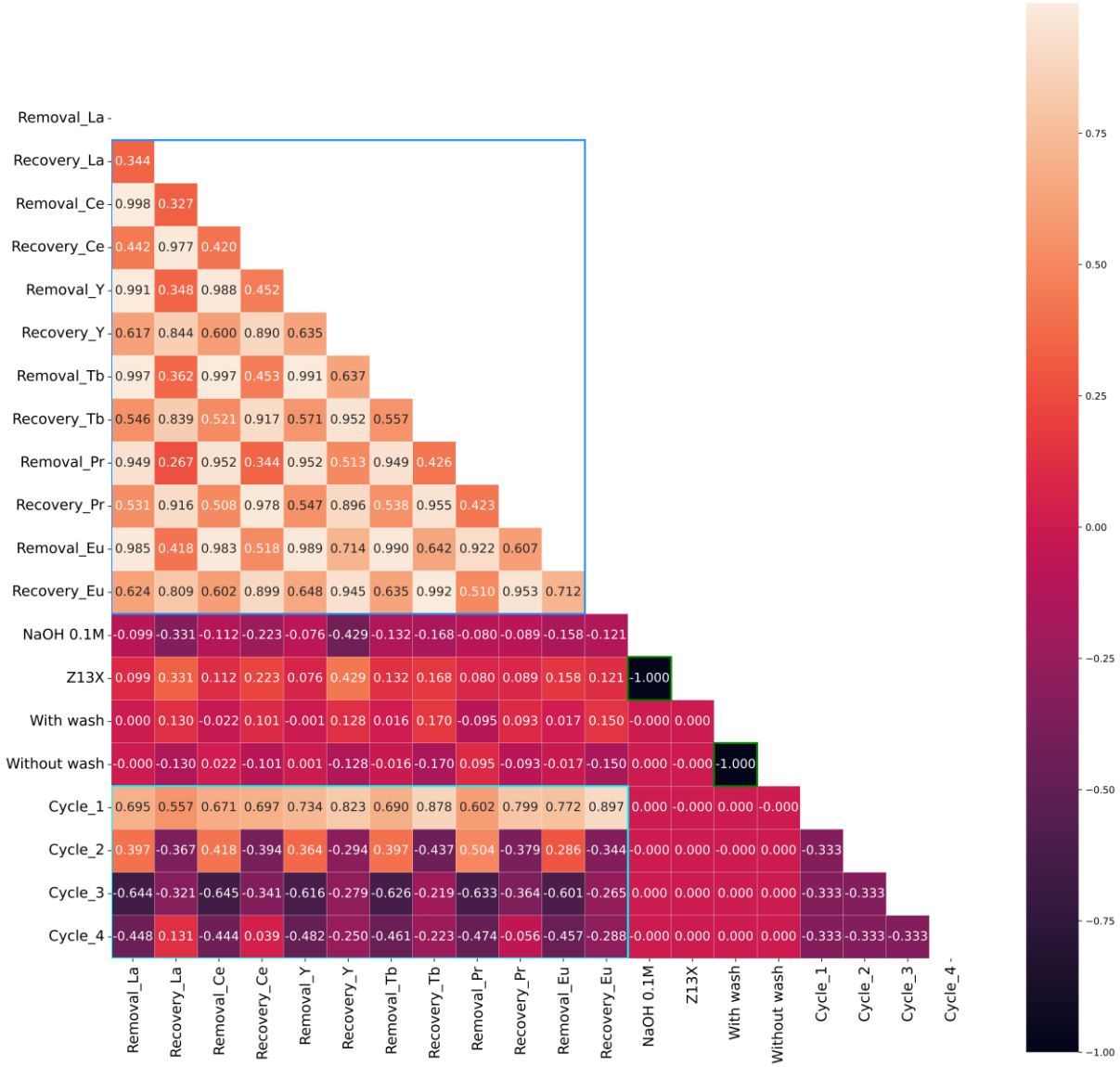

Figure 4.4: Heatmap representation of the correlation between different features used for the cycle evaluation. The left scale represents the different correlation values and the respective colors.

The heatmap shows 3 crucial relations. In a green square, the first one is the inverse correlation between the starting zeolites (Z13X and ZX_NaOH) and the washed samples (NW and WW, without and with washing, respectively). There is negative correlation for these two groups, which is expected since each sample is one zeolite or the other and the same happens regarding the washing.

The second square (light blue) refers to the correlation of the cycles and the different removals and recoveries of the REE. The first cycle is the one with the stronger correlation with both removal and recovery of the REE. As seen in **Figure 4.4**, the removal and recovery correlation got more negative,

inducing a poorer performance as the number of cycles grew. This supports that both the adsorption and the desorption lose efficiency over the cycles.

The last relation appears between the REE removals and recoveries. Each REE removal has a very high positive correlation (over 0.9) [24] with the removal of other REE, showing how the matrix entrapment of the different REE is similar and correlated. These analyses support some other observations in batch assays reported in the **Chapter 3**. Each REE removal and recovery have a moderate correlation (between 0.5 and 0.7) [24]. These correlations were expected to be stronger and this could be related to the fact that relatively poor recoveries are translated into a lower removal in the next cycle. A further evaluation of this hypothesis will be performed in the following sections. Each REE recovery has a very high positive correlation with the other recoveries. This is related to the fact that the oxidation number is the same (3+) for all the tested REE and even with some differences regarding the ionic radii, they behave similarly in the desorption process. The rest have a negligible correlation [24], except for the correlation between the different cycles, which has a low negative correlation [24]. This is due to the possible influence that incomplete recoveries would have over the removing in the following cycle.

The results of the adsorption and desorption will be analyzed separately in the following sections to understand better what may be improved. This analysis, especially for the desorption, could indeed give an important insight of what happened during the assay. A cycle analysis will be performed, since the overall results for both the adsorption and desorption (Erro! A origem da referência não foi encontrada.**, Figure S-4.1** and **Figure S-4.2**) are too overlapped, with dense information that makes the analyze too complex.

4.3.2.Sorption analysis of the continuous flow assays cycles

4.3.2.1. Adsorption analysis

The removal (%) is the result measured for specific time points 24, 48 and 72 h. The results are shown in **Figure S-4.6** to **Figure S-4.9** for the different cycles**.**

The results of the removal for the first cycle are similar in each analyzed time point, with no significant differences. As expected, the removal values increased over time, confirming the REE adsorption by the zeolite samples. For the second cycle, the total removal shows similar results, with most of the statistical tests having no significant difference.

The same behavior would be expected for the subsequent cycles. The results of total removal for the third cycle and fourth cycle show that no significant differences were found. These results indicate

that the ion exchange capacity of the zeolite attains the equilibrium, which is more visible for these cycles than the one obtained for the second cycle since a higher concentration was used .

The total removal of the REE for each tested condition was calculated and the results are shown in **Table 4.4**.

Table 4.4: Total removal of each REE for each zeolite tested after 4 cycles.

Removal (%)	La	Ce	Y	Tb	Pr	Eu
Z13X_NW	81.6 ± 6.5	83.3 ± 5.8	80.4 ± 6.7	83.8 ± 6.0	84.7 ± 5.7	83.6 ± 5.5
Z13X_WW	71.9 ± 0.4	74.7 ± 0.2	71.4 ± 2.2	76.2 ± 1.8	76.4 ± 0.8	75.6 ± 2.0
ZNaOH_NW	73.0 ± 3.0	73.6 ± 2.6	83.0 ± 2.0	72.7 ± 2.3	73.2 ± 2.9	72.7 ± 2.5
ZNaOH_WW	68.2 ± 4.1	70.9 ± 4.8	75.1 ± 4.5	72.3 ± 2.4	70.9 ± 3.6	70.7 ± 3.3

Overall, between 65 to 90 % of the total mass of REE present in the solutions to be treated were removed and the zeolite reveals similar affinity towards the different REE, for each of the four conditions (**Table 4.4**). No significant difference was found between the tested conditions (**Table S-4.1**), including the control zeolite, Z13X and the ZX_NaOH, as foreseen by previous batch assays, described in Chapter 3. This suggests that a pre-treatment of the zeolites will not improve the sorbent behavior.

A difference between the performance of zeolites with (WW) and without (NW) NaOH washing between cycles was forseen. It was expected that the washed beds (Z13X_WW and ZNaOH_WW) would reach higher removals as the OH^- from the NaOH could neutralize part of the H^+ from HNO_3, used in the desorption step. As this was not observed, probably the NaOH concentration used, 0.01M, was not enough for the purpose as it is 10 times lower than the acid concentration.

4.3.2.2. Desorption analysis

The desorption results for the four different cycles are shown in **Figure S-4.10** to **Figure S-4.13**. The desorption results for the first cycle are shallow, below 30 %, with no significant difference found for the different comparisons evaluated. For the second cycle, the desorption recovered below 11 %, with no significant differences. The same occurred for the third cycle, with recoveries below 10 % and for the fourth cycle, with recoveries below 14 %. No significant difference was found.

These results were not expected since the same concentration was used for the acid chosen to be the best one in batch assay. The same assessment reported that the NaOH 0.1 M zeolite had very high recovery.

The low recoveries of REE probably are related to the saturation of the zeolite surface [25]. Even though, this was not evident for the second cycle due to the lower initial REE concentration of 10 mg/L, supported by the adsorption results (**Figure S-4.7**). The third and fourth cycles had higher initial REE concentrations of 60 and 25 mg/L, respectively, but the low removal is more evident, as supported by the adsorption results (**Figure S-4.8** and **Figure S-4.9**).

This shows the importance of the desorption step in a multiple cycle assay in continuous flow through a column bed since good desorption may lead to a near total recovery of the REE from the zeolite. After that and during the second adsorption step, the zeolite would be available to remove more REE from the solution. The total recovery was calculated and shown in **Table 4.5**.

Table 4.5: Total recovery percentage of each REE for each zeolite sample tested after 4 cycles.

Recovery (%)	*La*	*Ce*	*Y*	*Tb*	*Pr*	*Eu*
Z13X_NW	9.5 ± 0.1	9.2 ± 0.2	11.0 ± 0.7	10.9 ± 1.1	9.4 ± 0.1	11.5 ± 0.5
Z13X_WW	7.9 ± 1.1	8.4 ± 1.1	10.7 ± 0.6	10.1 ± 0.7	8.3 ± 1.0	11.2 ± 0.6
ZNaOH_NW	11.7 ± 1.7	12.1 ± 2.2	10.5 ± 4.5	13.6 ± 3.5	13.8 ± 2.1	15.8 ± 2.9
ZNaOH_WW	14.9 ± 1.6	13.9 ± 0.8	14.9 ± 1.8	17.5 ± 0.9	16.0 ± 1.3	18.9 ± 1.1

The overall desorption results were below 20 %, with no significant differences (**Table S-4.2**). These results were meager and unexpected since higher recoveries were achieved in batch assays. This indicates that a higher concentration of the acid should be used in these assays, so the desorption step needs to be improved.

After the desorption process, the REE need to be concentrated so they be reused into new applications. The purification process may be consider the REE precipitation by addition of anions such as carbonate [26,27] or oxalate [28–32].

4.3.2.3. ML analysis of the desorption optimization

In the desorption batch assays from **Chapter 3**, 0.35 g of loaded zeolite was used with 0.1 L of HNO_3 at 0.1 M, which defines a ratio of 28.6 mmol of HNO_3 per g of zeolite. In these continuous flow assays, the ratio is 0.67 mmol of HNO_3 per g of zeolite. The proportion between the batch ratio and the column ratio is 43, which explains the reduced desorption efficiency in continuous flow assays. So, it was decided to perform new desorption assays in the continuous flow set-up with a ratio of 13.3 mmol of HNO_3 per g of the zeolite (2 L of 1 M of HNO_3 during 3 h with the same flow rate in close loop). The results obtained from the optimized desorption cycle are shown in **Figure 4.5**.

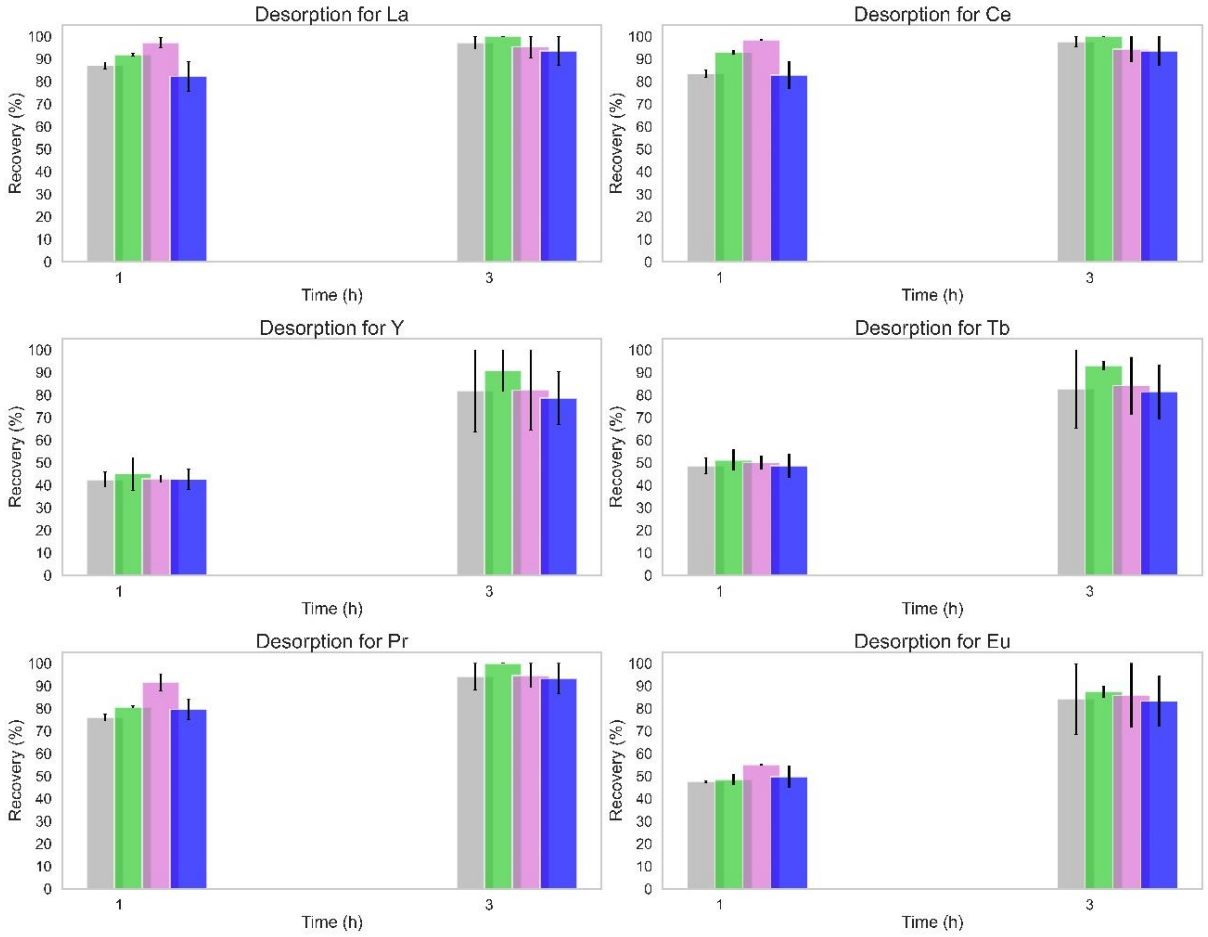

Figure 4.5: Total recovery for the different REE from loaded Z13X_NW ( ), Z13X_WW ( ), ZNaOH_NW ( ) and ZNaOH_WW ( ) for the 1 M eluent desorption. The NW refers to the assays without the washing step, and the WW refers to the assays with the NaOH 0.01 M washing step. Samples were taken from the accumulation Erlenmeyer with the outflow eluent.

The changes implemented for the desorption were definitive to improve the REE recoveries as seen in **Figure 4.5**. After 1 h of assays, over 70 % of La, Ce and Pr were removed from the zeolite, while the other REE had a lower recovery. This difference could be related to the accessibility of the cations located in the zeolite surface. The structural framework of zeolite Y or X (FAU) are distinguished by three main units: the hexagonal prism, the sodalite cavity and the supercage [33]. The recovery of these cations is facilitated if they are primarily located in the surface sites of the supercage or sodalite cavities. The different REE radii could be justify the observations since a smaller ion could easily enter into smaller structures of the zeolite and therefore, it would require more time to desorb from the zeolite.

After a 3 h leaching, the recoveries of REE are similar between them and over 80 %. It is important to add that no significant differences were found between the tested conditions and that the primary source of variation is the time for all tested REE.

The last time point results of all tested desorption cycles (the first 4 and the one with higher acid concentration) were compared for the same tested conditions. A significant difference, **Table S-4.3**, was found for all REE when any cycle is compared with cycle 5 (desorption with 1 M acid), as expected since this desorption presented recoveries up to 4 times higher than the ones from the previous cycles. Here, it was found that the primary source of variation is the cycle for all tested REE. After this desorption, an improved removal of the REE from the solution would be expected in a possible new adsorption cycle. This new adsorption cycle results could be better than to the ones obtained for cycles 3 and 4 since there will remain almost no REE in the zeolite. However, it is important to remember that the treatment could lead to changes in the structure, as a dealumination, which could reduce the negative charge of the zeolite and lead to a reduction of the REE adsorption.

The previous results show a great potential to produce a positive supervised ML analysis, since the results from **Figure 4.5** suggest that in this last cycle could have a higher mean value above 3.5, accordingly to **Table 4.3**. For that reason, a new DataFrame was built just considering the desorption results. This DataFrame consists in the previous 4 cycles and the results obtained from this new desorption cycle, with higher ratio of acid/zeolite. This DataFrame was used in a new ML analysis to investigate the impact of the amount of acid on the desorption efficiency.

From the results in **Figure S-4.14A**, four components were selected to build the PCA, confirmed by the Knee Locator method [23] and the result is shown in **Figure S-4.15**. The first 2 features explain 63.95 % of the variance of the samples as shown in **Figure 4.6A**. The PCA distribution results in two main groups, one on the right side, more influenced by cycle 5 (desorption with 1 M acid) and the recoveries of the different REE. The second group, on the left side, is more influenced by the first 4 cycles. This group can be divided into 2 smaller groups: the top group was more influenced by the ZX_NaOH zeolite, while the bottom group was more influenced by the Z13X. Each zeolite group can be further divided into two groups depending on the washing after cycles, with NW in the top and WW in the bottom.

The K-Means were made using three groups, as shown in **Figure S-4.14B,** confirmed by the Knee Locator method [23]. A clear group 1, in blue, which is from the ZX_NaOH zeolite for both NW and WW, can be seen in **Figure 4.6B**. The group 2, in green, is the fifth cycle of desorption with both zeolites and group 3, in purple is the Z13X zeolite. The other groups are mixed.

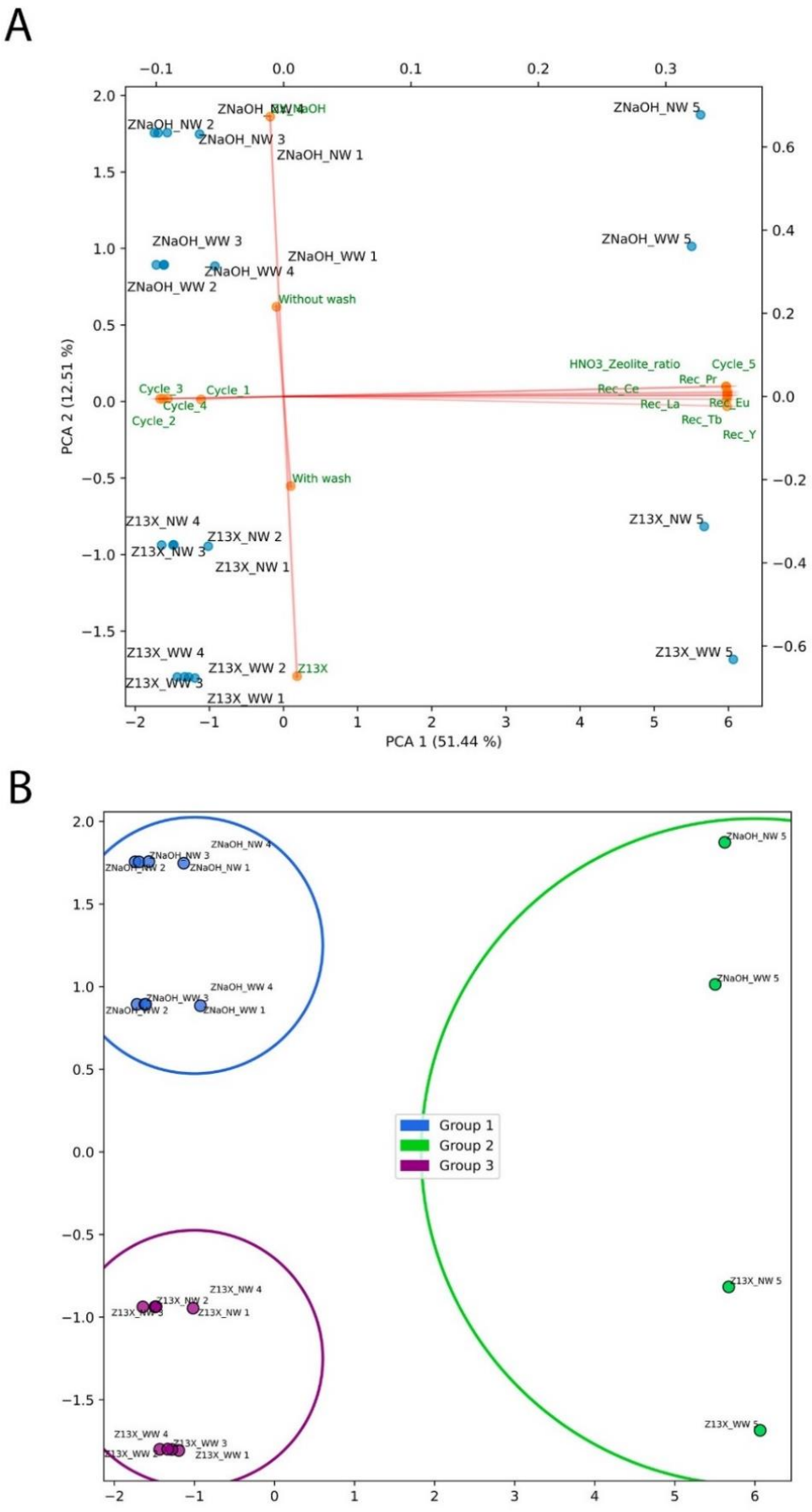

Figure 4.6: ML analysis: **A**) PCA; **B**) K-Means. The Rec refers to the recovery of each REE.

The ML classification algorithms were used to select the best desorption conditions, using the binary classification (**Table 4.3:** Binary classification used for each sample evaluated regarding the data from the adsorption (removal) and the desorption (recovery) assays.**Table 4.3**). For this case, 4 samples were considered good accordingly to **Table 4.3**. The 4 selected samples are the ones from the cycle 5, as expected, since the results shown in **Figure 4.5** show that this cycle was the best one. With this, the classification was carried out using 4 classifiers, KNN, Decision Tree, Random Forest and Logistic Regression. The results of the different classifiers are shown in **Figure 4.7**.

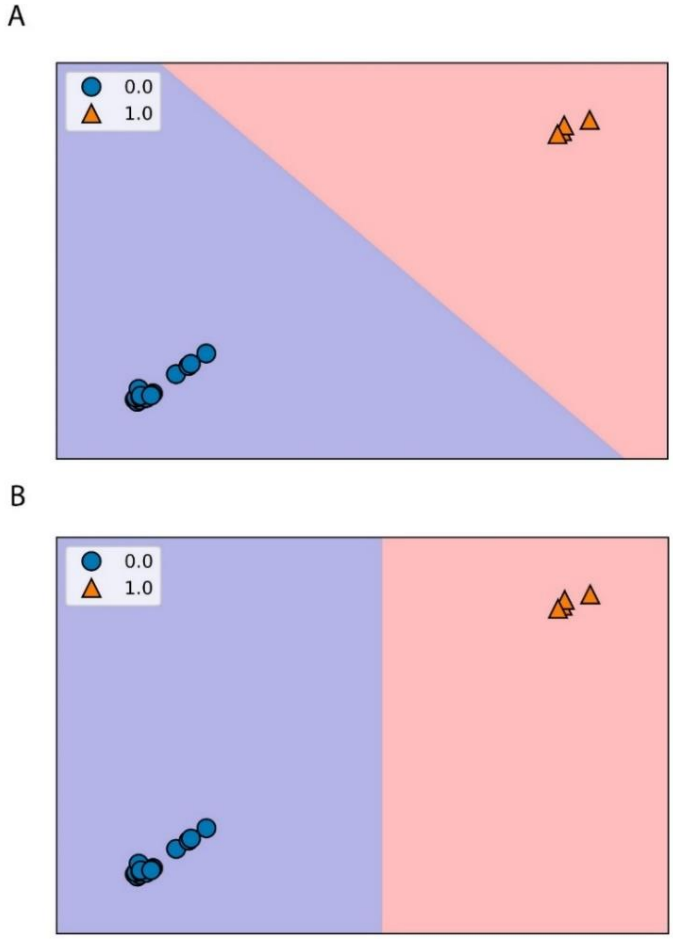

Figure 4.7: Conditions division according to the classifiers, **A)** KNN and logistic regression and **B**) decision tree and random forest. The different colors, violet and orange, represent the zone of a good or bad catalyst, respectively.

For the KNN, **Figure 4.7A,** three neighbors were selected accordantly to the accuracy values for both training and test sets, shown in **Figure S-4.14C.** The Decision Tree classifier, **Figure 4.7B**, has only one parameter, random state, with a value of 20. For the Random Forest, **Figure 4.7B**, the n estimator parameter was 10 and the random state was the same as for the Decision Tree classifier. Finally, the same value for the random state parameter was used for the Logic Regression, **Figure 4.7A**.

It is crucial to avoid overfitting of the training set for the classifiers, as it happens often with the model. A suitable generalization of the model from the training set can lead to a good classification of new and unseen data, which is the test set. All the tested classifiers could separate the 2 groups without any problem. Therefore, it is expected that the respective accuracy scores of the values (x and y values of training and test data) would be 100 %. The scores of the training and test using the four different classification algorithms are 100 % for all tested classifiers. Similar results were obtained using the classification report, which summarizes percentages of precision, recall and f1-scores. It is important to know that the precision is related to the accuracy of making good predictions, the recall is the value of the correctly identified positive predictions and the f1-score is the harmonic mean of the precision and recall. This evaluation used the real classification from the binary classification (*y_real*) and the predicted classification (*y_pred*) after training the model.

All classifiers presented a 100 % score for the precision, recall and f1-scores of the prediction of the model. Another vital metric to assess the classification used is the confusion matrix. All the classifiers evaluated are very similar between them and the overall result is shown in **Figure 4.8**.

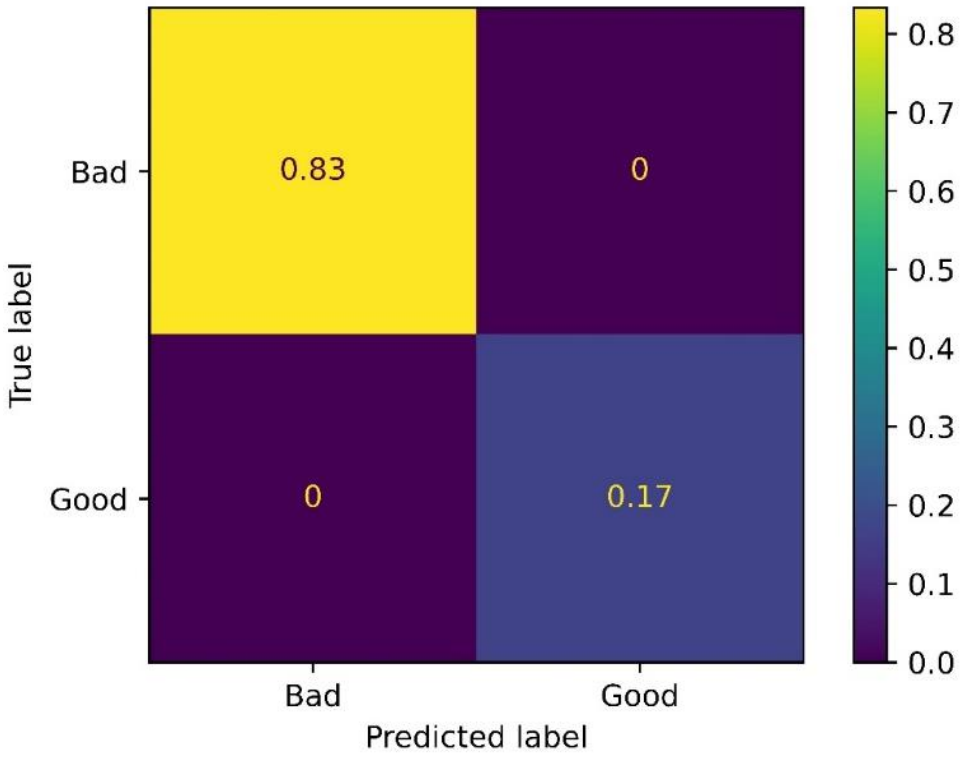

Figure 4.8: Graphical representation of the confusion matrix for all tested classifiers. The values shown refer to the fraction of the true correct predictions (when the model got it right) and false incorrect predictions (when the model got it wrong).

It was verified that there were only true positives (the model predicted it was a cycle with high desorption, and it was high) and true negatives (the model predicted it was a cycle with low desorption, and it was actually low).

A heatmap showing the Pearson correlations of the tested features was made as before, and the results are shown in **Figure 4.9**.

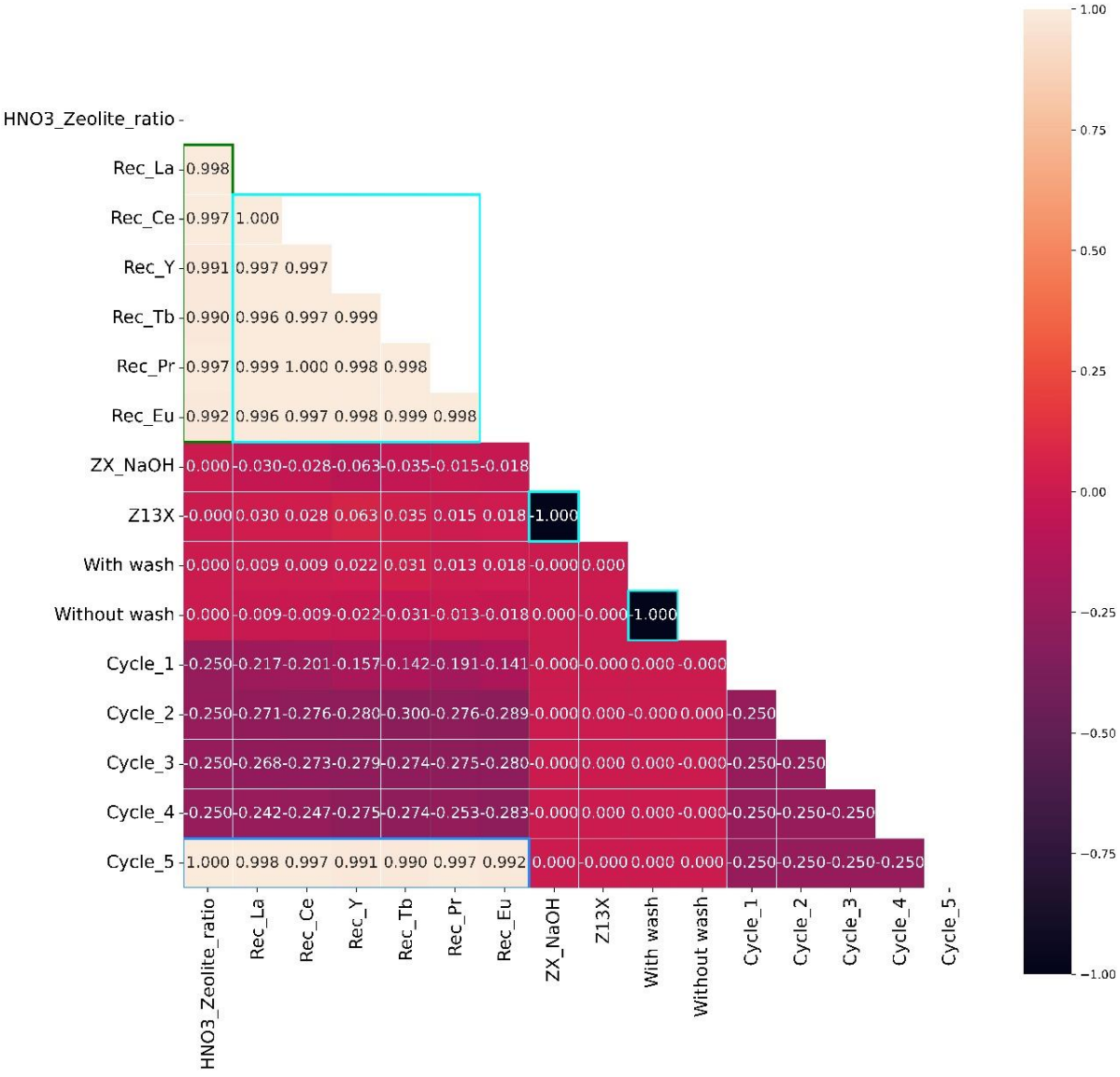

Figure 4.9: Heatmap representation of the correlation of the features used for the desorption obtained in the different cycles. The results for the maximization of the desorption are referenced as cycle 5. The left scale represents the different correlation values and the respective colors.

Overall, the correlation for the desorption cycles can be considered negligible, with 3 main exceptions. The first relates to the zeolites (Z13X and ZX_NaOH) and to the washing (NW and WW), which have a very high negative correlation, as shown in **Figure 4.4**. Also, the correlation of the recovery of

each REE is a very high positive, which is expected since all REE had a higher recovery. Finally, as expected, cycle 5 shows a very high positive correlation with the REE recoveries since it was the cycle with higher REE recoveries. The same happens for the HNO_3 zeolite ratio correlation with the REE recoveries for the same reason as said before. Also, this ratio has a very high positive correlation with the cycle 5 as expected, since the highest HNO_3 zeolite ratio was used in this cycle.

4.4. Conclusions

The column adsorption results confirmed that between 65 and 90 % of the total amount of REE was removed decreasing with the number of cycles. The desorption data were below 20 % during the different cycles analysis. After a maximization using 13.3 mmol of HNO_3 per g of the zeolite, the desorption achieved over 80 % of recovery after 3 h for each tested REE.

Considering the lack of significant differences between the zeolites tested, Z13X would be the best zeolite to be used in the multiple adsorption and desorption cycles, since the use of chemical pre-treated zeolite, ZX_NaOH, might not be justifiable. Adding to that, the eventual bed washing with NaOH 0.01 M also showed no improvement in the overall efficiency of the process and only increased costs. Overall, the adsorption and desorption of the REE could be performed in 4 cycles. The conditions tested for the adsorption could be further assessed using different REE concentrations. The application of the maximizing conditions leads to an improvement of the desorption step and have an important influence in the following adsorption cycles, improving the overall results obtained by this system to recover REE from wastewater.

The ML algorithms were applied successfully to the results of the continuous flow assays and can be helpful to select the best operation conditions, reinforcing the overall improvement with the desorption optimization. The heatmaps may be used to estimate all REE removals and recoveries just using the obtained values of one of the tested REE.

4.5. References

1. Qin, S.J.; Chiang, L.H. Advances and opportunities in machine learning for process data analytics. *Comput. Chem. Eng.* **2019**, *126*, 465–473.
2. Jordan, M.I.; Mitchell, T.M. Machine learning: Trends, perspectives, and prospects. *Science (80-.).* **2015**, *349*, 255–260.
3. Bi, Q.; Goodman, K.E.; Kaminsky, J.; Lessler, J. What is Machine Learning? A Primer for the Epidemiologist. *Am. J. Epidemiol.* **2019**, *188*, 2222–2239.
4. Samuel, A.L. Some studies in machine learning using the game of checkers. *IBM J. Res. Dev.* **2000**, *44*, 206–226.
5. El Naqa, I.; Murphy, M.J. Chapter 1: What Is Machine Learning? In *Machine Learning in Radiation Oncology*; Springer International Publishing: Cham, 2015; pp. 3–11 ISBN 9781119815075.
6. Peng, G.C.Y.; Alber, M.; Buganza Tepole, A.; Cannon, W.R.; De, S.; Dura-Bernal, S.; Garikipati, K.;

Karniadakis, G.; Lytton, W.W.; Perdikaris, P.; et al. Multiscale Modeling Meets Machine Learning: What Can We Learn? *Arch. Comput. Methods Eng.* **2021**, *28*, 1017–1037.
7. Nasteski, V. An overview of the supervised machine learning methods. *HORIZONS.B* **2017**, *4*, 51–62.
8. Torregrossa, D.; Leopold, U.; Hernández-Sancho, F.; Hansen, J. Machine learning for energy cost modelling in wastewater treatment plants. *J. Environ. Manage.* **2018**, *223*, 1061–1067.
9. Pang, J.-W.; Yang, S.-S.; He, L.; Chen, Y.-D.; Cao, G.-L.; Zhao, L.; Wang, X.-Y.; Ren, N.-Q. An influent responsive control strategy with machine learning: Q-learning based optimization method for a biological phosphorus removal system. *Chemosphere* **2019**, *234*, 893–901.
10. *Global Water Intelligence magazine The market leader in business information*;
11. Foroughi, M.; Ahmadi Azqhandi, M.H.; Kakhki, S. Bio-inspired, high, and fast adsorption of tetracycline from aqueous media using Fe3O4-g-CN@PEI-β-CD nanocomposite: Modeling by response surface methodology (RSM), boosted regression tree (BRT), and general regression neural network (GRNN). *J. Hazard. Mater.* **2020**, *388*, 121769.
12. Al-Gheethi, A.A.; Mohd Salleh, M.S.; Noman, E.A.; Mohamed, R.M.S.R.; Crane, R.; Hamdan, R.; Naushad, M. Cephalexin Adsorption by Acidic Pretreated Jackfruit Adsorbent: A Deep Learning Prediction Model Study. *Water* **2022**, *14*, 2243.
13. Zhang, K.; Zhong, S.; Zhang, H. Predicting Aqueous Adsorption of Organic Compounds onto Biochars, Carbon Nanotubes, Granular Activated Carbons, and Resins with Machine Learning. *Environ. Sci. Technol.* **2020**, *54*, 7008–7018.
14. Sigmund, G.; Gharasoo, M.; Hüffer, T.; Hofmann, T. Deep Learning Neural Network Approach for Predicting the Sorption of Ionizable and Polar Organic Pollutants to a Wide Range of Carbonaceous Materials. *Environ. Sci. Technol.* **2020**, *54*, 4583–4591.
15. Sadek, A.H.; Fahmy, O.M.; Nasr, M.; Mostafa, M.K. Predicting Cu(II) Adsorption from Aqueous Solutions onto Nano Zero-Valent Aluminum (nZVAl) by Machine Learning and Artificial Intelligence Techniques. *Sustainability* **2023**, *15*, 2081.
16. Abdi, J.; Mazloom, G. Machine learning approaches for predicting arsenic adsorption from water using porous metal–organic frameworks. *Sci. Rep.* **2022**, *12*, 16458.
17. Ke, B.; Nguyen, H.; Bui, X.-N.; Bui, H.-B.; Choi, Y.; Zhou, J.; Moayedi, H.; Costache, R.; Nguyen-Trang, T. Predicting the sorption efficiency of heavy metal based on the biochar characteristics, metal sources, and environmental conditions using various novel hybrid machine learning models. *Chemosphere* **2021**, *276*, 130204.
18. Lèbre, É.; Stringer, M.; Svobodova, K.; Owen, J.R.; Kemp, D.; Côte, C.; Arratia-Solar, A.; Valenta, R.K. The social and environmental complexities of extracting energy transition metals. *Nat. Commun.* **2020**, *11*, 4823.
19. Zheng, B.; Fan, J.; Chen, B.; Qin, X.; Wang, J.; Wang, F.; Deng, R.; Liu, X. Rare-Earth Doping in Nanostructured Inorganic Materials. *Chem. Rev.* **2022**, *122*, 5519–5603.
20. Pérez-Botella, E.; Valencia, S.; Rey, F. Zeolites in Adsorption Processes: State of the Art and Future Prospects. *Chem. Rev.* **2022**, *122*, 17647–17695.
21. Liu, T.; Johnson, K.R.; Jansone-Popova, S.; Jiang, D. Advancing Rare-Earth Separation by Machine Learning. *JACS Au* **2022**, *2*, 1428–1434.
22. Brião, G. de V.; Franco, D.S.P.; da Silva, F.V.; da Silva, M.G.C.; Vieira, M.G.A. Critical rare earth metal adsorption onto expanded vermiculite: Accurate modeling through response surface methodology and machine learning techniques. *Sustain. Chem. Pharm.* **2023**, *31*, 100938.
23. Satopaa, V.; Albrecht, J.; Irwin, D.; Raghavan, B. Finding a “Kneedle” in a Haystack: Detecting Knee Points in System Behavior. In Proceedings of the 2011 31st International Conference on Distributed Computing Systems Workshops; IEEE, 2011; pp. 166–171.
24. Mukaka, M.M. Statistics corner: A guide to appropriate use of correlation coefficient in medical research. *Malawi Med. J.* **2012**, *24*, 69–71.
25. Townsend, R.P. Chapter 10 Ion Exchange in Zeolites. In *Introduction to Zeolite Science and Practice*; van Bekkum, H., Flanigen, E.M., Jansen, J.C.B.T.-S. in S.S. and C., Eds.; Elsevier, 1991; Vol. 58, pp. 359–390 ISBN 0167-2991.
26. de Vasconcellos, M.E.; da Rocha, S.M.R.; Pedreira, W.R.; Queiroz, C.A. da S.; Abrão, A. Solubility behavior

of rare earths with ammonium carbonate and ammonium carbonate plus ammonium hydroxide: Precipitation of their peroxicarbonates. *J. Alloys Compd.* **2008**, *451*, 426–428.
27. Kim, P.; Anderko, A.; Navrotsky, A.; Riman, R.E. Trends in Structure and Thermodynamic Properties of Normal Rare Earth Carbonates and Rare Earth Hydroxycarbonates. *Minerals* 2018, *8*.
28. Ganguli, R.; Cook, D.R. Rare earths: A review of the landscape. *MRS Energy Sustain.* **2018**, *5*, 6.
29. Gupta, C.K.; Krishnamurthy, N. Extractive metallurgy of rare earths. *Int. Mater. Rev.* **1992**, *37*, 197–248.
30. Chi, R.; Xu, Z. A solution chemistry approach to the study of rare earth element precipitation by oxalic acid. *Metall. Mater. Trans. B* **1999**, *30*, 189–195.
31. Khawassek, Y.M.; Eliwa, A.A.; Gawad, E.A.; Abdo, S.M. Recovery of rare earth elements from El-Sela effluent solutions. *J. Radiat. Res. Appl. Sci.* **2015**, *8*, 583–589.
32. He, L.; Xu, Q.; Li, W.; Dong, Q.; Sun, W. One-step separation and recovery of rare earth and iron from NdFeB slurry via phosphoric acid leaching. *J. Rare Earths* **2022**, *40*, 338–344.
33. Seo, S.M.; Lim, W.T.; Seff, K. Crystallographic Verification that Copper(II) Coordinates to Four of the Oxygen Atoms of Zeolite 6-Rings. Two Single-Crystal Structures of Fully Dehydrated, Largely Cu 2+ -Exchanged Zeolite Y (FAU, Si/Al = 1.56). *J. Phys. Chem. C* **2012**, *116*, 963–974.

4.6. Supplementary material

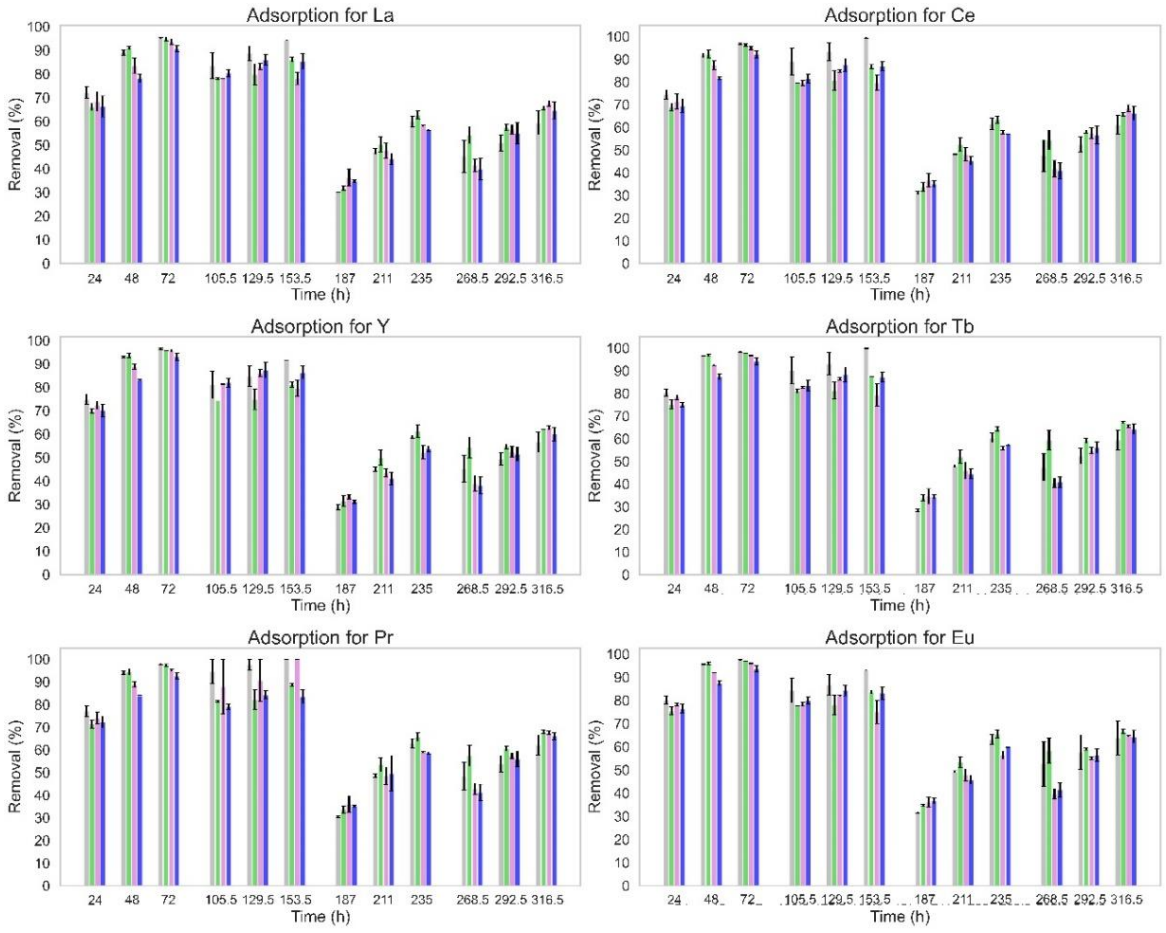

Figure S-4.1: Removal over time for the different REE adsorption by Z13X_NW ( ), Z13X_WW ( ), ZNaOH_NW ( ) and ZNaOH_NW ( ).The first cycle runs between 0 and 72h, the second cycle runs between 81.5 and 153.5 h, the third cycle runs between 163 and 235 h and finally the fourth cycle runs between 244.5 and 316.5 h.

Figure S-4.2: Total recovery for the different REE grouped by cycle and then grouped by sample tested for Z13X_NW (), Z13X_WW (), ZNaOH_NW () and ZNaOH_NW (). Cycle 1 had samples measured at 73.5, 74.5, 76.5 and 78.5 h, cycle 2 includes measurements at 155, 156, 158 and 160 h. For cycle 3, samples were measured at 236.5, 237.5, 239.5 and 241.5 h and finally cycle 4 includes measurements at 318, 319, 321, 323 h.

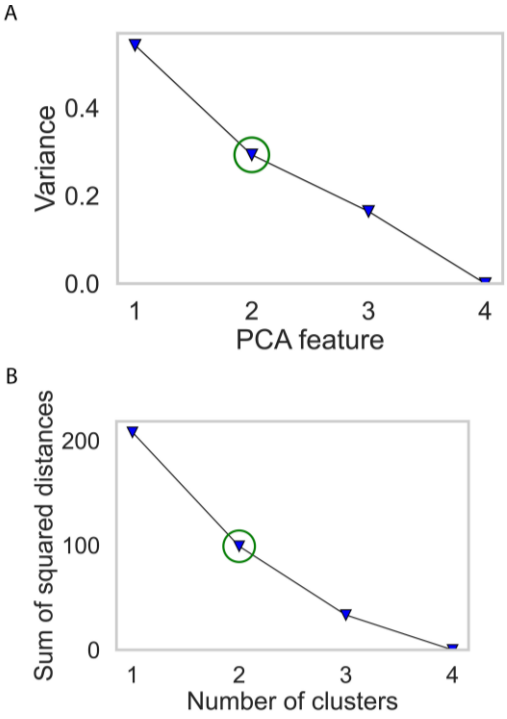

Figure S-4.3: Elbow method for selecting the best option for multiple adsorption and desorption cycles: **A)** PCA and **B)** K-Means.

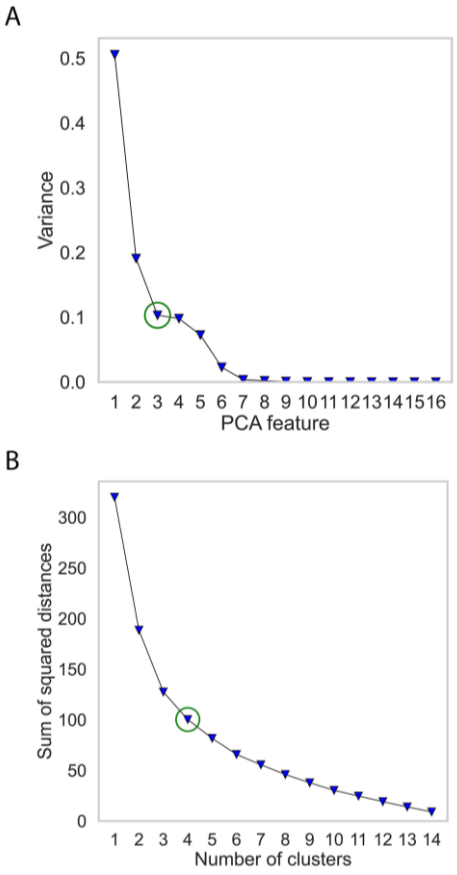

Figure S-4.4: Elbow method for selecting the best option of the cycle adsorption-desorption: **A)** PCA and **B)** K-Means.

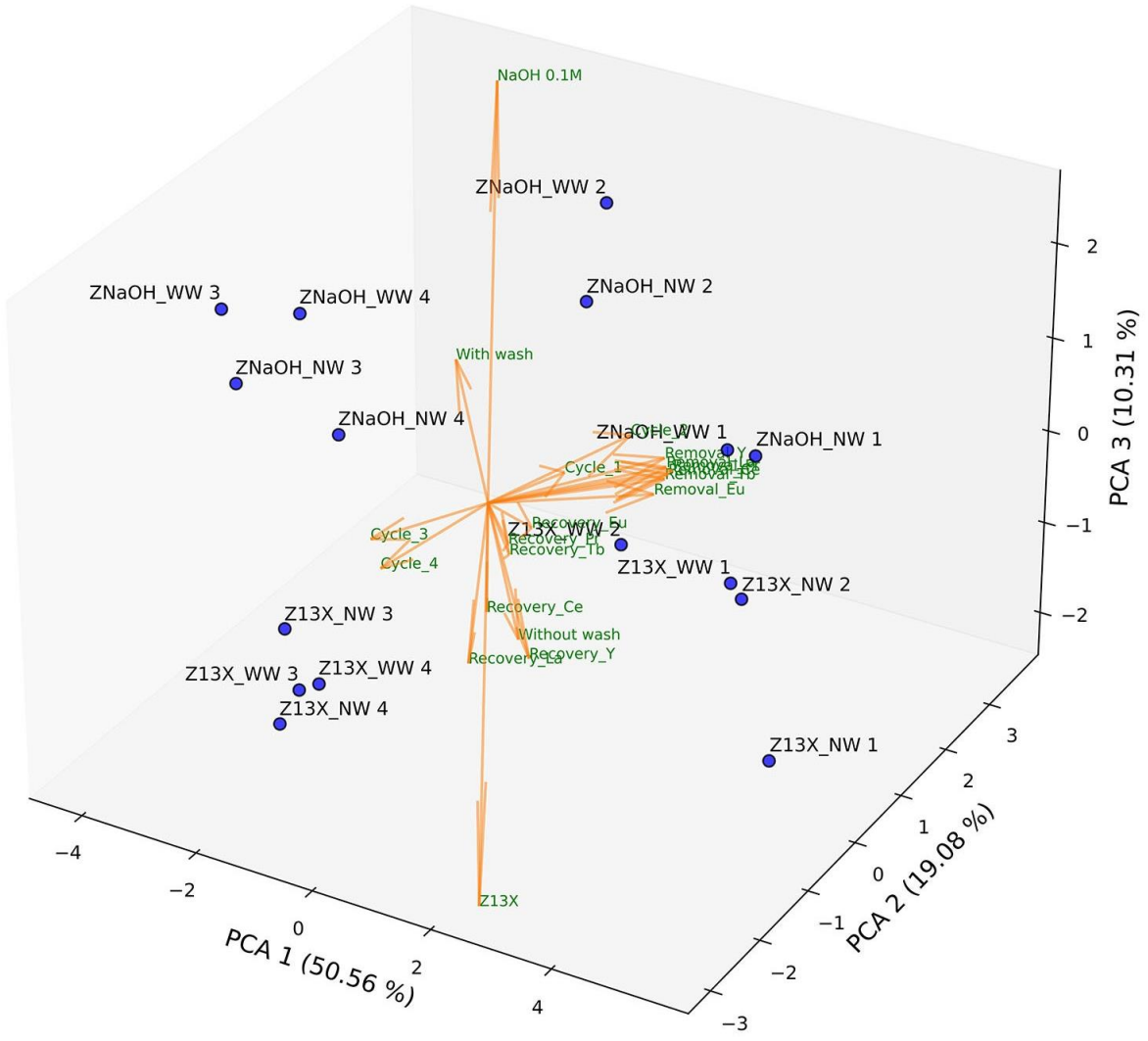

Figure S-4.5: PCA maps in 3D.

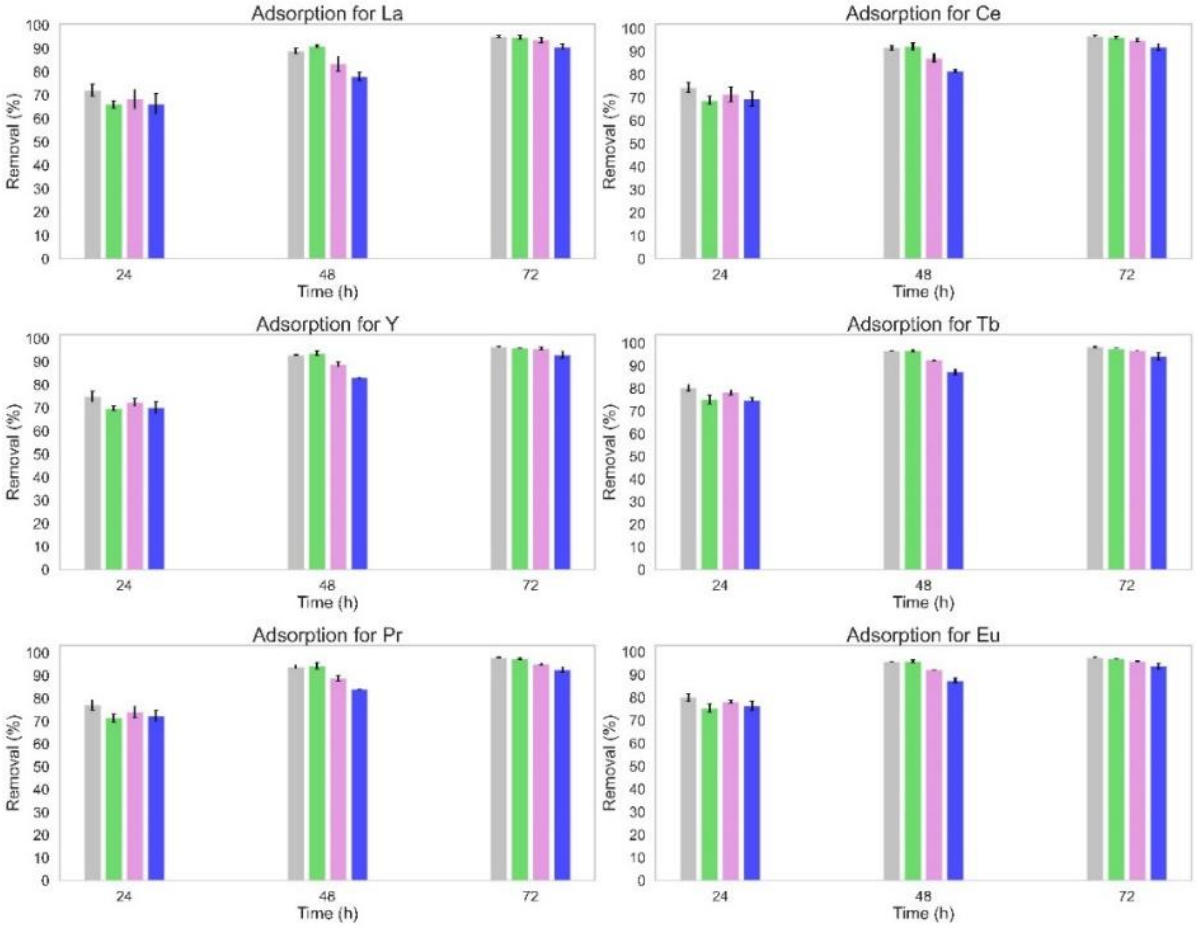

Figure S-4.6: Total removal for the different REE adsorption for Z13X_NW ( ), Z13X_WW ( ), ZNaOH_NW ( ) and ZNaOH_WW ( ) for the first adsorption cycle. The NW refers to the assays without the washing step, and the WW refers to the assays with the NaOH 0.01 M washing step. Samples were taken from the accumulation Erlenmeyer with the outflow eluent.

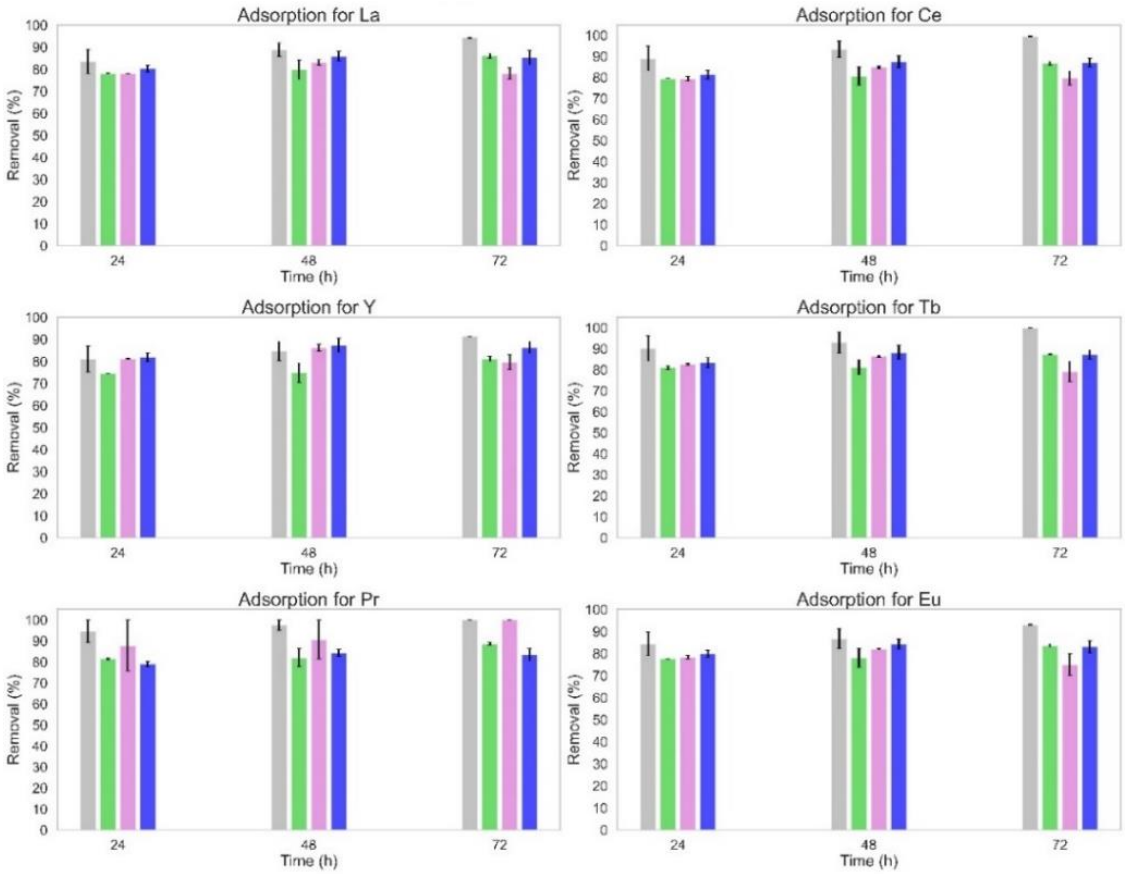

Figure S-4.7: Total removal for the different REE adsorption for Z13X_NW (), Z13X_WW (), ZNaOH_NW () and ZNaOH_WW () for the second adsorption cycle. The NW refers to the assays without the washing step, and the WW refers to the assays with the NaOH 0.01 M washing step. Samples were taken from the accumulation Erlenmeyer with the outflow eluent.

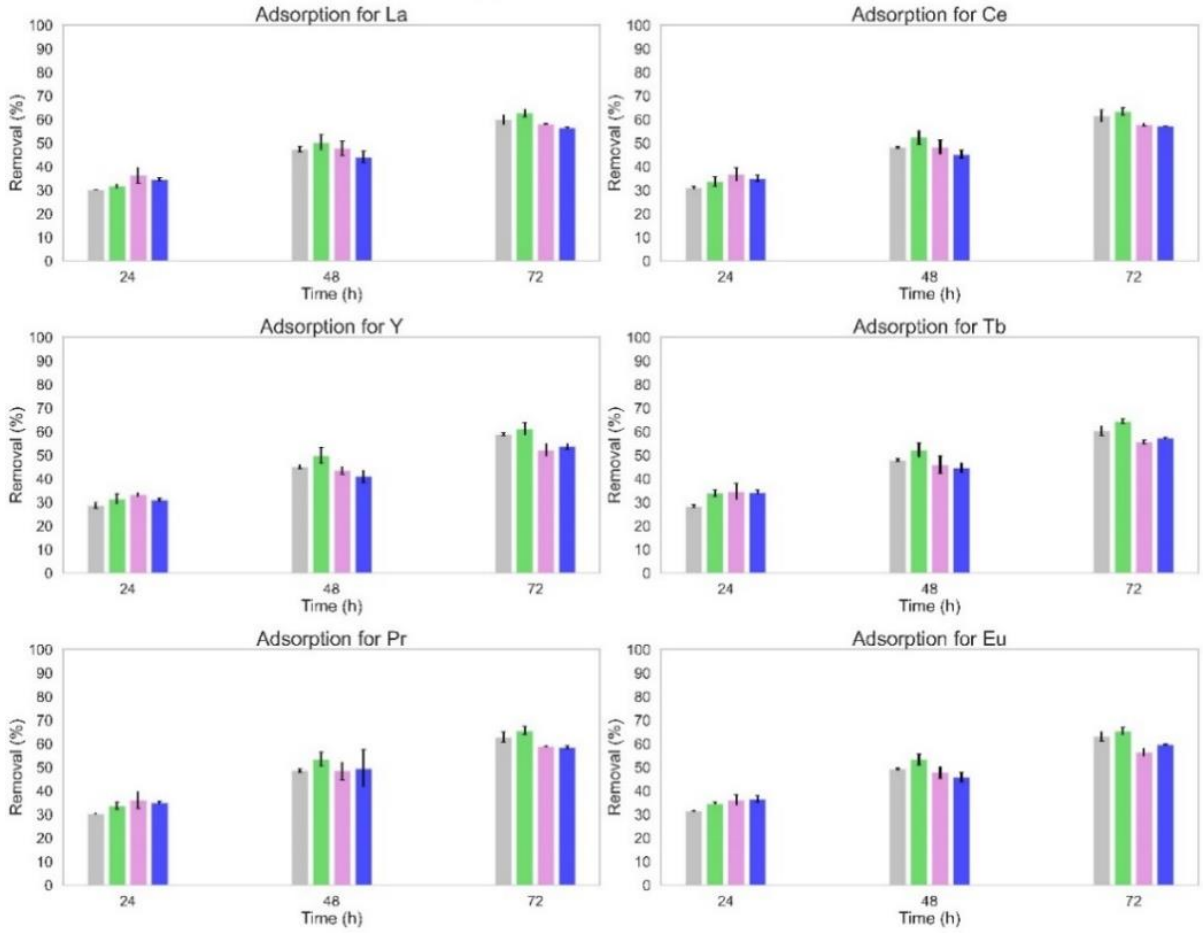

Figure S-4.8: Total removal for the different REE adsorption for Z13X_NW (), Z13X_WW (), ZNaOH_NW () and ZNaOH_WW () for the third adsorption cycle. The NW refers to the assays without the washing step, and the WW refers to the assays with the NaOH 0.01 M washing step. Samples were taken from the accumulation Erlenmeyer with the outflow eluent.

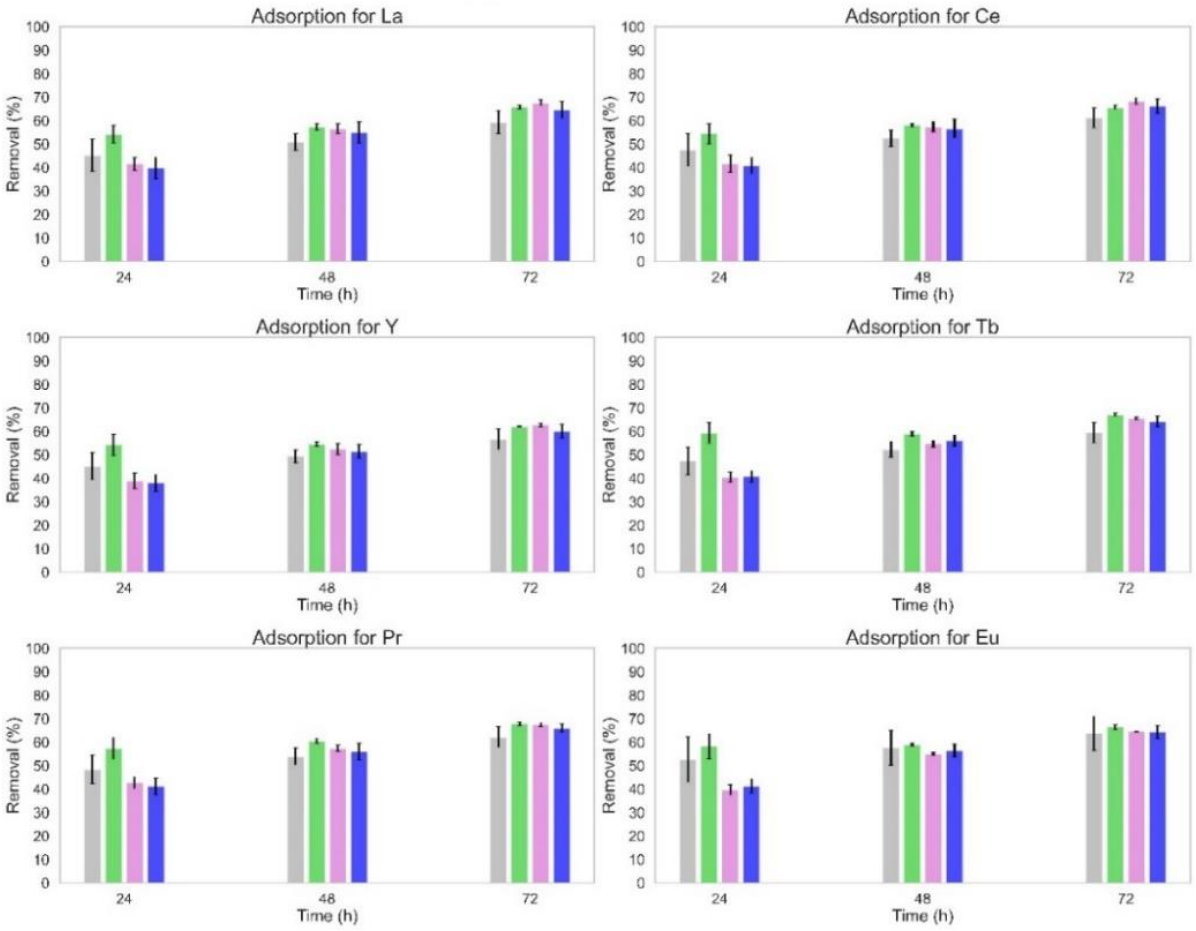

Figure S-4.9: Total removal for the different REE adsorption for Z13X_NW ( ), Z13X_WW ( ), ZNaOH_NW ( ) and ZNaOH_WW ( ) for the fourth adsorption cycle. The NW refers to the assays without the washing step, and the WW refers to the assays with the NaOH 0.01 M washing step. Samples were taken from the accumulation Erlenmeyer with the outflow eluent.

Table S-4.1: Two-Way ANOVA for the total removal percentage of REE after 4 cycles. The NW refers to the assays without the washing step, and the WW refers to the assays with the NaOH 0.01 M washing step.

Bonferroni's multiple comparisons tests	REE					
	La	Ce	Y	Tb	Pr	Eu
Z13X_NW vs. Z13X_WW	No (ns)	No (ns)	No (ns)	No (ns)	No (ns)	No (ns)
Z13X_NW vs. ZNaOH_NW	No (ns)	No (ns)	No (ns)	No (ns)	No (ns)	No (ns)
Z13X_NW vs. ZNaOH_WW	No (ns)	No (ns)	No (ns)	No (ns)	No (ns)	No (ns)
Z13X_WW vs. ZNaOH_NW	No (ns)	No (ns)	No (ns)	No (ns)	No (ns)	No (ns)
Z13X_WW vs. ZNaOH_WW	No (ns)	No (ns)	No (ns)	No (ns)	No (ns)	No (ns)
ZNaOH_NW vs. ZNaOH_WW	No (ns)	No (ns)	No (ns)	No (ns)	No (ns)	No (ns)

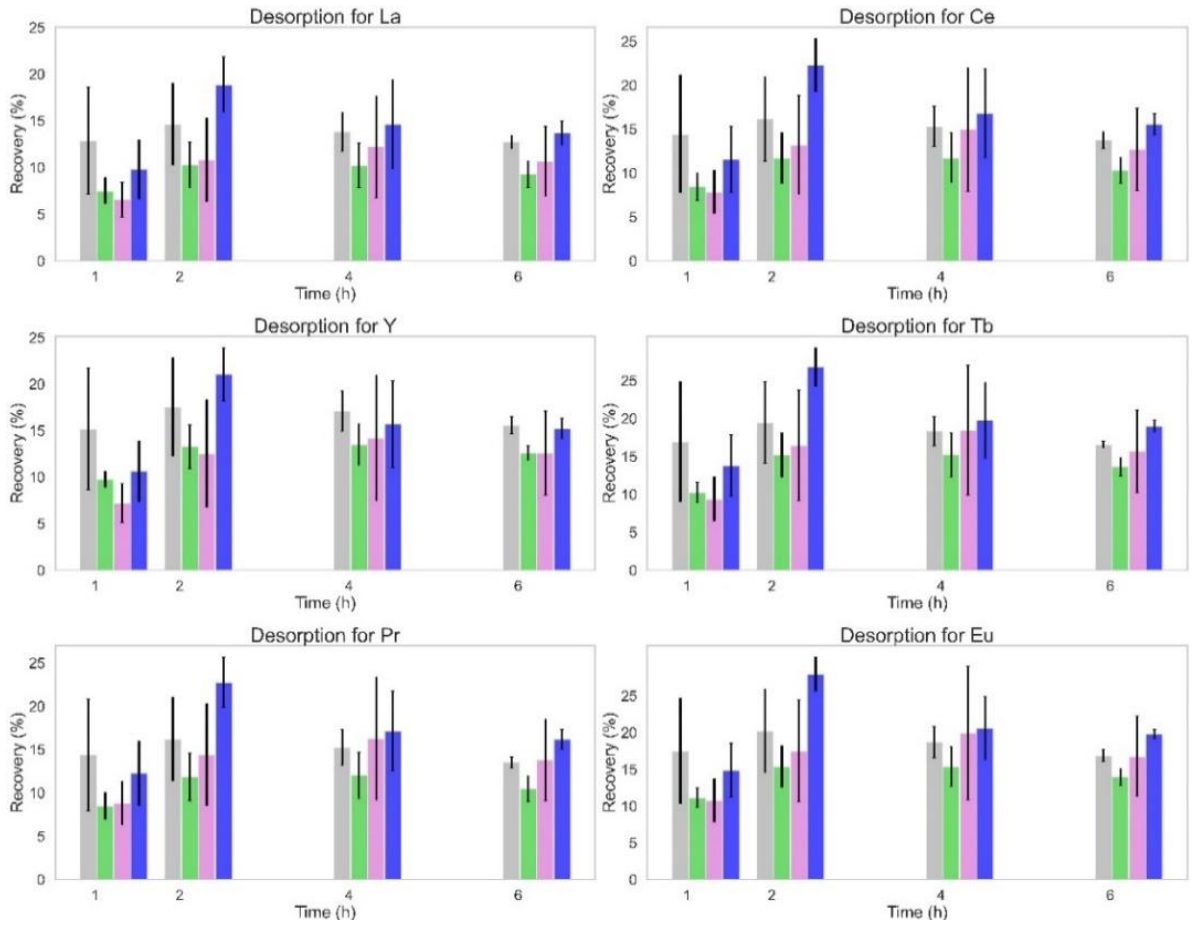

Figure S-4.10: Total recovery of the different REE from Z13X_NW ( ), Z13X_WW ( ), ZNaOH_NW ( ) and ZNaOH_WW ( ) for the first desorption step. The NW refers to the assays without the washing step and the WW refers to the assays with the NaOH 0.01 M washing step. Samples were taken from the accumulation Erlenmeyer with the outflow eluent.

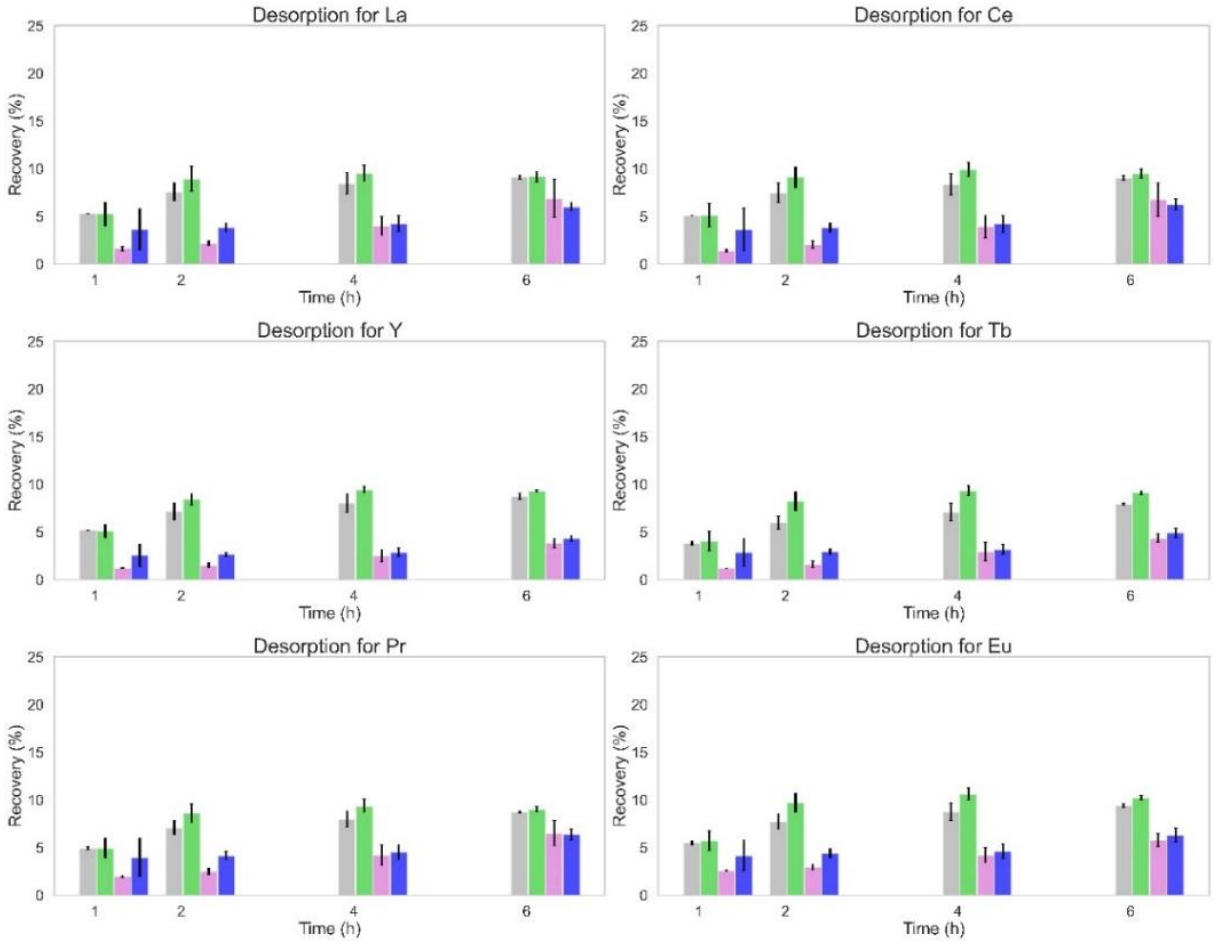

Figure S-4.11: Total recovery for Z13X_NW ( ), Z13X_WW ( ), ZNaOH_NW ( ) and ZNaOH_WW ( ) for the second desorption cycle. The NW refers to the assays without the washing step, and the WW refers to the assays with the NaOH 0.01 M washing step. Samples were taken from the accumulation Erlenmeyer with the outflow eluent.

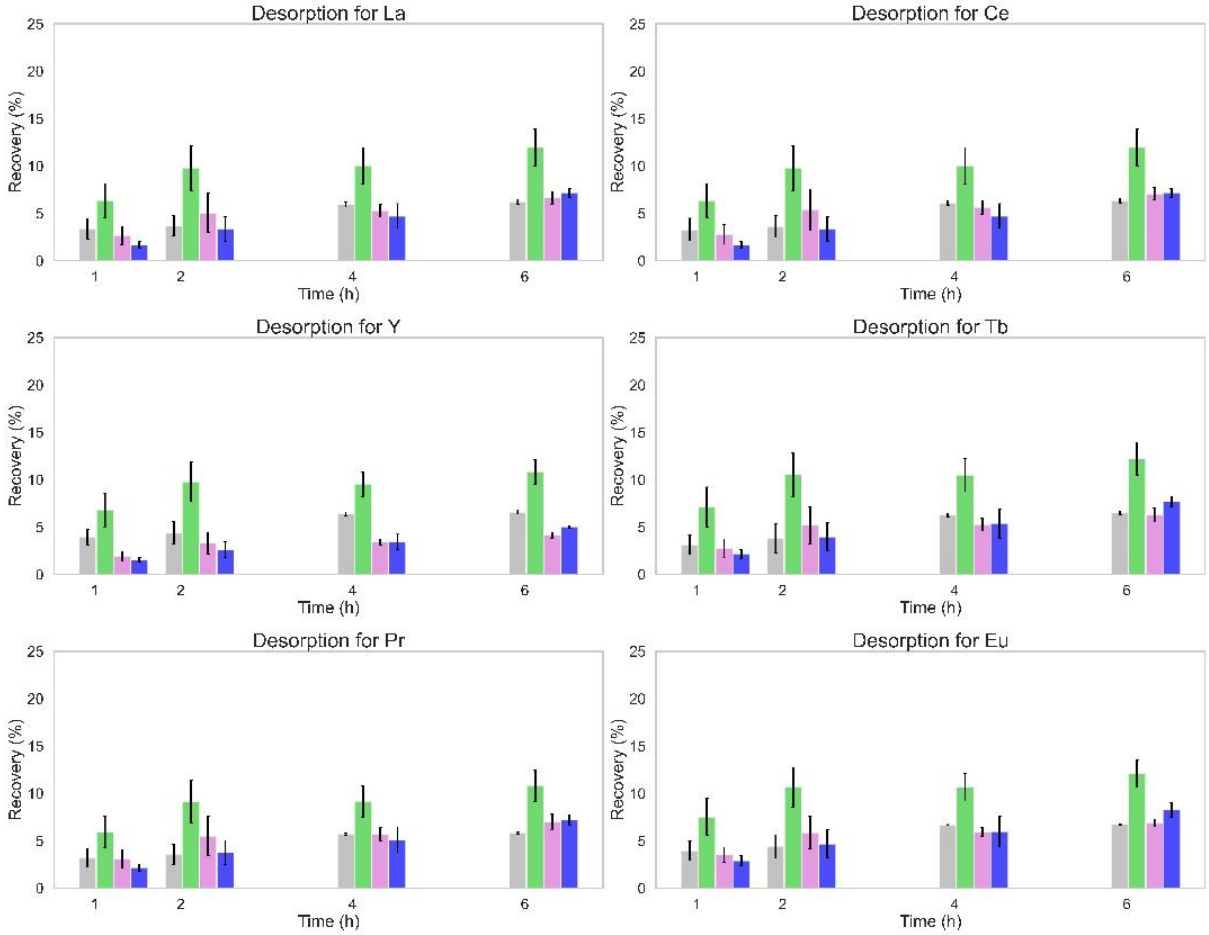

Figure S-4.12: Total recovery for the different REE for Z13X_NW (), Z13X_WW (), ZNaOH_NW () and ZNaOH_WW () for the third desorption cycle. The NW refers to the assays without the washing step, and the WW refers to the assays with the NaOH 0.01 M washing step. Samples were taken from the accumulation Erlenmeyer with the outflow eluent.

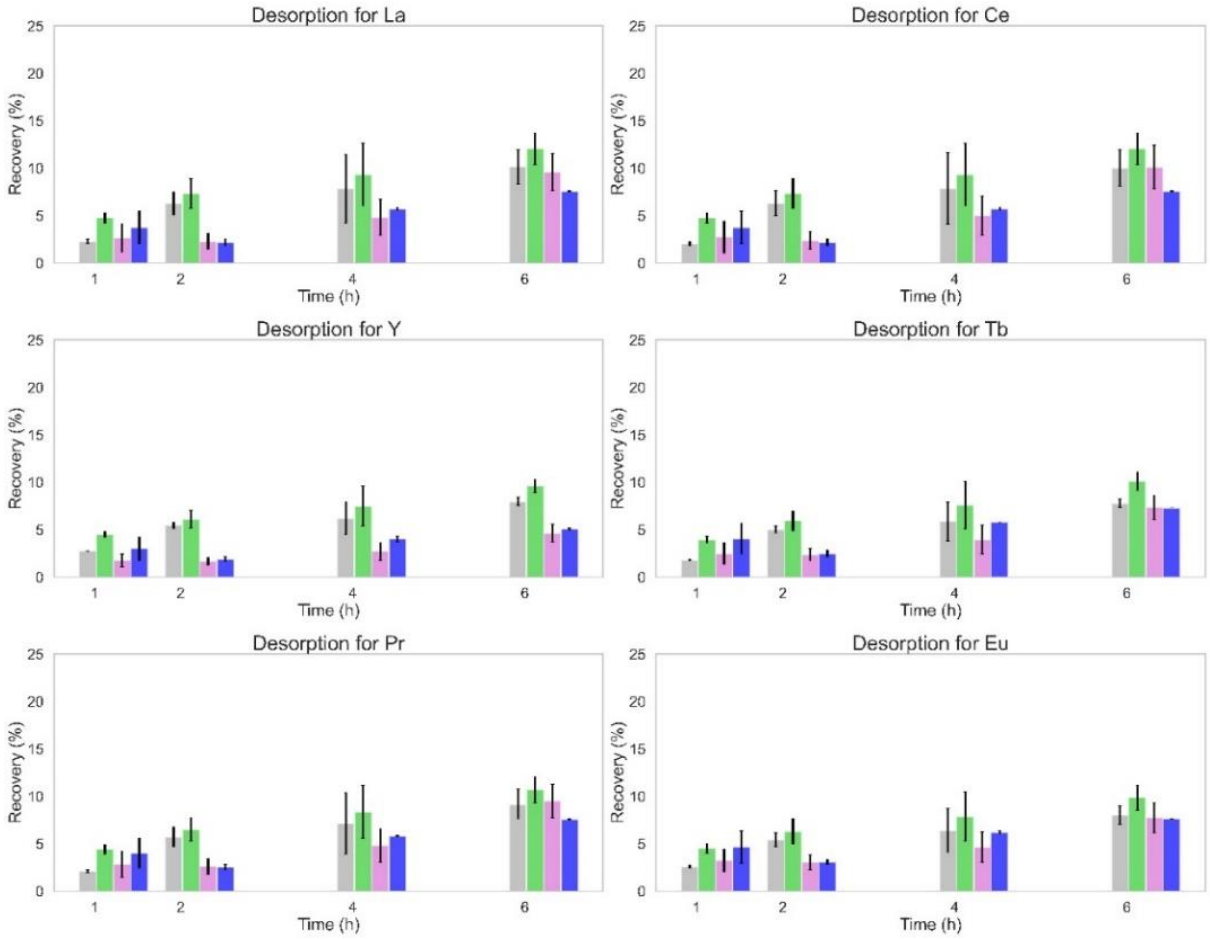

Figure S-4.13: Total recovery for Z13X_NW ( ), Z13X_WW ( ), ZNaOH_NW ( ) and ZNaOH_WW ( ) for the first desorption cycle. The NW refers to the assays without the washing step, and the WW refers to the assays with the NaOH 0.01 M washing step. Samples were taken from the accumulation Erlenmeyer with the outflow eluent.

Table S-4.2: Results for the Two-Way ANOVA for the total recovery percentage after 4 cycles. The NW refers to the assays without the washing step and the WW refers to the assays with the NaOH 0.01 M washing step.

Bonferroni's multiple comparisons tests	REE					
	La	Ce	Y	Tb	Pr	Eu
Z13X_NW vs. Z13X_WW	No (ns)	No (ns)	No (ns)	No (ns)	No (ns)	No (ns)
Z13X_NW vs. ZNaOH_NW	No (ns)	No (ns)	No (ns)	No (ns)	No (ns)	No (ns)
Z13X_NW vs. ZNaOH_WW	No (ns)	No (ns)	No (ns)	No (ns)	No (ns)	No (ns)
Z13X_WW vs. ZNaOH_NW	No (ns)	No (ns)	No (ns)	No (ns)	No (ns)	No (ns)
Z13X_WW vs. ZNaOH_WW	No (ns)	No (ns)	No (ns)	No (ns)	No (ns)	No (ns)
ZNaOH_NW vs. ZNaOH_WW	No (ns)	No (ns)	No (ns)	No (ns)	No (ns)	No (ns)

Table S-4.3: Statistical tests performed for all desorption cycles for each REE. The Two-Way ANOVA compares the total REE recovery from the zeolite. A comparison between each cycle for each tested condition was performed. The NW refers to the assays without the washing step and the WW refers to the assays with the NaOH 0.01 M washing step. The cycle with increased acid concentration is referred to as cycle 5.

REE	Bonferroni's multiple comparisons tests	Two way ANOVA			
		Z13X_NW	Z13X_WW	ZNaOH_NW	ZNaOH_WW
La	Cycle 1 vs. Cycle 2	No (ns)	No (ns)	No (ns)	No (ns)
	Cycle 1 vs. Cycle 3	No (ns)	No (ns)	No (ns)	No (ns)
	Cycle 1 vs. Cycle 4	No (ns)	No (ns)	No (ns)	No (ns)
	Cycle 1 vs. Cycle 5	Yes (****)	Yes (****)	Yes (****)	Yes (****)
	Cycle 2 vs. Cycle 3	No (ns)	No (ns)	No (ns)	No (ns)
	Cycle 2 vs. Cycle 4	No (ns)	No (ns)	No (ns)	No (ns)
	Cycle 2 vs. Cycle 5	Yes (****)	Yes (****)	Yes (****)	Yes (****)
	Cycle 3 vs. Cycle 4	No (ns)	No (ns)	No (ns)	No (ns)
	Cycle 3 vs. Cycle 5	Yes (****)	Yes (****)	Yes (****)	Yes (****)
	Cycle 4 vs. Cycle 5	Yes (****)	Yes (****)	Yes (****)	Yes (****)
Ce	Cycle 1 vs. Cycle 2	No (ns)	No (ns)	No (ns)	No (ns)
	Cycle 1 vs. Cycle 3	No (ns)	No (ns)	No (ns)	No (ns)
	Cycle 1 vs. Cycle 4	No (ns)	No (ns)	No (ns)	No (ns)
	Cycle 1 vs. Cycle 5	Yes (****)	Yes (****)	Yes (****)	Yes (****)
	Cycle 2 vs. Cycle 3	No (ns)	No (ns)	No (ns)	No (ns)
	Cycle 2 vs. Cycle 4	No (ns)	No (ns)	No (ns)	No (ns)
	Cycle 2 vs. Cycle 5	Yes (****)	Yes (****)	Yes (****)	Yes (****)
	Cycle 3 vs. Cycle 4	No (ns)	No (ns)	No (ns)	No (ns)
	Cycle 3 vs. Cycle 5	Yes (****)	Yes (****)	Yes (****)	Yes (****)
	Cycle 4 vs. Cycle 5	Yes (****)	Yes (****)	Yes (****)	Yes (****)
Y	Cycle 1 vs. Cycle 2	No (ns)	No (ns)	No (ns)	No (ns)
	Cycle 1 vs. Cycle 3	No (ns)	No (ns)	No (ns)	No (ns)
	Cycle 1 vs. Cycle 4	No (ns)	No (ns)	No (ns)	No (ns)
	Cycle 1 vs. Cycle 5	Yes (****)	Yes (****)	Yes (****)	Yes (****)
	Cycle 2 vs. Cycle 3	No (ns)	No (ns)	No (ns)	No (ns)
	Cycle 2 vs. Cycle 4	No (ns)	No (ns)	No (ns)	No (ns)
	Cycle 2 vs. Cycle 5	Yes (****)	Yes (****)	Yes (****)	Yes (****)
	Cycle 3 vs. Cycle 4	No (ns)	No (ns)	No (ns)	No (ns)
	Cycle 3 vs. Cycle 5	Yes (****)	Yes (****)	Yes (****)	Yes (****)
	Cycle 4 vs. Cycle 5	Yes (****)	Yes (****)	Yes (****)	Yes (****)
Tb	Cycle 1 vs. Cycle 2	No (ns)	No (ns)	No (ns)	No (ns)
	Cycle 1 vs. Cycle 3	No (ns)	No (ns)	No (ns)	No (ns)
	Cycle 1 vs. Cycle 4	No (ns)	No (ns)	No (ns)	No (ns)
	Cycle 1 vs. Cycle 5	Yes (****)	Yes (****)	Yes (****)	Yes (****)
	Cycle 2 vs. Cycle 3	No (ns)	No (ns)	No (ns)	No (ns)
	Cycle 2 vs. Cycle 4	No (ns)	No (ns)	No (ns)	No (ns)
	Cycle 2 vs. Cycle 5	Yes (****)	Yes (****)	Yes (****)	Yes (****)
	Cycle 3 vs. Cycle 4	No (ns)	No (ns)	No (ns)	No (ns)
	Cycle 3 vs. Cycle 5	Yes (****)	Yes (****)	Yes (****)	Yes (****)
	Cycle 4 vs. Cycle 5	Yes (****)	Yes (****)	Yes (****)	Yes (****)

Pr	Cycle 1 vs. Cycle 2	No (ns)	No (ns)	No (ns)	No (ns)
	Cycle 1 vs. Cycle 3	No (ns)	No (ns)	No (ns)	No (ns)
	Cycle 1 vs. Cycle 4	No (ns)	No (ns)	No (ns)	No (ns)
	Cycle 1 vs. Cycle 5	Yes (****)	Yes (****)	Yes (****)	Yes (****)
	Cycle 2 vs. Cycle 3	No (ns)	No (ns)	No (ns)	No (ns)
	Cycle 2 vs. Cycle 4	No (ns)	No (ns)	No (ns)	No (ns)
	Cycle 2 vs. Cycle 5	Yes (****)	Yes (****)	Yes (****)	Yes (****)
	Cycle 3 vs. Cycle 4	No (ns)	No (ns)	No (ns)	No (ns)
	Cycle 3 vs. Cycle 5	Yes (****)	Yes (****)	Yes (****)	Yes (****)
	Cycle 4 vs. Cycle 5	Yes (****)	Yes (****)	Yes (****)	Yes (****)
Eu	Cycle 1 vs. Cycle 2	No (ns)	No (ns)	No (ns)	No (ns)
	Cycle 1 vs. Cycle 3	No (ns)	No (ns)	No (ns)	No (ns)
	Cycle 1 vs. Cycle 4	No (ns)	No (ns)	No (ns)	No (ns)
	Cycle 1 vs. Cycle 5	Yes (****)	Yes (****)	Yes (****)	Yes (****)
	Cycle 2 vs. Cycle 3	No (ns)	No (ns)	No (ns)	No (ns)
	Cycle 2 vs. Cycle 4	No (ns)	No (ns)	No (ns)	No (ns)
	Cycle 2 vs. Cycle 5	Yes (****)	Yes (****)	Yes (****)	Yes (****)
	Cycle 3 vs. Cycle 4	No (ns)	No (ns)	No (ns)	No (ns)
	Cycle 3 vs. Cycle 5	Yes (****)	Yes (****)	Yes (****)	Yes (****)
	Cycle 4 vs. Cycle 5	Yes (****)	Yes (****)	Yes (****)	Yes (****)

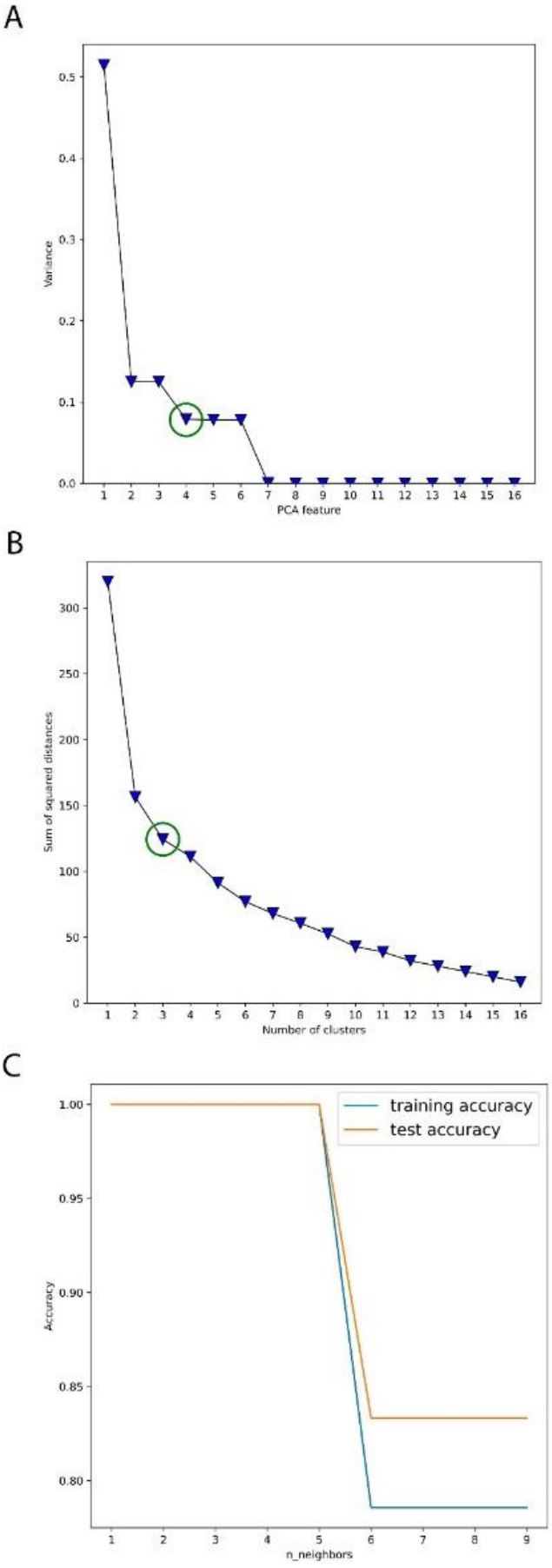

Figure S-4.14: Elbow method for selecting the best desorption: **A)** PCA, **B)** K-Means and **C)** KNN Classifier

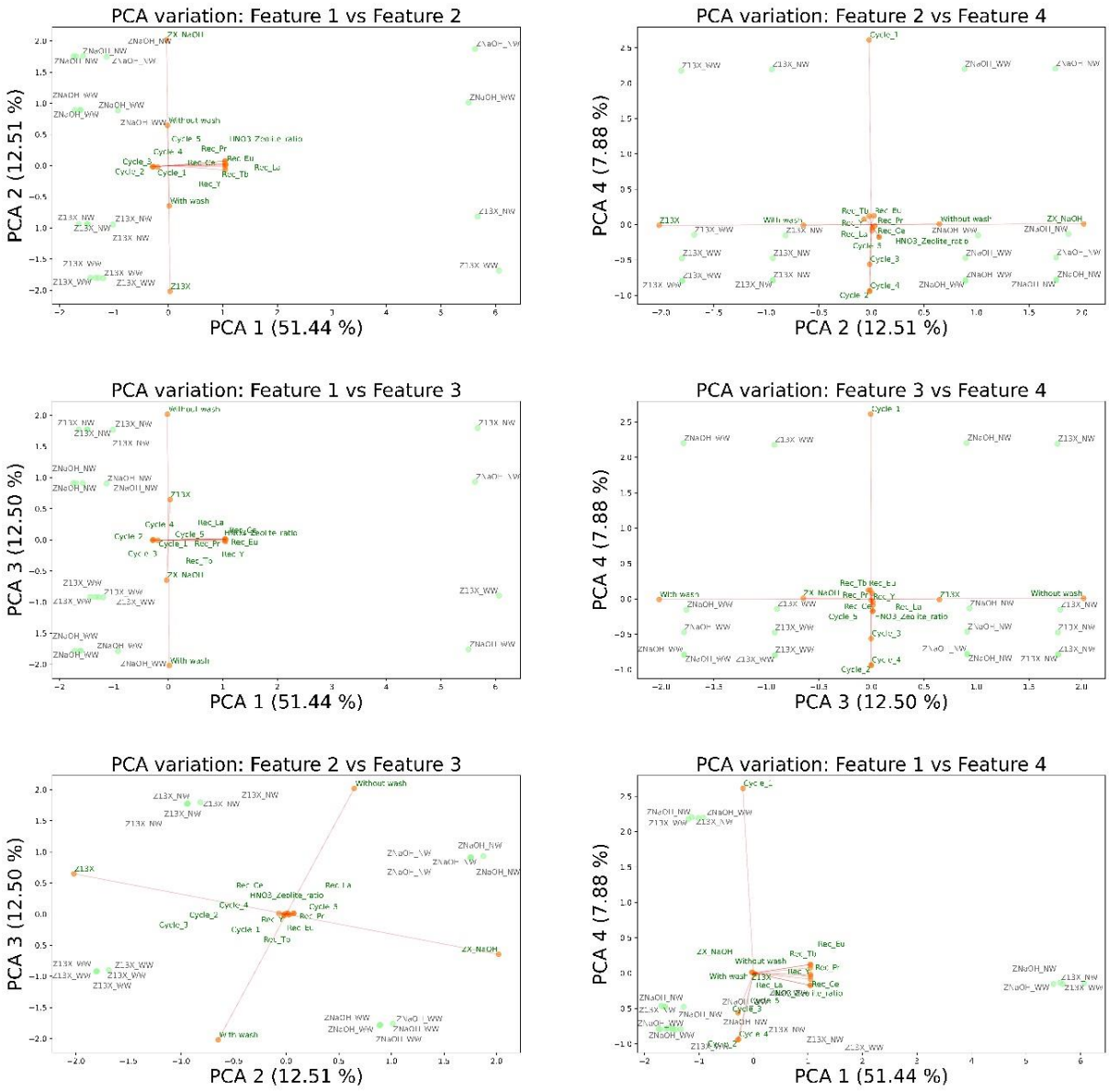

Figure S-4.15: PCA maps. Each map represents the distinct distribution for the selected features.

Chapter 5 – Development of REE/Fe-zeolite catalysts for Fenton-like reaction

Various heterogeneous catalysts based on rare earth elements (REE) and iron supported on zeolites were selected and evaluated by oxidation reactions. REE, which are crucial chemical elements that are used in various activities of our daily lives, including catalysis, were used in the preparation of multiple REE/Fe-zeolite catalysts with lanthanum, praseodymium or cerium, using FAU or MFI structures as supports and obtained by ion exchange or impregnation methods. The efficiency of these REE/Fe-zeolite catalysts was examined in Fenton-like reactions, in the degradation of tartrazine (Tar) and indigo carmine (IC) in aqueous solution. The REE/Fe-zeolite catalysts demonstrated outstanding performance, with Tar being degraded by over 80% and IC being degraded by over 95%. Machine learning algorithms were employed for clustering and classification of the different catalysts, based on their performance. Unsupervised learning algorithms like PCA and K-Means were used for pattern recognition while supervised classifiers were employed to classify catalysts, considering their ability to degrade dyes by Fenton reaction.

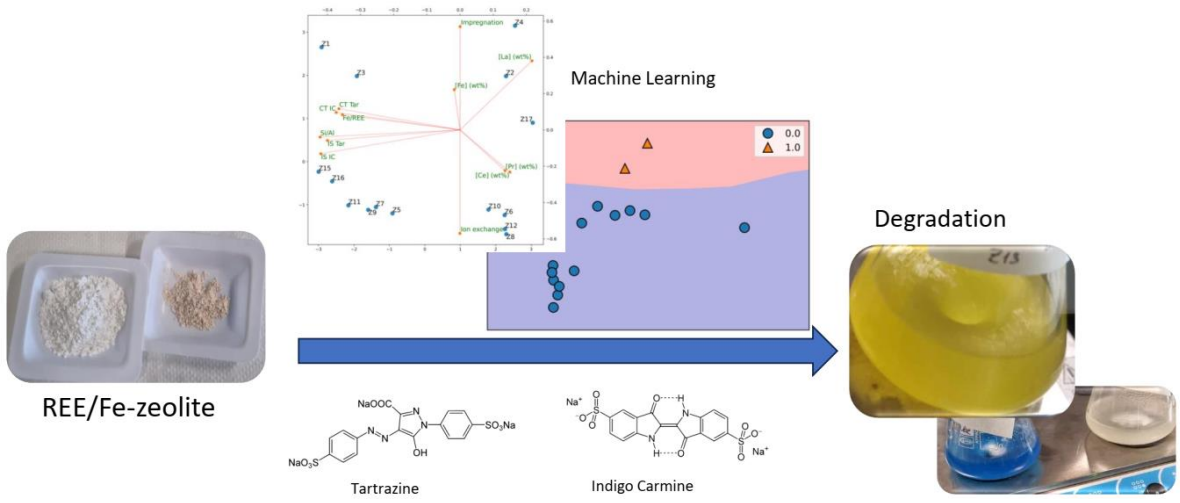

Adapted from: Barros, O.; Parpot, P.; Rombi, E.; Tavares, T.; Neves, I. C; Machine learning approach for classification of REE/Fe-zeolite catalysts for Fenton-like reaction – under revision.

5.1. Introduction

Rare earth elements (REE) are widely used due to their diversified properties such as optical, electrical, metallurgical, catalytic and magnetic [1–4], allowing different daily applications [5–7]. Due to the extensive demand and price, their reutilization is important, but the recycling technology is still in the early stages [8–12]. The hardship in REE recycling is mainly due to the complexity of the process and to the very different amounts of those elements in the end products, ranging from mg to kg [13].

The application of REE in catalysis is gaining attention, as there is a strong interest in designing and developing new heterogeneous catalysts, especially sustainable and cost-effective ones [14]. The definition of a heterogeneous catalyst loaded with recovered REE can be a key-factor for redox reactions applied in environment rehabilitation. Furthermore, these new catalysts can be applied in advanced oxidation processes (AOP) for wastewater treatment [14–17]. Zeolites, which have been reported as suitable supports [10,18–20], are inorganic crystalline microporous aluminosilicates [21–23] that have been used in many catalytic reactions for the production of high-value chemicals [22], including Fenton reactions [23,24]. The Fenton reaction is a process that utilizes hydrogen peroxide (H_2O_2) to degrade organic pollutants and is widely used for environmental remediation [25]. During the typical reaction, hydroxyl radicals (•OH) can be generated in the presence of H_2O_2 and Fe^{2+} [26,27], which are highly reactive and can effectively break down organic molecules [28] into non-toxic products such as CO_2, H_2O and inorganic salts [29].

Dyes are widely used in various industries such as food, pharmaceutical and cosmetic ones, to provide color and visual appeal to products. However, in recent years, their use has raised concerns about their potential health and environmental impacts. Two dyes that have received significant attention are tartrazine (E102) and indigo carmine (E132). Tartrazine (E102) is a synthetic yellow dye widely used in various food and beverage products [20,30] that is linked to some adverse health effects [31] such as allergic reactions, hyperactivity in children and migraines. Indigo carmine (E132) is a blue dye that colors various food and beverage products [30]. It has been linked to multiple adverse effects [31] such as allergic reactions, nausea and skin rashes. These dyes were proved to be degraded by heterogeneous Fenton-type reaction in the presence of H_2O_2 and Fe^{3+} [20].

Machine Learning (ML) approach is useful for selecting the best catalyst among a significant number of prepared REE-zeolite catalysts that were evaluated in the degradation of dyes in aqueous medium through Fenton-type reaction. ML is a branch of artificial intelligence that involves the development of algorithms and statistical models for pattern recognition, predictions or decisions without being explicitly programmed [32]. The capacity of ML algorithms to evaluate large amounts of data from

catalytic reactions and catalyst characterization can help to design the best catalyst according to its performance for a given reaction [33,34]. Various areas of both homogeneous and heterogeneous catalysis have been using ML [35].

The aim of this work is to evaluate the usage of zeolites loaded with REE recovered from contaminated wastewater to act as efficient heterogeneous catalyst for Fenton-like reaction. The prepared REE/Fe-zeolite catalysts will be tested in the degradation of tartrazine and indigo carmine and different ML algorithms will be used to select the best catalyst, also highlighting the importance of the ML approach in the determination of the effect of chemical properties of the catalyst on its performance.

5.2. Materials and Methods

5.2.1.Materials

REE used in this research were cerium [$Ce(NO_3)_3.6H_2O$; 99.5 %; Acros Organics], lanthanum, [$La(NO_3)_3.6H_2O$; 99.9 %; Alfa Aesar] and praseodymium ($PrCl_3.xH_2O$; 99.9 %; Alfa Aesar). These metals were used from previously prepared stock solutions at 1 g/L. The multi-element ICP quality control standard solution, with a concentration of each element under study of 200 mg/L, was purchased from CPAchem. The solution from iron (III) nitrate [$Fe(NO_3)_3.9H_2O$, Aldrich] was prepared as required. A stock solution of 90 mM of hydrogen peroxide (H_2O_2, 30 wt%, Merck) was prepared.

For this work, two zeolite structures were used: (NH_4)ZSM5 from MFI (CBV3024E, Si/Al = 15.00) and FAU with NaY (CBV100, Si/Al = 2.80) in powder form obtained from Zeolyst International, and NaX in powder or pellets, Sigma-Aldrich (Si/Al = 1.64 and Si/Al = 1.50, respectively).

The tartrazine dye ($C_{16}H_9N_4Na_3O_9S_2$, ≥ 90%) was purchased from Sigma Aldrich, while the indigo carmine ($C_{16}H_8N_2Na_2O_8S_2$, ≥ 90%) was obtained from Merck. Deionized water for dye solutions was produced with an ultrapure water system (Milli-Q, EQ 7000).

5.2.2.REE/Fe-zeolite catalysts preparation

The REE/Fe-zeolite catalysts were prepared by ion exchange or by impregnation method. In the first method, a solution of the individual REE (La, Ce or Pr) of 10 or 25 mg/L with or without a controlled pH (4.00) was added to a suspension containing 16 g/L of zeolite, with an orbital shaking of 120 rpm for 24 h. After the REE doping, the REE-zeolite was dried and added to the Fe^{3+} solution (10 mg/L) till a final concentration of 6 g/L was reached, with or without a controlled pH (4.00) and with an orbital shaking at 120 rpm for 24 h. Finally, the suspension was filtered, washed with deionized water, dried at 60 °C overnight and calcined at 350 °C for 4 h under a dry-air stream. For impregnation, the addition of the REE or Fe follows the same conditions used in the ion-exchange method, with the only exception being

the lack of a filtration. The resulting solution was decanted, leaving the catalysts to be dried and then calcinated. The prepared heterogeneous catalysts are displayed in **Table 5.1**.

Table 5.1: Designation and details of REE/Fe-zeolite catalysts and respective method of preparation.

Samples	Label	Zeolite type	pH	Method
$La_{10}Fe_{10}NaX$	A3	FAU powder	4.00	impregnation
$La_{10}Fe_{10}NaX$	A7	FAU pellet	4.00	impregnation
$La_{10}Fe_{10}ZSM5$	Z1	MFI	4.00	impregnation
$La_{10}Fe_{10}NaY$	Z2	FAU	4.00	impregnation
$La_{25}Fe_{10}ZSM5$	Z3	MFI	4.00	impregnation
$La_{25}Fe_{10}NaY$	Z4	FAU	4.00	impregnation
$La_{10}Fe_{10}ZSM5$	Z15	MFI	4.00	ion exchange
$La_{25}Fe_{10}ZSM5$	Z16	MFI	4.00	ion exchange
$La_{25}Fe_{10}NaY$	Z17	FAU	without adjustment	ion exchange
$Ce_{10}Fe_{10}ZSM5$	Z5	MFI	4.00	ion exchange
$Ce_{10}Fe_{10}NaY$	Z6	FAU	4.00	ion exchange
$Ce_{25}Fe_{10}ZSM5$	Z7	MFI	4.00	ion exchange
$Ce_{25}Fe_{10}NaY$	Z8	FAU	4.00	ion exchange
$Pr_{10}Fe_{10}ZSM5$	Z9	MFI	4.00	ion exchange
$Pr_{10}Fe_{10}NaY$	Z10	FAU	4.00	ion exchange
$Pr_{25}Fe_{10}ZSM5$	Z11	MFI	4.00	ion exchange
$Pr_{25}Fe_{10}NaY$	Z12	FAU	4.00	ion exchange

5.2.3.Catalysts characterization

Attenuated Total Reflectance Fourier Transform Infrared spectroscopy (ATR-FTIR) analysis was performed at room temperature using a PerkinElmer Spectrum Two spectrometer equipped with an ATR accessory. A diamond prism was used as the waveguide. All spectra were recorded with a resolution of 2 cm^{-1} in the wavelength region 4000-400 cm^{-1} by averaging 50 scans.

Elemental quantification of the La, Ce, Pr and Fe in the solutions used for metal addition to the zeolites was performed using an ICP-OES spectrometer (Optima 8000, PerkinElmer). The REE quantification is similar to the one described in **Chapter 3**, **3.2.4 Analytical quantification of REE**. The wavelength used for Fe was 238.204 nm with a radial plasma view.

The chemical analysis of the catalyst was performed to quantify La, Ce, Pr, Fe, Si, Al and Na in the solid samples (0.05 g). The samples were thermally treated at 500 ◦C for 12 h to remove the adsorbed water and subsequently placed in a platinum crucible. Then, the melting agent was added ($Li_2B_4O_7$:sample = 15:1 by weight), and the alkaline fusion was carried out in a muffle furnace at 1000 ◦C for 40 min. After cooling of the melt, the resultant fusion bead was transferred into a beaker and heated on a plate at 80 ◦C after addition of 100 mL of 5% HNO_3 (all the samples were found to completely dissolve within 40 min). Finally, the solution was transferred into a volumetric flask (250 mL) and diluted to the desired final volume with milliQ water. The resulting solution was analyzed with a 5110 Inductively Coupled Plasma Atomic Emission Spectroscopy (ICP-AES) spectrometer (Agilent Technologies).

5.2.4.Fenton-like reaction

Catalytic runs were carried out in a semi-batch reactor at atmospheric pressure and 40 °C, under continuous stirring (300 rpm), using a solution of 30 mg/L of tartrazine or of indigo carmine, at pH of 3.00 and a specific concentration of hydrogen peroxide (H_2O_2). The concentration of H_2O_2 used for the tartrazine was 90 mM, while for indigo carmine was 12 mM. The concentration of dyes, the pH and temperature were fixed at optimal values determined in a preliminary evaluation of the degradation of organic pollutants using similar zeolite-based LaFe catalysts [20]. The runs were divided into initial screening (IS) and catalytic tests (CT). Once the assay started, samples were taken at fixed time intervals and the reaction was stopped with the addition of an excess of $NaHSO_3$, which instantaneously consumes the unreacted H_2O_2. The suspension was centrifuged at 12000 rpm for 10 min, and the liquid was then analyzed for the pollutant by UV-vis. The quantification was performed using a microplate spectrophotometer Epoch 2 from Biotek, with the characteristic wavelengths (λ_{max}) at 427 nm and 610 nm for Tar and IC, respectively.

In order to select the best catalyst, an initial screening (IS) was carried out with sampling at the beginning of the run and after 180 min, using a catalyst concentration of 0.8 g/L with 0.5 mL of H_2O_2 at the respective concentration. The remaining conditions of the assay are equal to the ones described above.

The catalytic tests (CT) were carried out with the REE/Fe-zeolite catalysts with liquid samples taken at 0, 15, 30, 60, 90, 120, 180, 240 and 300 min, using a catalyst concentration of 0.8 g/L. The effects of the H_2O_2 load were assessed by using 5 or 0.5 mL at the respective concentration.

Usual Fenton-like reaction kinetics are described by a pseudo first-order model [24] that is used to evaluate the parameters of the degradation of the dyes and its non-linear equation is described by Eq. 5.1:

$$\frac{C_t}{C_0} = e^{-k*(\frac{W}{V})*t} \quad \text{(Eq. 5.1)}$$

C_t (mg/L) is the concentration of the dye at a given time t; C_0 (mg/L) is the initial concentration of dye; k (L/(g*min)) is the rate constant; V (L) is the volume of the solution; W (g) is the mass of catalyst used for the assay and t (min) is the time. Using Eq. 5.2, it is possible to simplify Eq. 5.1 to a more straightforward form (Eq. 5.3), since W and V are constant during the reaction:

$$m = k * (\frac{W}{V}) \quad \text{(Eq. 5.2)}$$

$$\frac{C_t}{C_0} = e^{-m*t} \quad \text{(Eq. 5.3)}$$

A linear form could be achieved according to the following equation:

$$\ln\left(\frac{C_t}{C_0}\right) = -m * t \quad \text{(Eq. 5.4)}$$

5.2.5.Machine learning analysis

ML analysis was conducted using a table designed as DataFrame, with the different catalysts produced as rows, while the different columns or features were filled with the REE and Fe concentrations obtained by the catalyst chemical analysis, the ratio between these two concentrations and the Si/Al ratio. Adding to that information, the dyes degradation reached in the IS and CT assays was also considered as feature.

Supervised and unsupervised ML approaches were applied to all catalytic results. For the unsupervised learner, the Principal Component Analysis, PCA, (method for reducing the dimensionality of data, leading to an increased interpretation and minimizing information loss) was used and K-Means clustering (division of the samples into groups or clusters that are more compatible with each other accordantly to the studied conditions). For this analysis a scaling or normalization of the data is required before using PCA and K-Means.

The supervised learner uses a classification to divide the tested catalysts into good or bad ones, accordantly to their results. K-nearest neighbors classifier (KNN), Decision Tree Classifier, Random Forest and Logistic Regressor Classifier were used to classify the samples. These classifiers are often used in a binary system. In this study, a binary classification approach was employed to evaluate the performance of each catalyst with respect to the degradation of the dye. Based on the obtained degradation results, each dye was classified according to the percentage of conversion. A mean value taking into account the

results obtained for different catalysts and experimental conditions, allows the preliminary selection of the best catalysts. This approach enables the efficiently evaluation and comparison of the performances of the catalysts in a standardized manner (**Table 3.2**).

To develop and evaluate the model's performance, the dataset was divided into two sets: a training set (70% of the data), which contains known output and enables the model to learn how to generalize and apply to new data, and a test set (30% of the data), which was used to evaluate the model's prediction accuracy. The data was divided using a stratified approach, ensuring that both the training and test sets had the same proportion of each class.

Table 5.2: Binary classification used for each REE/Fe-catalyst.

Degradation intervals, %	*Degradation Classification*	*Classification means*	*Binary Classification*
80 < Deg < 100	1		
60 < Deg < 80	2	≥ 4.75	1
40 < Deg < 60	3		
20 < Deg < 40	4	≤ 4.75	0
0 < Deg < 20	5		

All tests were performed using Spyder (Python 3.9) and the required modules for the python analysis as pandas, numpy, scikit-learn, matplotlib and seaborn.

5.2.6.Statistical analysis

The initial screening (IS) results were statistically analyzed using One-Way ANOVA, through which all samples were compared between themselves. The catalytic tests (CT) results were analyzed using Two-Way ANOVA. Bonferroni's multiple comparison test was used for the different comparisons performed.

The tests were performed using the software Graph Pad Prism version 8.0.2 (Graph Pad Software, Inc, San Diego, CA, USA). The results were considered significantly different only when the probability (p-value) was lower than 0.05, assuming a 95 % confidence interval.

5.3. Results and Discussion

In order to select the best FAU catalyst and to compare with the MFI-based ones, Tar degradation was carried out with the catalysts prepared from a solution with an initial concentration of La of 10 ppm. In a previous work [10], NaX was used to remove REE from aqueous solutions and it was found that this particular zeolite was an effective adsorbent [10]. For this reason, NaX prepared by impregnation in the same experimental conditions used for the other REE/Fe-zeolite catalysts, is also included for evaluation as a heterogeneous catalyst (in pellet or powder) for the Fenton-like reaction (**Figure 5.1**).

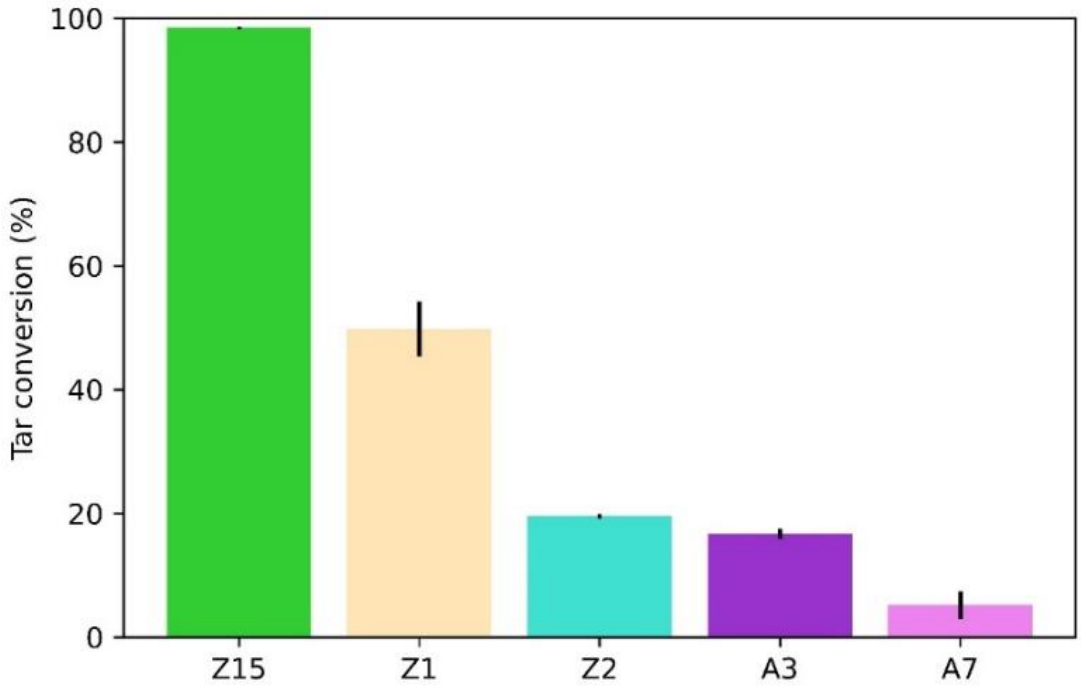

Figure 5.1: Tar degradation in the presence of $La_{10}Fe_{10}$ZSM5 (MFI): Z15, prepared by ion exchange ( ) and Z1, prepared by impregnation ( ); $La_{10}Fe_{10}$NaY (FAU), Z2, prepared by impregnation ( ), $La_{10}Fe_{10}$NaX powder (FAU), A3, prepared by impregnation ( ), and $La_{10}Fe_{10}$NaX pellet (FAU), A7, prepared by impregnation ( ). Conditions of the reaction: 20 mg of catalyst/25 mL of a 30 ppm solution of Tar; 0.5 mL of H_2O_2 90 mM; pH=3; T=40 ^{o}C; t = 180 min.

The best results were obtained with the catalysts based on MFI structure (Z15 and Z1), followed by NaY (Z2) and NaX (A3 and A7), as shown in **Table S-5.1**. The significant differences calculated by the column analysis performed using One-Way ANOVA are shown in **Table S-5.2**. The last one, the powder form (A3) favors the Fenton-like reaction in comparison with the pellets (A7), as the external mass transfer limitations are reduced when the average size of the catalysts particles diminishes. The lower degradation efficiency obtained for NaX was expected since this type of zeolite is mainly used for adsorption processes [10] rather than for catalysis. Moreover, Z2 ($La_{10}Fe_{10}$NaY) reached higher conversion

than any of the NaX catalysts, as NaY zeolite is widely used in catalytic applications [36–38] since it enhances the catalytic role of the supported metal. In addition, Z15 ($La_{10}Fe_{10}$ZSM5), prepared by the ion exchange method, reached higher degradation efficiency than Z1 ($La_{10}Fe_{10}$ZSM5), prepared by the impregnation method, probably due to fact that the metallic active sites are better distributed on the internal surface area. Since NaY and ZSM5 loaded with catalytic metals act as bifunctional catalysts, enhancing the metal role within the desired reaction, they are expected to have advantage over NaX as supports for heterogeneous catalysis. These last REE/Fe-zeolite catalysts were analyzed by FTIR (**Figure 5.2**).

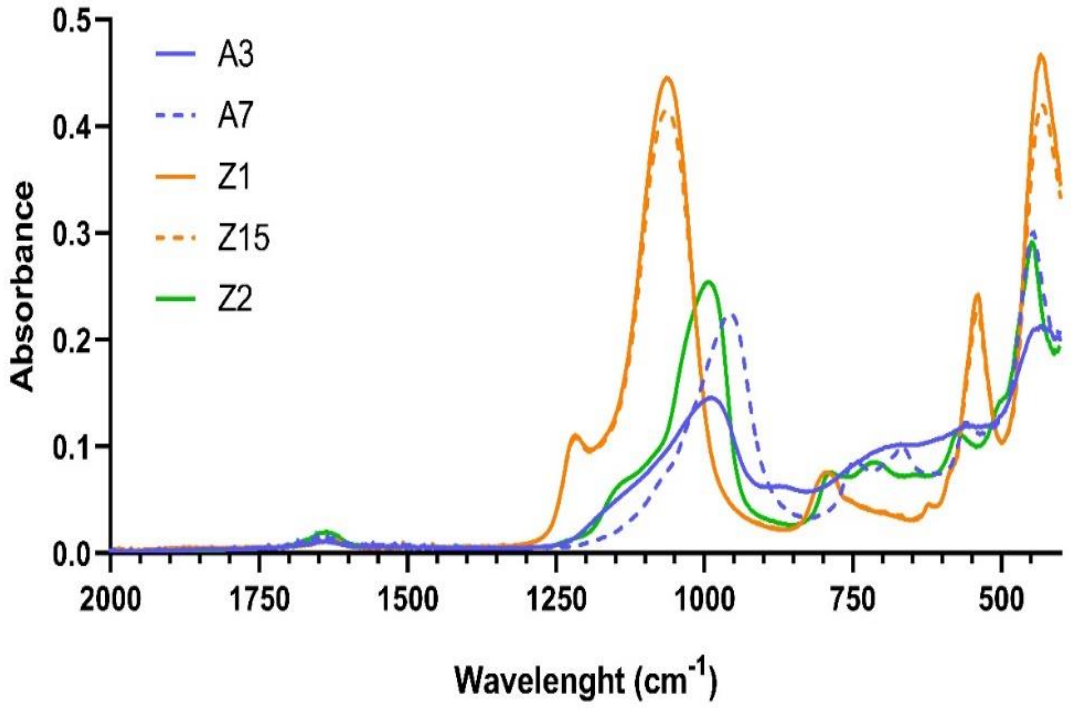

Figure 5.2: FTIR spectra of the REE/Fe-zeolite catalysts in the spectral region of 2000 to 450 cm^{-1}.

The characteristic bands of the pristine zeolite structures (FAU and MFI) dominate the spectra of all REE/Fe-zeolite catalysts. The band characteristic of the $\delta(H_2O)$ vibration mode of absorbed water on zeolite was identified at 1640 cm^{-1}, whereas the typical bands of the lattice vibrations of the framework are evidenced in the 1330-450 cm^{-1} range [20,39–41]. The band at 960 cm^{-1} is attributed to the asymmetric stretching of Si–O and Al–O bonds belonging to SiO_4 and AlO_4 tetrahedra [39–41], whereas the bands at 670 cm^{-1} and near 750 cm^{-1} are related to the Si–O symmetric stretching and oscillations of aluminosilicate oxygen tetrahedral chains [40,41]. The band at about 550 cm^{-1} is attributed to the symmetric stretching vibrations of bridge bonds Si–O–Si and bending vibrations of O–Si–O [42].

The granulometry of the NaX pristine structures may have an impact over the spectra of A3 (powder) and A7 (pellets) while the catalysts preparation method seems not to influence the spectra of the two ZSM5-based catalysts (Z1 and Z15).

In addition, the framework Si/Al ratio of the samples based on FAU structure can be determined by FTIR analysis using the following Eq. 5.5 [42]:

$$x=3.857-0.00621W_{DR} \quad \text{(Eq. 5.5)}$$

where $x = (1+Si/Al)^{-1}$ and W_{DR} is the wavenumber at 500-650 cm^{-1}, related to the vibrations of the FAU lattice [42] (**Table 5.3**).

Table 5.3: Framework Si/Al ratios obtained from the FTIR analysis.

Label	Samples	Framework Si/Al
-	NaY	2.80
-	NaX	1.64
A3	$La_{10}Fe_{10}NaX$	1.44
A7	$La_{10}Fe_{10}NaX$	1.64
Z2	$La_{10}Fe_{10}NaY$	2.49

The framework Si/Al values of FAU-based catalysts show that Z2 and A3 were the most affected by the introduction of both metals, La and Fe. The reduction of the Si/Al ratio for A3 may be related with the acid character of the metals solution. The powder form of A3, with larger surface area, makes it more sensitive to its circumstances than A7 with a pelleted form and smaller specific surface area. The lower degradation performance of A3 and Z2 is probably related to the impregnation method used in their preparation, which affects more the zeolite structure than the ion exchange method. The impregnation method results in a weak metal-support interaction and large metal sites are obtained, while ion exchange reaches a finer metal dispersion [43], with reactional advantages. The larger metal sites resulting from the impregnation method lead to a reduced conversion efficiency.

Based on the obtained catalytic results, ZSM5 and NaY structures were selected as the supports to prepare the REE/Fe-zeolite catalysts for degrading Tar and IC through the Fenton-like reaction. Tar degradation was carried out in the same reaction conditions as those in **Figure 5.1** [20]. IC degradation was instead performed using two different H_2O_2 concentrations, 12 and 90 mM. It was proven (data not shown) that a 7.5-fold increase in H_2O_2 concentration is not justified, as it does not lead to any improvement in degradation performance after 180 min of reaction.

5.3.1.Selection of the best REE/Fe-zeolite catalyst using IS results

The results for the PCA analysis are shown in **Figure S-5.1A**, after the scaling of the DataFrame. Two principal components, PCA 1 and PCA2 (variables created from the linear composites of the original variables with the highest variance), were selected to build the PCA, and the same value was obtained with the Knee Locator method [44]. The results obtained for PCA are shown in **Figure 5.3A**. These results are shown in a biplot where the bottom *x* and left *y* are used for samples distribution, while the top *x* and right *y* are used for the distribution of the different features.

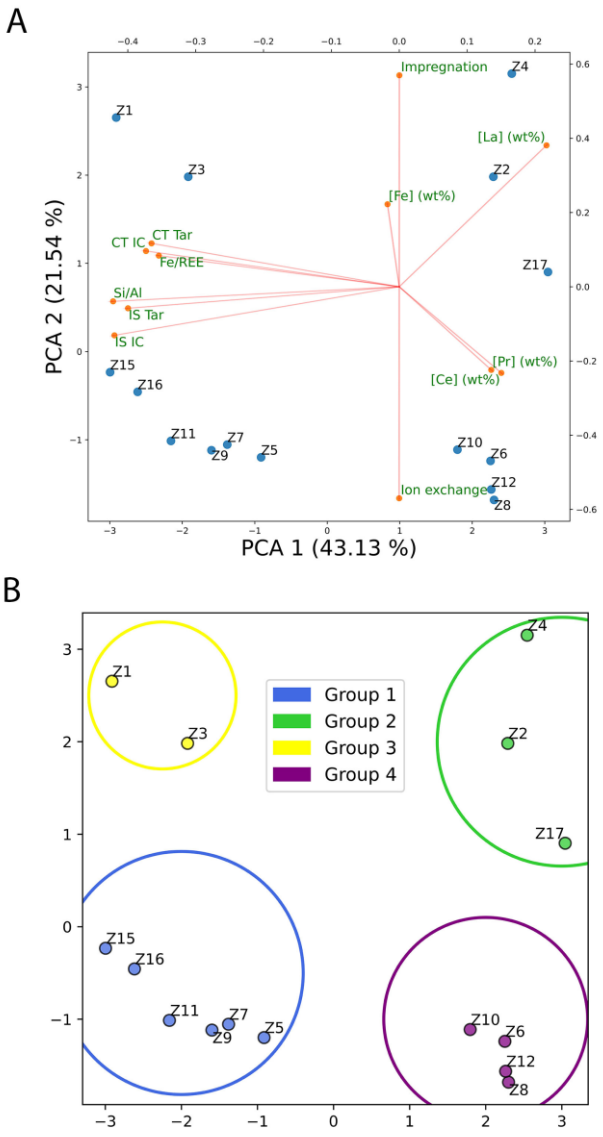

Figure 5.3: Graphical distribution of the ML analysis for the different catalysts: **A**) PCA analysis; **B**) K-Means algorithm. The IS and CT values are referred to initial screening and catalytical tests, respectively, for tartrazine (Tar) and for indigo carmine (IC).

The *cos* of the angle between the analyzed features indicates their correlation. Values close to 1 (angle near 0º) indicate that features are directly correlated, values near -1 (angle near 180º) indicate

indirect correlation and values next to 0 (angle near 90º) show no correlation. The CT for Tar and IC, the IS for Tar and IS, the Si/Al ratio and the Fe/REE ratio seem to have some direct correlation between each other. This positive correlation suggests that the ratios Si/Al and Fe/REE might have an influence on the degradation of the tested dyes, foreseeing that the catalysts with higher ratios have better catalytic properties. It is reported in different applications that catalysts with higher Si/Al ratio have a higher activity and higher selectivity [45]. Apparently, there is no correlation with the preparation methods or with the Fe concentration. Adding to that, a negative correlation between degradation and REE concentration in the zeolites was found, suggesting that increasing concentrations of REE seem not to improve dyes degradation. A higher amount of REE on the catalysts surface might not imply a better dye degradation, just larger active sites not as efficient as smaller but more dispersed ones. The Fe concentration has a positive correlation with the impregnation preparation method and a negative correlation with the ion exchange, indicating that the catalysts produced by impregnation could have a higher Fe concentration than the ones made via ion exchange. This higher quantity of Fe could be related to the selectivity of this metal by the zeolite.

The catalysts group division based on the results of the PCA could be performed in diverse ways and for that reason it was tested by K-Means algorithm, shown in **Figure 5.3B**. This analysis provided four clusters based on the Elbow method, presented in **Figure S-5.1B** and confirmed by the Knee Locator method. Group 1 consists in Z5, Z7, Z9, Z11, Z15 and Z16, group 2 in Z2, Z4 and Z17, group 3 in in Z1 and Z3 and finally, group 4 in Z6, Z8, Z10 and Z12. The groups 1 and 3 seem to be more influenced by the values of Si/Al and Fe/REE ratios as well as by the results of the degradation tests for both dyes. This suggests that these groups may include the best catalysts (possibly Z15, Z16 and Z3), mainly due to the stronger influence of the degradation results of Tar and IC. Group 2 appears to be primarily affected by the concentration of La and by the impregnation method, whereas in group 3 the key determinants were the concentrations of Pr and Ce, along with the ion exchange method. Important to mention that group 1 includes catalysts designed with all REE of interest, while group 3 and group 2 include only La catalysts and group 4 includes only Ce and Pr catalysts.

The combination shown in **Figure 5.3** helps to perform a division between groups considering the zeolite type and the preparation method. For example, the zeolite type division would consist of groups 1 and 3, both related to the higher Si/Al ratio, which is characteristic of the ZSM5 zeolite used as support for these catalysts, while groups 2 and 4 should have a lower Si/Al, characteristic of NaY zeolite. The preparation method division would consist in groups 2 and 3, as both used the impregnation method, while groups 1 and 4 used the ion exchange protocol. It is important to mention that the preparation

method division just includes the results for La catalysts, as this was the only REE involved in both methods. Therefore, these observations will help to assess the extent of the possible differences between the catalysts accordantly to the previously mention characteristics.

The dye degradation obtained with the catalysts based on the two zeolite types and the REE concentration on the starting solution are highlighted in **Figure 5.4**.

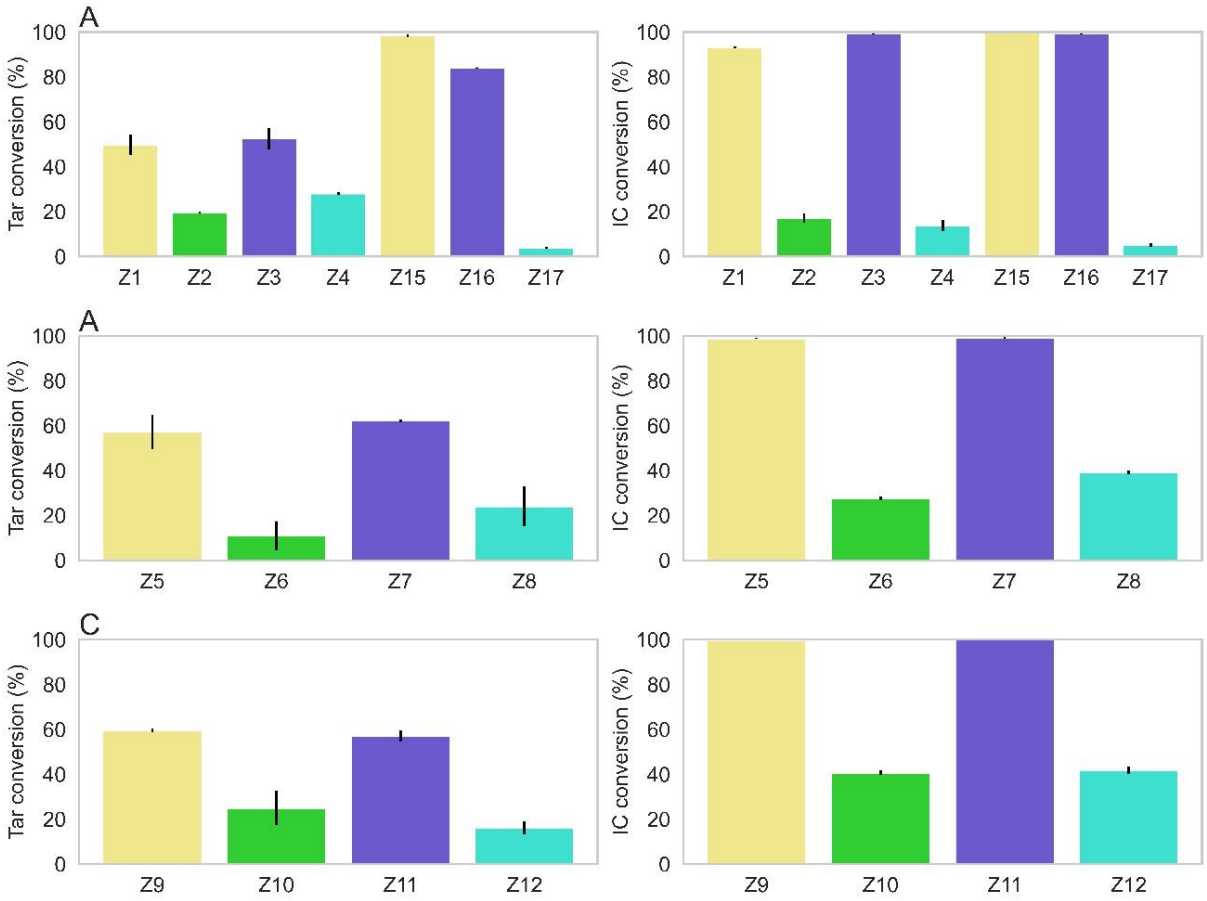

Figure 5.4: Degradation of Tar and IC using the REE/Fe-zeolite catalysts for **A**) La, **B**) Ce and **C**) Pr, after IS test. The catalysts are divided into ZSM5 (MFI) with a REE concentration of: 10 mg/L ( ) and 25 mg/L ( ); NaY (FAU) with a REE concentration of: 10 mg/L ( ) and 25 mg/L ( ). Conditions of the reaction: 20 mg of catalyst/25 mL at 30 ppm of dye; 0.5 mL of 90 mM of H_2O_2 for Tar and of 12 mM of H_2O_2 for IC; pH=3; T=40 °C and 3 h of reaction.

The best catalytic results for the degradation of both dyes by Fenton-like reaction were obtained for ZSM5 used as support, as shown in **Figure 5.4** and validated by the statistical differences presented in **Table S-5.3**. Remarkably, in the case of IC degradation, the performance of the catalysts is similar between La, Ce or Pr for the same support. The worst results considering these three metals were obtained with the NaY supported catalysts, with a slight IC degradation enhancement with the supported Ce or Pr (**Table S-5.3**). Overall, these results confirm the observations described in **Figure 5.3A**, with

a remarkable difference in the degradation of the dyes based on the zeolites used as supports of the catalysts. This was shown in **Figure 5.3A**, where catalysts with higher Si/Al ratio will also promote a higher conversion of the dyes in the IS and CT assays.

Only one significant difference was found between Z1 and Z16 (based on ZSM5 with different preparation methods) for Tar degradation in what concerns the effect of the REE concentration, as shown in **Table S-5.4**. The only difference suggests an improvement of the catalyst when using higher REE concentration in the preparation solution by ion exchange. For IC, the catalytic results may be divided into two groups. The first one includes the catalysts with Ce and with Pr. Only one significant difference was found between Z6 and Z8 (ZSM5) for the IC degradation with the increment of the REE concentration in starting solution from 10 to 25 mg/L, as shown in **Table S-5.4**. The second group includes the catalysts produced with La. Significant differences were found between Z1 and Z3 (based on ZSM5 by impregnation with preparation solution concentration of 10 and 25 mg/L La, respectively), Z1 and Z16 (based on ZSM5 and prepared by the two methods, with preparation solution concentration of 10 and 25 mg/L La, respectively) and Z2 and Z17 (based on NaY with different preparation methods, different pH approaches and with 10 and 25 mg/L La in the starting solution, respectively), in the IC degradation. In the first two cases, higher concentration of REE implies an improvement in the dye degradation. The same conclusion is not validated by the comparison between Z2 and Z17 as too many parameters are affecting simultaneously the degradation mechanism.

It is possible to evaluate the differences between the tested REE, **Figure 5.4**. For the same metal concentration in the starting solution and the same support, it can be seen that the conversions obtained with La catalyst were the best for Tar. Five significant differences were found for Tar conversion (four for ZSM5 and one for NaY), as shown by **Table S-5.5**. The significant differences between the La catalysts Z15 and Z16 versus Ce or Pr supported on ZSM5, imply that the La catalysts reach higher conversions during the IS assays than the other REE. The Z17 and Z8 NaY catalysts achieved low conversions, but with significant differences, which could indicate an influence of the REE in the catalyst performance. The preparation method, impregnation versus ion exchange, could also justify some differences, but this hypothesis was not supported as there was no significant difference between Z17 and Z12, NaY catalysts with Pr. Regarding the IC conversion, nine significant differences were found (two for ZSM5 and seven for NaY), as shown by **Table S-5.5**. The differences between the samples of La/Fe supported on ZSM5, Z1, confirm that this catalyst is not good for indigo degradation as shown in **Figure 5.4**. The detected differences are related not only with the REE but also with the catalysts preparation

method. On the other hand, NaY catalyst with Pr reached better conversion than with La or with Ce. In this case, these differences are more related with the REE rather than with the preparation method.

The last division shown in the PCA distribution, **Figure 5.3A**, regards the catalysts preparation method. The evaluation of the importance of this parameter only includes La/Fe-zeolite catalysts, the only ones prepared by the two methods, impregnation and ion exchange. NaY supported catalysts reached low degradations, but they will be kept in this analysis to assess the influence of the preparation method. The results are shown in **Figure 5.5**.

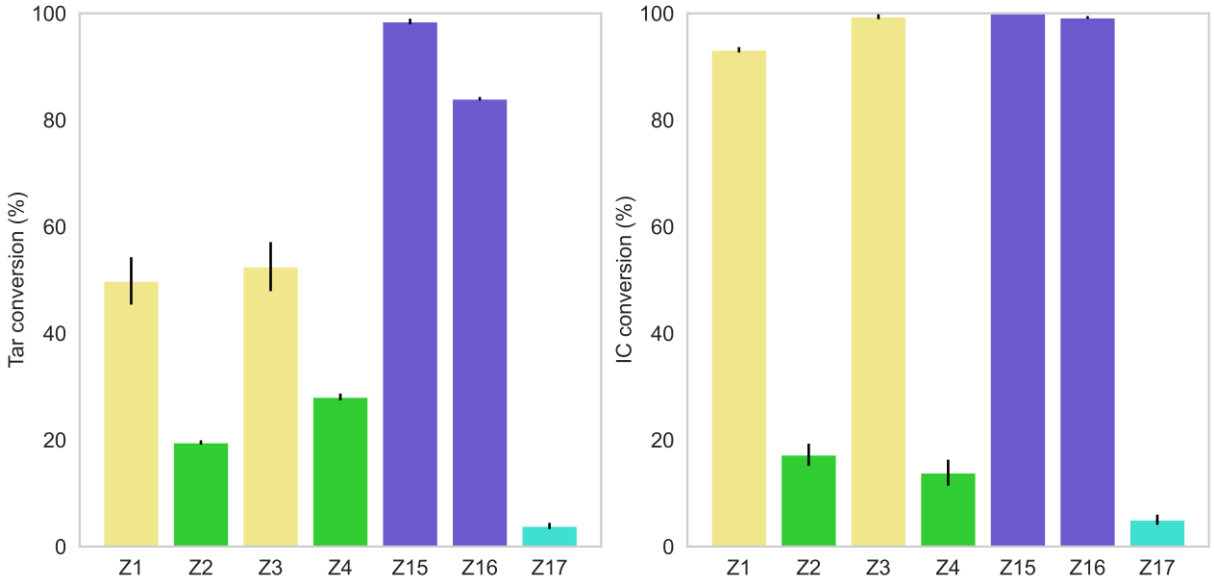

Figure 5.5: IS conversion of the two dyes by La/Fe catalysts prepared by different methods. The catalysts are divided into ZSM5 (MFI): impregnation ( ) and ion exchange ( ); NaY (FAU): impregnation ( ) and ion exchange ( ). Conditions of the reaction: 20 mg of catalyst/25 mL at 30 ppm of dye; 0.5 mL of 90 mM H_2O_2 for Tar and 12 mM H_2O_2 for IC; pH=3; T=40 °C and 3 h of reaction.

The catalytic performance of Z3 ($La_{25}Fe_{10}$ZSM5 by impregnation), Z15 ($La_{10}Fe_{10}$ZSM5 by ion exchange) and Z16 ($La_{25}Fe_{10}$ZSM5 by ion exchange) are very similar. The Z1 ($La_{10}Fe_{10}$ZSM5 by impregnation) have significant differences compared to those catalysts for the IC degradation, as shown in **Table S-5.4** and **Table S-5.6**. For Tar degradation, those differences are more visible, with the best catalytic results being obtained with the La/Fe-ZSM5 prepared by the ion-exchange method, Z15 and Z16 (**Table S-5.6**).

The NaY catalysts Z2 and Z4 provide better conversions with a significant difference when compared with the Z17 (**Table S-5.6**), which suggest that in this case, the impregnation method enhances the pollutant degradation, probably due to more REE/Fe in the catalyst, leading to an increase

of ·OH. However, the results obtained with the La/Fe-NaY catalysts are worse than the ones obtained with ZMS5 as support, as stated before.

The dye degradation results attained with La/Fe-ZSM5 suggest that the ion exchange method for the preparation the catalysts is better than the impregnation method. As previously stated, the impregnation method is related to a weak metal support interaction and large metal sites are obtained [43], while ion exchange reaches a finer metal dispersion [43], with reactional advantages.

The degradation dissimilarities are related to the different amounts of the metals added to the zeolites depending on the preparation method. A chemical analysis by ICP-AES of the solid REE/Fe-zeolite catalysts, after microwave assisted acid digestion, was performed (**Table 5.4**).

Table 5.4: Chemical analysis of the solid REE/Fe-zeolite catalysts.

Sample	Label	Si/Al	REE (wt%)	Fe (wt%)	Fe/REE
$La_{10}Fe_{10}ZSM5$	Z1	13.72	0.02	0.88	40.00
$La_{10}Fe_{10}NaY$	Z2	2.31	0.18	0.30	1.67
$La_{25}Fe_{10}ZSM5$	Z3	14.70	0.06	0.48	7.33
$La_{25}Fe_{10}NaY$	Z4	2.30	0.47	0.73	1.55
$La_{10}Fe_{10}ZSM5$	Z15	14.57	0.04	0.85	20.50
$La_{25}Fe_{10}ZSM5$	Z16	14.59	0.04	0.66	16.00
$La_{25}Fe_{10}NaY$	Z17	2.50	0.52	0.84	1.63
$Ce_{10}Fe_{10}ZSM5$	Z5	15.06	0.02	0.43	20.00
$Ce_{10}Fe_{10}NaY$	Z6	2.40	0.17	0.42	2.50
$Ce_{25}Fe_{10}ZSM5$	Z7	14.90	0.04	0.46	10.50
$Ce_{25}Fe_{10}NaY$	Z8	2.37	0.42	0.56	1.35
$Pr_{10}Fe_{10}ZSM5$	Z9	15.02	0.02	0.39	17.00
$Pr_{10}Fe_{10}NaY$	Z10	2.38	0.11	0.63	5.80
$Pr_{25}Fe_{10}ZSM5$	Z11	14.89	0.02	0.30	14.00
$Pr_{25}Fe_{10}NaY$	Z12	2.35	0.21	0.59	2.80

As expected, the ZSM5 are more selective for iron than for REE and NaY reach higher metal loading than the MFI structure, due to their lower Si/Al ratio, 2.80 for NaY compared to 15.00 for ZSM5, which results in a higher ion exchange capacity of the FAU structure. In addition, the amounts of La and of Ce in NaY are similar, with a ratio Fe/REE ranging from 1.67 to 1.55 for La and between 2.50 and

1.33 for Ce, depending on the concentrations of the initial solutions. The same effect is not observed for Pr on NaY, in which the ratio Fe/REE is higher than for the others REE, with 5.8 to 2.8 for a REE concentration of 0.11 and 0.21 wt %, respectively. Independently of the REE used on the FAU structure, a decrease in the total Si/Al ratio was registered in the samples prepared at pH 4.00 by impregnation (Z2 or Z4) or by ion-exchange (Z6, Z8, Z10 and Z12) when compared to the respective pristine zeolite. The sample Z17 prepared by ion-exchange without fixed pH shows a Si/Al ratio different from the pristine NaY (Si/Al = 2.80), which confirms that the acidic media affect the FAU structure by dealumination, especially the Fe solution with a pH of 3.37, while the pH of the La solution was 5.91.

The introduction of REE or Fe only slightly affects the MFI structure, especially in the case of Ce (Z5 and Z7) or Pr (Z9 and Z11), since the total Si/Al ratio of these samples are very close to the pristine zeolite, 15.00. The Si/Al ratio is more affected when the catalysts are prepared by impregnation (Z1 and Z3). With the increase in La concentration in sample Z3, the ratio of Fe/REE significantly decreases. A similar but not so severe effect was observed for the other REE, Pr (Z10 and Z12).

The REE adsorption on MFI structures, after 24 h assays, ranged between 23 and 35 % for La, 47 and 68 % for Ce, 24 and 38 % for Pr, of the original amount of the sorbates in solution, that could be 10 or 25 mg/L. FAU structures are even more efficient in adsorbing REE and Fe than MFI due to a lower Si/Al ratio and therefore they are more adequate for cations with high charge density. The difference in the ionic radius of sorbates: Fe^{3+} (0.63 Å), La^{3+} (1.032 Å), Ce^{3+} (1.01 Å) and Pr^{3+} (0.99 Å) justifies the selectivity of both structures for Fe in detriment of REE.

In summary, there is a clear difference between the two zeolite structures and the REE/Fe-ZSM5 catalysts have the best degradation results with both dyes by Fenton-like reaction. Adding to that, there is also a difference between the degradation achieved by the catalyst depending on the REE on its surface, as La catalyst tends to reach better results than the ones containing Ce and Pr. The ion exchange preparation method proved to be the best option for the REE/Fe-catalyst production. Finally, an increase in the REE concentration in the staring solution for catalysts preparation seems not to be relevant, given the similarity of the dye conversions for the same support and for same REE, with some exceptions. The lack of significant differences of the pollutant conversion can justify the use of the starting solution with the lowest concentration that allows an efficient degradation reaction.

Combining these pieces of information, it may be concluded that within the tested possibilities the best catalysts is the La/Fe-ZSM5 produced via the ion exchange method, with the minimal amount, 10 mg/L, of REE that promotes the dye degradation. The collected data will allow to evaluate the

performance of Machine Learning classification algorithms and their ability to correctly identify the best REE/Fe-zeolite catalyst, based on accurate information.

Each sample was considered using a binary classification, where 0 corresponds to a bad performance, while 1 is regarded as a good one. The binomial classification was carried out in agreement with **Table 3.2** and the results were added to the previous data frame. This classification resulted in two REE/Fe-catalysts with a classification of 1, while the rest had a classification of 0. Then, the classification was carried out using KNN, Decisions Trees, Random Forests classifiers and Logistic Regression. The results for the different classifiers are shown in **Figure 5.6**.

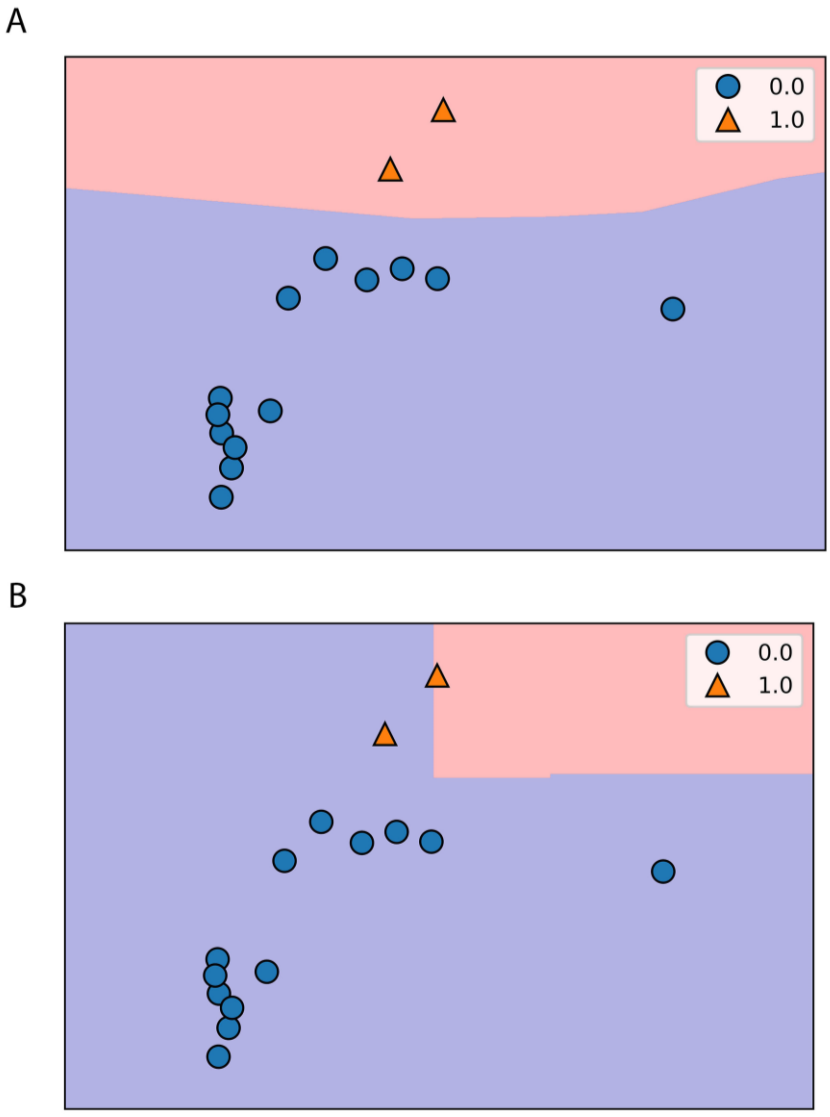

Figure 5.6: Classification of all different REE/Fe-zeolite catalysts using ML algorithms: **A**) KNN classifier, Decision Tree classifier and Logistic Regression **B**) Random Forest classifier. The 1 represent a good catalyst, while the 0 is a bad catalyst accordantly to the evaluation performed. The different colors, violet and orange, represent the zone of a good or bad catalyst, respectively.

The KNN Classifier, **Figure 5.6A**, selected one neighbor (n_neighbors) accordingly to the accuracy values for both training and test sets, as shown in **Figure S-5.1C**. The Decision tree (**Figure 5.6A**) used a random state of 20, the Random Forest (**Figure 5.6B**) used 10 for n estimators with the same random state and the Logistic Regression used the same random state (**Figure 5.6A**). For the classifiers, it is crucial to avoid overfitting concerning the training set, as it is for the learning process. A suitable generalization of the model from the training set should be validated by the test set in order to obtain a good classification for new and unseen data. Overall, the classifiers were able to separate the two best catalysts from all the tested ones, by using the data relating each catalyst to its classification.

Initially, each classifier was evaluated with the respective *scores* related to the accuracy of the values under consideration (*x* and *y* values of training and test data), as shown in **Table 5.5**.

Table 5.5: Scores obtained for the different classification algorithms.

Classifier	*KNN*	*Decision Tree*	*Random Forest*	*Logistic Regression*
Training score	100 %	100 %	80 %	90 %
Test score	100 %	100 %	90 %	100 %

The *scores* obtained for the different classifiers are mainly 100 % except for Random Forest and for Logistic Regression, this one for the training set, which is a good result considering that three over four classifiers presented 100 % of accuracy in the test set and two over four reached 100 % for the training set. An evaluation was performed using the classification report, which gives a summary of percentages values of precision, recall and f1-scores (**Table 5.6**). The precision is related to the accuracy of making good predictions, the recall is the value of the correctly identified positive predictions and the f1-score is the harmonic mean of the precision and recall. Another vital metric to assess the classification used is the confusion matrix. For this evaluation, the real classification from the binary classification (*y_real*) and the predicted classification (*y_pred*) calculated from the model were used.

Table 5.6: Classification of catalysts by classifier algorithms for the test set. The results include precision, recall and f1-score.

Classifier		KNN		Decision Tree		Random Forest		Logistic Regression	
Catalyst classification		*Bad*	*Good*	*Bad*	*Good*	*Bad*	*Good*	*Bad*	*Good*
Model Performance	*Precision*	100	100	100	100	80	0	100	100
	recall	100	100	100	100	100	0	100	100
	f1-score	100	100	100	100	89	0	100	100

All classifiers, with the exception of Random Forest, presented a 100 % score for the precision, recall and f1-scores of the prediction advanced by the model. All classifiers tested are very similar, except for Random Forests, and the overall result is shown in **Figure 5.7**. For the best models there were identified only true positives (the model predicted it was true, and it was actually true) and true negatives (the model predicted it was false and it was actually false).

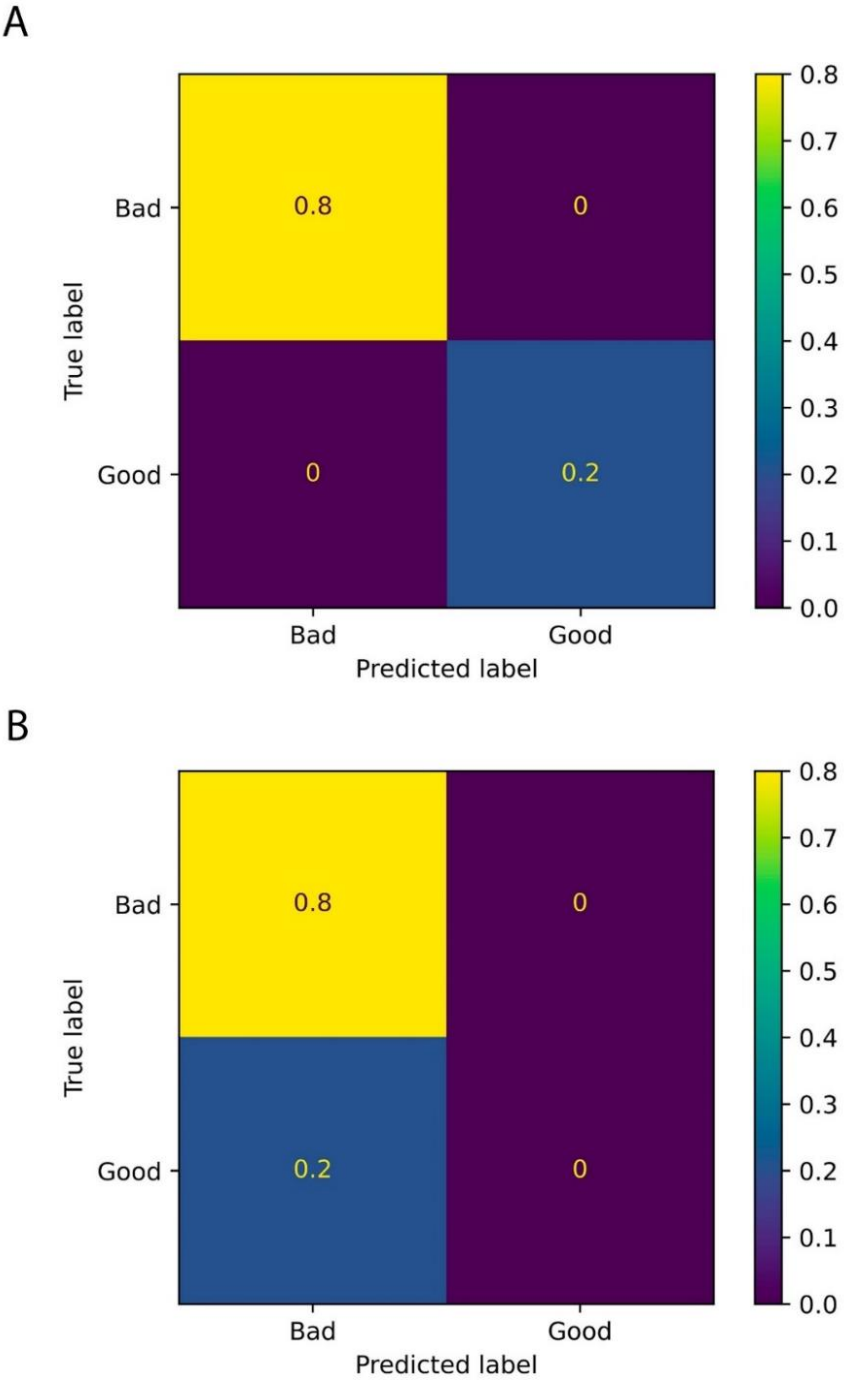

Figure 5.7: Confusion matrix for the test data for KNN, Decision Tree and Logistic Regression (**A**) and Random Forests (**B**). The values shown refer to the fraction of the true correct predictions (when the model got it right) and false incorrect predictions (when the model got it wrong).

This evaluation verified that two of the 15 REE/Fe-zeolite catalysts were selected as the best ones, namely Z15 ($La_{10}Fe_{10}$ZSM5) and Z16 ($La_{25}Fe_{10}$ZSM5). These catalysts were prepared with ZSM5, as **Figure 5.4** indicates this zeolite is the best support and shows that La is the best REE of the three tested for the catalytic reaction. From **Figure 5.4**, 10 and 25 mg/L were the initial solution concentrations selected for that support, confirming that there is no difference between the two in terms of pollutants degradation. Finally, these catalysts were prepared by the ion exchange method, as it was the best method for ZSM5, as shown in **Figure 5.5**.

The Pearson correlation was calculated to evaluate the relation of the different features used and to see how they correlate with each other, and the results are displayed as a heatmap, **Figure 5.8**.

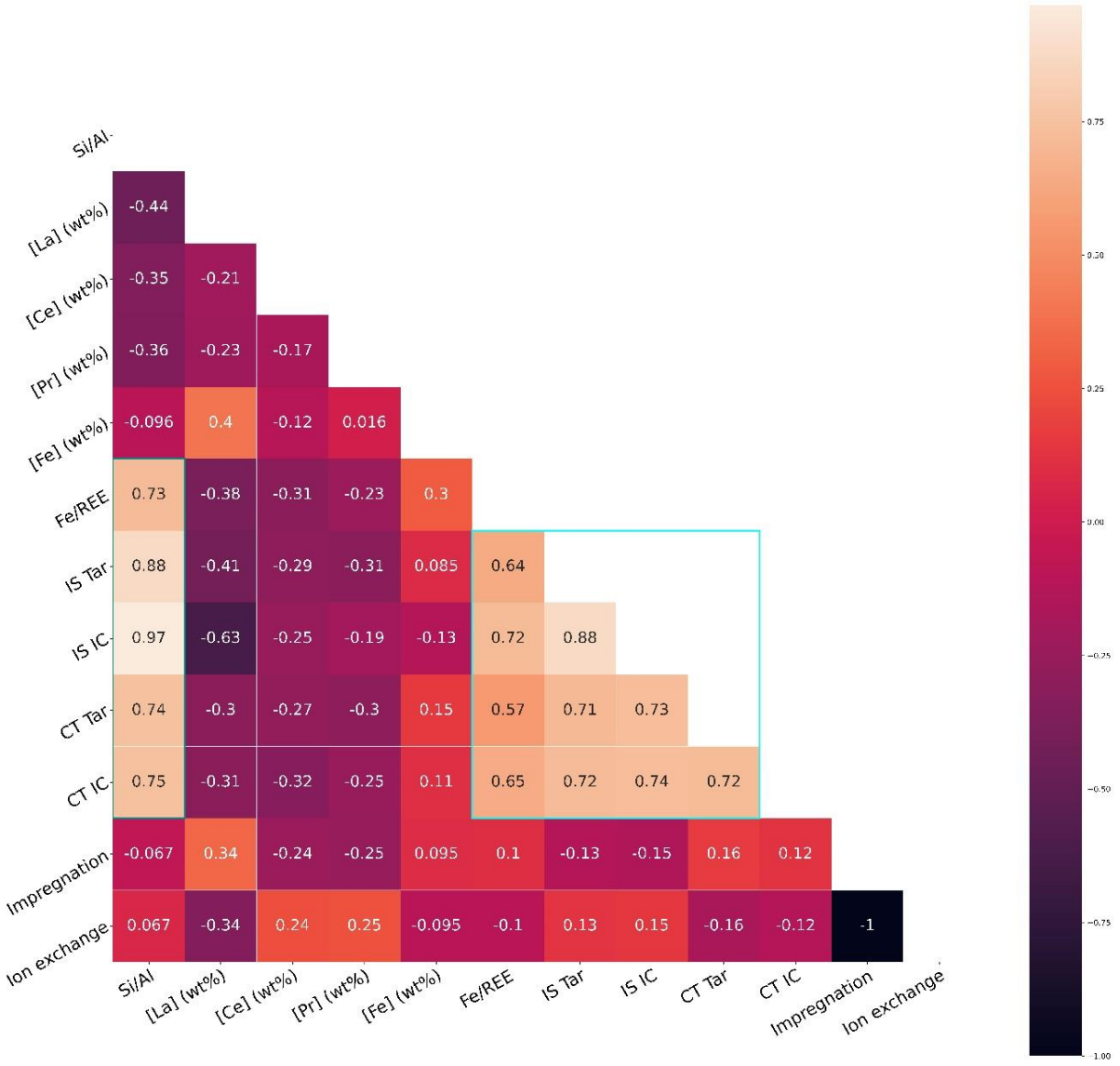

Figure 5.8: Heatmap representing the Pearson correlation between the different features considered on the degradation assays. The left scale represents the different correlation values and the respective colors.

The results of **Figure 5.8** display three important relations, one of them being that the correlation between the IS and CT results of both dyes is greater than 0.70. This suggests that a good catalyst would have good conversions in the tested assays. The Si/Al ratio and Fe/REE ratio have a high positive correlation (between 0.7 and 0.9) [46], suggesting that supports with higher Si/Al ratio, namely the ZSM5, will tend to prefer Fe over REE. The same high positive correlation is found between the Si /Al and the overall results for IS and CT, supporting that the ZSM5 zeolite was the best support used to build the catalysts. The Fe/REE ratio seemed to have moderate positive correlation (between 0.5 and 0.7) [46] with the results from IS and from CT, suggesting that it could be expected a better conversion of the tested dyes with higher values of Fe/REE ratio. The Fe/REE ratio have a low negative correlation (between - 0.3 and - 0.5) [46] with the REE concentrations used, as expected since the higher REE concentrations the smaller Fe/REE. In opposition, the Fe/REE have a low positive correlation (between 0.3 and 0.5) [46] with the Fe concentration, as expected. The CT and IS correlation with the La concentration is low negative, but with Ce and with Pr is negligible (between – 0.3 to 0.0) [46]. A more positive correlation between the CT and IS results and the La concentration could be expected, as the best conversions were obtained with this REE, however negative correlation could suggest that lower concentration can lead to higher degradations. There is a very high negative correlation (-0.9 to -1.0) [46] between the impregnation method and the ion exchange method. This is totally expected since the catalysts were made using one of the two procedures. Finally, the vast majority of the other correlations are negligible, as the values range between 0 and 0.3 or between 0 and -0.3 [46].

The ML algorithms are an important tool that allowed us to determine the main influences on each produced catalyst performance by using 12 features. It was possible to develop a classification model that successfully predicted the classes of unseen data and this is an important asset in selecting the best catalyst. Finally, it is possible to improve these models by increasing the number of characteristic features, a larger data collection (in this case, more catalysts) and by testing different algorithm parameters. These changes can lead to an improved model, which can provide a better understanding of the processes under consideration and the selection of the best solutions for the purpose. On the other hand, improving the data frames with more features may lead to the successful application of regression models, which could help to predict the degradation of untested catalysts or even some other characteristics.

Z15 ($La_{10}Fe_{10}$ZSM5) and Z16 ($La_{25}Fe_{10}$ZSM5) catalysts were used in kinetic studies, assessing the effect of La concentration on the catalyst performance over time.

5.3.2.Catalytic tests (CT)

The catalytic tests with 0.8 g/L of REE/Fe catalysts (Z15 and Z16) and within 300 min of reaction were carried out in two parts. First, the effect of the hydrogen peroxide concentration in the reaction was evaluated by the addition of two different volumes of H_2O_2 at specified concentrations, 0.5 and 5 mL for 90 mM or 12 mM, during the Fenton-like degradation of the dyes, shown in **Figure 5.9**. In the second part, a kinetic model was established for the best REE/Fe-ZSM5 catalysts for dyes degradation by Fenton-like reaction.

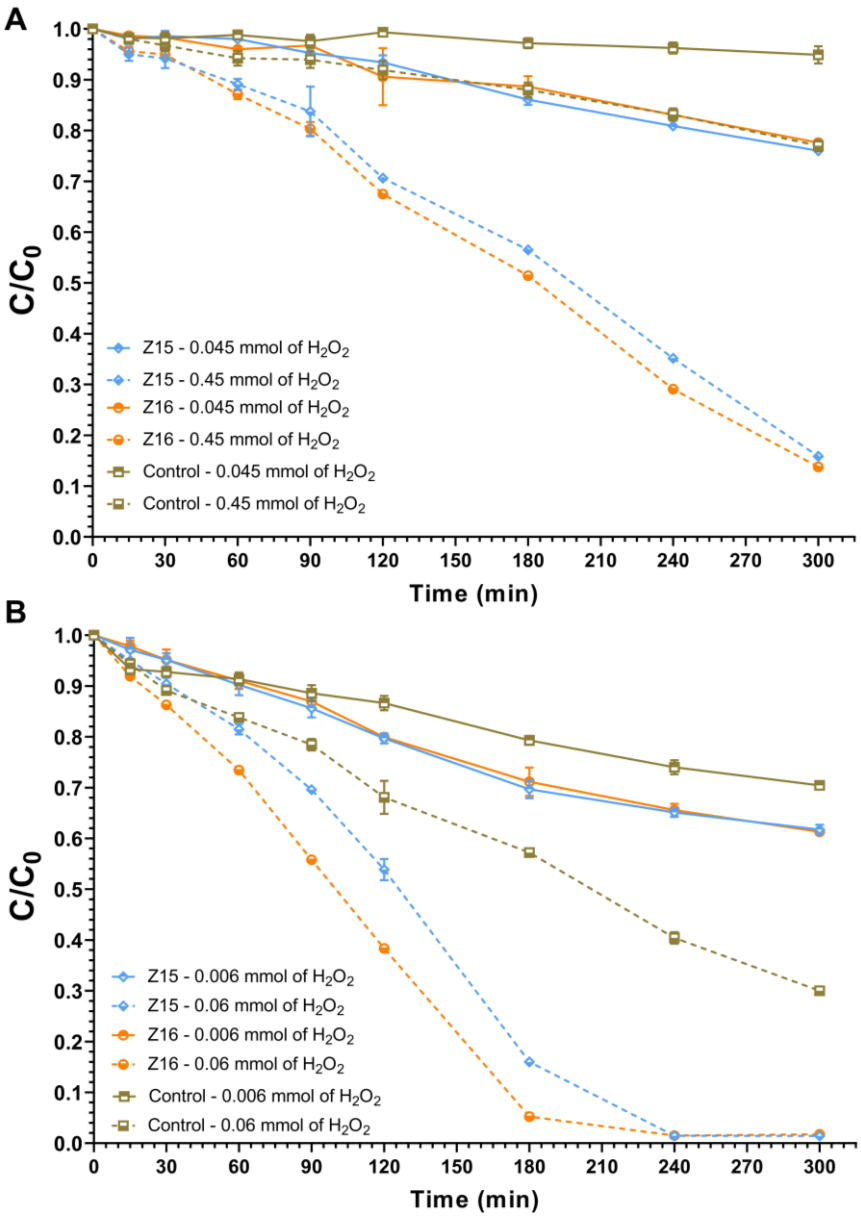

Figure 5.9: Conversion by Fenton-like reaction over time of Tar (**A**) and of IC (**B**) using the selected catalysts (Z15 and Z16) and the controls. The degradation assisted with 0.5 mL of H_2O_2 is represented with a full line, while the reaction with 5 mL of H_2O_2 used a dashed line. Conditions of reaction: 200 mg of catalyst/250 mL at 30 ppm of dye; 0.5 mL or 5 mL of 90 mM H_2O_2 for Tar and 12 mM H_2O_2 for IC; pH=3; T=40 °C and 300 min of reaction.

The dyes were degraded using the selected catalysts in the presence of H_2O_2 (**Figure 5.9**). As expected, bigger volumes of H_2O_2 enhance the degradation of the dyes (**Table S-5.7**). The best conditions for the degradation of the dyes (**Table S-5.8**) were identified. Z15 ($La_{10}Fe_{10}$ZSM5) and Z16 ($La_{25}Fe_{10}$ZSM5) catalysts differ in the La concentration in the preparation solution used and, therefore, in the amount of La ion-exchanged with the zeolite, justifying the eventual differences observed in the catalytic performances, but in fact, both samples have similar catalytic performance with no significant difference, as shown in **Table S-5.8Table S-5.8**.

As the select REE/Fe-ZSM5 catalysts and H_2O_2 have an important role in the degradation of the dyes by Fenton-like reaction, it would be interesting to examine the reaction rate. For that, the fitting parameters of the pseudo-first order model were obtained taking in account 50 % of the dyes degradation using the two selected catalysts. The non-linear and linear equations were used to fit the data with reduced errors. The results are shown in **Table 5.7Table 5.7**.

Table 5.7: Kinetic results for the degradation of both dyes using the non-linear (eq. 1) and the linear (eq. 4) forms of the pseudo-first order model equation.

	Dye	Tar		IC	
	Catalyst	Z15	Z16	Z15	Z16
non-linear	df[a]	25	27	23	19
	k[b]	0.0035	0.0039	0.0054	0.0073
	R^2	0.9556	0.9500	0.9550	0.9777
	Sy.x[c]	0.0299	0.0371	0.0344	0.0237
	SSR[d]	0.0224	0.0371	0.0273	0.0107
linear	df[a]	25	27	23	19
	k[b]	0.0039	0.0046	0.0039	0.0046
	R^2	0.9651	0.9645	0.9551	0.9776
	Sy.x[c]	0.0351	0.0433	0.0472	0.0332
	SSR[d]	0.0307	0.0505	0.0511	0.0209

[a] degrees of freedom; [b] k (L/(g*min)); [c] standard deviation of the residuals; [d] sum of squares due to regression.

The very good values of the R^2 for Tar or IC degradation were obtained from both forms of the equation, being very similar for Z15 and Z16 in the case of Tar and R^2 for Z15 is inferior to R^2 for Z16 in the case of IC . Therefore, the standard deviation of the residuals, Sy.x, and the sum of squares due to regression, SSR, were used to distinguish the fitting, since the R^2 are very similar. The value of Sy.x was

calculated from the fitting parameters using GraphPad Prism 8, while SSR was calculated from the Sy.x value using equation 5.6.

$$SSR = (n - K) * Sy.x^2 \qquad \text{(Eq. 5.6)}$$

In here, *n-K* is the number of degrees of freedom of the regression.

Considering the R^2, Sy.x and the SSR results, the non-linear form of the pseudo-first order model seems to fit better the experimental data than the linear form.

The highest values of the rate constant, *k*, are observed for Z16 catalyst for both dyes. The main difference between Z15 and Z16 for the IC degradation is that the Z16 catalyst required 30 min less than Z15 to reach a degradation near 50 % (**Figure 5.9**). The high kinetic constant is mainly related to the presence of the La^{3+} and Fe^{3+} in the zeolite, which favors the formation of HO· radicals responsible for dyes degradation.

5.4. Conclusions

Several REE/Fe-zeolite catalysts based on two zeolitic structures, FAU or MFI, were prepared and evaluated on Fenton-like reaction for the degradation of Tar and IC dyes. The selection of the best catalyst taking into account different parameters was achieved by machine learning approaches. La^{3+} together with Fe^{3+} and supported on a MFI zeolite structure prepared by ion-exchange reached the best catalytic results. Unsupervised ML tools like PCA and K-Means were a crucial help to visualize and to form clusters according to the best zeolite structure, the best REE used and the best synthesis method. The classifiers from the ML proved to be helpful in narrowing the number of catalysts from fifteen to only two, for the selection of the best one. The catalyst $La_{10}Fe_{10}$ZSM5, Z15, produced via the ion exchange method, was the one selected by ML with a significant dyes degradation efficiency by Fenton-like reaction.

5.5. References

1. Negrea, A.; Gabor, A.; Davidescu, C.M.; Ciopec, M.; Negrea, P.; Duteanu, N.; Barbulescu, A. Rare Earth Elements Removal from Water Using Natural Polymers. *Sci. Rep.* **2018**, *8*, 316.
2. An, F.; Gao, B.; Huang, X.; Zhang, Y.; Li, Y.; Xu, Y.; Zhang, Z.; Gao, J.; Chen, Z. Selectively removal of Al(III) from Pr(III) and Nd(III) rare earth solution using surface imprinted polymer. *React. Funct. Polym.* **2013**, *73*, 60–65.
3. Çelik, İ.; Kara, D.; Karadaş, C.; Fisher, A.; Hill, S.J. A novel ligandless-dispersive liquid–liquid microextraction method for matrix elimination and the preconcentration of rare earth elements from natural waters. *Talanta* **2015**, *134*, 476–481.
4. Unal Yesiller, S.; Eroğlu, A.E.; Shahwan, T. Removal of aqueous rare earth elements (REEs) using nano-iron based materials. *J. Ind. Eng. Chem.* **2013**, *19*, 898–907.
5. Zhao, F.; Repo, E.; Meng, Y.; Wang, X.; Yin, D.; Sillanpää, M. An EDTA-β-cyclodextrin material for the adsorption of rare earth elements and its application in preconcentration of rare earth elements

in seawater. *J. Colloid Interface Sci.* **2016**, *465*, 215–224.
6. Balaram, V. Rare earth elements: A review of applications, occurrence, exploration, analysis, recycling, and environmental impact. *Geosci. Front.* **2019**, *10*, 1285–1303.
7. Rostami, I.; Rezvani, H.; Hu, Z.; Shahmoradian, S.H. Breakthroughs in medicine and bioimaging with up-conversion nanoparticles. *Int. J. Nanomedicine* **2019**, *14*, 7759–7780.
8. Otto, R.; Wojtalewicz-Kasprzak, A. Method for Recovery of Rare Earths from Fluorescent Lamps 2012, 1–11.
9. Lyman, J.W.; Palmer, G.R. Recycling of Rare Earths and Iron from NdFeB Magnet Scrap. *High Temp. Mater. Process.* **1993**, *11*, 175–188.
10. Barros, Ó.; Costa, L.; Costa, F.; Lago, A.; Rocha, V.; Vipotnik, Z.; Silva, B.; Tavares, T. Recovery of Rare Earth Elements from Wastewater Towards a Circular Economy. *Molecules* **2019**, *24*, 1005.
11. Yang, F.; Kubota, F.; Baba, Y.; Kamiya, N.; Goto, M. Selective extraction and recovery of rare earth metals from phosphor powders in waste fluorescent lamps using an ionic liquid system. *J. Hazard. Mater.* **2013**, *254–255*, 79–88.
12. Gutiérrez-Gutiérrez, S.C.; Coulon, F.; Jiang, Y.; Wagland, S. Rare earth elements and critical metal content of extracted landfilled material and potential recovery opportunities. *Waste Manag.* **2015**, *42*, 128–136.
13. Binnemans, K.; Jones, P.T.; Blanpain, B.; Van Gerven, T.; Yang, Y.; Walton, A.; Buchert, M. Recycling of rare earths: a critical review. *J. Clean. Prod.* **2013**, *51*, 1–22.
14. Zheng, B.; Fan, J.; Chen, B.; Qin, X.; Wang, J.; Wang, F.; Deng, R.; Liu, X. Rare-Earth Doping in Nanostructured Inorganic Materials. *Chem. Rev.* **2022**, *122*, 5519–5603.
15. Sievers, M. Advanced Oxidation Processes. In *Treatise on Water Science*; Elsevier, 2011; Vol. 4, pp. 377–408 ISBN 9780444531933.
16. Miklos, D.B.; Remy, C.; Jekel, M.; Linden, K.G.; Drewes, J.E.; Hübner, U. Evaluation of advanced oxidation processes for water and wastewater treatment – A critical review. *Water Res.* **2018**, *139*, 118–131.
17. Giannakis, S.; Gamarra Vives, F.A.; Grandjean, D.; Magnet, A.; De Alencastro, L.F.; Pulgarin, C. Effect of advanced oxidation processes on the micropollutants and the effluent organic matter contained in municipal wastewater previously treated by three different secondary methods. *Water Res.* **2015**, *84*, 295–306.
18. Mosai, A.K.; Tutu, H. Simultaneous sorption of rare earth elements (including scandium and yttrium) from aqueous solutions using zeolite clinoptilolite: A column and speciation study. *Miner. Eng.* **2021**, *161*, 106740.
19. Mosai, A.K.; Chimuka, L.; Cukrowska, E.M.; Kotzé, I.A.; Tutu, H. The Recovery of Rare Earth Elements (REEs) from Aqueous Solutions Using Natural Zeolite and Bentonite. *Water, Air, Soil Pollut.* **2019**, *230*, 188.
20. Assila, O.; Barros, Ó.; Fonseca, A.M.F.; Parpot, P.; Soares, O.S.G.P.; Pereira, M.F.R.; Zerrouq, F.; Kherbeche, A.; Rombi, E.; Tavares, T.; et al. Degradation of pollutants in water by Fenton-like oxidation over LaFe-catalysts: Optimization by experimental design. *Microporous Mesoporous Mater.* **2023**, *349*, 112422.
21. Li, Y.; Yu, J. Emerging applications of zeolites in catalysis, separation and host–guest assembly. *Nat. Rev. Mater.* **2021**, *6*, 1156–1174.
22. Xu, R.; Pang, W.; Yu, J.; Huo, Q.; Chen, J. *Chemistry of Zeolites and Related Porous Materials*; Wiley, 2007; ISBN 9780470822333.
23. Sable, S.S.; Georgi, A.; Contreras, S.; Medina, F. Fenton-like oxidation of phenol with in-situ generated hydrogen peroxide and Pd/Fe-zeolite catalysts. *Water-Energy Nexus* **2021**, *4*, 95–102.
24. Gonzalez-Olmos, R.; Martin, M.J.; Georgi, A.; Kopinke, F.-D.; Oller, I.; Malato, S. Fe-zeolites as

heterogeneous catalysts in solar Fenton-like reactions at neutral pH. *Appl. Catal. B Environ.* **2012**, *125*, 51–58.
25. Jain, B.; Singh, A.K.; Kim, H.; Lichtfouse, E.; Sharma, V.K. Treatment of organic pollutants by homogeneous and heterogeneous Fenton reaction processes. *Environ. Chem. Lett.* **2018**, *16*, 947–967.
26. Imlay, J.A. Iron-sulphur clusters and the problem with oxygen. *Mol. Microbiol.* **2006**, *59*, 1073–1082.
27. Pignatello, J.J.; Oliveros, E.; MacKay, A. Advanced Oxidation Processes for Organic Contaminant Destruction Based on the Fenton Reaction and Related Chemistry. *Crit. Rev. Environ. Sci. Technol.* **2006**, *36*, 1–84.
28. Buxton, G. V.; Greenstock, C.L.; Helman, W.P.; Ross, A.B. Critical Review of rate constants for reactions of hydrated electrons, hydrogen atoms and hydroxyl radicals (·OH/·O− in Aqueous Solution. *J. Phys. Chem. Ref. Data* **1988**, *17*, 513–886.
29. Dong, C.; Ji, J.; Shen, B.; Xing, M.; Zhang, J. Enhancement of H2O2 Decomposition by the Co-catalytic Effect of WS2 on the Fenton Reaction for the Synchronous Reduction of Cr(VI) and Remediation of Phenol. *Environ. Sci. Technol.* **2018**, *52*, 11297–11308.
30. Silva, M.M.; Reboredo, F.H.; Lidon, F.C. Food Colour Additives: A Synoptical Overview on Their Chemical Properties, Applications in Food Products, and Health Side Effects. *Foods* **2022**, *11*, 379.
31. Neelam, M.; Mishra, S. Effects of Food Additives and Preservatives on Processed Food. *Asian J. Sci. Appl. Technol.* **2018**, *7*, 30–32.
32. Jordan, M.I.; Mitchell, T.M. Machine learning: Trends, perspectives, and prospects. *Science (80-.).* **2015**, *349*, 255–260.
33. Kitchin, J.R. Machine learning in catalysis. *Nat. Catal.* **2018**, *1*, 230–232.
34. Li, Z.; Wang, S.; Xin, H. Toward artificial intelligence in catalysis. *Nat. Catal.* **2018**, *1*, 641–642.
35. Yang, W.; Fidelis, T.T.; Sun, W.-H. Machine Learning in Catalysis, From Proposal to Practicing. *ACS Omega* **2020**, *5*, 83–88.
36. Shannon, R.D. Revised effective ionic radii and systematic studies of interatomic distances in halides and chalcogenides. *Acta Crystallogr. Sect. A* **1976**, *32*, 751–767.
37. Kuźniarska-Biernacka, I.; Carvalho, M.A.; Rasmussen, S.B.; Bañares, M.A.; Biernacki, K.; Magalhães, A.L.; Rolo, A.G.; Fonseca, A.M.; Neves, I.C. Copper(II)–imida-salen Complexes Encapsulated into NaY Zeolite for Oxidations Reactions. *Eur. J. Inorg. Chem.* **2013**, *2013*, 5408–5417.
38. Santos, B.L.C.; Parpot, P.; Soares, O.S.G.P.; Pereira, M.F.R.; Rombi, E.; Fonseca, A.M.; Correia Neves, I. Fenton-Type Bimetallic Catalysts for Degradation of Dyes in Aqueous Solutions. *Catalysts* **2020**, *11*, 32.
39. Picoli Nippes, R.; Derksen Macruz, P.; Heloísa Neves Olsen Scaliante, M. Photo-Fenton Oxidative System for Removing Tartrazine Yellow Dye in Aqueous Medium Using Y-fe Zeolite As Catalyst. **2021**.
40. Boroglu, M.S.; Gurkaynak, M.A. Fabrication and characterization of silica modified polyimide–zeolite mixed matrix membranes for gas separation properties. *Polym. Bull.* **2011**, *66*, 463–478.
41. Wang, W.; Zhang, W.; Chen, H.; Zhang, S.; Li, J. Synergistic effect of synthetic zeolites on flame-retardant wood-flour/polypropylene composites. *Constr. Build. Mater.* **2015**, *79*, 337–344.
42. Aronne, A.; Esposito, S.; Ferone, C.; Pansini, M.; Pernice, P. FTIR study of the thermal transformation of barium-exchanged zeolite A to celsian. *J. Mater. Chem.* **2002**, *12*, 3039–3045.
43. Kuźniarska-Biernacka, I.; Biernacki, K.; Magalhães, A.L.; Fonseca, A.M.; Neves, I.C. Catalytic behavior of 1-(2-pyridylazo)-2-naphthol transition metal complexes encapsulated in Y zeolite. *J.*

Catal. **2011**, *278*, 102–110.
44. Satopaa, V.; Albrecht, J.; Irwin, D.; Raghavan, B. Finding a "Kneedle" in a Haystack: Detecting Knee Points in System Behavior. In Proceedings of the 2011 31st International Conference on Distributed Computing Systems Workshops; IEEE, 2011; pp. 166–171.
45. Li, J.; Gao, M.; Yan, W.; Yu, J. Regulation of the Si/Al ratios and Al distributions of zeolites and their impact on properties. *Chem. Sci.* **2023**, *14*, 1935–1959.
46. Mukaka, M.M. Statistics corner: A guide to appropriate use of correlation coefficient in medical research. *Malawi Med. J.* **2012**, *24*, 69–71.

5.6. Supplementary material

Table S-5.1: Conversion results with respective errors for tartrazine (Tar) and Indigo Carmine (IC) for the initial screening assays (IS) and the catalytic tests (CT). Conditions of the reaction: 20 mg of catalyst/25 mL at 30 ppm of Tar; 0.5 mL of 90 mM H_2O_2; pH=3; T=40 ^{0}C and 3 h of reaction for IS and 5 h for CT. The same conditions for the IC for both IS and CT, with the exception of the H_2O_2 concentration used, which was 12 mM.

Samples	Label	Tar		IC	
		IS (%)	CT (%)	IS (%)	CT (%)
$La_{10}Fe_{10}NaX$	A3	16.7 ± 0.8	0	0	0
$La_{10}Fe_{10}NaX$	A7	5.2 ± 2.3	0	0	0
$La_{10}Fe_{10}ZSM5$	Z1	49.8 ± 4.5	93.5 ± 0.2	93.2 ± 0.5	98.9 ± 0.7
$La_{10}Fe_{10}NaY$	Z2	19.5 ± 0.4	0	17.2 ± 2.1	0
$La_{25}Fe_{10}ZSM5$	Z3	52.5 ± 4.6	97.1 ± 0.3	99.4 ± 0.5	99.1 ± 0.5
$La_{25}Fe_{10}NaY$	Z4	28.1 ± 0.6	0	13.9 ± 2.4	0
$La_{10}Fe_{10}ZSM5$	Z15	98.5 ± 0.5	83.5 ± 0.5	99.9 ± 0.1	98.6 ± 0.6
$La_{25}Fe_{10}ZSM5$	Z16	84.0 ± 0.3	85.5 ± 0.3	99.2 ± 0.3	0
$La_{25}Fe_{10}NaY$	Z17	3.9 ± 0.6	0	5.0 ± 1.0	0
$Ce_{10}Fe_{10}ZSM5$	Z5	57.2 ± 7.8	89.8 ± 0.4	98.8 ± 0.2	98.3 ± 0.6
$Ce_{10}Fe_{10}NaY$	Z6	11.0 ± 6.4	0	27.7 ± 0.9	0
$Ce_{25}Fe_{10}ZSM5$	Z7	62.2 ± 0.6	0	99.2 ± 0.4	0
$Ce_{25}Fe_{10}NaY$	Z8	24.0 ± 8.8	0	39.2 ± 0.9	0
$Pr_{10}Fe_{10}ZSM5$	Z9	59.7 ± 0.9	86.9 ± 0.9	99.8 ± 0.1	99.2 ± 0.6
$Pr_{10}Fe_{10}NaY$	Z10	25.0 ± 7.7	0	40.7 ± 1.0	0
$Pr_{25}Fe_{10}ZSM5$	Z11	57.0 ± 2.5	87.1 ± 0.4	100.0 ± 0.0	98.2 ± 0.8
$Pr_{25}Fe_{10}NaY$	Z12	16 ± 2.9	0	41.9 ± 1.7	0

Table S-5.2: One Way ANOVA results of the comparison with the catalysts based in ZSM5. NaY and NaX zeolites are in the same conditions for the degradation of Tar. The 95 % confidence interval of the difference is also included as 95.00% CI of diff.

Bonferroni's multiple comparisons test	Mean Diff	95% CI of diff	Significant
$La_{10}Fe_{10}$ZSM5 - Z1 vs. $La_{10}Fe_{10}$NaY - Z2	26.96	15.63 to 38.29	Yes (***)
$La_{10}Fe_{10}$ZSM5 - Z1 vs. $La_{10}Fe_{10}$NaX - A3	29.79	18.46 to 41.12	Yes (****)
$La_{10}Fe_{10}$ZSM5 - Z1 vs. $La_{10}Fe_{10}$NaX - A7	41.29	29.96 to 52.62	Yes (****)
$La_{10}Fe_{10}$ZSM5 - Z1 vs. $La_{10}Fe_{10}$ZSM5 - Z15	-51.99	-61.47 to -42.51	Yes (****)
$La_{10}Fe_{10}$NaY - Z2 vs. $La_{10}Fe_{10}$NaX - A3	2.835	-9.578 to 15.25	No (ns)
$La_{10}Fe_{10}$NaY - Z2 vs. $La_{10}Fe_{10}$NaX - A7	14.33	1.919 to 26.74	Yes (*)
$La_{10}Fe_{10}$NaY - Z2 vs. $La_{10}Fe_{10}$ZSM5 - Z15	-78.95	-89.70 to -68.20	Yes (****)
$La_{10}Fe_{10}$NaX - A3 vs. $La_{10}Fe_{10}$NaX - A7	11.5	-0.9166 to 23.91	No (ns)
$La_{10}Fe_{10}$NaX - A3 vs. $La_{10}Fe_{10}$ZSM5 - Z15	-81.78	-92.53 to -71.03	Yes (****)
$La_{10}Fe_{10}$NaX - A7 vs. $La_{10}Fe_{10}$ZSM5 - Z15	-93.28	-104.0 to -82.53	Yes (****)

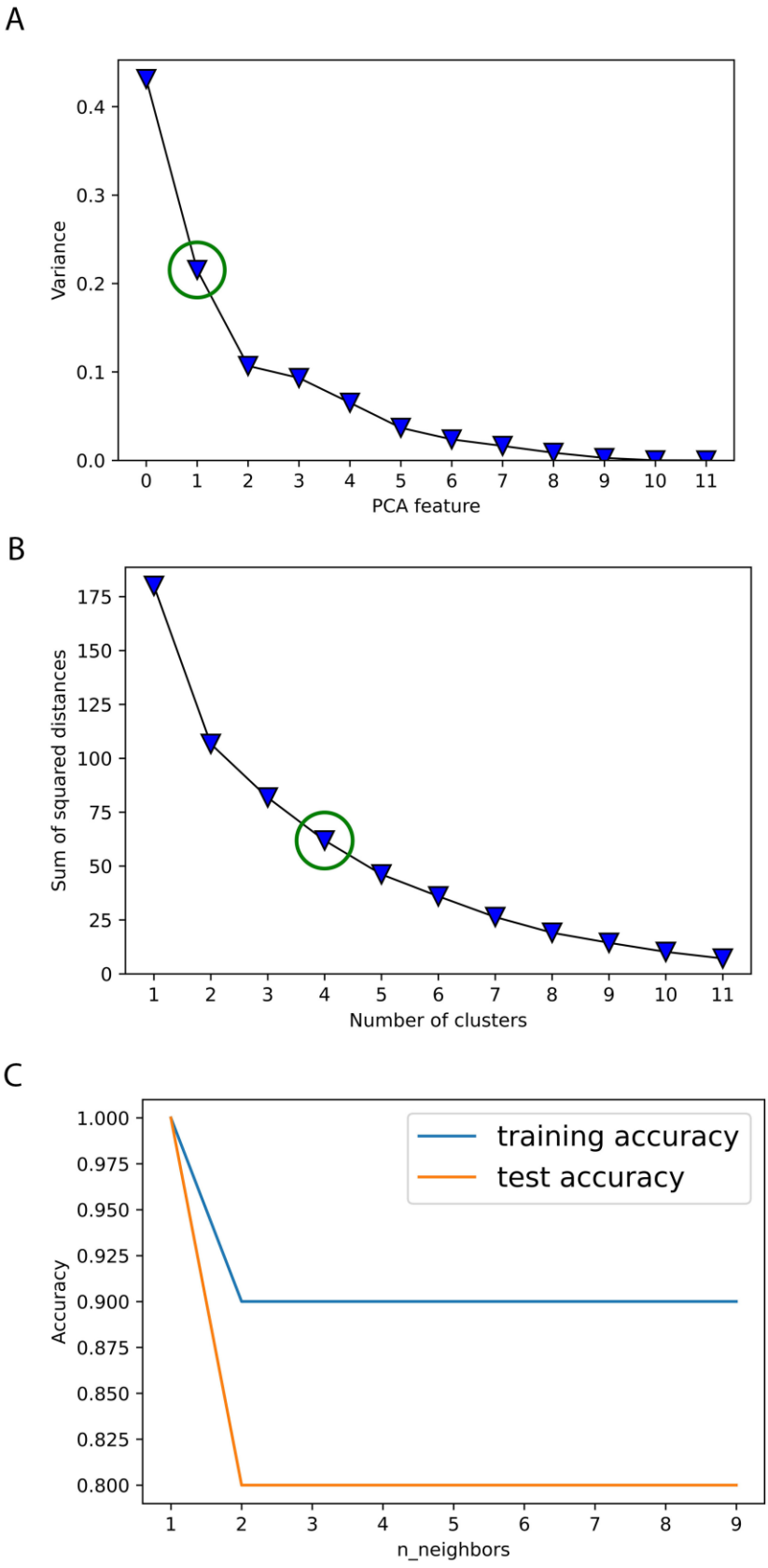

Figure S-5.1: Elbow method to select the best option for PCA (**A**), K-Means (**B**) and accuracy for the training and test sets for the K-Neighbors Classifier (**C**).

Table S-5.3: One Way ANOVA results using Bonferroni's multiple comparison tests with the REE/FE-catalysts based in NaY or in ZSM5 for the same REE. These tests were performed for both dyes. The 95 % confidence interval of the difference is also included as 95.00% CI of diff.

Dye	Bonferroni's multiple comparisons test	Mean Diff	95% CI of diff	Significant
Tartrazine	$La_{10}Fe_{10}$ZSM5 - Z1 vs. $La_{10}Fe_{10}$NaY - Z2	26.96	5.729 to 48.18	Yes (**)
	$La_{10}Fe_{10}$ZSM5 - Z1 vs. $La_{25}Fe_{10}$NaY - Z4	18.43	-2.796 to 39.66	No (ns)
	$La_{10}Fe_{10}$ZSM5 - Z1 vs. $La_{25}Fe_{10}$NaY - Z17	42.62	24.86 to 60.38	Yes (****)
	$La_{10}Fe_{10}$NaY - Z2 vs. $La_{25}Fe_{10}$ZSM5- Z3	-32.98	-54.20 to -11.75	Yes (****)
	$La_{10}Fe_{10}$NaY - Z2 vs. $La_{10}Fe_{10}$ZSM5 - Z15	-78.95	-99.09 to -58.81	Yes (****)
	$La_{10}Fe_{10}$NaY - Z2 vs $La_{25}Fe_{10}$ZSM5- Z16	-64.46	-84.60 to -44.32	Yes (****)
	$La_{25}Fe_{10}$ZSM5 - Z3 vs. $La_{25}Fe_{10}$NaY - Z4	24.45	3.223 to 45.68	Yes (**)
	$La_{25}Fe_{10}$ZSM5 - Z3 vs. $La_{25}Fe_{10}$NaY - Z17	48.64	30.88 to 66.40	Yes (****)
	$La_{25}Fe_{10}$NaY - Z4 vs. $La_{10}Fe_{10}$ZSM5- Z15	-70.42	-90.56 to -50.28	Yes (****)
	$La_{25}Fe_{10}$NaY - Z4 vs. $La_{25}Fe_{10}$ZSM5- Z16	-55.93	-76.07 to -35.79	Yes (****)
	$La_{10}Fe_{10}$ZSM5- Z15 vs. $La_{25}Fe_{10}$NaY - Z17	94.61	78.17 to 111.1	Yes (****)
	$La_{25}Fe_{10}$ZSM5- Z16 vs. $La_{25}Fe_{10}$NaY - Z17	80.12	63.68 to 96.56	Yes (****)
	$Ce_{10}Fe_{10}$ZSM5- Z5 vs $Ce_{10}Fe_{10}$NaY - Z6	46.21	24.99 to 67.44	Yes (****)
	$Ce_{10}Fe_{10}$ZSM5 - Z5 vs. $Ce_{25}Fe_{10}$NaY - Z8	33.2	11.98 to 54.43	Yes (****)
	$Ce_{10}Fe_{10}$NaY - Z6 vs. $Ce_{25}Fe_{10}$ZSM5 - Z7	-51.16	-72.38 to -29.93	Yes (****)
	$Ce_{25}Fe_{10}$ZSM5 - Z7 vs. $Ce_{25}Fe_{10}$NaY - Z8	38.14	16.92 to 59.37	Yes (****)
	$Pr_{10}Fe_{10}$ZSM5- Z9 vs. $Pr_{10}Fe_{10}$NaY - Z10	34.7	15.72 to 53.69	Yes (****)
	$Pr_{10}Fe_{10}$ZSM5- Z9 vs. $Pr_{25}Fe_{10}$NaY - Z12	43.65	24.67 to 62.64	Yes (****)
	$Pr_{10}Fe_{10}$NaY - Z10 vs $Pr_{25}Fe_{10}$ZSM5- Z11	-32	-50.99 to -13.02	Yes (****)
	$Pr_{25}Fe_{10}$ZSM5- Z11 vs. $Pr_{25}Fe_{10}$NaY - Z12	40.95	21.97 to 59.94	Yes (****)
Indigo Carmine	$La_{10}Fe_{10}$ZSM5 - Z1 vs. $La_{10}Fe_{10}$NaY - Z2	75.93	72.45 to 79.41	Yes (****)
	$La_{10}Fe_{10}$ZSM5 - Z1 vs. $La_{25}Fe_{10}$NaY - Z4	79.3	75.82 to 82.78	Yes (****)
	$La_{10}Fe_{10}$ZSM5 - Z1 vs. $La_{25}Fe_{10}$NaY - Z17	88.12	84.64 to 91.60	Yes (****)
	$La_{10}Fe_{10}$NaY - Z2 vs. $La_{25}Fe_{10}$ZSM5- Z3	-82.17	-85.65 to -78.70	Yes (****)
	$La_{10}Fe_{10}$NaY - Z2 vs. $La_{10}Fe_{10}$ZSM5 - Z15	-82.72	-86.20 to -79.24	Yes (****)
	$La_{10}Fe_{10}$NaY - Z2 vs $La_{25}Fe_{10}$ZSM5- Z16	-81.99	-85.47 to -78.51	Yes (****)
	$La_{25}Fe_{10}$ZSM5 - Z3 vs. $La_{25}Fe_{10}$NaY - Z4	85.55	82.07 to 89.03	Yes (****)
	$La_{25}Fe_{10}$ZSM5 - Z3 vs. $La_{25}Fe_{10}$NaY - Z17	94.37	90.89 to 97.84	Yes (****)
	$La_{25}Fe_{10}$NaY - Z4 vs. $La_{10}Fe_{10}$ZSM5- Z15	-86.09	-89.57 to -82.61	Yes (****)
	$La_{25}Fe_{10}$NaY - Z4 vs. $La_{25}Fe_{10}$ZSM5- Z16	-85.36	-88.84 to -81.88	Yes (****)
	$La_{10}Fe_{10}$ZSM5- Z15 vs. $La_{25}Fe_{10}$NaY - Z17	94.91	91.43 to 98.39	Yes (****)
	$La_{25}Fe_{10}$ZSM5- Z16 vs. $La_{25}Fe_{10}$NaY - Z17	94.18	90.70 to 97.66	Yes (****)
	$Ce_{10}Fe_{10}$ZSM5- Z5 vs $Ce_{10}Fe_{10}$NaY - Z6	71.05	67.57 to 74.53	Yes (****)
	$Ce_{10}Fe_{10}$ZSM5 - Z5 vs. $Ce_{25}Fe_{10}$NaY - Z8	59.6	56.12 to 63.08	Yes (****)
	$Ce_{10}Fe_{10}$NaY - Z6 vs. $Ce_{25}Fe_{10}$ZSM5 - Z7	-71.53	-75.01 to -68.05	Yes (****)
	$Ce_{25}Fe_{10}$ZSM5 - Z7 vs. $Ce_{25}Fe_{10}$NaY - Z8	60.08	56.60 to 63.56	Yes (****)
	$Pr_{10}Fe_{10}$ZSM5- Z9 vs. $Pr_{10}Fe_{10}$NaY - Z10	59.16	55.68 to 62.64	Yes (****)
	$Pr_{10}Fe_{10}$ZSM5- Z9 vs. $Pr_{25}Fe_{10}$NaY - Z12	57.91	54.43 to 61.38	Yes (****)
	$Pr_{10}Fe_{10}$NaY - Z10 vs $Pr_{25}Fe_{10}$ZSM5- Z11	-59.32	-62.80 to -55.84	Yes (****)
	$Pr_{25}Fe_{10}$ZSM5- Z11 vs. $Pr_{25}Fe_{10}$NaY - Z12	58.06	54.58 to 61.54	Yes (****)

Table S-5.4: One Way ANOVA results for the degradation comparing the different REE concentrations of the starting solutions tested. The 95 % confidence interval of the difference is also included as 95.00% CI of diff.

Dye	Bonferroni's multiple comparisons test	Mean Diff	95% CI of diff	Significant
Tartrazine	$La_{10}Fe_{10}$ZSM5 - Z1 vs. $La_{25}Fe_{10}$ZSM5 - Z3	-6.019	-25.01 to 12.97	No (ns)
	$La_{10}Fe_{10}$ZSM5 - Z1 vs. $La_{25}Fe_{10}$ZSM5- Z16	-37,5	-55,26 to -19,74	Yes (****)
	$La_{10}Fe_{10}$NaY - Z2 vs. $La_{25}Fe_{10}$NaY - Z4	-8.525	-31.78 to 14.73	No (ns)
	$La_{10}Fe_{10}$NaY - Z2 vs. $La_{25}Fe_{10}$NaY - Z17	15.66	-4.477 to 35.80	No (ns)
	$La_{10}Fe_{10}$ZSM5- Z15 vs. $La_{25}Fe_{10}$ZSM5- Z16	14.49	-1.953 to 30.93	No (ns)
	$Ce_{10}Fe_{10}$ZSM5 - Z5 vs. $Ce_{25}Fe_{10}$ZSM5 - Z7	-4.941	-23.93 to 14.05	No (ns)
	$Ce_{10}Fe_{10}$NaY - Z6 vs. $Ce_{25}Fe_{10}$NaY - Z8	-13.01	-36.26 to 10.24	No (ns)
	$Pr_{10}Fe_{10}$ZSM5- Z9 vs. $Pr_{25}Fe_{10}$ZSM5 - Z11	2.7	-16.29 to 21.69	No (ns)
	$Pr_{10}Fe_{10}$NaY - Z10 vs. $Pr_{25}Fe_{10}$NaY - Z12	8.95	-10.04 to 27.94	No (ns)
Indigo carmine	$La_{10}Fe_{10}$ZSM5 - Z1 vs. $La_{25}Fe_{10}$ZSM5 - Z3	-6.244	-9.722 to -2.765	Yes (****)
	$La_{10}Fe_{10}$ZSM5 - Z1 vs. $La_{25}Fe_{10}$ZSM5- Z16	-6,057	-9,536 to -2,579	Yes (****)
	$La_{10}Fe_{10}$NaY - Z2 vs. $La_{25}Fe_{10}$NaY - Z4	3.373	-0.1053 to 6.851	No (ns)
	$La_{10}Fe_{10}$NaY - Z2 vs. $La_{25}Fe_{10}$NaY - Z17	12.19	8.713 to 15.67	Yes (****)
	$La_{10}Fe_{10}$ZSM5- Z15 vs. $La_{25}Fe_{10}$ZSM5- Z16	0.733	-2.745 to 4.211	No (ns)
	$Ce_{10}Fe_{10}$ZSM5 - Z5 vs. $Ce_{25}Fe_{10}$ZSM5 - Z7	-0.4804	-3.959 to 2.998	No (ns)
	$Ce_{10}Fe_{10}$NaY - Z6 vs. $Ce_{25}Fe_{10}$NaY - Z8	-11.45	-14.93 to -7.969	Yes (****)
	$Pr_{10}Fe_{10}$ZSM5- Z9 vs. $Pr_{25}Fe_{10}$ZSM5 - Z11	-0.1576	-3.636 to 3.321	No (ns)
	$Pr_{10}Fe_{10}$NaY - Z10 vs. $Pr_{25}Fe_{10}$NaY - Z12	-1.256	-4.734 to 2.222	No (ns)

Table S-5.5: One Way ANOVA results for the degradation comparing the different REE for the same support and the same REE concentration. The 95 % confidence interval of the difference is also included as 95.00% CI of diff.

Dye	Bonferroni's multiple comparisons test	Mean Diff,	95,00% CI of diff,	Significant
Tartrazine	$La_{10}Fe_{10}$ZSM5 - Z1 vs. $Ce_{10}Fe_{10}$ZSM5- Z5	-10,75	-29,74 to 8,233	No (ns)
	$La_{10}Fe_{10}$ZSM5 - Z1 vs. $Pr_{10}Fe_{10}$ZSM5 - Z9	-13,18	-32,16 to 5,810	No (ns)
	$La_{10}Fe_{10}$NaY - Z2 vs. $Ce_{10}Fe_{10}$NaY - Z6	8,504	-14,75 to 31,76	No (ns)
	$La_{10}Fe_{10}$NaY - Z2 vs. $Pr_{10}Fe_{10}$NaY - Z10	-5,431	-26,66 to 15,80	No (ns)
	$La_{25}Fe_{10}$ZSM5- Z3 vs. $Ce_{25}Fe_{10}$ZSM5- Z7	-9,675	-28,66 to 9,311	No (ns)
	$La_{25}Fe_{10}$ZSM5- Z3 vs. $Pr_{25}Fe_{10}$ZSM5 - Z11	-4,458	-23,44 to 14,53	No (ns)
	$La_{25}Fe_{10}$NaY - Z4 vs. $Ce_{25}Fe_{10}$NaY - Z8	4,018	-19,24 to 27,27	No (ns)
	$La_{25}Fe_{10}$NaY - Z4 vs. $Pr_{25}Fe_{10}$NaY - Z12	12,04	-9,184 to 33,27	No (ns)
	$La_{10}Fe_{10}$ZSM5 - Z15 vs. $Ce_{10}Fe_{10}$ZSM5 - Z5	-41,24	-59,00 to -23,48	Yes (****)
	$La_{10}Fe_{10}$ZSM5 - Z15 vs. $Pr_{10}Fe_{10}$ZSM5 - Z9	-38,81	-56,57 to -21,05	Yes (****)
	$La_{25}Fe_{10}$ZSM5 - Z16 vs. $Ce_{25}Fe_{10}$ZSM5 - Z7	-21,81	-39,57 to -4,046	Yes (**)
	$La_{25}Fe_{10}$ZSM5 - Z16 vs. $Pr_{25}Fe_{10}$ZSM5 - Z11	-27,02	-44,78 to -9,264	Yes (***)
	$La_{25}Fe_{10}$NaY – Z17 vs. $Ce_{25}Fe_{10}$NaY - Z8	20,17	0,02945 to 40,31	Yes (*)
	$La_{25}Fe_{10}$NaY – Z17 vs. $Pr_{25}Fe_{10}$NaY - Z12	12,14	-5,619 to 29,90	No (ns)
	$Ce_{10}Fe_{10}$ZSM5- Z5 vs. $Pr_{10}Fe_{10}$ZSM5- Z9	-2,423	-21,41 to 16,56	No (ns)
	$Ce_{10}Fe_{10}$NaY - Z6 vs. $Pr_{10}Fe_{10}$NaY - Z10	-13,94	-35,16 to 7,293	No (ns)
	$Ce_{25}Fe_{10}$ZSM5 - Z7 vs. $Pr_{25}Fe_{10}$ZSM5 - Z11	5,218	-13,77 to 24,20	No (ns)
	$Ce_{25}Fe_{10}$NaY - Z8 vs. $Pr_{25}Fe_{10}$NaY - Z12	8,026	-13,20 to 29,25	No (ns)
Indigo Carmine	$La_{10}Fe_{10}$ZSM5 - Z1 vs. $Ce_{10}Fe_{10}$ZSM5- Z5	-10,75	-29,74 to 8,233	Yes (****)
	$La_{10}Fe_{10}$ZSM5 - Z1 vs. $Pr_{10}Fe_{10}$ZSM5 - Z9	-13,18	-32,16 to 5,810	Yes (****)
	$La_{10}Fe_{10}$NaY - Z2 vs. $Ce_{10}Fe_{10}$NaY - Z6	8,504	-14,75 to 31,76	Yes (****)
	$La_{10}Fe_{10}$NaY - Z2 vs. $Pr_{10}Fe_{10}$NaY - Z10	-5,431	-26,66 to 15,80	Yes (****)
	$La_{25}Fe_{10}$ZSM5- Z3 vs. $Ce_{25}Fe_{10}$ZSM5- Z7	-9,675	-28,66 to 9,311	No (ns)
	$La_{25}Fe_{10}$ZSM5- Z3 vs. $Pr_{25}Fe_{10}$ZSM5 - Z11	-4,458	-23,44 to 14,53	No (ns)
	$La_{25}Fe_{10}$NaY - Z4 vs. $Ce_{25}Fe_{10}$NaY - Z8	4,018	-19,24 to 27,27	Yes (****)
	$La_{25}Fe_{10}$NaY - Z4 vs. $Pr_{25}Fe_{10}$NaY - Z12	12,04	-9,184 to 33,27	Yes (****)
	$La_{10}Fe_{10}$ZSM5 - Z15 vs. $Ce_{10}Fe_{10}$ZSM5 - Z5	-41,24	-59,00 to -23,48	No (ns)
	$La_{10}Fe_{10}$ZSM5 - Z15 vs. $Pr_{10}Fe_{10}$ZSM5 - Z9	-38,81	-56,57 to -21,05	No (ns)
	$La_{25}Fe_{10}$ZSM5 - Z16 vs. $Ce_{25}Fe_{10}$ZSM5 - Z7	-21,81	-39,57 to -4,046	No (ns)
	$La_{25}Fe_{10}$ZSM5 - Z16 vs. $Pr_{25}Fe_{10}$ZSM5 - Z11	-27,02	-44,78 to -9,264	No (ns)
	$La_{25}Fe_{10}$NaY – Z17 vs. $Ce_{25}Fe_{10}$NaY - Z8	20,17	0,02945 to 40,31	Yes (****)
	$La_{25}Fe_{10}$NaY – Z17 vs. $Pr_{25}Fe_{10}$NaY - Z12	12,14	-5,619 to 29,90	Yes (****)
	$Ce_{10}Fe_{10}$ZSM5- Z5 vs. $Pr_{10}Fe_{10}$ZSM5- Z9	-2,423	-21,41 to 16,56	No (ns)
	$Ce_{10}Fe_{10}$NaY - Z6 vs. $Pr_{10}Fe_{10}$NaY - Z10	-13,94	-35,16 to 7,293	Yes (****)
	$Ce_{25}Fe_{10}$ZSM5 - Z7 vs. $Pr_{25}Fe_{10}$ZSM5 - Z11	5,218	-13,77 to 24,20	No (ns)
	$Ce_{25}Fe_{10}$NaY - Z8 vs. $Pr_{25}Fe_{10}$NaY - Z12	8,026	-13,20 to 29,25	No (ns)

Table S-5.6: One Way ANOVA results for the degradation comparing the different preparation methods for La on both supports. The 95 % confidence interval of the difference is also included as 95.00% CI of diff.

Dye	Bonferroni's multiple comparisons test	Mean Diff.	95,00% CI of diff.	Significant
Tartrazine	$La_{10}Fe_{10}$ZSM5 - Z1 vs. $La_{10}Fe_{10}$ZSM5- Z15	-51,99	-60,70 to -43,29	Yes (****)
	$La_{10}Fe_{10}$ZSM5 - Z1 vs. $La_{25}Fe_{10}$ZSM5- Z16	-37,5	-46,21 to -28,80	Yes (****)
	$La_{25}Fe_{10}$ZSM5 - Z3 vs. $La_{10}Fe_{10}$ZSM5- Z15	-45,97	-54,68 to -37,27	Yes (****)
	$La_{25}Fe_{10}$ZSM5 - Z3 vs. $La_{25}Fe_{10}$ZSM5- Z16	-31,48	-40,19 to -22,78	Yes (****)
	$La_{10}Fe_{10}$NaY - Z2 vs. $La_{25}Fe_{10}$NaY - Z17	15,66	5,791 to 25,53	Yes (***)
	$La_{25}Fe_{10}$NaY - Z4 vs. $La_{25}Fe_{10}$NaY - Z17	24,19	14,32 to 34,06	Yes (****)
Indigo Carmine	$La_{10}Fe_{10}$ZSM5 - Z1 vs. $La_{10}Fe_{10}$ZSM5- Z15	-6,79	-10,54 to -3,041	Yes (****)
	$La_{10}Fe_{10}$ZSM5 - Z1 vs. $La_{25}Fe_{10}$ZSM5- Z16	-6,057	-9,806 to -2,309	Yes (***)
	$La_{25}Fe_{10}$ZSM5 - Z3 vs. $La_{10}Fe_{10}$ZSM5- Z15	-0,5464	-4,295 to 3,202	No (ns)
	$La_{25}Fe_{10}$ZSM5 - Z3 vs. $La_{25}Fe_{10}$ZSM5- Z16	0,1865	-3,562 to 3,935	No (ns)
	$La_{10}Fe_{10}$NaY - Z2 vs. $La_{25}Fe_{10}$NaY - Z17	12,19	8,443 to 15,94	Yes (****)
	$La_{25}Fe_{10}$NaY - Z4 vs. $La_{25}Fe_{10}$NaY - Z17	8,818	5,070 to 12,57	Yes (****)

Table S-5.7: Two Way ANOVA results from the comparison between the different volumes (0.5 or 5 mL) of H_2O_2. The H_2O_2 concentration for the Tar degradation was 90 mM, while for IC was 12 mM. The 95 % confidence interval of the difference is also included as 95.00% CI of diff.

Dye	Bonferroni's multiple comparisons test	Mean Diff.	95.00% CI of diff.	Significant
Tartrazine	Control – 0.5 mL of H_2O_2 vs. Control -5 mL of H_2O_2	-6.61	-10.68 to -2.542	Yes (****)
	Z15 - 0.5 mL of H_2O_2 vs. Z15 -5 mL of H_2O_2	-18.64	-34.45 to -2.830	Yes (**)
	Z16 - 0.5 mL of H_2O_2 vs. Z16 -5 mL of H_2O_2	-20.75	-36.94 to -4.552	Yes (**)
Indigo Carmine	Control – 0.5 mL of H_2O_2 vs. Control -5 mL of H_2O_2	-14.51	-27.54 to -1.481	Yes (*)
	Z15 - 0.5 mL of H_2O_2 vs. Z15 -5 mL of H_2O_2	-26.11	-47.33 to -4.898	Yes (**)
	Z16 - 0.5 mL of H_2O_2 vs. Z16 -5 mL of H_2O_2	-32.74	-53.92 to -11.57	Yes (***)

Table S-5.8: Two Way ANOVA results from the comparisons between the control and the catalysts for the same volume (5 mL) of H_2O_2. The H_2O_2 concentration for the Tar degradation was 90 mM, while for IC was 12 mM. The 95 % confidence interval of the difference is also included as 95.00% CI of diff.

Dye	Bonferroni's multiple comparisons test	Mean Diff.	95.00% CI of diff.	Significant?
Tartrazine	Control -5 mL of H_2O_2vs. Z15 -5 mL of H_2O_2	-19.32	-34.83 to -3.816	Yes (**)
	Control -5 mL of H_2O_2vs. Z16 -5 mL of H_2O_2	-21.98	-37.86 to -6.110	Yes (**)
	Z15 -5 mL of H_2O_2 vs. Z16 -5 mL of H_2O_2	-2.661	-23.56 to 18.23	No (ns)
Indigo Carmine	Control - 5 mL of H_2O_2vs. Z15 - 5 mL of H_2O_2	-14.68	-37.71 to 8.338	No (ns)
	Control - 5 mL of H_2O_2vs. Z16 - 5 mL of H_2O_2	-20.79	-43.77 to 2.190	No (ns)
	Z15 - 5 mL of H_2O_2vs. Z16 - 5 mL of H_2O_2	-6.108	-33.73 to 21.51	No (ns)

Chapter 6 – Final Remarks

This chapter contains the principal conclusions drawn from the work described in the previous chapters and proposes recommendations/suggestions for further research.

6.1. General conclusions

Rare earth elements (REE) are a crucial group of valuable elements used in diverse and relevant applications in our daily lives. Zeolites are crystalline microporous aluminosilicates that can be used as adsorbents and catalysts. These materials can suffer surface treatments to increase their ion exchange and adsorbent capacities. Adsorption processes have been extensively used to remove different pollutants from wastewater, such as heavy metals. This process is simple and competitive with high recovery efficiency, availability of a wide range of sorbents and effective with low pollutant concentrations. Heterogeneous catalysis involves solid materials while the reactants can be in liquid state and it has been applied in Advanced Oxidation Processes (AOP). AOPs are an emerging technology, and within them the Fenton reaction allows different organic pollutants to be oxidized into non-toxic products. Machine learning (ML) is an evolving branch of computational algorithms widely used in diverse fields.

In **Chapter 3**, the REE adsorption capacities of the FAU (13X) and LTA (4A) zeolites were tested after surface chemical treatments by acid and base solutions. The different zeolites were characterized, which led to the conclusion that the chemical modifications performed in the zeolites were only at the surface. From the comparison of the results obtained from the modified zeolites and the controls used, it could be possible to see that the acid treatments for the FAU did not improve the natural adsorption capacity of the zeolite. In some cases, a significant difference was found between the controls and the modified zeolites. On the other hand, the alkali treatment for both tested zeolite structures (Z13X and Z4A) led to an enhancement of the REE removal from aqueous solutions. The zeolite ZX_NaOH 0.1 M (FAU 13X treated with an alkali solution of NaOH 0.1 M) removed over 80 % of each tested REE in the solution, except for Ce, and it was closely followed by the ZX_KOH 0.1 M (FAU 13X treated with an alkali solution of KOH 0.1 M). The previous zeolites were selected and used in the follow-up assays. Regarding the LTA zeolite, the ZA_NaOH 0.5 M (4A treated with an alkali solution of NaOH 0.5 M) removed over 80 % of each tested REE, except for La and Ce. However, for the LTA zeolite, there might be some possible precipitation of the REE and this ended its use in the leaching tests. The ML algorithms were used to test their applicability to these systems, to obtain different insights from the collected experimental data and to have a better understanding of the overall process. All modified zeolites were used. In unsupervised learning, it was possible to apply the PCA and K-Means algorithms, which identified the characteristics that influenced the most the modified zeolites and associated them in groups according to those characteristics. In supervised learning, a classification algorithm was applied to train a model that correctly selected the best modified zeolites accordingly to their REE removal capacity and the results from the classification agreed with those obtained in the adsorption assays. At the same time, a regression

model was successfully tested that used the C/C_0 of one REE to predict the C/C_0 of the other tested REE. In the desorption of the REE, it was shown that water leaching is ineffective, as the recovery was less than 5 % of the tested REE after 3 h. Regarding the acid leaching, the best recoveries were achieved at 0.5 h. The selected modified FAU presented a statistically significant improvement in the recoveries compared to the control zeolites. HNO_3 eluent at 0.10 M was selected for further assays because it presents good recoveries and is a weaker acid when compared to the others tested. The zeolite ZX_NaOH 0.10 M presented the best parameters in the tested kinetic models, showing an overall improvement in capacity and rate compared to the untreated zeolites. Therefore, this designed sorbent can be used in continuous flow assays to test its capacity for adsorption and desorption for REE recovery from wastewater.

In **Chapter 4**, the assays were carried out using the modified zeolite selected from **Chapter 3**, ZX_NaOH 0.10 M (designed only as ZX_NaOH) and an untreated zeolite (Z13X) as control. In the adsorption assays it was possible to remove between 65 and 90 % of the total amount of REE during the 4 adsorption - desorption cycles. Adding to that, a decrease in the removal per cycle of adsorption was observed. In terms of desorption, only 20 % of the total REE entrapped in the zeolite was recovered for each 4 desorption cycle. For each cycle, a reduction of the recovery explained the poorer results in the adsorption tests. After comparing the HNO_3/ zeolite ratio from the batch assays (**Chapter 3**) with the same ratio used in the continuous flow assays, a 43-fold difference was identified and the HNO_3/ zeolite ratio was increased. It was possible to recover over 80 % of each REE, after 3 h leaching. As expected, this improvement showed a statistical difference from the results of the previous 4 cycles, demonstrating an improvement in the REE recovery in the continuous flow assays. The eventual bed washing with NaOH 0.01 M also showed no improvement in the overall efficiency of the process and no REE leaching was detected.

ML algorithms can be successfully applied to continuous flow assays. The unsupervised learning allowed the evaluation of the influence of each characteristic using PCA and the grouping of the different conditions using K-Means. The classification results from the supervised learning showed that none of the tested conditions improved compared to the others for the overall analysis. The exception was the desorption analysis using all cycles, including the maximized one, which was the best overall, as expected from the desorption results analysis. The heatmap results from the regression suggest that it is possible to develop a model that allows the prediction of the REE concentrations for the adsorption and desorption of the different tested REE, using the values of one of them. From all results, there is a lack of significant differences between the zeolites tested, Z13X and ZX_NaOH, opposite to what was observed in the batch

assays (**Chapter 3**). This suggests that the chemical pre-treatment might not be justifiable in the continuous flow assays.

In **Chapter 5**, several REE/Fe zeolite catalysts were produced based on two zeolitic structures, FAU (NaX and NaY) and MFI (ZSM5) and evaluated on Fenton-like reaction for the degradation of tartrazine or indigo carmine dyes in liquid phase. An initial tartrazine degradation was performed to compare the different La/Fe zeolite catalysts produced from the three types of zeolites used and it was shown that the NaX zeolite do not have any catalytical properties, as expected. This also helped to explain why different zeolites were used in this research. Overall, the NaY catalysts had higher concentrations of REE than the ZSM5 catalysts, due to the different Si/Al ratios. However, the initial screening assays for both tartrazine and indigo carmine showed that the NaY catalysts had a lower degradation activity for both dyes when compared to those produced with ZSM5. In addition, between the different tested REE (La, Ce and Pr), the catalysts loaded with La achieved better degradation for tartrazine than the ones produced with Ce or Pr. At the same time, for indigo carmine, the results were very similar for the catalysts produced with ZSM5. Finally, it was also possible to assess the La/Fe ZSM5 catalysts preparation, comparing the ion exchange method, that allowed higher degradation ability, with the impregnation one. The conjugation of these results led to the conclusion that La^{3+} together with Fe^{3+} and supported on MFI zeolite structure prepared by ion exchange, reached the best catalytic results. The best catalysts were Z15 ($La_{10}Fe_{10}$ZSM5 by ion exchange) and Z16 ($La_{25}Fe_{10}$ZSM5 by ion exchange), with degradations over 80 % for tartrazine and nearly 100 % for indigo carmine. ML tools were also successfully implemented in this analysis, where unsupervised learning (PCA and K-Means) helped visualize and form clusters according to the best zeolite structure, the best REE used and the best synthesis method. The classifiers from the supervised learning proved to help narrowing the number of catalysts from fifteen to only two for selecting the best degradation promoter. The kinetics modelling was very similar for Z15 ($La_{10}Fe_{10}$ZSM5 by ion exchange) and for Z16 ($La_{25}Fe_{10}$ZSM5 by ion exchange), from which Z15 was selected as the best catalyst for the degradation of the tested dyes. This demonstrated that the use more of La to produce the Z16 catalyst is unjustified.

6.2. Future work

Further work is yet to be done to better understand and develop the full potential of these systems, in the adsorption or in the catalysis perspectives.

I. The sorption assays in batch and continuous flow assays can be further developed by:

- Using other types of zeolite structures with and without chemical modifications, using the same or different chemicals for the modification to evaluate the influence of these modifications in the REE adsorption in batch assays.
- Characterizing the resulting zeolites with other techniques such as X-ray diffraction (XRD) and N_2 adsorption isotherms fittings as Brunauer-Emmett-Teller (BET) to determine specific surface areas and pore volumes.
- Quantifying the Al and Si in the solid matrices during the adsorption and desorption assays should be performed as it could help to identify an eventual dealumination or not by the chemical treatments.
- Testing the use of different microorganisms in biosorption assays to assess their capacity of REE retention. The best suitable microorganisms can be grown in supported biofilm on the best suitable modified zeolite and this combination should be tested in continuous flow assays.
- Optimizing the eluent nature and concentration in terms of leaching efficiency and zeolites degradation minimization.
- Testing the adsorption after the optimized desorption steps in the continuous flow assays to improve the overall process.
- Selecting the best concentrations of the NaOH for the eventual bed washing between the desorption and the adsorption steps in the continuous flow assays.
- Further developing the ML models with more critical features (from the characterization), with more data and even with different and optimized algorithm parameters so it could be possible to promote a better understanding of the process and, therefore, an improved model for the batch assays.
- Applying and developing the regression models considering the optimizations performed in the batch assays for the REE concentration prediction in the continuous flow assays.

II The catalysts assays can be further developed by:

- Producing more catalysts with different relevant characteristics with possible chemical or physical modification with an extended characterization of the produced material by X-ray Photoelectron Spectroscopy (XPS), for example.
- Assessing the degradation of different dyes (with or without combinations of them), different organic pollutants, such as polycyclic aromatic hydrocarbons (PAH), persistent organic pollutants (POP) and emerging organic contaminants (EOC).
- As for the sorption processes, improving and developing the ML models, especially models that predict the catalytic capacity of pollutant degradation. It would be interesting to establish a correlation between some catalyst characteristics and the degradation of specific pollutants.